SCUOLA DI DOTTORATO
UNIVERSITÀ DEGLI STUDI DI MILANO-BICOCCA

Department of Earth and Environmental Sciences (DISAT)

PhD program in Chemical, Geological and Environmental Sciences

Cycle XXXI

Curriculum in Environmental Sciences

Quantitative reconstructions of climatic series in mountain environment based on paleoecological and ecological data

Surname: Furlanetto

Name: Giulia

Registration number: 809217

Tutor: Prof. Maggi Valter

Supervisor: Dr. Ravazzi Cesare

Coordinator: Prof. Frezzotti Maria Luce

ACADEMIC YEAR 2017/2018

Acknowledgements

I wish to acknowledge the help provided by many people: Cesare Ravazzi and Roberta Pini for fruitful discussions and for their help during field work and in the laboratory; Valter Maggi, Michele Brunetti, Federica Badino and Roberto Comolli for their support and comments; I am grateful to the two external advisors Antonello Provenzale and Thomas Giesecke; Francesca Vallè for her help with climate reconstructions; José María Fernández-Palacios for the PhD period of research abroad. I acknowledge the many people helping during field and laboratory work: Andrea Tramelli, Marco Zanon, Davide Margaritora, Lorenzo Castellano, Enrico Croce, Massimo Domenico Novellino, Renata Perego, Fioretta Brameri, Silvia Poletti, Edoardo Secchi, Matteo Rosi and Rifugio Fratelli Longo for the logistic support.

Index

Abstract

Montane vegetation is traditionally known to be particularly sensitive to climate changes. The strong elevational climatic gradient that characterises mountain areas results in a steep ecological slope, with several ecotones occurring in a small area. Pollen sequences investigated in or shortly above the modern timberline ecotone are ideal archives to analyze the relationships between climate and ecosystems. Quantitative reconstruction of past climate conditions from fossil pollen records requires understanding modern pollen representation along climatic and ecological gradients. The model calibration with elevational transects could allow to obtain good paleoclimate reconstructions in high-elevation environments, particulary sensitive to rapid climate changes.

The aims of this PhD research are:

- the development of modern pollen-vegetation-climate elevational transects
- looking for new high-resolution natural archives to obtain proxy data and to reconstruct paleoenvironmental and palaeoclimatic changes during the Holocene
- model processing and validation for evaluating pollen-climate relationships thanks to elevational gradients
- the application of these models to pollen-stratigraphical data
- comparing the results with different proxy-based reconstructions

In **Manuscript 1** the importance of local elevational transects of modern pollen samples with site-specific temperature as a tool for paleoclimate reconstructions in the Alps was demonstrated. The two elevational transects (La Thuile Valley and Upper Brembana Valley) were developed to derive consistent local pollen-climate correlations, to find sensitive pollen taxa useful for paleoclimate reconstructions; to estimate the effects of local parameters (elevational lapse rate, climate, uphill pollen transport and human impact) and were used as test sets to evaluate pollen-climate models based on calibration sets extracted from the European Modern Pollen Database.

Both test sets and calibration sets benefit from site-specific climate information obtained by applying well-performing interpolation techniques from a high-density climate-station network. This is an improvement that assists in the reconstruction of past climate in mountain settings. This procedure can be applied to other high mountain ranges with

Alpine-types of elevational biodiversity gradients in the mid-latitudes of the Eurasian and American continents.

In **Manuscript 2** modern pollen assemblages-vegetation-climate relationships along an elevational gradient in the Upper Brembana Valley were investigated. Here modern pollen assemblages (pollen traps and moss samples), vegetation, elevation and climate have been collected at 16 sampling sites placed along an elevational gradient stretching from 1240 m asl to 2390 m asl. The results of CCA analysis demonstrated a general good agreement with previous studies, which identified elevation as the main gradient in the variation of modern pollen and vegetation assemblages in mountain areas.

The uphill transport of pollen by wind to subalpine and alpine zones implies wider pollen belts with less defined boundaries than vegetation. This is mainly due to the increase in extra-local transport of strong pollen producers (e.g. *Pinus sylvestris/mugo*, *Picea*, *Castanea*, *Corylus* and *Ostrya*) and lead to some homogenization of pollen assemblages. Thus, if it is possible to identify the major vegetation types by means of their modern pollen deposition, it becomes more difficult to identify specific thresholds (e.g. treeline). To overcome these limitations, potential indicator pollen taxa of alpine/subalpine belts (*Vaccinium*, *Rhododendron*, *Loiseleuria*) documented in this study could be useful for this purpose.

The stratigraphic study of paleoecological and sedimentary proxies in the Armentarga peat bog allowed to reconstruct the vegetation and climate history during the last 10 ka in a high-elevation, oceanic district of the Italian Alps (**Manuscript 3**). Quantitative reconstructions of Tjuly and Pann were obtained and validated by applying numerical transfer functions built on an extensive calibration pollen-climate dataset. These models proved to be effective even on the modern landscape marked by weak to moderate human impact, with the exclusion of Middle Age phases that suffered stronger alterations due to deforestation and pastoralism. The reconstruction of timberline structure and elevations was supported by an additional elevational transect on modern and past Pollen Accumulation Rates of the main tree and shrub species building the timberline ecotone.

In this area, the modern timberline ecotone shows a peculiar arrangement with a widespread belt of broad-leaved dwarf forest, in agreement with high annual precipitation, while the continental timberline formed by *Pinus cembra* is absent.

The palaeobotanical record of the Armentarga peat bog has shown this elevational vegetation arrangement to be primarily driven by a Middle to late Holocene precipitation increase, substantially independent from the millennial sequence of thermal anomalies already known from other high-elevation Alpine proxies (i.e. glaciers, timberline, chironomids, speleothems).

Changes in annual precipitation occurred in three main steps during the Holocene, starting with a moderately humid early Holocene marked by early occurrence of the *Alnus viridis* dwarf forests, and followed by a first step of precipitation increase starting at 6.2 ka cal BP. A prominent step forward occurred at the Middle to Late Holocene transition, dated between 4.7 and 3.9 ka at the Armentarga site, which led to present values typical for oceanic mountain climates (Pann 1700-1850 mm) and was probably accompanied by increased snowfall and runoff, and had a major impact on timberline depression and grassland expansion. Evidence for a concurrent trigger by human activities at the Late Neolithic / Bronze Age transition are weak, although climate change favored a subsequent development of pastoralism in the Alpine highlands.

Introduction

Since 1990, global mean temperatures have probably been higher than at any previous time during the last 1000 years (Osborn and Briffa, 2006). In the current discussion about past climatic variability and climatic change, an often-asked question is whether (and if so, why) comparably warm periods occurred earlier, in particular during the present interglacial: the Holocene (the last 11700 calendar yr b2k). Climate variability during the Holocene is relatively subtle if compared with the larger amplitude that characterized the last glacial period. Nonetheless, several proxy data (pollen and macrofossils, glacier length variations, lake level oscillations, tree rings width, lacustrine carbonates, stalagmites and ice cores) indicate detectable changes in temperature and/or moisture during this period. Early Holocene (10000 to 5000 years ago) warmth is followed by ~0.7°C cooling through the middle to late Holocene (<5000 years ago), culminating in the coolest temperatures of the Holocene during the Little Ice Age, about 200 years ago. This cooling is largely associated with ~2°C change in the North Atlantic. Current global temperatures of the past decade have not yet exceeded peak interglacial values but are warmer than during ~75% of the Holocene temperature history (Marcott et al., 2013).

Montane vegetation is traditionally known to be particularly sensitive to climate changes (Birks and Ammann, 2000; Wick, 2000). The strong elevational climatic gradient that characterises mountain areas results in a steep ecological slope, with several ecotones occurring in a small area. Regional climate signal is amplified with elevation (Beniston et al., 1997), and this effect is illustrated by the strong impact of recent climate variations on montane ecosystems (Houghton et al., 2001; Qin et al., 2009; Pepin et al., 2015). Being able to assess the impacts of climatic fluctuations on past biodiversity in mountain regions will help in choosing suitable management strategies in the near future. Pollen sequences investigated in or shortly above the modern timberline ecotone are ideal archives to analyze the relationships between climate and ecosystems, offering a millennial perspective to the ongoing trends and allowing to decouple the role of different predictors (e.g. July temperature, annual precipitation, pastoralism), acting at different time scales (Tinner and Theurillat, 2003; Badino et al., 2018).

While the suitability of pollen data for paleoenvironmental reconstructions has long been tested and proved, its potential for quantitative paleoclimate estimations has not yet been fully explored and understood. The application of calibration and regression techniques on

paleoecological records offers the opportunity to obtain pollen-based quantitative estimations of past climate variables (temperature and precipitation) (Seppä and Birks, 2001; Connor and Kvavadze, 2008; Lu et al., 2011; Viau et al., 2012). Quantitative reconstruction of past climate conditions from fossil pollen records requires understanding modern pollen representation along climatic and ecological gradients (Connor et al., 2004; Cañellas-Boltà et al., 2009; Fall, 2012). The model calibration with elevational transects could allow to obtain good paleoclimate reconstructions in high-elevation environments, particulary sensitive to rapid climate changes.

Paleoclimate reconstructions can be compared with other proxy data: diatoms, chironomids, glacier length variations, lake levels variations (Magny 2004; Holzhauser et al. 2005; Le Roy et al. 2015).

1. Basic principles and assumptions for climate reconstructions from pollen data

The basic principle of all quantitative climate reconstructions from biological data is the “methodological uniformitarianism” (Birks and Birks, 1980; Birks and Seppä, 2004; Brewer et al., 2007; Birks et al. 2010) which means, specifically for pollen data, that modern pollen-climate data and relationships between them can be used as analogue or model to infer past conditions because those relationships have not changed throughout time. In **Fig.1** it is schematized the uniformitarianism principle and the major requirement, namely, the existence of a modern calibration set composed by modern pollen assemblages and associated climate variables.

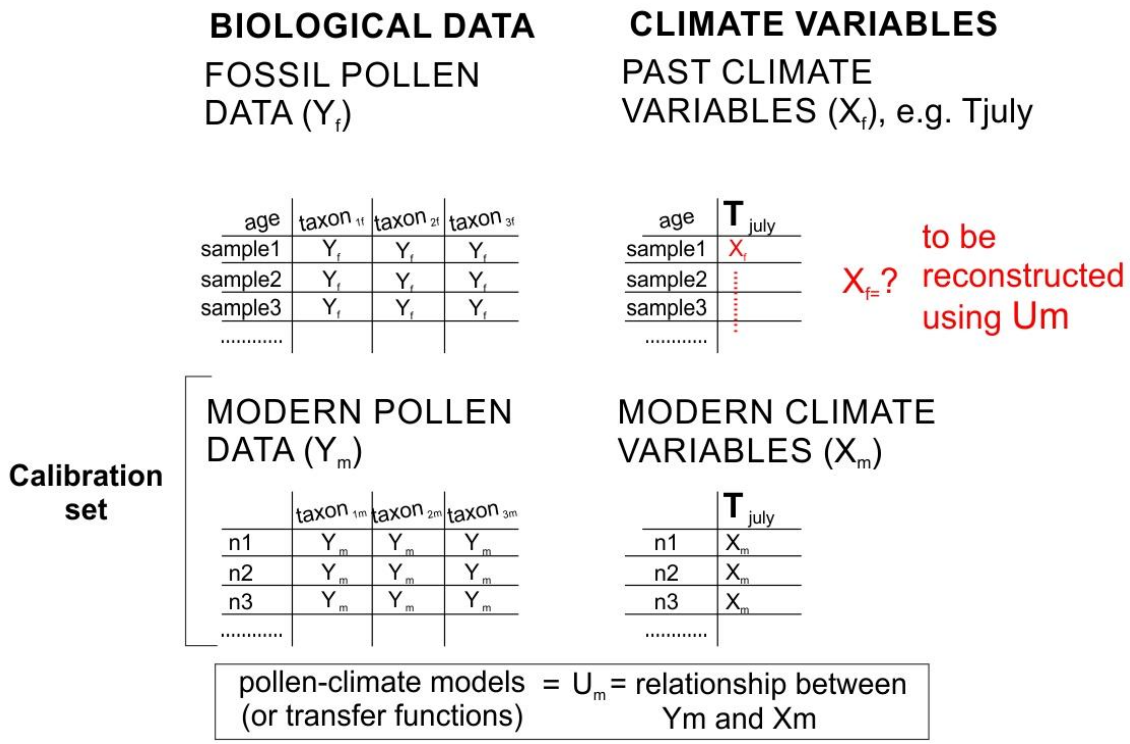

Fig. 1 scheme of the basic principles for quantitative climate reconstructions from pollen data. Y are pollen *taxon* abundances (percentages), X are climate variables. X_f, the unknown climatic variable, to be reconstructed from fossil pollen assemblages Y_f, the essential role of a modern calibration set consisting of n= modern pollen assemblages and associated climate values, and the resulting transfer function (U_m) (modified from Birks and Seppä, 2004 and Birks et al. 2010).

Generally, deriving quantitative reconstructions from pollen data involves "three steps" (Juggins and Birks, 2012) (**Fig. 2**): (1) the development of a calibration set representative for the variable to be reconstructed, (2) the application of numerical methods to the modern pollen-climate data to model their relationships (or finding the transfer function), and (3) the application of the best model (or transfer function) to the stratigraphical-pollen records to finally estimate the past climate values, the validation of the models developed and the obtained reconstruction.

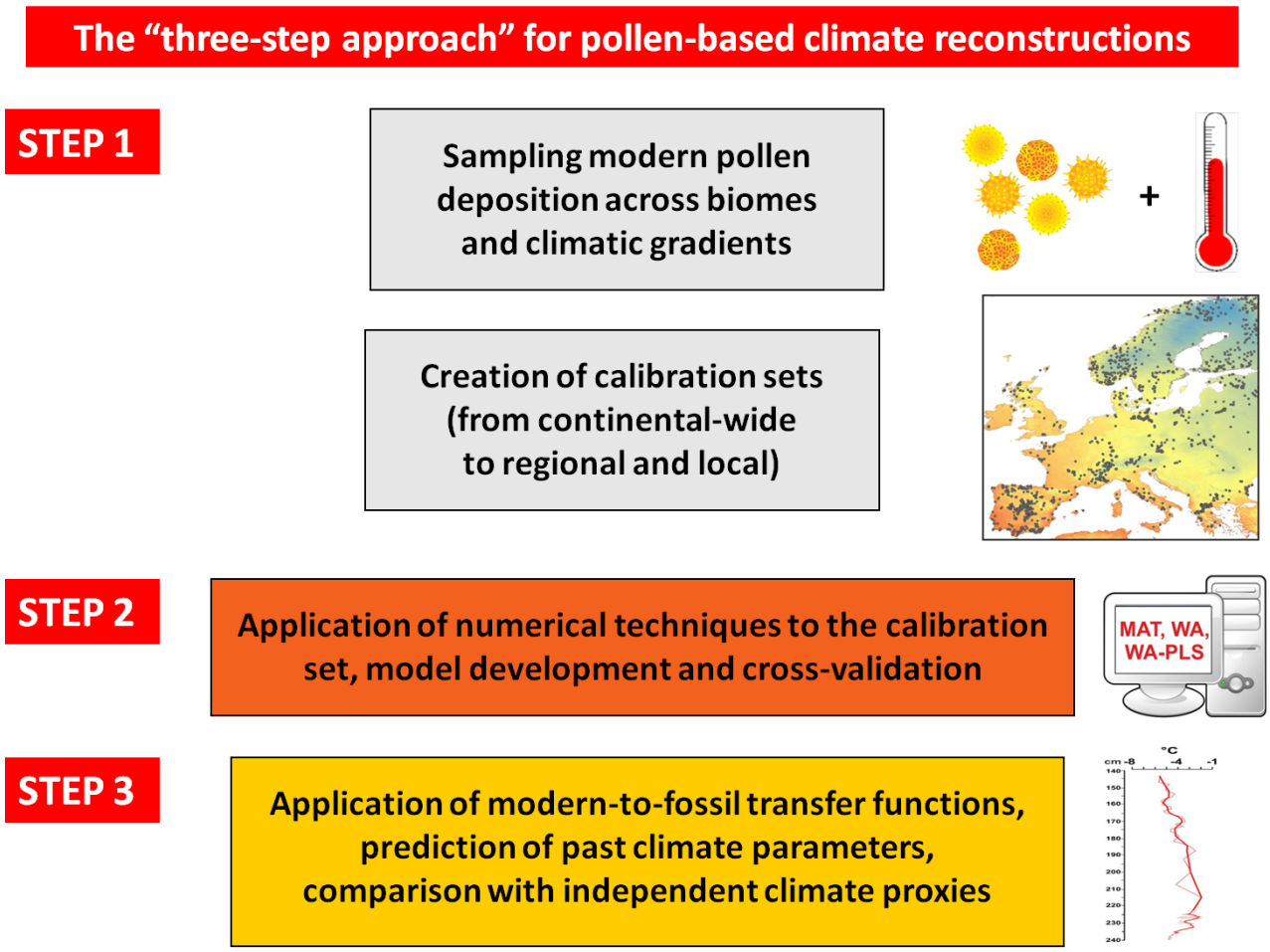

Fig. 2 scheme of the "three-step approach" for pollen-based climate reconstructions based on Juggins and Birks (2012).

1.1. Modern calibration sets (pollen data and related climate variables)

The base for developing pollen-climate models (or transfer functions) is the calibration data-set composed by modern pollen assemblages and associated measured climate variables. The development or selection of the calibration set must be adequate to the environmental context from which the fossil pollen record is obtained, and the goodness of the climate reconstructions depend mostly on the ecological and climate structures and distribution of the modern calibration set. A calibration set is arranged in two matrices (**Fig.1**). The first matrix includes the modern pollen assemblages which indeed represent samples of the modern pollen deposition possibly occurring in different sedimentary environments. Since most of the fossil pollen records allowing a continuous registration of past environmental and climate changes in high-elevation sites are from small lake basin or mires, a focus on the ways to sample the modern pollen deposition in those

environmental contexts is summarized in **Fig. 3**. Moss samples are commonly used as surface samples for local modern pollen deposition. They are assumed to record an average of several years of pollen deposition (Räsänen et al., 2004; Pardoe et al., 2010; Lisitsyna and Hicks, 2014) and can be profitably used as analogues for fossil pollen assemblages because they are easily and quickly obtained and widely distributed (in contrast to core tops). Instead, pollen traps can be espressed both as percentages and Pollen Accumulation Rates (PAR). PAR measurements can be used as a modern reference to estimate past plant population densities buffering the study site (Hicks, 2001; Tinner and Theurillat, 2003; Badino et al., 2018).

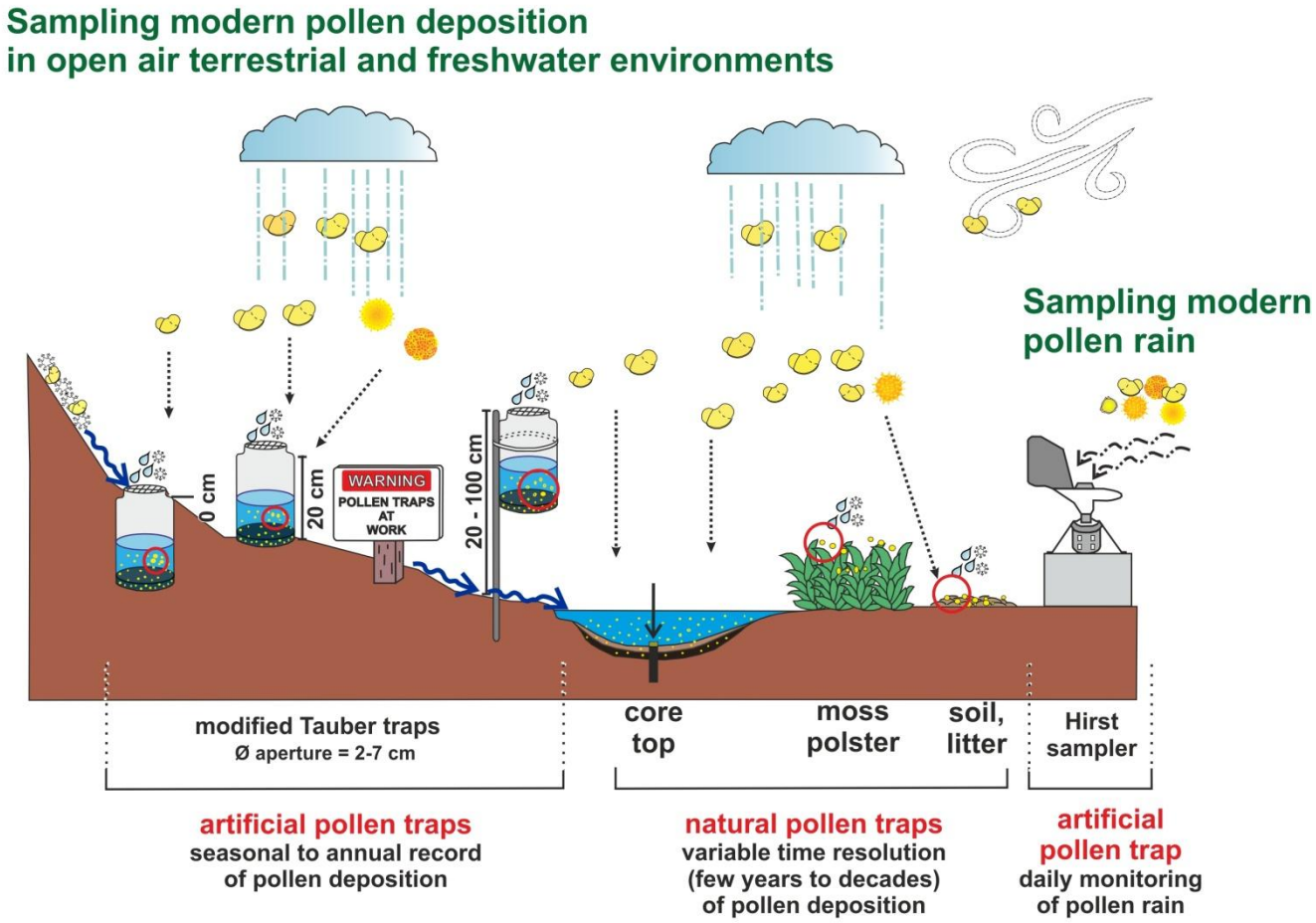

Fig. 3 Sketch illustrating the different ways to sample the modern pollen deposition in open air terrestrial and freshwater environments, such as a small basin in mountain or subalpine area. Processes such as snow and river runoffs are presented with dark blue wavy arrows. At the right edge of the figure, it is also shown how the modern pollen rain (= pollen content in the air masses) is sampled.

During the last years, different pollen-climate databases at continental or regional scales became available thanks to the contribution of the several analysts. As far as Europe is concerned there is the European Modern Pollen Database (EMPD; Davis et al., 2013) which consists of more than 4200 modern pollen samples from the Eurasia regions (**Fig. 4**). The modern pollen assemblages of the EMPD were sampled in the different ways illustrated in **Fig. 3**, excluding pollen traps because of their short time recording (Davis et al., 2013). This continental scale dataset used as source for statistically-based comparisons between fossil and modern pollen spectra. Although the relevance of this dataset is undeniable, several points need to be fixed in order to provide the Eurasian pollen-community with an ecologically sound and complete tool for paleoclimate reconstructions.

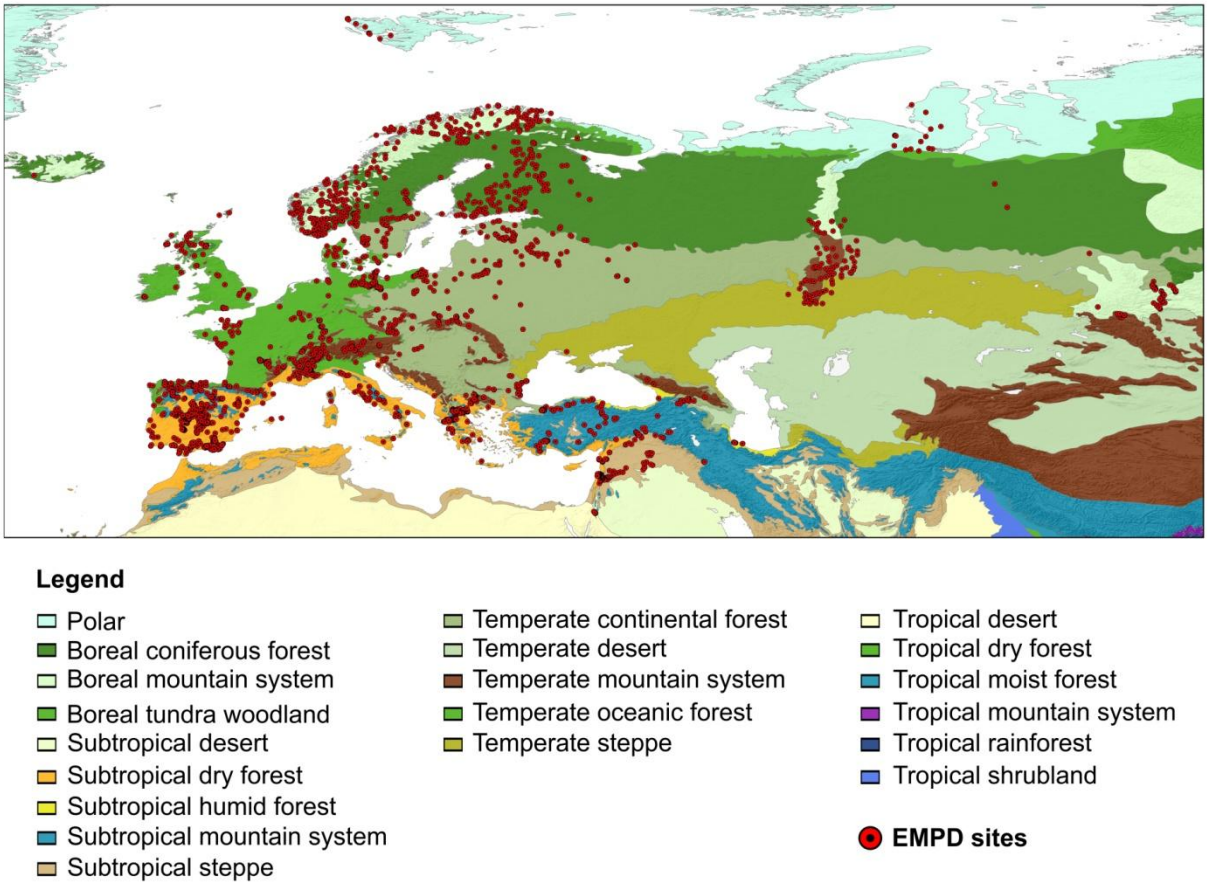

Fig. 4 Geographical extent of the European Modern Pollen Database (EMPD: Davis et al., 2013) excluding north African samples. Red dots indicate the location of the 4270 sampling sites superimposed on the spatial distribution of global ecological zones (GEZ) proposed by the Global Forest Resources Assessments (GRFA) of FAO (http://www.fao.org/forest-resources-assessment/remote-sensing/global-ecological-zones-

gez/en/). Metadata, as well as pollen and climate data associated to each EMPD site shown in the map can be downloaded at http://www.europeanpollendatabase.net/wiki/doku.php?id=empd_download_database.

Global climatological datasets do not differentiate the local scale. This is even more true when remote sites are considered. For this reason, the climate information for each sampling site was reconstructed in a more precise way using the techniques provided in Brunetti et al. (2014), Crespi et al. (2018), and Brunetti et al. (2012), which are appropriate to depict local climates in complex mountain regions. In order to obtain the modern climate variables, the interpolation method is applied to the specific location of each sampling site providing more precise reconstruction than using the available gridded products (e.g. Fick and Hijmans, 2017). In fact, in the alpine region elevation gradients are very strong and within a 1km^2 grid cell elevation can vary up to, or even more than, 500 m that, for a lapse rate of about -0.5°C/100m, can provide with an additional error of more than 1°C in the local temperature estimation.

Multivariate analyses of the calibration sets, both unconstrained (e.g. Detrended Correspondence Analysis, DCA) or constrained (e.g. Canonical Correspondence Analysis, CCA) help exploring the ecological and climate gradients lengths and the relationships between the pollen taxa and the climate variables associated. The analysis of the calibration sets is necessary to know what can and cannot be reconstructed, avoiding to and explicitly address the dangers of reconstructing surrogate and confounded variables (Juggins, 2013).

1.2. Numerical methods to develop pollen-climate models and transfer functions

1.2.1 Method based on similarity: modern analogue technique (MAT)

The Modern Analogue Technique (MAT) (e.g. Guiot, 1990; Juggins and Birks, 2012) is based on the similarity between fossil pollen assemblages and the modern pollen samples (or analogs) available in the calibration set. The resemblance is evaluated based on squared-chord distances, which consist of a prior transformation of pollen percentages by taking the square root in order to reduce the influence of the few relatively abundant taxa in the samples (Brewer et al. 2007). Once the modern analogs have been selected, the

climatic values can be attributed to the fossil sample as a weighted average of the climate of the modern samples. The weights used are the inverse of the chord distance, which allows the most similar analogs to have the greater influence on the climate estimates obtained. The number of analogs is chosen during the process of internal cross-validation. MAT diagnostics allow the recognition of the possible "no-analogue" situations (Juggins and Birks, 2012).

1.2.2. Methods based on taxon-climate response models: Weighted Averaging (WA) and Weighted Average – Partial Least Squares (WA-PLS)

The methods based on the taxa response models to the climate variables imply that species occupy different niches in climate space, and that these niches can be characterized by parameters that describe the niche centre (optima) and niche breadth (tolerance) (e.g. Birks et al. 2010; Juggins and Birks 2012) and can be described as a regression-calibration procedure. ecological response function is the unimodal relationship in which taxon abundance varies across the environmental gradient, with an optimum at a particular value. The technique of weighted averaging (WA) (ter Braak and Looman, 1986) allows these unimodal response functions to be used in climatic reconstructions (Brewer et al. 2007; Juggins and Birks, 2012). The regression step of WA consists of estimating the optima of the selected taxa for a given climatic or environmental parameter by a simple weighted average of the climate values over the modern assemblages where the species is found (Birks et al., 2010; Juggins and Birks, 2012). The regression step consists of the estimation of the past climate parameter by weighted average of the optima estimated for all taxa present in the fossil sample based on their abundances (Brewer et al., 2007). WA-PLS method combines WA method and partial least square (ter Braak and Juggins, 1993) and tries to solve the "edge effect" of which WA suffers, by using residuals correlations. The WAPLS method uses different components (up to 5) calculated as weighted average of the taxa scores in the regression step.

1.2 Aims of the present work

The aims of this PhD research are:

- the development of modern pollen-vegetation-climate elevational transects (**a**,**b**)

- looking for new high-resolution natural archives to obtain proxy data and to reconstruct paleoenvironmental and palaeoclimatic changes during the Holocene (**c**)

- model processing and validation for evaluating pollen-climate relationships thanks to elevational gradients (**a**)

- the application of these models to pollen-stratigraphical data (**c**)

- comparing the results with different proxy-based reconstructions (**c**)

a) We analyze the pollen deposition captured by surface samples (mosses), in relation to July temperature, in two elevational transects in the Western and Central Alps (respectively La Thuile and Upper Brembana Valleys), stretching from the montane to the alpine vegetation belts in order to (1) to derive consistent pollen-climate correlations, both collectively and individually in Alpine regions that have differences in local climates and human pressure; (2) to find potential indicator taxa useful for paleoclimate reconstructions; (3) to estimate the effect of local parameters on the relationships between pollen percentage variations, elevation, and climate and put forward new proposals for reconstruction of fossil sites; (4) to evaluate and quantify the error of pollen-climate models developed for high-elevational site based on a calibration set extracted from the EMPD using as test sets the two elevational transects and finally (5) to integrate the newly-obtained pollen spectra into the European Modern Pollen Database.

This part of the research is presented in **Manuscript 1** (**Elevational transects of modern pollen samples - site specific temperatures as a tool for paleoclimate reconstructions in the Alps**) The Holocene accepted.

b) We investigated modern pollen assemblages-vegetation-climate relationships along an elevational gradient in the Upper Brembana Valley. Here modern pollen assemblages (pollen traps and moss samples), vegetation and climate have been collected at 16 sampling sites placed along an elevational gradient stretching from 1240 m asl to 2390 m asl. The transect has been designed to (1) understand how is the modern vegetation reflected in modern pollen assemblages from pollen traps and moss samples; (2) estimate

the relationships linking modern assemblages, vegetation, elevation and climate; (3) provide a robust modern reference for reliable palaeoenvironmental and quantitative interpretations of past vertical shifts and changes in vegetation composition, as recognized in the pollen records from high-elevation sites.

This part of the research is presented in **Manuscript 2** (**Modern pollen assemblages-vegetation-climate relationships along an elevational transect in the Upper Brembana Valley (Central Alps)**) in preparation for Review of Palaeobotany and Palynology.

c) We reconstructed the vegetation and climate history during the last 10 ka in a high-elevation sedimentary record (Armentarga peat bog, 2345 m asl) on the southern flank of the European Alps. (1) An expanded array of biological proxies, including pollen and other microbiological particles, pollen-slide microcharcoal, sieved charcoal, and biogeochemical proxies was obtained from the study site; (2) we included a specific elevational transect of modern Pollen Accumulation Rates for timberline-forming trees and shrubs (*Alnus viridis, Pinus sylvestris/mugo, Pinus cembra*); (3) we obtained quantitative reconstructions of July temperature and annual precipitation by applying numerical transfer functions built on an extensive pollen-climate calibration set from the European Alps.

This part of the research is presented in **Manuscript 3** (**Holocene vegetation history and quantitative climate reconstructions in a high-elevation oceanic district of the Italian Alps. Evidence for a middle to late Holocene precipitation increase.**) Quaternary Science Reviews 200 (2018) 212-236.

References

Badino, F., Ravazzi, C., Vallè, F., Pini, R., Aceti, E., Brunetti, M., Champvillair, E., Maggi, V., Maspero, F., Perego, R., Orombelli, G., 2018. 8800 years of high-altitude vegetation and climate history at the Rutor Glacier forefield, Italian Alps. Evidence of middle Holocene timberline rise and glacier contraction. Quaternary Science Reviews 185, 41-68.

Beniston, M., Diaz, H.F., Bradley, R.S., 1997. Climatic change at high elevation sites: an overview. Climate Change 36, 233-251.

Birks, H.H., Ammann, B., 2000. Two terrestrial records of rapid climatic change during the glacial–Holocene transition (14,000–9,000 calendar years B.P.) from Europe. PNAS 97, 1390-1394.

Birks, H.J.B., Birks, H.H., 1980. Quaternary Palaeoecology. Edward Arnold, London.

Birks, H.J.B., Heiri, O., Seppä, H., Bjune, A.E., 2010. Strengths and weaknesses of quantitative climate reconstructions based on Late-Quaternary biological proxies. The Open Ecology Journal 3, 68-110.

Birks, H.J.B., Seppä, H., 2004. Pollen-based reconstructions of late-Quaternary climate in Europe e progress, problems, and pitfalls. Acta Palaeobotanica 44, 317-334.

Birks, H.J.B., Heiri, O., Seppä, H., Bjune, A.E., 2010. Strengths and Weaknesses of Quantitative Climate Reconstructions Based on Late-Quaternary. The Open Ecology Journal, 3(1).

Brewer, S., Guiot, J., Barboni, D., 2007. Pollen data as climate proxies, in: Elias SA (Ed) Encyclopedia of quaternary science, (4). Elsevier, New York, pp. 2498-2510.

Brunetti, M., Lentini, G., Maugeri, M., Nanni, T., Simolo, C., Spinoni, J. 2012. Projecting North Eastern Italy temperature and precipitation secular records onto a high-resolution grid. Physics and Chemistry of the Earth 40–41, 9–22.

Brunetti, M., Maugeri, M., Nanni, T., Simolo, C., Spinoni, J., 2014. High-resolution temperature climatology for Italy: interpolation method intercomparison. International Journal of Climatology 34(4), 1278–1296.

Cañellas-Boltà, N., Rull, V., Vigo, J., Mercadé, A., 2009. Modern pollen-vegetation relationships along an altitudinal transect in the central Pyrenees (southwestern Europe). The Holocene 19(8), 1185-1200.

Connor, S.E., Thomas, I., Kvavadze, E.V., Arabuli, G.J., Avakov, G.S., Sagona, A., 2004. A survey of modern pollen and vegetation along an altitudinal transect in southern Georgia, Caucasus region. Review of Palaeobotany and Palynology 129, 229-250.

Connor, S.E., Kvavadze, E.V., 2008. Modelling late Quaternary changes in plant distribution, vegetation and climate using pollen data from Georgia, Caucasus. Journal of Biogeography 36, 529-545.

Crespi, A., Brunetti, M., Lentini, G., Maugeri, M., 2018. 1961–1990 high-resolution monthly precipitation climatologies for Italy. International Journal of Climatology 38, 878–895.

Davis, B.A.S., Zanon, M., Collins, M., Mauri, A., Bakker, J., Barboni, D., Barthelmes, A., Beaudouin, C., Birks, H.J.B., Bjune, A.E., et al., 2013. The European modern pollen database (EMPD) project. Vegetation History and Archaeobotany 22(6), 521-530.

Fall, P.L., 2012. Modern vegetation, pollen and climate relationships on the Mediterranean island of Cyprus. Review of Palaeobotany and Palynology 185, 79-92.

Fick, S.E., Hijmans, R.J., 2017. WorldClim 2: new 1-km spatial resolution climate surfaces for global land areas. International Journal of Climatology 37, 4302–4317.

Guiot, J., 1990. Methodology of the last climatic cycle reconstruction in France from pollen data. Palaeogeography Palaeoclimatoloy Palaeoecology 80(1), 49-69.

Hicks, S., 2001. The use of annual arboreal pollen deposition values for delimiting tree-lines in the landscape and exploring models of pollen dispersal. Review of Palaeobotany and Palynology 117(1-3), 1-29.

Holzhauser, H., Magny, M., Zumbühl, H.J., 2005. Glacier and lake-level variations in west-central Europe over the last 3500 years. The Holocene 15(6), 789-801.

Houghton, J.T., Ding, Y., Griggs, D.J., Noguer, M., van der Linden, P.J., Dai, X., Maskell, K., Johnson, C.A., 2001. IPCC, 2001: Climate Change 2001: The Scientific Basis. Contribution of Working Group I to the Third Assessment Report of the Intergovernmental Panel on Climate Change. Cambridge University Press, Cambridge, United Kingdom and New York, NY, USA, pp. 881.

Juggins, S., 2013. Quantitative reconstructions in palaeolimnology: new paradigm or sick science? Quaternary Science Reviews 64, 20-32.

Juggins, S., Birks, H.J.B., 2012. Quantitative Environmental Reconstructions from Biological Data, Chapter 14, in: Birks, H.J.B., et al. (Eds.), Tracking Environmental Change Using Lake Sediments, Developments in Palaeoenvironmental Research 5. Springer Science+Business Media, pp. 431-483. B.V. 2012.

Le Roy, M., Nicolussi, K., Deline, P., Astrade, L., Edouard, J.L., Miramont, C., Arnaud, F., 2015. Calendar-dated glacier variations in the western European Alps during the Neoglacial: the Mer de Glace record, Mont Blanc Massif. Quaternary Science Reviews 108, 1-22.

Lisitsyna, O.V., Hicks, S., 2014. Estimation of pollen deposition time-span in moss polsters with the aid of annual pollen accumulation values from pollen traps. Grana 53(3), 232–248.

Lu, H., Wu, N.Q., Liu, K.-B., Zhu, L.P., Yang, X.D., Yao, T.D., Wang, L., Li, Q., Liu, X.Q., Shen, C.M., Li, X.Q., Tong, G.B., Jiang, H., 2011. Modern pollen distributions in Qinghai-Tibetan Plateau and the development of transfer functions for reconstructing Holocene environmental changes. Quaternary Science Reviews 30, 947-966.

Magny, M., 2004. Holocene climate variability as reflected by mid-European lake-level fluctuations and its probable impact on prehistoric human settlements. Quaternary International 113, 65-79.

Marcott, S.A., Shakun, J.D., Clark, P.U., Mix, A.C., 2013. A Reconstruction of Regional and Global Temperature for the Past 11,300 Years. Science 339(6124), 1198-1201.

Osborn, T.J., Raper, S.C.B., Briffa, K.R., 2006. Simulated climate change during the last 1,000 years: comparing the ECHO-G general circulation model with the MAGICC simple climate model. Climate Dynamics 27, 185–197.

Pardoe, H.S., Giesecke, T., van der Knaap, W.O., Svitavská-Svobodová, H., Kvavadze, E.V., Panajiotidis, S., Gerasimidis, A., Pidek, I.A., Zimny, M., Święta-Musznicka, J., Latałowa, M., Noryśkiewicz, A.M., Bozilova, E., Tonkov, S., Filipova-Marinova, M.V., van Leeuwen, J.F.N., Kalniņa, L., 2010. Comparing pollen spectra from modified Tauber traps and moss samples: examples from a selection of woodlands across Europe. Vegetation History and Archaeobotany 19, 271–283.

Pepin, N., Bradley, R.S., Diaz, H.F., Baraer, M., Caceres, E.B., Forsythe, N., Fowler, H., Greenwood, G., Hashmi, M.Z., Liu, X.D., Miller, J.R., Ning, L., Ohmura, A., Palazzi, E., Rangwala, I., Schöner, W., Severskiy, I., Shahgedanova, M., Wang, M.B., Williamson, S.N., Yang, D.Q., 2015. Elevation-dependent warming in mountain regions of the world. Nature Climate Change 5(5), 424-430.

Qin, J., Yang, K., Liang, S., Guo, X., 2009. The altitudinal dependence of recent rapid warming over the Tibetan Plateau. Climatic Change 97, 321–327.

Räsänen, S., Hicks, S., Odgaard, B.V., 2004. Pollen deposition in mosses and in a modified ‘Tauber trap’ from Hailuoto, Finland: what exactly do the mosses record? Review of Palaeobotany and Palynology 129, 103–116.

Seppä, H., Birks, H.J.B., 2001. July mean temperature and annual precipitation trends during the Holocene in the Fennoscandian tree-line area: pollen-based climate reconstructions. The Holocene 11, 527-539.

ter Braak, C.J.F., Juggings, S., 1993. Weighted averaging partial least squares regression (WA-PLS): an improved method for reconstructing environmental variables from species assemblages. Hydrobiologia 269/270, 485–502.

ter Braak, C.J.F., Looman, C.W.N., 1986. Weighted averaging, logistic regression and the Gaussian response model. Vegetatio 65, 3–11.

Tinner, W., Theurillat, J.P., 2003. Uppermost limit, extent, and fluctuations of the timberline and treeline ecocline in the Swiss Central Alps during the past 11,500 years. Arctic, Antarctic, and Alpine Research 35(2), 158-169.

Viau, A.E., Ladd, M., Gajewski, K., 2012. The climate of North America during the past 2000 years reconstructed from pollen data. Global and Planetary Change 84-85, 75-83.

Wick, L., 2000. Vegetational response to climatic changes recorded in Swiss Late Glacial lake sediments. Palaeogeography Palaeoclimatoloy Palaeoecology 159, 231–250.

Manuscript 1

(The Holocene accepted)

Elevational transects of modern pollen samples - site specific temperatures as a tool for paleoclimate reconstructions in the Alps

Giulia Furlanetto[1,2], Cesare Ravazzi[2], Federica Badino[2,3], Michele Brunetti[4], Elena Champvillair[1], Valter Maggi[1]

1 University of Milano - Bicocca, Department of Environmental and Earth Sciences, Milano, Italy

2 CNR - Institute for the Dynamics of Environmental Processes (IDPA), Laboratory of Palynology and Palaeoecology, Milano, Italy

3 University of Bologna, Department of Cultural Heritage, Ravenna, Italy

4 CNR- Institute of Atmospheric Sciences and Climate (ISAC), Bologna, Italy

Abstract

The potential of quantitatively reconstructing climate from modern pollen assemblages from high mountain environments has been widely debated but seldom tested. We analyzed the pollen deposition in 53 surface samples (mosses) in relation to July temperature in two elevational transects in the European Alps. Each surface-sample site was assigned climate data derived from the local-scale climate. We compared our results with a larger calibration set extracted from the European Modern Pollen Database (EMPD) and centred on the European Alps. This also was assigned local climate data. The main calibration set (234 pollen samples) had *Alnus* harmonized at genus level; in contrast, a second set was selected (174) that retained the taxonomic resolution of *Alnus viridis*, which is one of the main climate indicators in the timberline ecotone. The overall and individual pollen responses to July temperature were inferred by canonical correspondence analysis (CCA), generalized linear regression (eHOF), and weighted averaging (WA). Quantitative climate reconstructions for each sample-site of the two

elevational transects were obtained using transfer functions, ie weighted averaging (WA) and weighted averaging partial least squares (WA-PLS) regressions. In each calibration set around 30% of the pollen taxa show a relationship with July temperature through monotonic or unimodal functions. The best transfer function obtained has a good statistical performance, with a determination coefficient (r^2) of 0.74. We propose new calibration procedures formulated to include the full climate space of the modelled taxa, as well as to account for uphill pollen transport in the high mountains and for human activity.

Keywords Modern pollen samples, elevational transects, calibration, transfer functions, climate, Alps

1. Introduction

The interpretation of past pollen records solely in terms of the known biology of the taxa involved is puzzling, because of the uncertainties related to pollen production, dispersal, and preservation, as well as the location and extent of the pollen source and the size and features of the catchment area (Birks and Birks, 1980; Faegri et al., 1989; Moore et al., 1991; Traverse, 1994; Tyson, 1995). Climate and human activities trigger further variability, both in time and space, in vegetation and pollen production. Calibration studies allow to investigate problems related to these factors by providing a straightforward correlation between the pollen signal and vegetation and environment (Birks, 1995, 1998; Jackson and Williams, 2004). Studies on modern pollen assemblages have been developed in different parts of the world, but mostly in Europe (e.g. Hicks, 1992, 1993; Hjelle 1997; van der Knaap et al., 2001; Bunting, 2002, 2003; Nielsen and Odgaard, 2005; Court-Picon et al., 2005, 2006; Mazier et al., 2006; Finsinger et al., 2007; Räsänen et al., 2007). However, there are few studies of modern pollen rain in mountain environments of southern European countries (Court-Picon et al., 2005, 2006; Cañellas-Boltà et al., 2009; Ortu et al., 2010).

Montane vegetation is particularly sensitive to climate changes (Birks and Ammann, 2000). The strong elevational climatic gradient that characterises mountain areas results in a steep ecological gradient, with several ecotones occurring in a small area. This situation is an amplification of the global climate signal (Beniston et al., 1997). Vegetation responses

to climatic changes are more pronounced at higher elevations than in lowland areas (Birks and Ammann, 2000). Recent climate variations have had a particularly strong effect on montane ecosystems (Houghton et al., 2001). Being able to assess the impacts of climatic fluctuations on the past biodiversity in mountain regions will help in choosing suitable management strategies in the near future. Montane pollen sequences through time are ideal archives for the study of past climate changes.

The use of continental-scale datasets as modern analogues for mountain environments is problematic because the accuracy of paleoclimatic estimations is influenced by the following factors: (1) the “multiple-analogue” problem, where the fossil assemblage is similar to several modern samples originating from areas with different climatic conditions (Birks, 1998; Finsinger et al., 2007); this issue is particularly important when a small number of pollen taxa of high taxonomic rank, for example at family level, is used in the calibration (Birks, 1998); (2) the scarcity of surface samples from the subalpine and alpine belts in the available data sets; (3) the effects of wind-driven uphill transport of tree pollen into the subalpine and alpine zones; (4) the great dependence of relative pollen percentages in spectra from elevated sites on the local physiographic conditions (slopes, exposure to dominant winds) (Ortu et al., 2006, 2010); (5) the multiple analysts variability, since samples are commonly analyzed by a number of different analysts, and (6) taxonomic consistency in the identifications may become an issue when quantitative paleoenvironmental reconstructions are implemented (Birks, 1998; Finsinger et al., 2007). In the European Alps, further complicating factors affecting paleoclimate reconstruction from pollen data are: (7) the large variations in local climates (from oceanic external ranges to continental inner districts) which may affect the realized elevational niche of the dominant vegetation species; (8) human modification of some of the main components of pristine vegetation and their response curve to climate parameters, since the onset of Neolithic in some valley floors (Colombaroli et al., 2013) and later at high elevations (Pini et al., 2017).

A new methodology for mountains was proposed by Ortu et al. (2006). This includes more local studies along elevational gradients orientated to facilitate the interpretation of past vertical shifts and changes in vegetation composition, in order to infer past climate changes and land-use changes (Ortu et al., 2006). Investigations by Court-Picon et al. (2005, 2006), Cañellas-Boltà et al. (2009), Ortu et al. (2010) in the Alps, and Rull (2006) in the Andes are examples of this procedure.

In this paper, we analyze the pollen deposition captured by surface samples (mosses), in relation to July temperature, in two elevational transects in the Western and Central Alps (respectively La Thuile and Upper Brembana Valleys), stretching from the montane to the alpine vegetation belts. Results were compared with a larger calibration set from the European Alps extracted from the EMPD (European Modern Pollen Database, Davis et al., 2013).

The general aim is to improve paleoecological and paleoclimate interpretation based on pollen. Specific objectives are: (1) to derive consistent pollen-climate correlations, both collectively and individually in Alpine regions that have differences in local climates and human pressure; (2) to find potential indicator taxa useful for paleoclimate reconstructions; (3) to estimate the effect of local parameters on the relationships between pollen percentage variations, elevation, and climate and put forward new proposals for reconstruction of fossil sites; (4) to evaluate and quantify the error of pollen-climate models based on a calibration set extracted from the EMPD using as test sets the two elevational transects and finally (5) to integrate the newly-obtained pollen spectra into a new version of the European Modern Pollen Database (EMPD Stage 2).

1.1. The elevational ecological gradients in the European Alps

The European Alps display the largest climatic and ecological gradients of the western Eurasian continent (Ozenda, 2002). Coastal sclerophyll evergreen woodlands of Mediterranean climates (0 to 400 m asl, locally 1700 m asl), are followed uphill by a variety of mixed broad-leaved deciduous forests of warm to cool and wet temperate conditions (500 to 1700 m asl). Boreal conifer forests (the so-called subalpine belt; Ellenberg, 1988) develop between 1500 and 2500 m asl, thinning in the timberline ecotone (Holtmeyer, 2009). Here a steep climate-controlled gradient is mirrored by sharp changes in tree taxa and forest canopy density. Timberline species (*Pinus cembra, Alnus viridis, Picea abies, Larix decidua*) show the strongest ecological responses to climate. The upper limit of the timberline ecotone borders on to grasslands and glaciers. The composition of the timberline ecotone reflects continentality (Ellenberg, 1988) with major regional differences in the elevations of thresholds and the abundance of indicator species. Over the last 5000 years, human impact has led to the expansion of pastures, resulting in the lowering or even dismantling of the timberline ecotone, with large differences from site to site. The

effects of human activities on Alpine timberline structure are reflected in pollen assemblages by an array of anthropogenic indicators. Most of them are not introduced plants but are apophytes which occurred in pristine vegetation in low abundances.

1.2. Modern vegetation-climate relationships of the studied elevational transects

Considering regional variations of the continentality gradient and prehistoric to historic human pressure, we developed our climate-pollen test sets in two climatically different areas of the Alps. The Upper Brembana Valley elevational transect (**Fig. 1c**) was chosen in an oceanic, outer district of the Central Alpine chain strongly modified by mining and pastoralists. The La Thuile elevational transect (**Fig. 1b**) is in a continental inner valley of the Western Alps, weakly impacted by humans at least in its upper belts (Badino et al., 2018).

Here we present the overall elevational ecosystem structure in relation to climate. Details on single sites are given in **Supplementary Table S1a,b**.

The La Thuile Valley elevational transect extends from 900 to 2670 m asl. The natural wet mixed forest of *Abies alba, Alnus incana,* and *Tilia cordata* of valley floor is modified by human settlements. Mowed meadows are dominated by Poaceae and Compositae and are rich in synanthropic plants (e.g. *Plantago lanceolata*). Coppicing and reduction of shade at the forest-meadow edges favour the development of *Corylus avellana* communities up to 1400 m asl. Instrumental TJuly is between 17 and 15°C. A dark spruce belt (*Picea abies*) between 1400 and 1900 m asl is interrupted by avalanche tracks, stream beds, and wet cliffs hosting extrazonal *Alnus incana* thickets. In the spruce-dominated belt *Alnus viridis* occurs as a sporadic shrub, in contrast to the wetter and snowy districts of the Central Alps, where it displays a much wider response curve downhill to 1200 m (see below, Upper Brembana Valley elevational transect). Between 1900 and 2100 m the subalpine conifer forest includes both spruce, Swiss stone pine (*Pinus cembra*), and larch (*Larix decidua*), with a TJuly between 12° and 10.7 °C. The timberline ecotone is formed by *Pinus cembra* and *Alnus viridis* shrubs, with an open forest limit at 2360 m asl at 8.9°C TJuly; an upper tree limit runs at 2455 m at 8.1°C TJuly (Badino et al., 2018). Dwarf Ericaceae and juniper heaths (*Vaccinium*, *Loiseleuria,* and *Juniperus nana*) develop in the timberline ecotone but do not extend much further above the treeline. Alpine short-grass pastures (graminoid-dominated, i.e. *Nardus stricta*),

xerophytic tussock grasslands (graminoid-dominated, i.e. *Festuca* spp) and snow-bed, partly woody tundra (*Salix herbacea* and Fabaceae) forms a continuous belt up to 2800 m asl, but such a continuous herbaceous carpet is missing in the area glaciated during the Little Ice Age. Indeed, the Rutor Glacier foreland (**Fig. 1b**) at 2100-3000 m asl is still occupied by pioneer cushion plants and ruderal communities (Caccianiga et al., 2002), rich in moderate-pollen producing Fabaceae and Compositae species. The Equilibrium Line Elevation of the Rutor Glacier provides an independent climate proxy for calibration (2850 m asl in 1991 AD, Villa et al., 2007).

The Upper Brembana Valley elevational transect extends along the uppermost section of a typical pre-alpine valley open to moist southern winds orographically forced uphill, between 1100 m and the headwalls at 2500-2700 m asl (**Fig. 1c**). A belt of deciduous broad-leaved forest, largely fragmented by clearings, mowed meadows, and human settlements, extends between 1100 and 1400 m on sunny aspects. Here the dominant taxa are *Acer pseudoplatanus* and *Corylus avellana*. Chestnut and walnut trees (*Castanea sativa* and *Juglans regia*) have been planted up to 1100 m asl on sunny slopes, ie up to a Tjuly limit of about 16°C. A dark coniferous forest (*Picea abies, Abies alba, Larix decidua*) occurs only on shaded slopes, while wide areas in the subalpine belt (1400 to 2200 m asl) are covered by low pollen-producing larch forest. The canopy density of the larch forest is usually low, allowing the massive development of *Alnus viridis* understory thickets. Open larch forests with reduced understory allow local winds forced uphill to reach the ground. The timberline is very complex in this district, due to the disruption of the subalpine forest by pastoralism and mining, especially on sunny slopes. The open forest upper limit is formed by larch at 2140 m asl. The uppermost limit of *Alnus viridis* dwarf forest is at 2240 m. Larch treeline reaches up 2220 m at about 10.1°C TJuly and 1870 mm annual rainfall. At dry edaphic sites, isolated stands of mountain dwarf pine (*Pinus mugo*) form part of the timberline structure at 1800-2000 m asl. The crown cover of *Pinus cembra* is negligible. The wide development of graminoid-dominated alpine pastures and of xerophytic grasslands at timberline elevations and up to 2600 m is driven primarily by oceanic climates and by human impact in the last 4 ka (Furlanetto et al., 2018). The Equilibrium Line Elevation under current conditions of climate warming exceeds the tops of main peaks; it was about 2600 m in 1994 AD (Caccianiga et al., 1994).

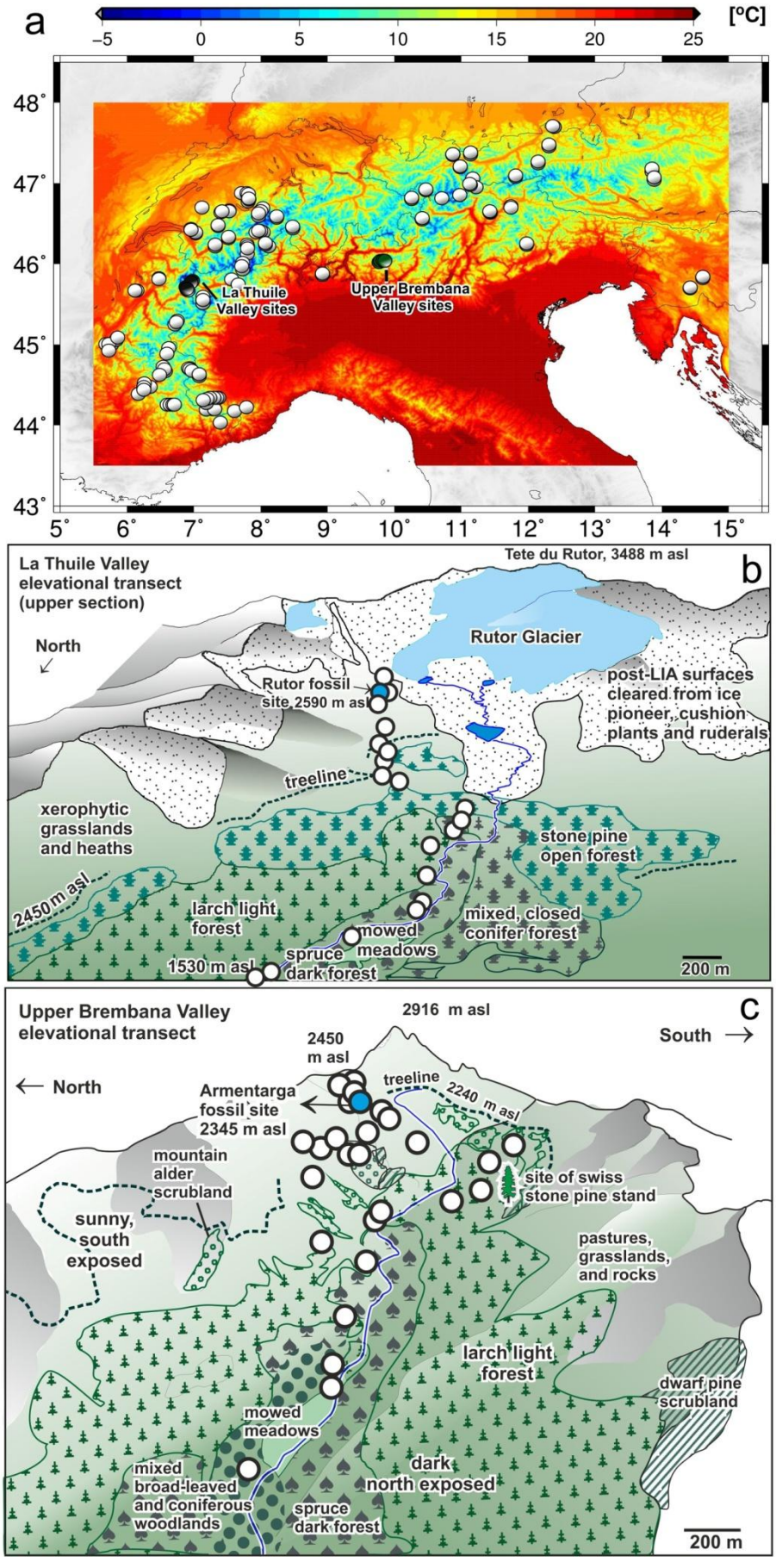
a
[°C]
−5
0
5
10
15
20
25
48°
47°
46°
45°
44°
43°
5°
6°
7°
8°
9°
10°
11°
12°
13°
14°
15°
La Thuile Valley sites
Upper Brembana Valley sites
La Thuile Valley elevational transect (upper section)
Tete du Rutor, 3488 m asl
b
North
Rutor Glacier
Rutor fossil site 2590 m asl
post-LIA surfaces cleared from ice pioneer, cushion plants and ruderals
treeline
xerophytic grasslands and heaths
stone pine open forest
2450 m asl
larch light forest
mixed, closed conifer forest
mowed meadows
spruce dark forest
1530 m asl
200 m
Upper Brembana Valley elevational transect
2916 m asl
c
South
2450 m asl
North
treeline
2240 m asl
Armentarga fossil site 2345 m asl
mountain alder scrubland
site of swiss stone pine stand
sunny, south exposed
pastures, grasslands, and rocks
larch light forest
dwarf pine scrubland
mowed meadows
dark north exposed
mixed broad-leaved and coniferous woodlands
spruce dark forest
200 m

Fig. 1 (a) Map of July climatogy (1961-1990) with EMPD sites and elevational transects sites plotted; (b and c) Sketches summarizing the altitudinal arrangement of the main ecosystems in the two study areas: La Thuile elevational transect (b) and Upper Brembana Valley elevational transect (c). The panorama views were drawn on Google Earth images. The scale bar (down on the right) refers to the foreground frame. The linear distance covered by elevational transect (b) is 6 km, by elevational transect (c) is 7 km.

2. Methods

2.1. Pollen data and other microfossils

A total of 27 sites from La Thuile Valley (from the lowermost TRS 1 to the uppermost TRS 27) and 26 sites from the Upper Brembana Valley (L 1 to L 17) were used for this study (**Fig. 1a,b,c**) and compared with 234 modern samples from the European Alps (EMPD sites, **Fig. 1a**). In each site, three moss polsters were collected within a circular area of 1.8 m radius (ca 10 m^2) and mixed into one sample. Mosses were sampled down to, but not including, the mineral soil. Moss samples were used because of their known suitability as pollen traps and their frequent occurrence in the two elevational transects. Furthermore, their pollen content is an average pollen deposition of several years (Räsänen et al., 2004; Pardoe et al., 2010; Lisitsyna and Hicks, 2014), more similar to sediments, so they can be profitably used as analogues for fossil pollen assemblages. Samples were processed following standard methods at the Laboratory of Palynology and Palaeoecology of CNR-IDPA in Milano, after adding *Lycopodium* tablets for pollen and pollen-slide microcharcoal concentration estimations (Stockmarr, 1971). A minimum of 600 pollen grains was counted. Aquatics, spores and non-pollen palynomorphs were excluded from the pollen sum. Identification was carried out at x400, x630 and x1000 magnifications under a Leica DM-LB light microscope. Pollen identification followed Moore et al. (1991), Punt and Blackmore (1976-2009), Reille (1992-1998), Beug (2004) and the CNR pollen reference collection. Pollen of *Pinus cembra* is separated from *Pinus sylvestris/mugo* type on the following criteria: (1) presence of verrucae on the ventral surface of the grain body, (2) shape of sacci, more elongated than in *Pinus sylvestris*, (3) occurrence of a slightly undulating outer layer on the proximal surface of the grain body towards the sacci. Size classes of Poaceae pollen were distinguished by measuring grain and pore + annulus diameters. Grains larger than 47 µm and pore + annulus diameter > 11 µm have been referred to cereals (*Avena-Triticum* group and *Secale cereale*). Microbiological particles were named after van Geel (1978) and van Geel et al. (1981). Pollen-slide microcharcoal

particles were recorded under a light microscope at 400x. Black, completely opaque and angular fragments (Clark, 1988) were identified as charcoal, distinguished in two size classes (10–50 μm and 50–250 μm length). Pollen diagrams were drawn using TILIA 2.0.41 (Grimm, 2015) and Corel Draw X7 for further graphic elaborations.

2.2. Climate data

Global climatological datasets do not differentiate the local scale. This is even more true when remote sites are considered. For this reason, we reconstructed the climate information for each sampling site in a more precise way using the techniques provided in Brunetti et al. (2014), Crespi et al. (2018), and Brunetti et al. (2012), which are appropriate to depict local climates in complex mountain regions. In the present work the interpolation method is applied to the specific location of each sampling site providing more precise reconstruction than using the available gridded products (e.g. Fick and Hijmans, 2017). In fact, in the alpine region elevation gradients are very strong and within a 1km^2 grid cell elevation can vary up to, or even more than, 500 m that, for a lapse rate of about -0.5°C/100m, can provide with an additional error of more than 1°C in the local temperature estimation.

Specifically, site-specific temperature and precipitation series, covering the 1951-2015 period, were constructed for each sampling site in the two elevational transects and of the 234 alpine sites selected from the EMPD-European Modern Pollen Database (Davis et al., 2013), by means of the anomaly method (New et al., 2000; Mitchell and Jones, 2005) as described in Brunetti et al. (2012). The climate values, characterized by remarkable spatial gradients, were constructed by evaluating the local dependence of the meteorological variable on elevation (Brunetti et al., 2014; Crespi et al., 2018), utilising a high spatial density network of stations (even if with a limited temporal coverage); Climate normals over a given reference period were constructed (i.e. climatologies) together with the anomalies (i.e. the departures from the climatological means). Anomalies (linked to climate variability) are characterized by a higher spatial coherence and a more simple interpolation technique and a low spatial density of stations is enough, but long temporal coverage and accurate homogenization (i.e. the procedure that removes the non-climatic signals introduced by stations and instruments relocation, changes in measurement practices and

so on) are mandatory. Finally, the two fields were superimposed to get temperature and precipitation monthly series in absolute values for each sampling site.

From these monthly series, mean temperature of the warmest month (July), summer temperature and the total annual precipitation over the 1951–2000 period were calculated for the sampled sites in the two elevational transects and for the 234 alpine sites selected from the EMPD mean July and summer temperature.

2.3. Numerical analyses

Numerical analysis includes a set of interdependent standard methods commonly used in pollen calibration studies aimed at: (1) assessing the overall dependence of each pollen assemblage on July temperature, (2) determining the individual response of taxa to July temperature by estimating their optimum and tolerance (3) testing the significance of these responses and (4) obtaining climate reconstructions for each site of the two elevational transects and comparing the results with instrumental data. Prior to all numerical analysis, the modern pollen percentage values were square root-transformed to stabilize the variance and to minimize the “signal to noise” ratio in the data (Prentice, 1980). The overall dependence of modern pollen assemblages on July and summer temperature was inferred through canonical correspondence analysis (CCA) (ter Braak, 1986) for each elevational transect and calibration set. The statistical significance of the relationship between modern pollen assemblage and climate was assessed by an ANOVA permutation test (999 unrestricted permutations). Only the mean temperature of the warmest month (July) was chosen because it explains more variance in both the test and the calibration sets (see **Table 1**). Finsinger et al. (2007) have previously shown that modern pollen assemblages in the Alpine area respond mostly to July temperatures. All computations were made using R 3.2.3 version (R core team 2013) and vegan package (version 2.4-0; Oksanen et al., 2016). The weighted average (WA) method, which implies Gaussian species response curves is used to calculate optima and tolerances in order to summarize the range of variation in the taxa responses to July temperature (ter Braak and Looman, 1986). The WA optima and tolerances were estimated with the rioja package (Juggins, 2017). The statistical significance of these individual responses was tested using the Extended Huisman-Olff-Fresco fitting method, which considers a set of hierarchical models in a generalized linear modelling framework (Huisman et al., 1993; Jansen and Oksanen,

2013) using eHOF package (Jansen and Oksanen, 2017). These models are designed as I (flat response, no optima), II (monotonic, optima is at the gradient extremes), III (plateau, there is an optimum range), IV (symmetric unimodal, single point optima), V (skewed unimodal, single point optima), VI (symmetric bimodal, two optima) and VII (skewed bimodal, two optima). The minimum number of occurrences of a taxon to be considered for eHOF analysis was 10. Quantitative climate reconstructions for each test set were obtained using a calibration set of 234 modern pollen samples from the EMPD (Alpine 234 - **Fig. 1a**). The modern pollen data were harmonised with the EMPD by combining *Alnus* and *Pinus* pollen types to genus. A second calibration set (Alpine 170), composed of 170 sites, was obtained from the EMPD by retaining only those samples where *Alnus viridis* and *Alnus glutinosa/incana* pollen types were distinguished, thus retaining the potential indicator value of these taxa. Pollen-climate transfer functions were derived from weighted averaging (WA) and weighted averaging partial least squares (WA-PLS) regressions (ter Braak and Juggings, 1993; ter Braak, 1995). All taxa within the pollen sum were included in the calibration analysis to increase the statistical performance (Birks, 1994), percentages were square-root transformed and rare taxa were downweighted. The analysis was carried out in the R environment using the rioja package (Juggins, 2017). The optimal number of components was selected on the basis of the lower root mean square error of prediction (RMSEP), low maximum bias, high determination coefficient (r^2) between observed and predicted values of July temperature, and the smallest number of "useful" components (Birks, 1998) and randomization t-test (van der Voet, 1994).

3. Results

3.1. Pollen assemblages

A total of 108 pollen and spore types was recorded in samples from the La Thuile Valley elevational transect: 42 selected taxa are shown in the simplified percentage diagram (**Fig. 2**). In general, the lower elevation samples (TRS 1–TRS 5) are dominated by *Pinus sylvestris/mugo* type, *Picea*, *Betula,* and *Corylus*. Poaceae are abundant, whereas most of the other herb types and shrubs are poorly represented. The dung spore *Sporormiella* reaches its maximum value in the site TRS 5 (1,7%) (**Fig. 2a**). Pollen-slide microcharcoal concentration shows the highest values in these samples (up to 1000 particles/cm^3). At

higher elevations, especially above 2450 m asl, herbs become more abundant, while tree pollen decreases.

From TRS 6 to TRS 15 the pollen diagram is characterized by the dominance of *Picea* and the relatively high abundance of *Pinus cembra*, *Pinus sylvestris/mugo* (dark coniferous forest) and *Larix*. *Alnus glutinosa* type is the commonest deciduous tree. Besides grasses, other herb pollen types are Umbelliferae, Caryophyllaceae, Ranunculaceae, *Aster* type and Cichorioideae. High AP (arboreal pollen) values up to 70-80% correspond to closed coniferous forests (see **Supplementary Table S1**). The TRS 7 site is still related to dark coniferous forests but has a lower AP value. This is in agreement with its open structure (dry meadows surrounded by coniferous forests) and the abundance of mowed meadows/grazed areas (*Plantago lanceolata* up to 8%). Samples TRS 16–TRS 21 (2143–2348 m asl) are above the closed forest and encompass the timberline ecotone. Compared with the lower belts, *Picea* shows lower percentages, *Pinus cembra* maintains steady percentages, while higher values are recorded of *Pinus sylvestis/mugo* type. An increase in both abundance and diversity of herb and shrub pollen is also evident. Among shrubs, *Alnus viridis* records its highest values (up to 8%), together with relatively high abundances of *Vaccinium* and *Juniperus*. A general increase in percentages of Poaceae, Cichorioideae, Caryophyllaceae, Brassicaceae, Cyperaceae and dung spores (Sordariaceae and *Sporormiella*) is also recorded. The apophyte taxon *Rumex acetosa* type reaches its maximum value in the site TRS 20 (9,9%) which is well above its pristine baseline found in a nearby fossil site (Badino et al., 2018). Above the treeline (TRS 22–TRS 27) the modern pollen spectra are characterized by the high abundance of Poaceae and a general decrease of tree pollen. Besides grasses, other herb pollen types are Cichorioideae, Brassicaceae, *Aster* type, *Plantago alpina* type, *Phyteuma*, *Geum* type and Saxifragaceae. The only pollen grain of *Cerealia* identified in the whole transect was found in site TRS 25. Low pollen percentages of cultivated trees (*Juglans, Castanea* and *Olea*) occur in most samples of the elevational transect.

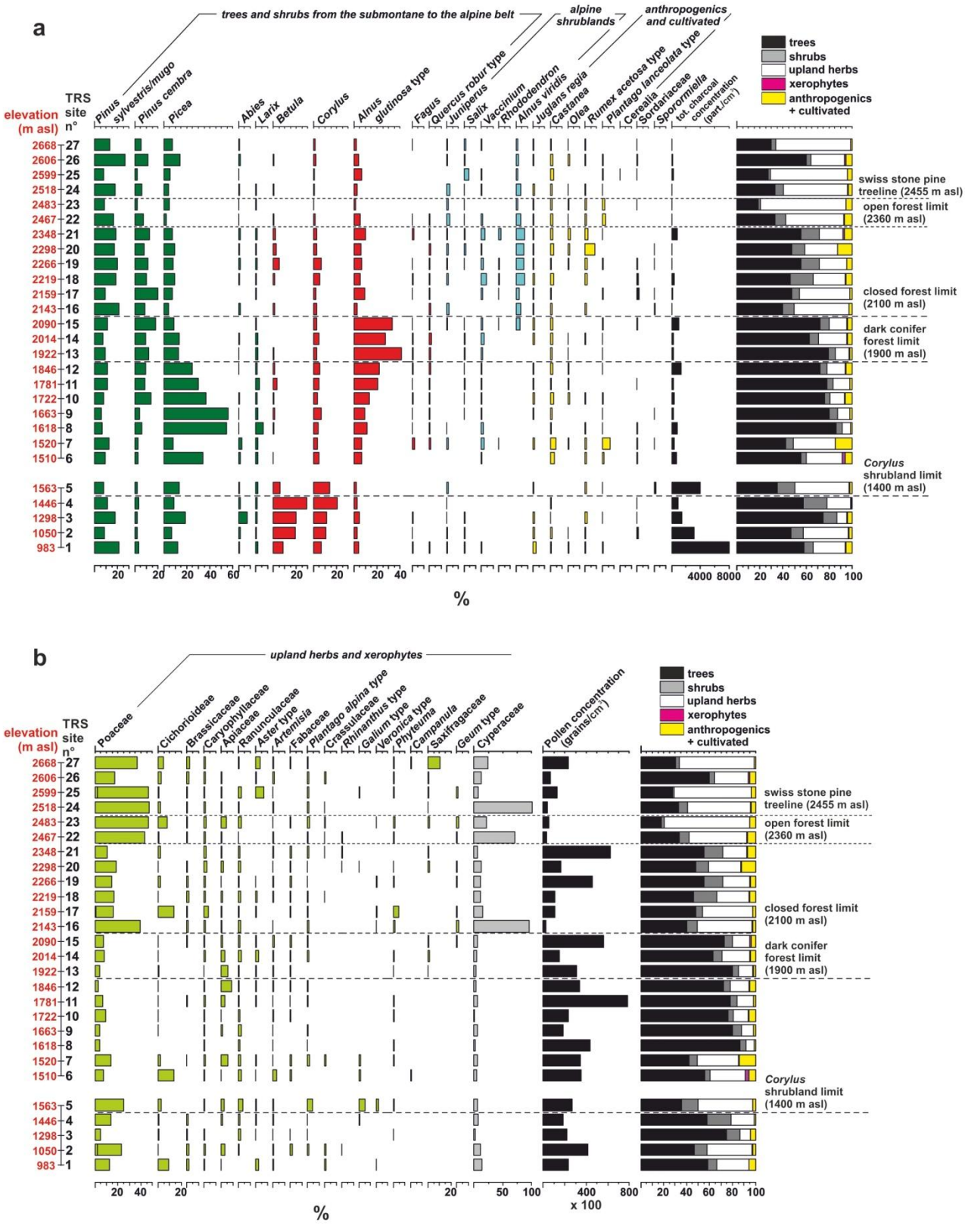

Fig. 2 (a) and (b) Percent diagram of the La Thuile Valley elevational transect showing selected pollen taxa and main vegetation zones. The summary diagram is shown twice to allow comparison.

A total of 149 pollen and spore types was recorded in samples from the Upper Brembana Valley elevational transect: 57 of them are shown in the simplified percentage diagram (**Fig. 3**). In contrast to the La Thuile Valley elevational transect, the pollen spectra are dominated by upland herbs and shrubs. In the lower part of the transect (L 1–L 7) the dominant taxa are *Corylus*, *Ostrya* type, *Fraxinus excelsior* type, *Pinus sylvestris/mugo,* and *Larix*. *Alnus viridis* reaches high percentages (20–40%) in samples L 3 and L 4, taken next to streams. Among herbs Poaceae are the most abundant. Other herb pollen types are Brassicaceae, Apiaceae (e.g. *Bupleurum*), *Galium* type, *Plantago coronopus* type, and Rosaceae. Manuring of either mowed or grazed areas (L 2, L 5 and L 6) is indicated by the presence of dung spores *Sporormiella* and *Podospora* (**Fig. 3a**). From L 8 to L 13 the pollen diagram is characterized by the dominance of trees and shrubs (e.g. *Pinus sylvestris/mugo*, *Picea*, *Corylus*, *Alnus viridis,* and *Castanea*); Poaceae increase in samples L 11 and L 13. Site L 10, like the lower sites L 3 and L 4, is located in an avalanche corridor/stream and is characterized by *Alnus viridis* and upland herbs (e.g. Poaceae, Apiaceae, Brassicaceae, Scrophulariaceae). The samples L 12–L 20 are located in the upper subalpine belt with Ericaceae moorlands (*Vaccinium*, *Rhododendron,* and *Juniperus*) and *Alnus viridis* thickets with *Larix decidua* individuals; the treeline is located at 2200 m. These samples are dominated by *Alnus viridis*, *Pinus sylvestris/mugo,* and Poaceae. Above 2100 m asl the wind-driven uphill transport of pollen from the lower belts (e.g. *Betula*, *Corylus*, *Ostrya* type, *Fagus,* and *Carpinus betulus*) shows increased percentages. Samples L 14–L 24 are located in an extensive pasture, reflected by the high percentages of Poaceae and dung spores (Sordariaceae, *Sporormiella,* and *Podospora*) and of taxa transported uphill from the lower belts (e.g. *Pinus sylvestris/mugo*, *Picea*, *Betula*, *Corylus*, *Ostrya* type, *Fagus,* and *Castanea*). The apophyte taxon *Rumex acetosa* type occurs in most samples of the elevational transect, but its percentages are even lower than in its pristine baseline shown in a nearby fossil site (see **Fig. 6** in Furlanetto et al., 2018). In contrast, *Plantago lanceolata* type, *Ranunculus acris* type, and *Urtica* have higher percentages than in the pre-anthropic (pre-Neolithic) section of the fossil record (Furlanetto et al., 2018). Average pre-anthropic values can be used as "pristine baseline values" for site interpretation procedures (see discussion (4.3.)).

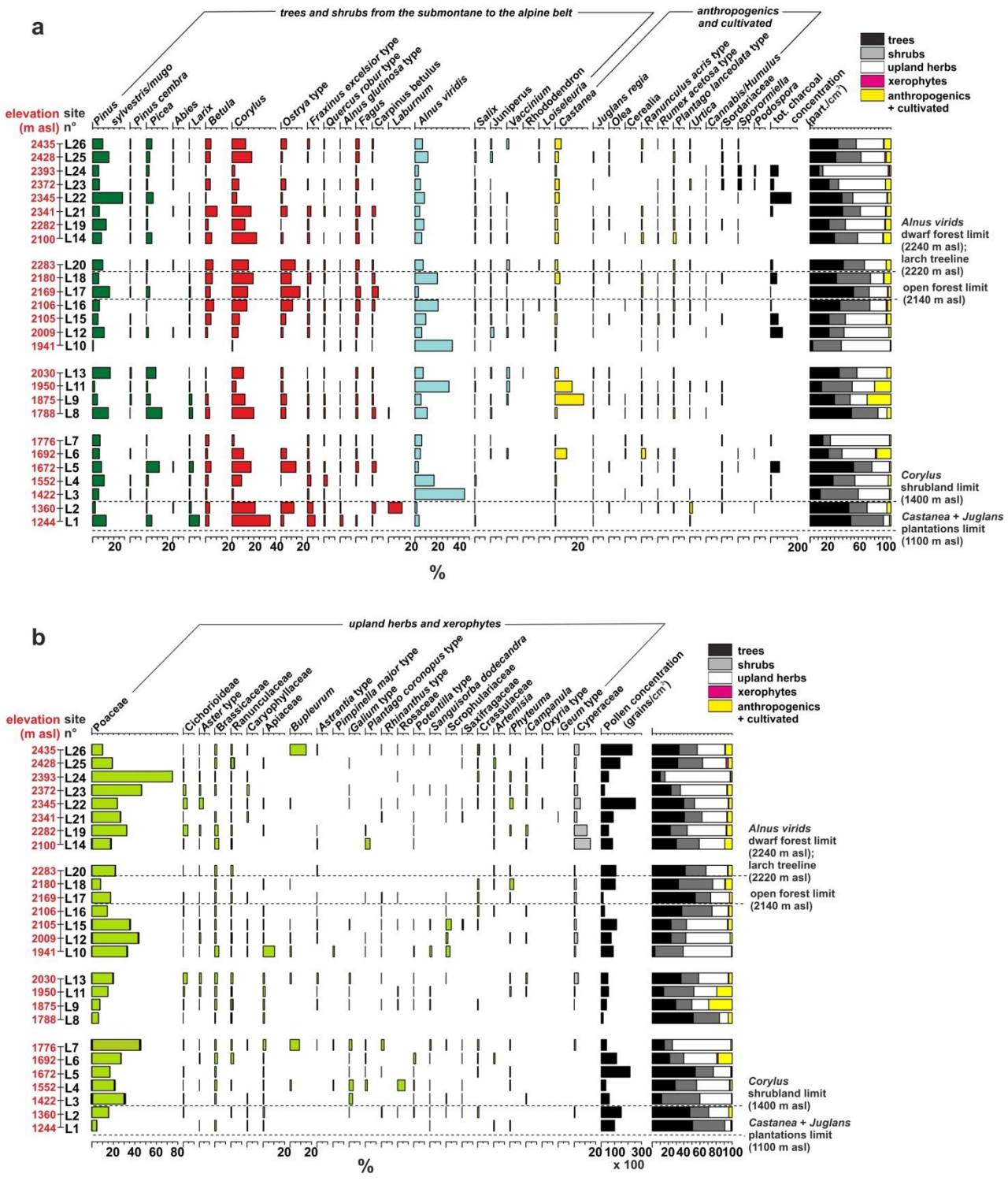

Fig. 3 (a) and (b) Percent diagram of the Upper Brembana Valley elevational transect showing selected pollen taxa and main vegetation zones. The summary diagram is shown twice to allow comparison.

3.2. Numerical analysis and calibration

Results of canonical correspondence analysis (CCA), performed using July and summer temperatures as the sole constraining variables, for each elevational transect and for the two calibration sets are shown in **Table 1**. All the datasets show significant correlations with July and summer temperature (p = 0.001, after 999 unrestricted permutations).

	Tjuly			Tsumm		
La Thuile Valley	CCA1	CA 1	λ1/λ2	CCA1	CA 1	λ1/λ2
Eigenvalue	0.09601	0.1072	0.89562	0.0956	0.1072	0.89179
Percentage variance (%)	12.328	13.76		12.28	13.76	
P-value	0.001 ***			0.001 ***		
Upper Brembana Valley	CCA1	CA 1		CCA1	CA 1	
Eigenvalue	0.07313	0.1207	0.60588	0.07088	0.1207	0.58724
Percentage variance (%)	8.238	13.6		7.984	13.6	
P-value	0.001 ***			0.001 ***		
234 EMPD sites	CCA1	CA 1		CCA1	CA 1	
Eigenvalue	0.08348	0.15151	0.55099	0.08254	0.15194	0.54324
Percentage variance (%)	4.751	8.623		4.698	8.648	
P-value	0.001 ***			0.001 ***		
170 EMPD sites	CCA1	CA 1		CCA1	CA 1	
Eigenvalue	0.1043	0.1718	0.6071	0.10342	0.1723	0.60023
Percentage variance (%)	6.32	10.41		6.268	10.44	
P-value	0.001 ***			0.001 ***		

Table 1 Results of canonical correspondence analysis (CCA) for each elevational transect and calibration set; all taxa in the pollen sum were sqrt transformed and downweighted.

WA optimum and tolerance values of the pollen taxa included in the analysis of the two elevational transects are shown in **Supplementary Tables 3-4**. In the La Thuile Valley elevational transect 71.3% of the taxa have their optimum below the closed forest limit, while 16.3% have optima between the closed forest and the treeline and 12.5% have optima above the treeline. eHOF fitting shows that 26% of the pollen taxa show a relationship with July temperature (**Supplementary Table 3**), 2 being monotonic (*Corylus*

and Saxifragaceae), 3 symmetric unimodal (*Pinus cembra, Larix,* and *Alnus viridis*) and 4 skewed bimodal (*Betula*, *Picea*, *Alnus glutinosa* type, and Poaceae < 37 µm). In the Upper Brembana Valley elevational transect 90.5% of the taxa found have their optimum below the treeline, while 9.5% have optima above the treeline. eHOF fitting shows that 13% of the pollen taxa have a significant relationship with July temperature (Supplementary Table 4), 2 being monotonic (*Larix* and *Fraxinus excelsior* type), 1 symmetric unimodal (Apiaceae) and 4 skewed bimodal (*Alnus viridis*, *Corylus*, *Castanea sativa*, Poaceae < 37 µm).

In both elevational transects, the following high pollen producers are related to TJuly: *Pinus cembra, Alnus viridis, Corylus, Betula, Picea, Alnus glutinosa, Poaceae, Castanea sativa, Fraxinus excelsior*.

High pollen producing trees growing in lower mountain belts (e.g. *Ostrya* and *Corylus*) show lower optima and larger tolerances in the Upper Brembana Valley elevational transect, as a consequence of a more efficient uphill wind dispersal of pollen to higher elevations thus having lower temperatures (see **Table 2**). Major differences also occur in the realized altitudinal niche of the dominant subalpine species *Alnus viridis* (**Table 2** and **Fig. 4**), which has an estimated optimum of 11.3 °C in the Upper Brembana Valley and of 9.0 °C in the La Thuile Valley. This offset is related to variations in local climates (from oceanic external ranges to continental inner districts). Intriguingly, both wind dispersal and regional differences in ecological responses affect climate reconstructions based on pollen deposition.

In the alpine calibration set of 234 modern pollen samples (Alpine 234) eHOF fitting shows that 27.9% of the pollen taxa have a significant relationship with July temperature (**Supplementary Table S5**), 20 being monotonic (e.g. *Alnus* undifferentiated, *Artemisia*, *Betula*, *Carpinus*, *Corylus*, *Fraxinus* undifferentiated, *Quercus*, *Salix*, *Tilia*), 3 plateau (*Plantago maritima/alpina* type, *Plantago* type, and *Potentilla* type), 5 symmetric unimodal (*Acer* type, *Larix*, *Ostrya* type, *Rhododendron,* and *Vaccinium*), 1 skewed unimodal (*Pinus* undifferentiated) and 5 skewed bimodal (*Abies*, *Castanea sativa*, *Fagus*, Poaceae, and *Picea*). In the alpine calibration set of 170 modern pollen samples (Alpine 170) eHOF fitting shows that 27.1% of the pollen taxa have a significant relationship with July temperature (**Supplementary Table S6**), 14 being monotonic (e.g. *Alnus glutinosa* type, *Artemisia*, *Carpinus*, *Juniperus*, *Quercus*, *Salix*), 2 plateau (*Alnus viridis* and *Plantago maritima/alpina* type), 5 symmetric unimodal (*Acer*, *Larix*, *Pinus* undifferentiated,

Rhododendron, and *Vaccinium*) and 6 skewed bimodal (*Abies*, *Castanea sativa*, *Corylus*, *Fraxinus* undifferentiated, Poaceae, and *Picea*). The performance of the different transfer functions obtained using the two calibration sets (Alpine 234 and Alpine 170) is shown in **Table 3**.

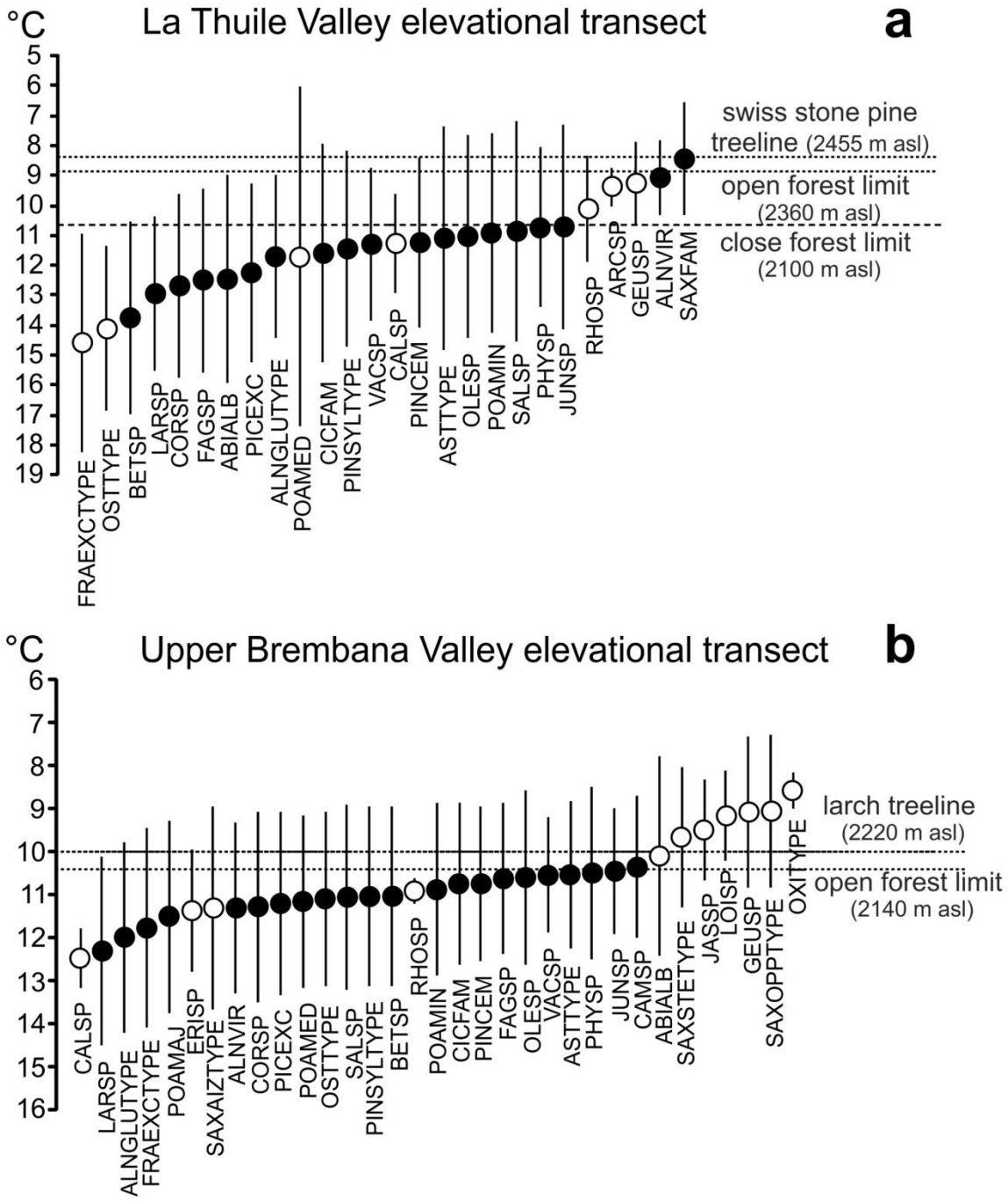

Fig. 4 Thermal arrangement of weighted averaging (WA) optima (circles) and tolerances (error bars) for selected taxa included in the pollen sum; (a) La Thuile Valley, (b) Brembana Valley. Solid circles indicate taxa with 10 or more occurrences. See Tables S2, S3 for taxa codes.

Taxon	La Thuile valley optima	Upper Brembana valley optima	Alpine 234 optima	Alpine 170 optima	La Thuile valley tolerances	Upper Brembana valley tolerances	Alpine 234 tolerances	Alpine 170 tolerances
Alnus glutinosa type	11.7	12.0		12.8	2.7	2.2		3.6
Alnus viridis	9.0	11.3		11.2	1.3	2.0		2.9
Alnus undifferentiated			12.1				3.5	
Betula	13.7	11.0	13.2	12.9	3.2	2.1	3.7	3.7
Castanea sativa	11.4	10.9	14.1	14.1	3.1	1.8	4.3	4.3
Corylus	12.6	11.3	13.8	13.4	3.1	2.2	3.7	3.7
Fagus	12.5	10.6	13.7	13.6	3.1	1.7	3.5	3.4
Fraxinus excelsior type	14.5	11.8			3.6	2.3		
Fraxinus ornus type		11.3				1.9		
Fraxinus			13.8	14.0			3.6	3.6
Ostrya type	14.1	11.1	15.5	11.4	2.8	2.0	4.3	4.1
Pinus cembra	11.2	10.7			2.8	1.8		
Pinus sylvestris/mugo type	11.4	11.0			3.3	2.1		
Pinus undifferentiated			12.7	11.8			3.6	3.3
Apiaceae	11.8	12.0	13.5	13.3	2.9	1.6	3.6	3.5
Asteroideae			12.4	11.8			3.5	3.3
Aster type	11.1	11.5			3.7	1.7		
Cichorioideae	11.6	10.7	11.7	11.2	3.6	1.9	3.4	3.1
Poaceae < 37 µm	10.9	10.9			3.4	2.0		
Poaceae 37-47 µm	11.7	11.1			5.7	2.0		
Poaceae > 47 µm anulus < 11 µm		11.5				2.2		
Poaceae			12.0	11.6			3.6	3.4

Table 2 July mean temperature weighted average optima (°C) and tolerances (°C) of selected taxa from the two elevational transects and the two calibration sets.

234 EMPD sites

Components	**RMSEP**	r^2	Max. bias
1	2.2088	0.6306	3.1562
2	2.0887	0.6696	3.5779
3	2.0847	0.6741	3.4699

170 EMPD sites

Components	**RMSEP**	r^2	Max. bias
1	1.9003	0.7070	2.9008
2	1.7906	0.7396	3.3712
3	1.8488	0.7253	2.7594

Table 3 Summary performance statistics of the five first components of the WA-PLS transfer function for each calibration set (234 and 170 EMPD sites). RMSEP, root mean square error of prediction (°C), r^2, coefficient of determination between predicted and modern July mean temperature (°C). These statistics are all based on leave-one-out cross-validation.

The best transfer function for both calibration sets was a two-component WA-PLS model (**Table 3**). The observed and predicted July temperature (r^2 = 0.74; RMSEP = 1.79°C) show higher correlations in the second calibration set (Alpine 170). The results of the WA and WA-PLS reconstructions for each elevational transects compared to instrumental data are shown in **Fig. 5**.

In the La Thuile Valley elevational transect Poaceae were removed from the pollen sum of sites TRS 1–7 in the mountain belt. The site TRS 26 from rocky slopes with low percentages of vegetation cover was not considered for climate reconstructions. In the Upper Brembana Valley elevational transect sites L 10 and L 21 were removed before climate reconstructions. The correlation between pollen-inferred climate reconstructions and instrumental data gives the opportunity to determine which model better reconstructs the climate of the two study areas. In the La Thuile Valley the WA (234 sites) reconstruction shows the highest correlation to instrumental data (r^2 = 0.74) while in the Upper Brembana Valley the WA-PLS two components (234 sites) has the highest correlation (r^2 = 0.66). Two principal biases remain: (1) the underestimated values of July temperature from the lower elevation sites especially in La Thuile Valley elevational transect and (2) the overestimated values of July temperature of the sites above the closed forest.

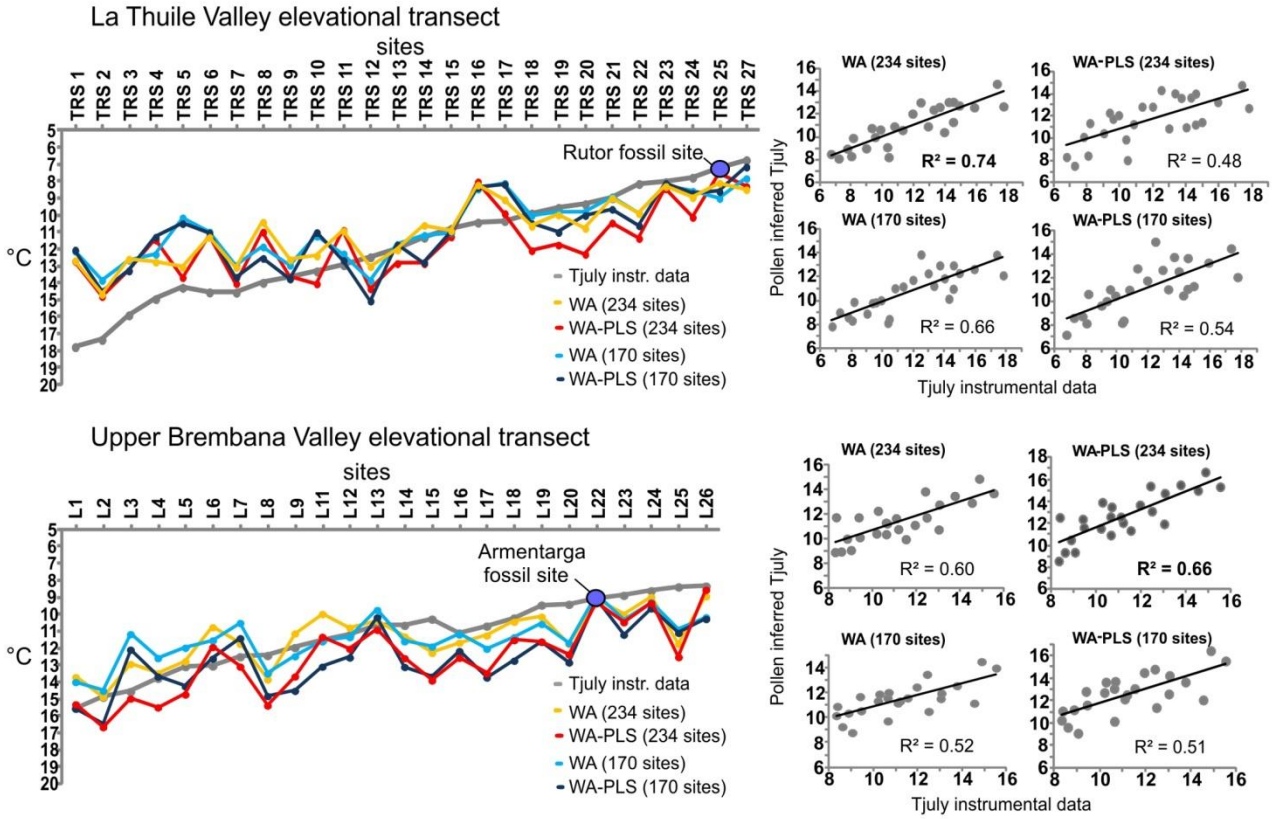

Fig. 5 On the left comparison between pollen inferred climate reconstructions using the WA and WA-PLS approach and instrumental data; on the right correlation graphs for each elevational transect.

4. Discussion: The potential of elevational transects as a tool for paleoclimate reconstructions in Alpine mountains

Numerical analyses show that the two calibration sets (Alpine 234 and Alpine 170) have significant correlations with July temperature (see **Table 1**) and that their model performances are similar to other studies of the same nature based on pollen and other biological proxies (**Table 3**; r^2 = 0.74–0.67; RMSEP = 1.79–2.08°C), although model performances obtained in different calibration sets are not directly comparable because of their calibration set dependency. A representative literature review of papers using the same methods on pollen data shows that correlations (r^2) range from 0.33 to 0.89, whereas root mean square errors of prediction (RMSEP) are between 0.89°C and 2.57°C, which represents 8.8–22.2% of the total temperature gradient (Lotter et al., 2000; Rosén et

al., 2001; Seppä and Birks, 2001; Bigler et al., 2002; Seppä et al., 2004). Furthermore, our prediction accuracies are improved by estimating a local temperature lapse rate, which in these elevational transects ranges from 0.56 ^{o}C per 100 m elevation in the mountain belt to 0.77 ^{o}C per 100 m elevation above the tree limit.

The correlation between pollen-inferred climate reconstructions obtained for each site of the two elevational transects and instrumental data determines which reconstruction model better estimates the climate of the two study areas. In the La Thuile Valley the WA (234 sites) reconstruction shows the highest correlation with instrumental data (r^2 = 0.74) while in the Upper Brembana Valley the WA-PLS two components (234 sites) has the highest correlation (r^2 = 0.66) (see **Fig. 5**).

In this study there is a large spatial variability in the elevational structure of the vegetation and climate gradients, and also in the contribution of uphill pollen transport. We have shown that all these factors affect the individual ecological responses of indicator species. This is not surprising: our experiment takes place in the European Alps, where the largest climate and ecological gradients of the western Eurasian continent occur (see discussion (4.1.)). Below, we also discuss the site-specific calibration (accounting for topography, uphill pollen transport and local human impact, see discussions 2-3) and the calibration for the alpine region (i.e. further expansion of calibration sets specifically designed to account for the response curves of climatic-sensitive pollen taxa).

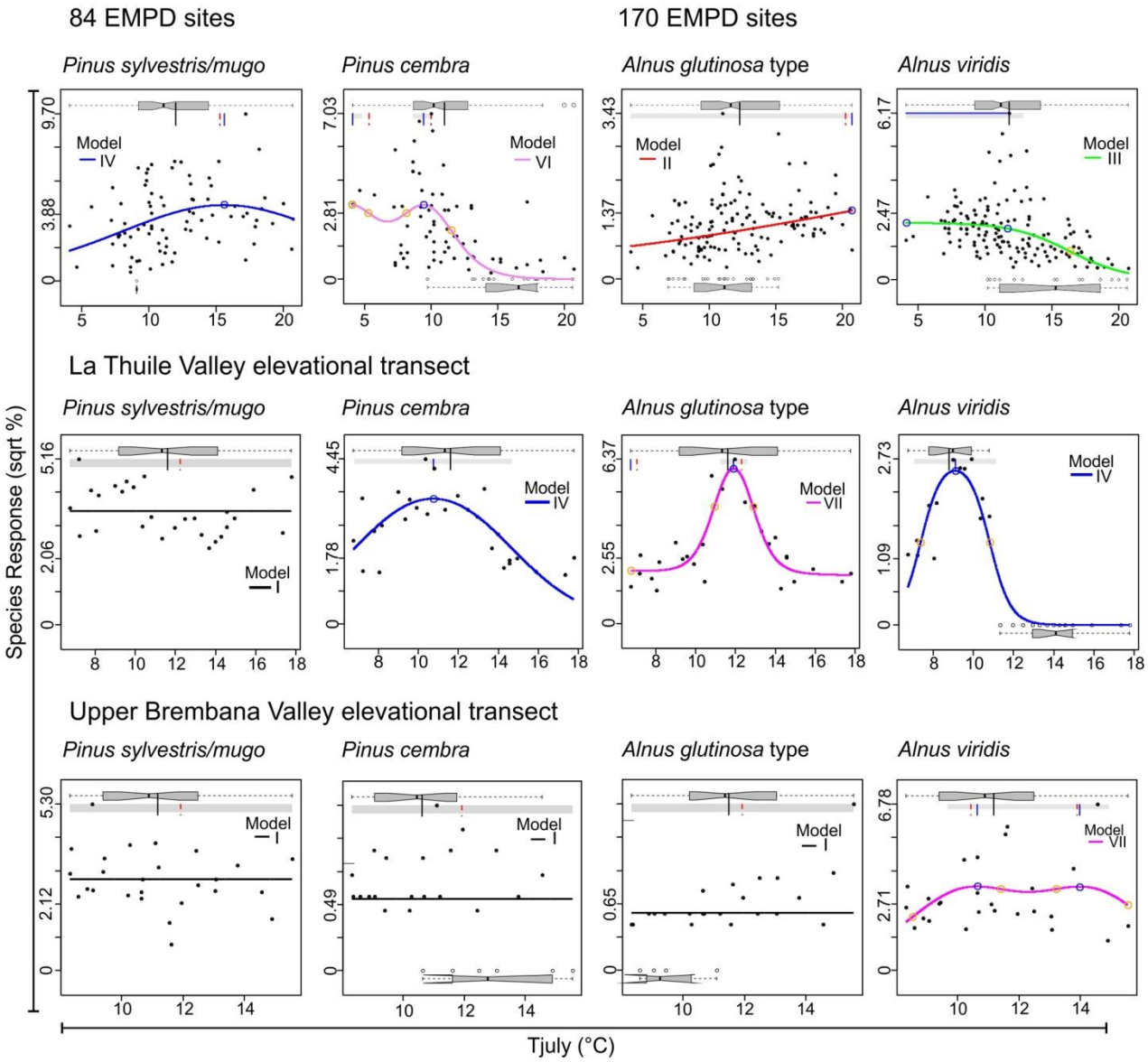

Fig. 6 Diagrams showing the simplest statistically significant response model for *Pinus sylvestris*/mugo, *Pinus cembra*, *Alnus glutinosa* type and *Alnus viridis* from the EMPD sites and the two elevational transects in relation to July temperature as assessed by a hierarchical set of taxon response models within the framework of generalized linear modelling. Legend is shown in Fig. 7.

4.1. Indicator species response to local climates and optima estimation

Taxonomic resolution of pollen analysis often reaches only the family or genus level, thus the original climatic value of many important indicator species is lost. For example *Rhododendron* and *Vaccinium* show a symmetric unimodal response to July temperature in both Alpine 234 (optima respectively 9.7°C and 10.0°C) and Alpine 170 (optima respectively 9.8°C and 9.9°C) and differ from the family Ericaceae that have a higher optima (11.9°C in the Alpine 234 and 11.5°C in the Alpine 170) and a wider tolerance (see **Supplementary Tables S5-6**). Diagrams showing the simplest statistically significant response models for *Pinus sylvestris/mugo*, *Pinus cembra*, *Alnus glutinosa* type, and *Alnus viridis* from the EMPD sites in which they were distinguished (84 EMPD sites for *Pinus sylvestris/mugo* and *Pinus cembra* and 170 EMPD sites for *Alnus viridis* and *Alnus glutinosa/incana* type) in relation to July temperature, as assessed by eHOF models (**Fig. 6**), depict notable differences in the optima. In the two elevational transects there are major differences in the range of the dominant subalpine vegetation species *Alnus viridis* (**Table 2** and **Fig. 6**). It has an estimated WA optimum of 9.0°C (tolerance 1.3°C) in the La Thuile Valley and of 11.3°C (tolerance 2.0°C) in the Upper Brembana Valley. In the Alpine 170 calibration set (**Table 2**) *Alnus viridis* has an estimated WA optimum of 11.2 °C. Therefore, *Alnus viridis* shows a unimodal response model in the La Thuile Valley elevational transect and a skewed bimodal response in the Upper Brembana Valley elevational transect (**Fig. 6**). This offset is related to variations in local climates (from oceanic external ranges to continental inner districts). *Alnus viridis* vegetation needs a continuous water supply during the growing season, enhanced by high annual snowfall rate and good soil water balance (Richard, 1968, 1969; Mauri and Caudullo, 2016). In Alpine oceanic climates, its ecological range expands downstream especially along avalanche corridors but also on northern slopes, due to a general increase in soil moisture, and thus optima are shifted towards higher temperatures. The identification of climatic-sensitive pollen taxa, especially for middle and subalpine elevation forest ecosystems (e.g. *Picea, Abies, Pinus sylvestis/mugo*, *Pinus cembra,* and *Alnus viridis*), must be pursued as far as the taxonomical standards of the calibration set will allow.

Differences between pollen-inferred climate reconstructions and instrumental data (**Fig. 5**, sites TRS 1–6 and L 1–7) might be due to an uneven sampling of the gradient in the calibration sets which affects the WA optima estimations (ter Braak and Looman, 1986; Telford and Birks, 2011) especially for species of the mountain belt with a skewed bimodal

distribution (e.g. *Betula*, *Castanea sativa*, *Corylus*, *Fagus,* and *Fraxinus*). Notably differences occur between the optima shown in the eHOF models (**Fig. 7**) and the optima estimated by WA (**Table 2**). A solution to this problem could be enlarging the calibration set to obtain an evenly sampled gradient to provide a better estimate of the species optima from the under-sampled part of the gradient. Furthermore, using the optima provided by eHOF models (Jansen and Oksanen, 2013) could improve the climate reconstruction.

4.2. How can we adjust for the effects of uphill pollen transport?

Topographical variation and the resulting variation in temperature with elevation have been found to be a complicating factor in many pollen-based climate reconstructions. Pollen transport by wind from low-elevation sites to the treeless high-elevation sites may result in reconstructed temperatures that are too high at high-elevation sites. High-elevation lakes and peat bogs may receive non-local pollen from lower-elevation belts ("extralocal component") as well as from vegetation at greater distances ("regional component").

The uphill transport of pollen by wind to subalpine and alpine zones was first recorded in the European Alps (Markgraf. 1980; David, 1997; Frei, 1997; Brugiapaglia et al., 1998; Ortu, 2002) and has also been found in the mountains of Africa, South America, New Guinea (Flenley, 1973), Tibet (Shen et al., 2006; Lu et al., 2011), New Zealand (Moar, 1970; Randall, 1990) as well in the Canary Islands (De Nascimento et al., 2015). Markgraf (1980) showed that, in a steep valley-slope system of Alpine type, the proportion of pollen dispersal from local uphill winds in daytime decreases with increasing elevation in favor of regional (medium-distance) dispersal. This high-elevation dispersal component relies significantly on pollen washout by rain, which cleans the atmosphere of suspended pollen (Markgraf, 1980).

In oceanic areas such as Upper Brembana Valley, pollen taxa from broad-leaved tree species 10 to 20 km distant from the lowermost site in the elevational transect (e.g. *Castanea*, and *Ostrya* type) are washed out by orographic rain or transported by winds and occur in high proportions (**Fig. 3**). Between 2100 and 2300 m asl (L 16–20) (**Fig. 5**), in the Upper Brembana Valley the WA-PLS overestimate July temperatures. The WAPLS corrects the skewed bimodal distribution of the species of the mountain belt transported uphill by wind (e.g. *Betula*, *Castanea sativa*, *Corylus*, *Fagus,* and *Fraxinus,* **Table 2** and

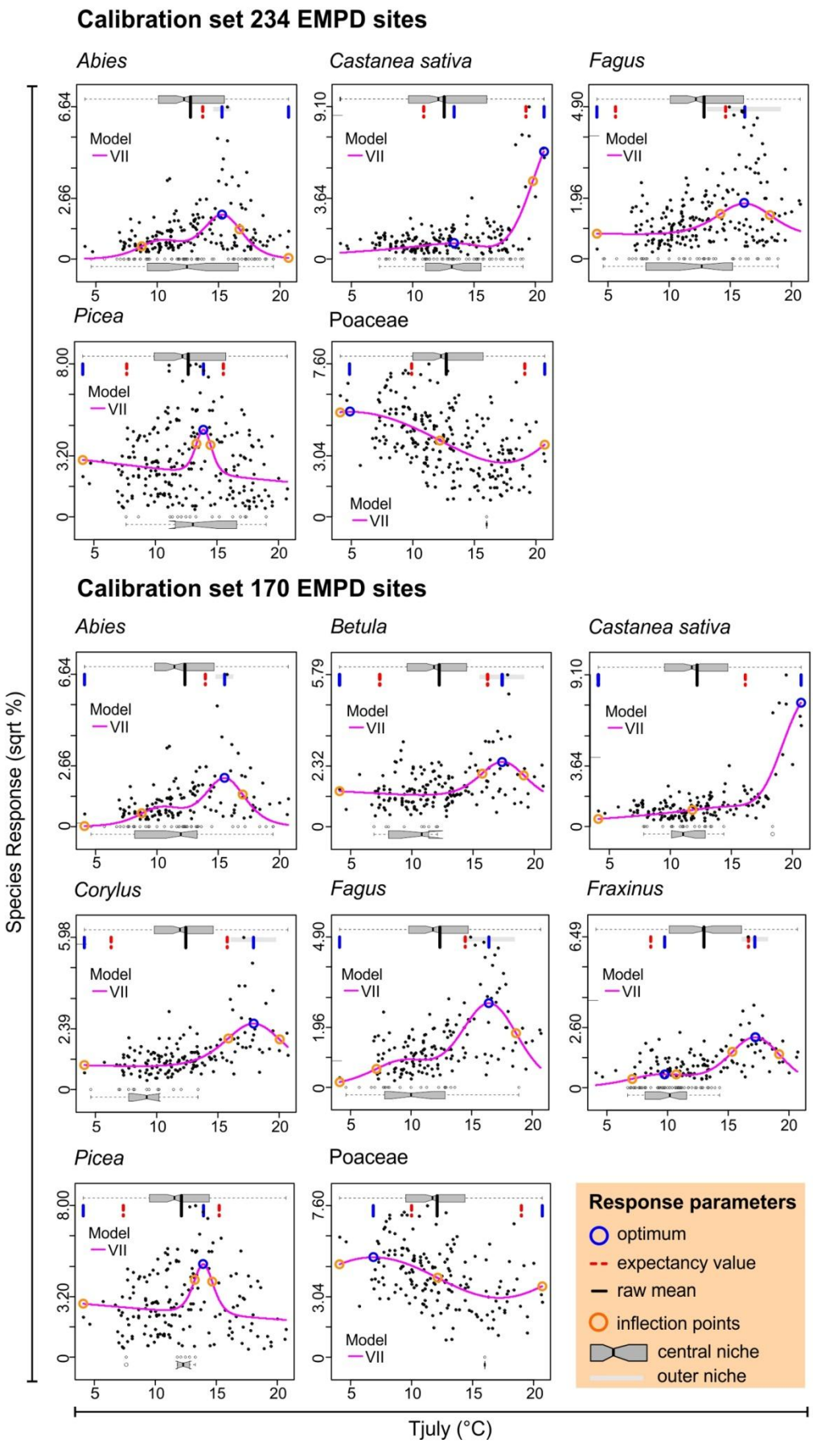
Calibration set 234 EMPD sites
Abies
Castanea sativa
Fagus
Picea
Poaceae
Calibration set 170 EMPD sites
Abies
Betula
Castanea sativa
Corylus
Fagus
Fraxinus
Picea
Poaceae
Model
VII
Species Response (sqrt %)
Tjuly (°C)
Response parameters
optimum
expectancy value
raw mean
inflection points
central niche
outer niche

Figure 7 Diagrams showing the simplest statistically significant response model for pollen types from the two calibration sets (234 EMPD sites and 170 EMPD sites) in relation to July temperature as assessed by a hierarchical set of taxon response models within the framework of generalized linear modelling.

Fig. 7) but reconstructs higher temperatures than by using WA method as shown in the comparison with instrumental data (**Fig. 5**). The Upper Brembana Valley elevational transect represents currently one extreme wet orographic climate of the Alps, where washout of regionally-transported pollen is enhanced by the extraordinary high values of annual precipitation (see **Supplementary Table S1b**). The Alpine calibration sets (both Alpine 234 and Alpine 170) only partly account for species response in wet elevational ecosystems and climates, given that oceanic-type timberlines from the Eastern Alps are still poorly represented in the EMPD (**Fig. 1a**).

Treeless elevational ecosystems fail to provide an array of indicator types, due to the reduced abundance of anemophilous pollen producers, and to the fact that high-elevation mountain meadows taxa are poorly resolved in pollen taxonomy of calibration sets (e.g. Poaceae and Asteraceae). Calibration sets for elevational belts need further work in order to better detect the climate signal from pollen assemblages of local treeless vegetation. This requires expanding the number of high-elevational sites, adding new herb pollen descriptors in the mountain belt, and recognizing the component carried by local winds and pollen washout. On the other hand, areas devoid of vegetation (screes and glaciers) are expected to act as a sink for extralocal and regionally uphill-transported pollen (see Festi et al., 2015 for pollen deposition on glacier firn in the Alps).

Some suggestions for improving paleoclimate reconstructions:

(1) Not considering medium- to long-distance transported pollen types (e.g. *Castanea*, and *Ostrya* type broad-leaved tree species 10 to 20 km distant from our elevational transect)

(2) Need to expand the Alpine calibration set in wet elevational ecosystems and climates in Eastern Alps, maintaining a high taxonomic resolution.

(3) Presenting the reconstructed climate variable of interest as departures from the modern inferred value(s) (Huntley, 1994; Cheddadi et al., 1997); assuming that the bias in each study area remained the same during the study period. Offsets between the modern

pollen-inferred value(s) and site-specific climatologies allow for a site calibration of the bias due to locally uneven factors, such as topography and wind transport effects.

4.3. How much do human-induced vegetation changes affect climate calibrations?

Human impact on vegetation is a potential source of bias in pollen-based climate reconstruction models. Forest clearance may distort the relative abundances within the modern vegetation-climate relationships. However, anthropogenic vegetation is also affected by climate and therefore it is correct to include human-shaped landscapes in pollen-climate calibration sets. Both our elevational transects include synanthropic vegetation types especially in the montane belts where lower gentle slopes have been extensively deforested for farming and settlements.

In the mountain belt of La Thuile Valley we observed an underestimated temperature in sites rich in synanthropic herbs (e.g. Apiaceae, Asterioideae, Cichorioideae, Poaceae). These pollen taxa identified at a family level do not allow the distinction between high-elevation mountain meadows from lowland meadows. In the calibration sets these taxa show a monotonic and skewed bimodal responses with their optima around 10.4-12.0°C (**Supplementary Tables S5-6**) with temperatures characteristics of the subalpine and alpine ecosystems. In the reconstruction shown in **Fig. 5** Poaceae were excluded from the pollen sum (sites TRS 1–6), but differences between pollen-inferred temperatures and instrumental data are still evident. Actually, this difference is mainly due to the lower optima reconstructed with a symmetric unimodal response model for deciduous broad-leaved trees and shrubs forming the lower belts (see section 3.2.).

A similar underestimate also affects elevational grasslands whose pollen production is enhanced by pastoralism and fertilization, so that tree indicators from the timberline ecotone will consequently be proportionally reduced**.**

From the results of this work, we recommend that a modern calibration for the surface sample of any fossil site be made, in order to evaluate the relationships between human alterations to herbaceous vegetation and their pollen assemblages in modern surface samples collected at the core site. Anthropogenic indicators could be calibrated by considering their baseline in pristine vegetation (see Dietl et al., 2015), thus allowing

recent or specific intervals of intense pastoralism at specific sites to be recognized and, if not negligible, to be excluded from climate reconstructions. This will aid in the interpretation of palaeoecological and palaeoenvironmental reconstructions from the fossil site.

5. Conclusions

We have demonstrated the importance of local elevational transects of modern pollen samples with site-specific temperature as a tool for paleoclimate reconstructions in the Alps. The two elevational transects were developed to derive consistent local pollen-climate correlations, to find sensitive pollen taxa useful for paleoclimate reconstructions; to estimate the effects of local parameters (elevational lapse rate, climate, uphill pollen transport and human impact) and were used as test sets to evaluate pollen-climate models based on calibration sets extracted from the European Modern Pollen Database.

Both test sets and calibration sets benefit from site-specific climate information obtained by applying well-performing interpolation techniques from a high-density climate-station network. This is an improvement that assists in the reconstruction of past climate in mountain settings. This procedure can be applied to other high mountain ranges with Alpine-types of elevational biodiversity gradients in the mid-latitudes of the Eurasian and American continents.

When modelling modern data for paleoclimate reconstructions, the following factors should be considered:

(1) Taxonomic resolution of pollen identifications. Several high pollen-producer tree species are important indicators for climate factors. When taxonomic harmonization and downgrading of pollen types has to be undertaken, the original climatic value of important indicators at the biogeographical scale of the mountain range may be lost. We encourage the development of specialized calibration sets from different climatic and vegetational mountain areas to enable the full climate space of the main indicator taxa to be used. These can of course, be incorporated as subsets of larger continental datasets.

(2) Pollen transport by wind from lower vegetation belts to the treeless high-elevation sites may lead to overestimation of reconstructed temperatures at higher elevations.

Overestimation appears to be higher in regions with strong local winds and pollen washout. Calibration sets and WA and WA-PLS transfer functions can only partly account for these effects. The reconstructed climate parameter at fossil sites should be presented as the departure from the modern inferred mean, assuming that the bias in each study area has remained the same during the study period.

(3) Human impact on vegetation is a potential source of bias in pollen-based climate reconstruction models, but if anthropogenic pollen taxa are also considered, they allow these effects to be identified and eventually removed. From the results of this work, we recommend that a modern calibration for the surface sample of any fossil site be made, in order to evaluate the relationships between human alterations to herbaceous vegetation and their pollen assemblages in modern surface samples collected at the core site. This will aid in the interpretation of paleoecological and paleoenvironmental reconstructions from the study area.

Future perspectives

We have discussed the importance of reaching the highest taxonomical level for climate-sensitive pollen taxa in order to create a specifically designed modern calibration set for high-elevation site climate reconstructions. For example, since *Pinus cembra* is an important species of the European Alps ecosystem, its pollen type needs to be distinguished from *Pinus sylvestris/mugo* type in order to maximize its response to climate. The optima calculation could be improved using eHOF models as suggested by Jansen and Oksanen (2013). To investigate the human effects on modern and past pollen assemblages local baselines of anthropogenic taxa should be quantified.

Acknowledgements

This paper is a result of Giulia Furlanetto's PhD research project sponsored by the Milano-Bicocca University, Dept. of Earth and Environmental Sciences, with the co-tutoring and support of the CNR-IDPA. Suggestions provided by three anonymous referees improved the quality of the manuscript. Authors are indebted to Prof. Hilary H. Birks (Univ. of Bergen) for language editing. This paper is a contribution to the CNR-IDPA Research

Project DTA.AD001.112 "Quaternary environmental history, ecological changes and mutual interactions with human societies". Special thanks go to Migliorini Enzo, manager of the Rifugio Longo and to CAI for logistic support. EMPD contributors are gratefully acknowledged for sharing their data.

Funding

This research was supported by a grant from Parco Regionale delle Orobie Bergamasche (Delib. 12/2017). Setting up of transfer functions benefited from the CNR project of interest NextData.

Data accessibility

Data will be archived in EMPD Stage 2.

References

Badino, F., Ravazzi, C., Vallè, F, Pini, R., Aceti, E., Brunetti, M., Champvillair, E., Maggi, V., Maspero, F., Perego, R., Orombelli, G., 2018. 8800 years of high-altitude vegetation and climate history at the Rutor Glacier forefield, Italian Alps. Evidence of middle Holocene timberline rise and glacier contraction. Quaternary Science Reviews 185, 41–68.

Beniston, M., Diaz, H.F., Bradley, R.S., 1997. Climatic change at high elevation sites: an overview. Climate Change 36, 233–251.

Beug, H.J., 2004. Leitfaden der Pollenbestimmung für Mitteleuropa und angrenzende Gebiete. Verlag Dr. Friedrich Pfeil, München, Germany.

Bigler, C., Larocque, I., Peglar, S.M., Birks, H.J.B., Hall, R.I., 2002. Quantitative multiproxy assessment of long-term patterns of Holocene environmental change from a small lake near Abisko, northern Sweden. The Holocene 12, 481–496.

Birks, H.H., Ammann, B., 2000. Two terrestrial records of rapid climatic change during the glacial–Holocene transition (14,000–9,000 calendar years B.P.) from Europe. Proceedings of the National Academy of Sciences of the United States of America 97, 1390–1394.

Birks, H.J.B., Birks, H.H., 1980. Quaternary Palaeoecology. Edward Arnold, London.

Birks HJB (1994). The importance of pollen and taxonomic precision in quantitative palaeoenvironmental reconstructions. Review of Palaeobotany and Palynology 83, 107–117.

Birks, H.J.B., 1995. Quantitative Palaeoenvironmental reconstructions, in: Wigley, T.M.L., Ingram, M.J., Farmer, G. (Eds) Statistical modelling of Quaternary science data. Quaternary Research Association, Cambridge, pp 161-254.

Birks, H.J.B., 1998. Numerical tools in palaeolimnology – Progress, potentialities, and problems. Journal of Paleolimnology 20, 307-332.

Brugiapaglia, E., Beaulieu, J.L., Guiot, J., Reille, M., 1998. Transect de pluie pollinique et étagement de la végétation dans le massif du Taillefer (Isère France). Géographie physique et Quaternaire 52, 209–218.

Brunetti, M., Lentini, G., Maugeri, M., Nanni, T., Simolo, C., Spinoni, J. 2012. Projecting North Eastern Italy temperature and precipitation secular records onto a high-resolution grid. Physics and Chemistry of the Earth 40–41, 9–22.

Brunetti, M., Maugeri, M., Nanni, T., Simolo, C., Spinoni, J., 2014. High-resolution temperature climatology for Italy: interpolation method intercomparison. International Journal of Climatology 34(4), 1278–1296.

Bunting, M.J., 2002. Detecting woodland remnants in cultural landscapes: modern pollen deposition around small woodlands in northwest Scotland. The Holocene 12, 291–301.

Bunting, M.J., 2003. Pollen-vegetation relationships in non-arboreal moorland taxa. Review of Palaeobotany and Palynology 125, 285–298.

Caccianiga, M., Ravazzi, C., Zubiani, P., 1994. Storia del Ghiacciaio del Trobio (Alpi Orobie, Bergamo) e colonizzazione della vegetazione nelle aree liberate dopo la Piccola Età Glaciale. Natura Bresciana 29, 65–96.

Caccianiga, M., Luzzaro, A., Turri, D., Viapiana, G., Andreis, C., 2002. Indagini sulla flora del Ghiacciaio del Rutor (La Thuile-AO). Revue Valdotaine Histoire Naturelle 56, 15–35.

Cañellas-Boltà, N., Rull, V., Vigo, J., Mercadé, A., 2009. Modern pollen-vegetation relationships along an altitudinal transect in the central Pyrenees (southwestern Europe). The Holocene 19(8),1185–1200.

Cheddadi, R., Yu, G., Guiot, J., Harrison, S.P., Prentice, I.C., 1997. The climate of Europe 6000 years ago. Climate Dynamics 14, 883–890.

Clark, J.S., 1988. Particle motion and the theory of charcoal analysis: source area, transport, deposition, and sampling. Quaternary Research 30(1), 67–80.

Colombaroli, D., Beckmann, M., van der Knaap, W.O., Curdy, P., Tinner, W., 2013. Changes in biodiversity and vegetation composition in the central Swiss Alps during the transition from pristine forest to first farming. Diversity and Distributions 19, 157–170.

Court-Picon, M., Buttler, A., Beaulieu, J.-L., 2005. Modern pollen-vegetation relationships in the Champsaur valley (French Alps) and their potential in the interpretation of fossil pollen records of past cultural landscapes. Review of Palaeobotany and Palynology 135, 13–39.

Court-Picon, M., Buttler, A., Beaulieu, J.-L., 2006. Modern pollen/vegetation/land-use relationships in mountain environments: an example from the Champsaur valley (French Alps). Vegetation History and Archaeobotany 15, 151–168.

Crespi, A., Brunetti, M., Lentini, G., Maugeri, M., 2018. 1961–1990 high-resolution monthly precipitation climatologies for Italy. International Journal of Climatology 38, 878–895.

David, F., 1997. Holocene tree limit history in the northern French Alps stomata and pollen evidence. Review of Paleobotany and Palynology 97, 227–237.

Davis, B.A.S., Zanon, M., Collins, M., Mauri, A., Bakker, J., Barboni, D., Barthelmes, A., Beaudouin, C., Birks, H.J.B., Bjune, A.E., et al., 2013. The European modern pollen database (EMPD) project. Vegetation History and Archaeobotany 22(6), 521–530.

De Nascimento, L., Nogué, S., Fernández-Lugo, S., Méndez, J., Otto, R., Whittaker, R.J., Willis, K.J., Fernández-Palacios, J.M., 2015. Modern pollen rain in Canary Island ecosystems and its implications for the interpretation of fossil records. Review of Palaeobotany and Palynology 214, 27–39.

Dietl, G.P., Kidwell, S.M., Brenner, M., Burney, D.A., Flessa, K.W., Jackson, S.T., Koch, P.L., 2015. Conservation Paleobiology: Leveraging knowledge of the past to inform conservation and restoration. Annual Review of Earth and Planetary Sciences 43, 79–103.

Ellenberg, H., 1988. Vegetation ecology of central Europe. Cambridge University Press.

Faegri, K., Iversen, J., 1989. Textbook of pollen analysis. 4th edn by Faegri, K., Kaland, P.E., Krzywinski, K. John Wiley and Sons, Chichester, pp. 328.

Festi, D., Kofler, W., Bucher, E., Carturan, L., Mair, V., Gabrielli, P., Oeggl, K., 2015. A novel pollen-based method to detect seasonality in ice cores: a case study from the Ortles glacier, South Tyrol, Italy. Journal of Glaciology 61(229), 815–824.

Fick, S.E., Hijmans, R.J., 2017. WorldClim 2: new 1-km spatial resolution climate surfaces for global land areas. International Journal of Climatology 37, 4302–4317.

Finsinger, W., Heiri, O., Valsecchi, V., Tinner, W., Lotter, A.F., 2007. Modern pollen assemblages as climate indicators in southern Europe. Global Ecology and Biogeography 16, 567–582.

Flenley, J.R., 1973. The use of modern pollen rain samples in the study of the vegetational history of tropical regions, in: Birks, H.J.B., West, R.G. (Eds) Quaternary Plant Ecology. Oxford: Blackwell, pp. 131–141.

Frei, T., 1997. Pollen distribution at high elevation in Switzerland: Evidence for medium range transport. Grana 36, 34–38.

Furlanetto, G., Ravazzi, C., Pini, R., Vallè, F., Brunetti, M., Comolli, R., Novellino, M.D., Garozzo, L., Maggi, V., 2018. Holocene vegetation history and quantitative climate reconstructions in a high-elevation oceanic district of the Italian Alps. Evidence for a middle to late Holocene precipitation increase. Quaternary Science Reviews 200, 212-236.

Grimm, E.C., 2015. Tilia/TGView 2.0.41. Illinois State Museum, Research and Collections Center, Springfield, IL.

Hicks, S., 1992. Modern pollen deposition and its use in interpreting the occupation history of the island Hailuoto, Finland. Vegetation History and archaeobotany 1, 75–86.

Hicks, S., 1993. Present and past pollen records of Lapland forests. Review of Palaeobotany and Palynology 82, 17–35.

Hjelle, K.L., 1997. Relationships between pollen and plants in human-influenced vegetation types using presence-absence data in western Norway. Review of Palaeobotany and Palynology 99, 1–16.

Holtmeyer, F.K., 2009. Mountain Timberlines. Ecology, Patchiness, and Dynamics. Advances in Global Change Research, vol 36. Springer, Berlin.

Houghton, J.T., Ding, Y., Griggs, D.J., Noguer, M., van der Linden, P.J., Dai, X., Maskell, K., Johnson, C.A., 2001. IPCC, 2001: Climate Change 2001: The Scientific Basis. Contribution of Working Group I to the Third

Assessment Report of the Intergovernmental Panel on Climate Change. Cambridge University Press, Cambridge, United Kingdom and New York, NY, USA, pp. 881.

Huisman, J., Olff, H., Fresco, L.F.M., 1993. A hierarchical set of models for species response analysis. Journal of Vegetation Science 4, 37–46.

Huntley, B., 1994. Late Devensian and Holocene palaeoecology and palaeoenvironments of the Morrone Birkwoods, Aberdeenshire, Scotland. Journal of Quaternary Science 9, 311–336.

Jackson, S.T., Williams, J.W., 2004. Modern analogs in Quaternary paleoecology: here today, gone yesterday, gone tomorrow? Annual Reviews Earth and Planetary Sciences 32, 495–537.

Jansen, F., Oksanen, J., 2013. How to model species responses along ecological gradients – Huisman–Olff–Fresco models revisited. Journal of Vegetation Science 24, 1108–1117.

Jansen, F., Oksanen, J., 2017. Extended HOF (Huisman-Olff-Fresco) Models. R Package Version 1.8.

Juggins, S., 2017. Rioja: Analysis of Quaternary Science Data, R package version 0.9-15. Available at: http://cran.r-project.org/package=rioja.

Lisitsyna, O.V., Hicks, S., 2014. Estimation of pollen deposition time-span in moss polsters with the aid of annual pollen accumulation values from pollen traps. Grana 53(3), 232–248.

Lotter, A.F., Birks, H.J.B., Eicher, U., Hofmann, W., Schwander, J., Wick, L., 2000. Younger Dryas and Alleröd summer temperatures at Gerzensee (Switzerland) inferred from fossil pollen and cladoceran assemblages. Palaeogeography, Palaeoclimatology, Palaeoecology 159, 349–361.

Lu, H., Wu, N.Q., Liu, K.-B., Zhu, L.P., Yang, X.D., Yao, T.D., Wang, L., Li, Q., Liu, X.Q., Shen, C.M., Li, X.Q., Tong, G.B., Jiang, H., 2011. Modern pollen distributions in Qinghai-Tibetan Plateau and the development of transfer functions for reconstructing Holocene environmental changes. Quaternary Science Reviews 30, 947–966.

Markgraf, V., 1980. Pollen Dispersal in a Mountain Area. Grana 19, 127–146.

Mauri, A., Caudullo, G., 2016. *Alnus viridis* in Europe: distribution, habitat, usage and threats, in: San-Miguel-Ayanz, J., De Rigo, D., Caudullo, G., Houston Durrant, T., Mauri, A. (Eds) European Atlas of Forest Tree Species. Publication Office of the European Union, Luxembourg, p. 68.

Mazier, F., Galop, D., Brun, C., Buttler, A., 2006. Modern pollen assemblages from grazed vegetation in the western Pyrenees, France: a numerical tool for more precise reconstruction of past cultural landscapes. The Holocene 16, 91–103.

Mitchell, T.D., Jones, P.D., 2005. An improved method of constructing a database of monthly climate observations and associated high-resolution grids. International Journal of Climatology 25, 693–712.

Moar, N.T., 1970. Recent pollen spectra from three localities in the South Island, New Zealand. New Zealand Journal of Botany 8, 210–221.

Moore, P.D., Webb, J.A., Collinson, M.E., 1991. Pollen analysis. Blackwell Scientific Publications, Oxford.

New, M., Hulme, M., Jones, P., 2000. Representing twentieth-century space-time climate variability. Part II: Development of 1901–96 monthly grids of terrestrial surface climate. Journal of Climate 13, 2217–2238.

Nielsen, B.A., Vad Odgaard, B., 2005. Reconstructing land cover from pollen assemblages from small lakes in Denmark. Review of Palaeobotany and Palynology 133(1–2), 1–21.

Oksanen, J., Blanchet, F.G., Kindt, R., Legendre, P., Minchin, P.R., O'Hara, R.B., Simpson, G.L., Solymos, P., Stevens, M.H.H., Wagner, H., 2016. VEGAN: community ecology package, version 2.4-1.

Ortu, E., 2002. Reconstruction sur base pollinique de la dynamique de la végétation tardiglaciaire et holocène dans les Alpes Maritimes Italiennes. PhD Thesis, University d'Aix-Marseille III, F.

Ortu, E., Brewer, S., Peyron, O., 2006. Pollen-inferred palaeoclimate reconstructions in mountain areas: problems and perspectives. Journal of Quaternary Science 21(6), 615–627.

Ortu, E., Klotz, S., Brugiapaglia, E., Caramiello, R., Siniscalco, C., 2010. Elevation-induced variations of pollen assemblages in the North-western Alps: An analysis of their value as temperature indicators. Comptes Rendus Biologies 333, 825–835.

Ozenda, P., 2002. Perspectives pour une géobiologie des montagnes. Presses Polytechniques et Universitaires Romandes, Lausanne.

Pardoe, H.S., Giesecke, T., van der Knaap, W.O., Svitavská-Svobodová, H., Kvavadze, E.V., Panajiotidis, S., Gerasimidis, A., Pidek, I.A., Zimny, M., Święta-Musznicka, J., Latałowa, M., Noryśkiewicz, A.M., Bozilova, E., Tonkov, S., Filipova-Marinova, M.V., van Leeuwen, J.F.N., Kalniņa, L., 2010. Comparing pollen spectra from modified Tauber traps and moss samples: examples from a selection of woodlands across Europe. Vegetation History and Archaeobotany 19, 271–283.

Pini, R., Ravazzi, C., Raiteri, L., Guerreschi, A., Castellano, L., Comolli, R., 2017. From pristine forests to high-altitude pastures: an ecological approach to prehistoric human impact on vegetation and landscapes in the western Italian Alps. Journal of Ecology 105, 1580–1597.

Prentice, I.C., 1980. Multidimensional scaling as a research tool in Quaternary palynology: a review of theory and methods. Review of Palaeobotany and Palynology 31, 71–104.

Punt, W., Blackmore, S. (Eds), 1976–2009. The Northwest European Pollen Flora. Vol. I-IX. Elsevier Publishing Company.

R Core Team, 2013. R: A language and environment for statistical computing. R Foundation for Statistical Computing, Vienna, Austria. Available at: http://www.R-project.org/.

Randall, P.M., 1990. A study of modern pollen deposition, Southern Alps, South Island, New Zealand. Review of Palaeobotany and Palynology 64, 263–272.

Räsänen, S., Hicks, S., Odgaard, B.V., 2004. Pollen deposition in mosses and in a modified 'Tauber trap' from Hailuoto, Finland: what exactly do the mosses record? Review of Palaeobotany and Palynology 129, 103–116.

Räsänen, S., Suutari, H., Nielsen, B.A., 2007. A step further towards quantitative reconstructions of past vegetation in Fennoscandian boreal forests: pollen productivity estimates for six dominant taxa. Review of Palaeobotany and Palynology 147, 208–220.

Reille, M., 1992-1998. Pollen et spores d'Europe et d'Afrique du Nord. Laboratoire de Botanique historique et palynologie, Marseille.

Richard, L., 1968. Écologie de l'aune vert (*Alnus viridis*): facteurs climatiques et édaphiques. Documents pour la Carte de Végétation des Alpes 6, 107–158.

Richard, L., 1969. Une interprétation éco-physiologique de la répartition de l'aune vert (*Alnus viridis*). Documents pour la Carte de Végétation des Alpes 7, 7–23.

Rosén, P., Segerström, U., Eriksson, L., Renberg, I., Birks, H.J.B., 2001. Holocene climatic change reconstructed from diatoms, chironomids, pollen and near-infrared spectroscopy at an alpine lake (Sjuodjijaure) in northern Sweden. The Holocene 11, 551–562.

Rull, V., 2006. A high mountain pollen-altitude calibration set for palaeoclimatic use in the tropical Andes. The Holocene 16, 105–107.

Seppä, H., Birks, H.J.B., 2001. July mean temperature and annual precipitation trends during the Holocene in the Fennoscandian tree-line area: pollen-based climate reconstructions. The Holocene 11, 527-539.

Seppä, H., Birks, H.J.B., Odland, A., Poska, A., Veski, S., 2004. A modern pollen–climate calibration set from northern Europe: developing and testing a tool for palaeo-climatological reconstructions. Journal of Biogeography 31, 251–267.

Shen, C., Liu, K., Tang, L., Overpeck, J.T., 2006. Quantitative relationships between modern pollen rain and climate in the Tibetan Plateau. Review of Palaeobotany and Palynology 140, 61–77.

Stockmarr, J., 1971. Tablets with spores used in absolute pollen analysis. Pollen et Spores 13, 615–621.

Telford, R.J., Birks, H.J.B., 2011. Effect of uneven sampling along an environmental gradient on transfer-function performance. Journal of Paleolimnology 46, 99–106.

ter Braak, C.J.F., 1986. Canonical Correspondence Analysis: A New Eigenvector Technique for Multivariate Direct Gradient Analysis. Ecology 67, 1167–1179.

ter Braak, C.J.F., Looman, C.W.N., 1986. Weighted averaging, logistic regression and the Gaussian response model. Vegetatio 65, 3–11.

ter Braak, C.J.F., Juggins, S., 1993. Weighted averaging partial least squares regression (WA-PLS): an improved method for reconstructing environmental variables from species assemblages. Hydrobiologia 269/270, 485–502.

ter Braak, C.J.F., 1995. Non-linear methods for multivariate statistical calibration and their use in palaeoecology: a comparison of inverse (k-nearest neighbours, partial least squares and weighted averaging partial least squares) and classical approaches. Chemometrics and Intelligent Laboratory Systems 28**,** 165–180.

Traverse, A., (Ed.), 1994. Sedimentation of organic particles. Cambridge University Press.

Tyson, R.V., 1995. Sedimentary organic matter. Chapman and Hall.

van der Knaap, W.O., van Leeuwen, J.F.N., Ammann, B., 2001. Seven years of annual pollen influx at the forest limit in the Swiss Alps studied by pollen traps: relations to vegetation and climate. Review of Palaeobotany and Palynology 117, 31–52.

van der Voet, H., 1994. Comparing the predictive accuracy of models using a simple randomization test. Chemometr Intell Lab Syst 25, 313–323.

van Geel, B., 1978. A palaeoecological study of Holocene peat bog sections in Germany and The Netherlands, based on the analysis of pollen, spores and macro- and microremains of fungi, algae, cormophytes and animals. Review of Palaeobotany and Palynology 25, 1–120.

van Geel, B., Bohncke, S.J.P., Dee, H., 1981. A palaeoecological study of an upper Late Glacial and Holocene sequence from 'De Borchert', The Netherlands. Review of Palaeobotany and Palynology 31, 367–449.

Villa, F., De Amicis, M., Maggi, V., 2007. GIS analysis of Rutor Glacier (Aosta Valley, Italy) volume and terminus variations. Geografia Fisica e Dinamica Quaternaria 30(1), 87-95.

Appendix A. Supplementary data

Site acronym	Landscape and vegetation main features (from site centre to 100 m radius)	Latitude (site centre)	Longitude (site centre)	Elevation m asl	Tjuly (1951-2000)	Pann (1951-2000)
TRS 27	Little Ice Age moraine colonized by dry grasslands (eg *Achillea moschata, Trifolium badium* and isolated patches of *Carex curvula*).	45°40'12.44560"N	6°59'53.19031"E	2668	6.7	1047
TRS 26	Rocky slope covered by dwarf shrubs (eg *Salix herbacea*).	45°40'21.02228"N	6°59'48.15957"E	2606	7.2	1052
TRS 25	Wet meadow (*Nardus stricta* and *Leontodon* cf *helveticus*) surrounded by dwarf scrubs (eg *Salix herbacea*).	45°40'20.59097"N	6°59'45.67814"E	2599	7.2	1052
TRS 24	Mire surrounded by dry grasslands on steep slopes with scattered shrubs(eg *Juniperus nana, Rhododendron ferrugineum, Vaccinium gaultherioides* and *Vaccinium uliginosum*).	45°40'22.72214"N	6°59'26.31072"E	2518	7.8	1054
TRS 23	Small spring with mire plants (eg *Carex foetida, Carex fusca*). In the surrounding area: alpine meadows (eg *Nardus stricta*) on the east facing slopes.	45°40'33.73127"N	6°59'09.14109"E	2483	8.0	1043
TRS 22	Small mire surrounded by dry meadows on rocky slopes (*Nardus stricta* and *Leontodon helveticus*). *Pinus cembra* krummholz on rocky patches.	45°40'38.67876"N	6°59'00.56391"E	2467	8.2	1046
TRS 21	Cold moorland with Ericaceae heaths (eg *Rhododendron ferrugineum, Vaccinium gaultherioides* and *Vaccinium myrtillus*) mixed with dwarf shrubs (eg *Salix herbacea* and *Salix foetida*). Scattered trees, the nearest at ca 70 m far is a *Pinus cembra* tree individual.	45°40'44.39524"N	6°58'52.41553"E	2348	9.0	1043
TRS 20	Wet grassland surrounded by scattered *Larix decidua*, *Pinus cembra* and *Alnus viridis* tree individuals.	45°40'45.82689"N	6°58'48.56166"E	2298	9.3	1044
TRS 19	Scree slope with scattered *Larix decidua*, *Pinus cembra* and *Alnus viridis*.	45°40'48.77154"N	6°58'44.08702"E	2266	9.6	1046
TRS 18	Low-pressure grazed pasture with scattered *Larix decidua*, *Pinus cembra*, *Alnus viridis*. At ca 50 m distance, there is a lodge with ruderal species.	45°40'48.05674"N	6°58'38.60473"E	2219	9.9	1045
TRS 17	Dry grassland (*Agrostis*) on the top of a rocky emergence. In the surrounding area: *Pinus cembra* and *Larix decidua* trees.	45°40'40.66425"N	6°58'28.93368"E	2159	10.3	1032
TRS 16	Mire surrounded by scattered *Larix decidua* and *Pinus cembra* tree individuals.	45°40'39.66540"N	6°58'30.28653"E	2143	10.4	1040
TRS 15	*Pinus cembra* - *Larix decidua* open forest.	45°40'34.55567"N	6°58'06.43781"E	2090	10.8	1030
TRS 14	*Pinus cembra* - *Larix decidua* open forest with shrubs (eg Ericaceae).	45°40'36.07078"N	6°58'01.84590"E	2014	11.3	1031

TRS 13	Tall herb megaforb community in *Larix decidua* and *Pinus cembra* woodland.	45°40'38.66495"N	6°58'00.13285"E	1922	12.0	1031
TRS 12	Avalanche rill with scattered *Larix decidua* and *Pinus cembra* trees. Grazed dry meadows in the surroundings.	45°40'49.23728"N	6°58'00.18381"E	1846	12.5	1035
TRS 11	Sunny opening in wooded area (*Picea abies, Larix decidua*, *Pinus cembra*, *Alnus glutinosa*). At ca 100 m distance a lodge surrounded by mown meadows and megaforbs (eg *Rumex* and *Epilobium*).	45°40'59.35931"N	6°57'50.62548"E	1781	12.9	1030
TRS 10	Small opening in *Picea abies* woodland with *Sorbus aria* tree individuals.	45°41'03.64927"N	6°57'42.47135"E	1722	13.3	1013
TRS 9	Small hollow within dense *Picea abies* woodland, also including *Larix decidua*, *Acer pseudoplatanus* and *Salix* cf *caprea*.	45°41'07.04184"N	6°57'42.10082"E	1663	13.7	1014
TRS 8	Shaded small opening in wooded area with *Picea abies, Larix decidua* and sparse *Pinus cembra* tree individuals.	45°41'23.82291"N	6°57'46.88648"E	1618	14.0	1023
TRS 7	Grazed dry meadows (*Nardus stricta*) with scattered shrub groves (*Juniperus communis, Juniperus nana, Berberis vulgaris*) surrounded by *Larix* and *Picea* forest.	45°42'02.87050"N	6°57'41.40393"E	1520	14.6	997
TRS 6	Shaded small opening in wooded area with *Picea abies* and *Larix decidua.*	45°42'00.36854"N	6°57'42.23790"E	1510	14.5	996
TRS 5	Mown meadows near a track surrounded by an open deciduous thicket (*Corylus, Betula, Fraxinus excelsior*) and coniferous trees (*Larix decidua, Picea abies* and *Pinus sylvestris*).	45°45'02.03072"N	7°01'03.29547"E	1563	14.3	790
TRS 4	*Molinia coreulea* slope mire with open woodland (eg *Betula alba, Alnus incana, Acer pseudoplatanus, Larix decidua*).	45°44'58.08240"N	7°01'19.50509"E	1446	14.9	804
TRS 3	Opening in *Abies alba* forest with subordinated *Larix decidua, Picea abies, Sorbus aucuparia, Populus tremula, Betula alba.*	45°44'43.19404"N	7°01'56.00547"E	1298	15.9	780
TRS 2	Mown meadows surrounded by deciduous trees (eg *Fraxinus excelsior, Betula alba, Corylus avellana, Larix decidua*).	45°44'55.58848"N	7°02'21.61815"E	1050	17.3	763
TRS 1	Heavily grazed meadows in a rural context. Open thickets with *Acer pseudoplatanus*, *Fraxinus excelsior, Tilia cordata, Juglans, Picea abies, Larix decidua.*	45°45'03.71943"N	7°02'08.88244"E	983	17.8	773

Supplementary Table S1a La Thuile Valley elevational transect.

Site acronym	Landscape and vegetation main features (from site center to 100 m radius)	Latitude (site centre)	Longitude (site centre)	Elevation m asl	Tjuly (1951-2000)	Pann (1951-2000)
L 26	Cushion plant formation over a ridge top; NE-exposed slope covered by graminoid tussocks with *Rhododendron ferrugineum* groves; SE-exposed slope with graminoid tussocks accompanied by with juniper.	46° 2'31.68"N	9°52'36.61"E	2435	8.3	1850
L 25	Coarse pebble, unconsolidated scree with only sparse pioneer petrophytic vegetation (*Achillea moscata)* and scatted graminoid tussocks (*Festuca* gr. *varia*) on stable blocks.	46° 2'35.48"N	9°52'42.70"E	2428	8.4	1849
L 24	Open air shed ("bàrech") with droppings and discontinuous ruderal vegetation, in the distance petrophytic herb vegetation.	46° 2' 33.189" N	9° 52' 43.901" E	2393	8.6	1849
L 23	Continuous tussock grassland (*Festuca* and *Nardus*) and herding enclosing area with nitrophilous plants (*Rumex)*.	46° 2' 29.397" N	9° 52' 49.651" E	2372	8.9	1843
L 22	Wet, low-tall grassland (*Nardus*) bordering a sedge peat bog and parcels of snow-bed and scree vegetation (*Salix herbacea, Chrysanthemum alpinum*).	46° 2' 26.642" N	9° 52' 44.263" E	2345	9.0	1844
L 21	Tussock grassland (*Festuca* and *Nardus*)	46° 2' 25.534" N	9° 52' 44.319" E	2341	9.1	1844
L 20	Juniper-Ericaceae dwarf heath (Vaccinium and Rhododendron) beyond the treeline, not grazed.	46° 2' 14.601" N	9° 52' 4.840" E	2283	9.4	1863
L 19	Tussock grasslands (*Festuca spp*.) and low-tall grasslands (*Nardus*), scattered juniper and *Rhododendron*.	46° 2'19.60"N	9°52'45.39"E	2282	9.4	1844
L 18	Continuous *Rhododendron*-heath with larch tree individuals (4 m high, 30/40 years old).	46° 2' 15.344" N	9° 51' 51.616" E	2180	10.2	1870
L 17	Ericaceae heaths in mosaic with low tall grassland and scattered larch trees.	46° 2' 26.690" N	9° 52' 6.433" E	2169	10.3	1858
L 16	Mountain alder scrub with continuous understory of Ericaceae heath, and residual pasture clearings.	46° 2' 18.490" N	9° 51' 48.631" E	2106	10.6	1870
L 15	Tussock grassland (*Festuca* gr. *varia*) with mountain alder groves and scattered larch individuals.	46° 2' 28.870" N	9° 51' 40.735" E	2105	10.6	1869
L 14	Extensive tussock grassland (Festuca gr. varia), including scattered juniper groves and larch individuals on rock emergences.	46° 2'2.60"N	9°52'23.65"E	2100	10.7	1862
L 13	Juniper-Ericaceae dwarf heaths in mosaic with small peat bogs and tussock grasslands (*Festuca*), scattered larch; a single spruce individual noticed at spruce treeline.	46° 1'25.80"N	9°52'32.00"E	2030	11.1	1823
L 12	Tussock grassland (*Festuca* gr. *varia*) in mosaic with juniper and Ericaceae dwarf scrub and a parcel of pasture	46° 2' 22.194" N	9° 51' 43.051" E	2009	11.2	1870

L 11	Mountain alder scrub with rich tall herb vegetation in the understory.	46° 1'29.73"N	9°51'46.73"E	1950	11.5	1855
L 10	Mountain alder scrub with thickets of the endemic tall herb *Sanguisorba dodecandra*.	46° 2' 18.621" N	9° 51' 18.009" E	1941	11.6	1870
L 9	Pasture and larch parkland; small groves of mountain dwarf pine (*Pinus mugo*) and three individuals of stone pine (*Pinus cembra*). At the plot border there is an isolated wood of stone pine and extensive scrubs formed by mountain dwarf pine.	46° 1'24.36"N	9°51'17.52"E	1875	12.0	1866
L 8	Open, mixed coniferous forest (*Picea-Larix),* broad-leaved scrubs (*Laburnum*, *Alnus viridis*, *Acer pseudoplatanus)* and tall herbs (*Cicerbita).*	46° 1'29.51"N	9°50'44.41"E	1788	12.4	1865
L 7	Grassland rich in basophilous herbs and petrophytic vegetation along an avalanche corridor.	46° 1' 57.943" N	9° 50' 21.535" E	1776	12.5	1847
L 6	Pasture at the border of a *Molinia*-peat bog. Larch woodlands in the distance.	46° 1'51.72"N	9°51'1.19"E	1692	13.0	1872
L 5	Pasture at the border of a mixed coniferous forest (*Larix* and *Picea*).	46° 1' 37.134" N	9° 49' 45.206" E	1672	13.1	1841
L 4	Tussock grasslands (*Festuca* gr. *varia*), legume bushes (*Genista radiata*) in mosaic with mountain alder scrubs and tall herbs; thickets of the endemic tall herb *Sanguisorba dodecandra*.	46° 1' 36.211" N	9° 49' 17.909" E	1552	13.8	1834
L 3	River corridor and waterfalls with mountain alder scrub and tall herbs (including *Sanguisorba dodecandra*). In the surroundings, coniferous woodlands (*Picea-Larix), Larburnum* understory and mowed leans (*Pimpinella* and *Rumex)*.	46° 1' 33.239" N	9° 48' 48.401" E	1422	14.5	1826
L 2	Mowed leans surrounded by thickets of broad-leaved trees (*Acer, Fraxinus*)	46° 1' 35.235" N	9° 48' 30.007" E	1360	14.9	1827
L 1	Hazelnut scrubland and mixed coniferous (*Picea-Larix*), broad-leaved forests (*Sorbus aucuparia*, *Sorbus aria*), petrophytic habitats.	46° 1' 29.681" N	9° 47' 53.160" E	1244	15.5	1788

Supplementary Table S1b Upper Brembana Valley elevational transect.

	Longitude	Latitude	Elevation	July temperature
Barboni a1461	14.4333	45.7500	610	17.6
Barboni a1464	14.5833	45.8666	350	19.5
Barboni a58	7.6000	44.1400	2080	11.4
Barboni a75	7.4500	44.0500	2090	11.4
Barboni a76	6.5300	45.7700	1784	13
Barboni a79	6.5487	44.7782	1066	17.5
Barboni a825	7.7330	45.8750	2050	10.6
Barboni a831	7.6500	45.7830	1841	12.2
Barboni a833	7.6170	45.8500	1800	12.3
EPDcoretop E1055	7.9763	46.5972	1850	10.8
EPDcoretop E1056	8.0246	46.3886	2017	10
EPDcoretop E1061	8.0215	46.6694	2265	8.2
EPDcoretop E1064	7.9833	46.3847	2330	7.9
EPDcoretop E1065	7.9716	46.3835	2290	8.2
EPDcoretop E1072	7.0725	46.3262	1780	11.9
EPDcoretop E1075	7.2333	44.1500	2260	10.2
EPDcoretop E1092	8.1124	46.2106	1635	12.8
EPDcoretop E1093	8.9541	45.9091	990	17.2
EPDcoretop E1095	7.8450	46.1963	1710	12.4
EPDcoretop E1097	7.7911	46.0114	2334	8.6
EPDcoretop E1098	8.0359	46.6729	2339	7.7
EPDcoretop E1102	7.8432	46.2820	1535	13.4
EPDcoretop E1108	7.0046	46.3637	1891	11.2
EPDcoretop E1109	10.3106	46.7836	1546	12.9
EPDcoretop E1121	8.0235	46.2524	2017	10.2
EPDcoretop E1138	8.2613	46.5471	2315	7.8
EPDcoretop E1143	7.7619	45.9833	2757	5.7
EPDcoretop E1146	8.5172	46.4440	1892	10.7
EPDcoretop E1151	7.4439	46.5769	1831	11
EPDcoretop E1153	7.8417	46.7942	1190	14.4
EPDcoretop E1155	7.9765	46.6800	1935	10.2
EPDcoretop E1157	7.8476	46.7435	1450	13
EPDcoretop E1158	7.7068	45.9908	2552	7.2
EPDcoretop E1159	7.2847	46.6703	1046	15.2
EPDcoretop E1160	10.4798	46.8697	1721	11.7
EPDcoretop E1161	8.0114	46.2303	1885	11.1
EPDcoretop E1166	7.8627	46.7607	1470	13
EPDcoretop E1167	10.4340	46.5425	2490	7.3
EPDcoretop E1169	7.4788	46.3113	1500	13.6
EPDcoretop E1170	7.4022	46.4274	1885	11
EPDcoretop E1176	7.7339	46.8206	980	15.4
EPDcoretop E1178	11.7988	47.0242	1875	11
EPDcoretop E1179	11.0014	47.2110	1880	10.9
EPDcoretop E1180	10.9764	47.2917	797	16.4
EPDcoretop E1184	11.1903	47.3226	1177	14.5

EPDcoretop E1189	12.3583	47.4714	826	15.7
EPDcoretop E1193	11.6783	46.7608	870	17.7
EPDcoretop E1194	11.4944	46.6447	1780	11.9
EPDcoretop E1195	11.4589	46.6400	2080	9.9
EPDcoretop E1196	11.4583	46.6661	2050	10.2
EPDcoretop E1197	11.4319	46.6664	2033	10.2
EPDcoretop E1198	11.1697	47.0840	2155	8.6
EPDcoretop E1199	11.1921	46.9942	2190	8.5
EPDcoretop E1200	11.1410	46.9965	2285	7.8
EPDcoretop E1201	11.8024	47.0244	1880	11.1
EPDcoretop E1202	11.0239	46.8433	2267	8.3
EPDcoretop E1213	12.1389	47.2431	1590	12.2
EPDcoretop E1214	10.8256	46.8292	2760	4.7
EPDcoretop E1227	7.3381	46.2335	640	18.4
EPDcoretop E1265	5.8067	45.0689	1130	17.3
EPDcoretop E133	7.8431	46.2592	2061	10.1
EPDcoretop E208	13.8667	47.1667	1700	11.1
EPDcoretop E242	13.9000	47.1167	1680	11.1
EPDcoretop E715	11.0250	46.8583	2150	9.2
EPDcoretop E739	6.5942	44.9189	1800	13.2
EPDcoretop E742	12.3000	47.6500	664	16.3
EPDcoretop E907	6.6333	44.9975	2248	10.2
EPDcoretop E980	7.5433	46.6458	989	15.6
Knaap a1	8.0263	46.3907	2000	10.1
Knaap a11	8.0311	46.3878	2215	8.6
Knaap a17	8.0482	46.3791	1840	11.3
Knaap a20	8.0155	46.3740	2130	9.3
Knaap a23	8.0166	46.3730	2150	9.1
Knaap a26	8.0157	46.3712	2215	8.7
Knaap a29	8.0147	46.2342	1855	11.3
Knaap a33	8.0205	46.2322	2055	10
Knaap a36	8.0232	46.2307	2130	9.6
Knaap a39	8.0262	46.2308	2185	9.2
Knaap a50	8.0106	46.6544	2020	9.8
Knaap a54	8.0122	46.6556	2120	9.2
Knaap a57	8.0151	46.6582	2270	8.2
Knaap a60	8.0201	46.6612	2390	7.3
Knaap a63	8.0105	46.6532	1955	10.2
Knaap a66	7.9980	46.6495	1725	11.7
Knaap a68	8.0352	46.6736	2340	7.7
Knaap a71	8.0658	46.7171	1525	12.7
Knaap a77	7.7752	46.0054	2240	9.1
Knaap a80	7.7862	46.0049	2320	8.6
Knaap a83	7.7813	46.0013	2520	7.3
Knaap a86	7.7796	45.9873	2915	4.6
Knaap a89	7.7809	45.9822	3000	4.1
Ortu a1	7.1333	44.2333	2240	10.4

Ortu a11	7.2479	44.2461	1960	12.2
Ortu a13	7.3260	44.1490	2175	10.8
Ortu a14	7.3340	44.1610	2070	11.4
Ortu a4	7.1000	44.2667	2130	11.1
Ortu a9	7.7292	44.2000	1624	14.4
Ortu b1	7.2090	45.5600	1728	13.3
Ortu b10	7.2140	45.5460	1980	11.6
Ortu b11	7.2160	45.5460	2080	10.9
Ortu b13	7.2190	45.5450	2167	10.3
Ortu b14	7.2210	45.5470	2190	10.1
Ortu b15	7.2220	45.5440	2309	9.3
Ortu b16	7.2250	45.5440	2405	8.6
Ortu b17	7.2270	45.5430	2461	8.2
Ortu b18	7.2300	45.5430	2533	7.7
Ortu b19	7.2390	45.5420	2680	6.7
Ortu b20	7.2330	45.5430	2631	7
Ortu b21	7.2090	45.5740	1680	13.6
Ortu b22	7.1980	45.6450	1260	16.2
Ortu b23	7.2030	45.6650	1177	16.6
Ortu b24	6.8280	45.3300	2316	9.5
Ortu b25	6.8240	45.3300	2364	9.2
Ortu b26	6.8190	45.3250	2352	9.2
Ortu b27	6.8160	45.3220	2311	9.5
Ortu b28	6.8310	45.3240	2243	10
Ortu b29	6.8280	45.3190	2071	11.2
Ortu b3	7.2100	45.5690	1794	12.8
Ortu b30	6.8340	45.3130	1986	11.8
Ortu b31	6.8240	45.3050	1751	13.4
Ortu b33	6.7950	45.2560	1284	16.3
Ortu b34	7.0500	44.6180	1603	14.5
Ortu b35	7.0620	44.6150	1793	13.3
Ortu b36	7.0660	44.6140	1871	12.8
Ortu b37	7.0690	44.6150	1978	12.1
Ortu b38	7.0750	44.6160	2023	11.8
Ortu b41	6.9780	44.6890	2738	7
Ortu b42	6.9760	44.6900	2651	7.6
Ortu b43	6.9750	44.6890	2684	7.4
Ortu b44	6.9760	44.6890	2697	7.3
Ortu b45	6.9780	44.6880	2633	7.7
Ortu b46	6.9770	44.6860	2758	6.9
Ortu b47	6.9780	44.6850	2700	7.3
Ortu b49	6.9840	44.6830	2570	8.1
Ortu b51	6.9870	44.6760	2380	9.4
Ortu b52	6.9840	44.6660	2179	10.7
Ortu b54	6.9690	44.6950	2579	8.1
Ortu b55	6.9490	44.7000	2380	9.4
Ortu b56	6.9280	44.7090	2193	10.7

Ortu b57	6.9190	44.7140	2107	11.2
Ortu b58	7.2200	44.3090	856	18.9
Ortu b59	7.2820	44.3100	755	19.5
Ortu b60	7.3280	44.3030	756	19.5
Ortu b61	7.1540	44.3010	951	18.4
Ortu b62	7.1510	44.2930	1082	17.6
Ortu b64	7.1460	44.2920	1170	17.1
Ortu b66	7.1370	44.2800	1300	16.3
Ortu b67	7.1250	44.2650	1550	14.8
Ortu b69	7.1090	44.2430	1800	13.2
Ortu b7	7.1970	45.6230	1391	15.4
Ortu b70	7.1130	44.2310	1915	12.5
Ortu b71	7.1160	44.2420	2003	11.9
Ortu b73	7.1260	44.2260	2130	11.1
Ortu b74	7.1450	44.2110	2310	9.9
Ortu b75	7.1480	44.2050	2360	9.6
Ortu b76	6.0880	45.6210	1024	17.8
Ortu b77	6.0890	45.6210	1049	17.6
Ortu b79	6.0910	45.6190	1136	17.2
Ortu b81	6.0920	45.6190	1195	16.9
Ortu b82	6.0930	45.6190	1233	16.7
Ortu b83	6.0930	45.6200	1251	16.6
Ortu b85	6.0930	45.6210	1330	16.1
Ortu b88	6.1020	45.6270	1350	16
Ortu b9	7.2130	45.5460	1885	12.2
Ortu b90	6.1140	45.6380	1460	15.3
Ortu b93	6.1130	45.6420	1722	13.5
Ortu b94	6.1160	45.6420	1685	13.7
Ortu b95	6.1150	45.6410	1658	14
Ortu b98	6.1150	45.6380	1515	14.9
Ortu b99	6.1160	45.6350	1400	15.7
Ortu c11	5.9340	45.0700	2075	11.5
Ortu c12	5.9330	45.0700	2050	11.7
Ortu c13	5.9340	45.0680	2000	12
Ortu c14	5.9320	45.0670	1900	12.7
Ortu c15	5.9310	45.0650	1870	12.9
Ortu c16	5.9300	45.0660	1860	12.9
Ortu c17	5.9250	45.0650	1850	13
Ortu c18	5.9240	45.0670	1840	13.1
Ortu c19	5.9230	45.0670	1830	13.1
Ortu c20	5.9210	45.0640	1820	13.2
Ortu c21	5.9190	45.0640	1810	13.3
Ortu c22	5.9150	45.0600	1800	13.3
Ortu c23	5.9100	45.0580	1700	13.9
Ortu c24	5.9070	45.0570	1640	14.3
Ortu c25	5.9040	45.0550	1620	14.4
Ortu c26	5.8830	45.0540	1580	14.6

Ortu c27	5.8820	45.0530	1560	14.7
Ortu c28	5.8650	45.0230	1350	16.1
Ortu c29	5.8500	45.0440	1250	16.4
Ortu c30	5.8440	45.0410	1150	17
Ortu c31	5.8480	45.0460	1050	17.3
Ortu c32	5.8460	45.0470	960	17.8
Ortu c33	5.8460	45.0490	950	17.9
Ortu c34	5.8440	45.0480	920	18
Ortu c35	5.8350	45.0400	850	18.6
Ortu c36	5.8360	45.0440	750	19.2
Ortu c37	5.8290	45.0400	650	20
Ortu c38	5.8260	45.0380	550	20.6
Ortu c39	5.8220	45.0430	540	20.7
Ortu c7	5.9450	45.0760	2350	9.7
Ortu c8	5.9450	45.0740	2320	9.8
Ortu d10	6.3020	44.4220	1200	16.9
Ortu d16	6.2930	44.4520	800	19
Ortu d17	6.3860	44.4490	860	18.6
Ortu d18	6.3890	44.4570	820	18.9
Ortu d24	6.3700	44.5020	1400	15.7
Ortu d25	6.3700	44.5020	1200	16.8
Ortu d27	6.4630	44.4880	1520	15
Ortu d31	6.4650	44.4920	1490	15.2
Ortu d32	6.4650	44.4990	1100	17.3
Ortu d33	6.5780	44.6030	1480	15.2
Ortu d35	6.5640	44.6100	1280	16.3
Ortu d36	6.5590	44.6130	1030	17.6
Ortu d37	6.5570	44.6130	1030	17.6
Ortu d40	6.5530	44.6160	960	18
Ortu d41	6.6110	44.7080	920	18.2
Ortu d44	6.6010	44.7470	1600	14.6
Ortu d45	6.6010	44.7470	1480	15.3
Ortu d46	6.5950	44.7460	1250	16.5
Ortu d47	6.5900	44.7450	1070	17.4
Ortu d48	6.5840	44.7450	946	18
Ortu d49	6.6360	44.2450	1400	15.8
Ortu d51	6.6550	44.2430	1720	13.8
Ortu d52	6.6590	44.2460	1800	13.3
Ortu d53	6.6750	44.2450	1800	13.3
Ortu d54	6.6860	44.2480	1920	12.5
Ortu d55	6.6930	44.2490	2050	11.7
Ortu d56	6.6930	44.2490	2150	11
Ortu d57	6.6930	44.2490	2120	11.2
Ortu d8	6.2980	44.3990	1160	17.2
Ortu d9	6.2880	44.4070	1322	16.3
Sadori a1	12.0357	46.2678	600	18.8
Sadori a2	12.0310	46.2651	770	17.9

Sadori a3	12.0284	46.2602	900	17.2

Supplementary Table S2 Calibration set 234 EMPD sites. Sites are arranged in alphabetical order.

Taxon	codes	optima (°C)	tolerances (°C)	n° of occurrences	type of eHOF response models
Ephedra fragilis	EPHFRA	15.9	3.0	1	
Plantago major type	PLAMAJTYPE	15.9	3.0	1	
Astragalus	ASTTYPE	14.9	3.0	1	
Liliaceae	LILFAM	14.9	3.0	1	
Rosaceae	ROSFAM	14.9	3.0	1	
Trifolium repens type	TRIREPTYPE	14.5	0.5	2	
Taxus	TAXSP	14.3	3.0	1	
Fraxinus excelsior type	FRAEXCTYPE	14.5	3.6	9	
Onobrychis	ONOSP	14.6	3.0	1	
Ostrya	OSTTYPE	14.1	2.8	6	
Sambucus	SAMSP	14.0	0.6	2	
Betula	BETSP	13.7	3.2	20	VII
Helleborus	HELSP	13.7	3.0	1	
Galium	GALTYPE	13.5	2.7	6	
Tilia	TILSP	13.5	4.3	8	
Sedum	SEDTYPE	13.2	2.9	2	
Larix	LARSP	12.9	2.6	22	IV
Labiatae	LABFAM	12.8	3.0	15	I
Corylus	CORSP	12.6	3.1	27	II
Abies	ABIALB	12.4	3.5	24	I
Fagus	FAGSP	12.5	3.1	18	I
Crassulaceae	CRAFAM	12.4	4.8	9	
Veronica type	VERTYPE	12.1	3.3	6	
Picea	PICEXC	12.2	3.0	27	VII
Juglans	JUGSP	12.2	3.4	22	I
Ephedra distachya	EPHDIS	12.2	2.8	6	
Sorbus	SORSP	12.1	1.1	8	
Vitis	VITSP	12.1	2.7	4	
Epilobium	EPISP	12.1	1.8	3	
Rhamnus	RHATYPE	12.0	3.0	1	
Scrophulariaceae	SCRFAM	12.0	3.0	1	
Apiaceae	APIFAM	11.8	2.9	24	I

Ranunculaceae	RANFAM	11.8	2.9	25	I
Artemisia	ARTSP	11.7	3.3	26	I
Quercus robur type	QUEROBTYPE	11.7	2.4	17	I
Fabaceae	FABFAM	11.7	3.0	17	I
Poaceae 37-47 µm	POAMED	11.7	5.7	3	
Alnus glutinosa type	ALNGLUTYPE	11.7	2.7	27	VII
Juglans nigra	JUGNIG	11.7	7.4	2	
Cichorioideae	CICFAM	11.6	3.6	25	I
Plantago lanceolata type	PLALANTYPE	11.5	3.3	20	I
Pinus sylvestris/mugo type	PINSYLTYPE	11.4	3.3	27	I
Castanea sativa	CASSAT	11.4	3.1	26	I
Chenopodiaceae	CHENFAM	11.3	3.3	6	
Carpinus betulus	CARBET	11.3	2.9	2	
Calluna	CALSP	11.2	1.6	5	
Vaccinium	VACSP	11.2	2.5	20	I
Pinus cembra	PINCEM	11.2	2.8	27	IV
Rumex acetosa type	RUMACETYPE	11.2	3.2	19	I
Plantago alpina type	PLAALPTYPE	11.1	3.2	23	I
Aster type	ASTTYPE	11.1	3.7	17	I
Caryophyllaceae	CARFAM	11.0	3.0	26	I
Brassicaceae	BRAFAM	11.0	3.9	18	I
Olea	OLESP	11.0	3.4	16	I
Poaceae < 37 µm	POAMIN	10.9	3.3	27	VII
Salix	SALSP	10.8	3.7	19	I
Hypericum	HYPSP	10.9	3.2	7	
Phyteuma	PHYSP	10.7	2.7	17	I
Juniperus	JUNSP	10.7	3.4	18	I
Aconitum	ACOSP	10.6	1.8	4	
Acer	ACESP	10.5	4.8	2	
Rhinanthus type	RHITYPE	10.4	4.0	4	
Anthemis type	ANTTYPE	10.4	3.2	20	I
Helianthemum	HELSP	10.2	2.5	4	
Campanulaceae	CAMFAM	10.1	5.5	2	
Rhododendron	RHOSP	10.1	1.7	6	
Ambrosia type	AMBSP	10.0	3.3	12	I
Melampyrum	MELSP	9.6	3.0	1	
Arctostaphylos	ARCSP	9.3	0.6	2	
Geum	GEUSP	9.2	1.4	8	
Alnus viridis	ALNVIR	9.0	1.3	13	IV
Sanguisorba minor type	SANMIN	8.9	2.2	4	
Ulmus	ULMSP	8.8	4.0	2	

Saxifragaceae	SAXFAM	8.4	1.9	10	II
Cotinus coggyria	COTCOG	8.4	2.0	3	
Cerealia	CERFAM	7.2	3.0	1	
Frangula alnus	FRAALN	7.2	3.0	1	
Gentiana pneumonanthe type	GENPNETYPE	7.2	3.0	1	
Polygonum aviculare type	POLAVITYPE	7.2	3.0	1	
Rumex acetosella type	RUMACETOTYPE	7.2	3.0	1	

Supplementary Table S3 La Thuile Valley elevational transect: codes, optima, tolerances and number of occurrences of all taxa included in the pollen sum. Taxa are arranged in optima order. The response models are restricted to taxa with ten or more occurrences in the elevational transect.

Taxon	codes	optima (°C)	tolerances (°C)	n° of occurrences	type of eHOF response models
Laserpitium	LASSP	15.5	1.8	1	
Sambucus racemosa type	SAMRACTYPE	15.5	1.8	1	
Laburnum	LABSP	14.4	1.7	2	
Ligustrum	LIGSP	13.8	1.8	1	
Other Rosaceae	OTHROSFAM	14.2	1.8	1	
Rubus	RUBSP	13.4	2.0	3	
Lysimachia	LYSSP	13.2	3.0	2	
Centaurea jacea type	CENTJACTYPE	13.2	1.4	3	
Anagallis type	ANATYPE	13.2	3.3	3	
Hypericum	HYPSP	13.1	2.2	3	
Viburnum	VIBSP	13.1	1.2	5	
Dipsacaceae	DIPSFAM	13.0	1.8	1	
Plantago tenuiflora type	PLATENTYPE	13.0	1.8	1	
Ericaceae	ERIFAM	13.0	2.6	4	
Sorbus	SORSP	12.8	1.6	5	
Sanguisorba minor	SANMIN	12.7	1.3	3	
Bifaria type	BIFTYPE	12.5	1.8	1	
Chaerophyllum	CHASP	12.5	1.8	1	
Aconitum	ACOSP	12.5	1.5	6	
Calluna	CALSP	12.5	0.7	3	
Pimpinella major type	PIMMAJTYPE	12.5	1.1	3	
Symphytum	SYMSP	12.5	0.0	2	
Gentiana pneumonanthe type	GENPNEUTYPE	12.4	1.8	1	

Lilium	LILSP	12.4	1.8	1	
Plantago maritima type	PLAMARTYPE	12.4	1.8	1	
Polygonum bistorta	POLBIS	12.4	1.8	10	I
Galium type	GALTYPE	12.4	2.0	13	I
Larix	LARSP	12.3	2.2	23	II
Cerealia	CERFAM	12.3	1.3	7	
Sanguisorba dodecandra	SANDOD	12.2	1.9	12	I
Mentha type	MENTYPE	12.1	2.9	3	
Acer	ACESP	12.0	2.7	14	I
Alnus glutinosa type	ALNGLUTYPE	12.0	2.2	22	I
Apiaceae	APIFAM	12.0	1.6	19	IV
Trifolium pratense type	TRIPRATYPE	12.0	1.8	1	
Rumex scutatus type	RUMSCUTYPE	11.9	2.0	20	I
Rhamnus type	RHATYPE	11.9	1.0	3	
Trifolium repens type	TRIREPTYPE	11.8	0.2	2	
Potentilla type	POTTYPE	11.8	2.0	15	I
Fraxinus excelsior type	FRAEXCTYPE	11.8	2.3	23	II
Liliaceae	LILFAM	11.8	0.9	2	
Plantago coronopus type	PLACORTYPE	11.7	1.6	9	
Vitis	VITSP	11.7	2.1	10	I
Ulmus	ULMSP	11.6	2.2	19	I
Quercus robur type	QUEROBTYPE	11.6	2.1	23	I
Scrophulariaceae	SCRFAM	11.5	2.5	6	
Poaceae > 47 µm anulus < 11 µm	POAMAJ	11.5	2.2	18	I
Rhinanthus type	RHITYPE	11.5	2.0	13	I
Astragalus type	ASTRTYPE	11.4	0.3	2	
Euphorbia	EUPHSP	11.4	1.1	6	
Helianthemum	HELSP	11.4	2.4	5	
Rumex acetosa type	RUMACETYPE	11.4	1.8	19	I
Gentianella germanica type	GENGERTYPE	11.4	0.3	2	
Verbascum	VERBSP	11.4	1.4	6	
Erica	ERISP	11.4	1.4	5	
Fraxinus ornus type	FRAORNTYPE	11.3	1.9	13	I
Quercus ilex	QUEILE	11.3	1.9	18	I
Alnus viridis	ALNVIR	11.3	2.0	26	VII
Saxifraga aizoides type	SAXAIZTYPE	11.3	2.4	7	
Carpinus betulus	CARBET	11.3	2.0	23	I
Corylus	CORSP	11.3	2.2	26	VII
Cedrus	CEDSP	11.2	1.2	5	

Daphne	DAPSP	11.2	1.8	1	
Juglans	JUGSP	11.2	1.9	22	I
Echium	ECHSP	11.2	2.3	3	
Picea excelsa	PICEXC	11.2	2.1	25	I
Plantago major type	PLAMAJTYPE	11.2	2.0	4	
Poaceae 37-47 µm	POAMED	11.1	2.0	26	I
Urtica	URTSP	11.1	2.5	17	I
Veronica type	VERTYPE	11.1	1.7	8	
Brassicaceae	BRAFAM	11.1	1.9	24	I
Sambucus nigra type	SAMNIGTYPE	11.1	1.8	14	I
Ostrya type	OSTTYPE	11.1	2.0	23	I
Salix	SALSP	11.0	2.2	26	I
Pinus sylvestris/mugo type	PINSYLTYPE	11.0	2.1	26	I
Scrophularia type	SCRTYPE	11.0	0.3	3	
Betula	BETSP	11.0	2.1	25	I
Ranunculus acris type	RANACRTYPE	11.0	1.7	21	I
Tilia	TILSP	11.0	2.5	9	
Rosaceae	ROSFAM	10.9	2.1	8	
Castanea sativa	CASSAT	10.9	1.8	26	VII
Rhododendron	RHOSP	10.9	0.3	4	
Poaceae < 37 µm	POAMIN	10.9	2.0	26	VII
Plantago lanceolata type	PLALANTYPE	10.7	1.8	22	I
Sedum type	SEDTYPE	10.8	2.3	5	
Caryophyllaceae	CARFAM	10.7	2.5	13	I
Cichorioideae	CICFAM	10.7	1.9	23	I
Pinus cembra	PINCEM	10.7	1.8	20	I
Ranunculaceae	RANFAM	10.7	1.7	22	I
Cirsium	CIRSP	10.7	2.4	9	
Astrantia type	ASTTYPE	10.7	1.1	12	I
Bupleurum	BUPSP	10.7	2.1	9	
Fagus	FAGSP	10.6	1.7	24	I
Olea	OLESP	10.6	2.0	13	I
Plantaginaceae	PLAFAM	10.6	1.4	7	
Ranunculus	RANSP	10.6	1.9	14	I
Vaccinium	VACSP	10.5	1.3	15	I
Aster type	ASTTYPE	10.5	1.7	20	I
Phyteuma	PHYSP	10.5	2.0	15	I
Chenopodiaceae	CHENFAM	10.5	2.0	18	I
Ambrosia	AMBSP	10.5	1.6	14	I

Crassulaceae	CRAFAM	10.5	2.1	10	I
Juniperus	JUNSP	10.5	1.4	19	I
Campanula	CAMSP	10.4	1.6	11	I
Lotus type	LOTTYPE	10.3	1.8	9	
Primula	PRISP	10.3	1.8	1	
Anemone	ANESP	10.2	1.8	1	
Cannabis/Humulus	CANHUM	10.2	1.2	12	I
Gentiana sp.	GENSP	10.1	1.6	5	
Abies alba	ABIALB	10.1	2.3	9	
Artemisia	ARTSP	10.0	2.1	13	I
Anthemis type	ANTTYPE	10.0	1.6	10	I
Saxifraga stellaris type	SAXSTETYPE	9.7	1.6	2	
Jasione	JASSP	9.5	1.2	3	
Filipendula	FILSP	9.4	1.8	1	
Loiseleuria	LOISP	9.2	1.1	4	
Geum	GEUSP	9.1	1.8	1	
Prunus	PRUSP	9.1	1.8	1	
Campanulaceae	CAMFAM	9.0	1.8	1	
Centaurea sp.	CENSP	9.0	1.8	1	
Saxifraga oppositifolia type	SAXOPPTYPE	9.0	1.8	1	
Trifolium sp.	TRISP	9.0	1.8	1	
Trifolium alpinum	TRIALP	8.6	1.8	1	
Oxyria type	OXITYPE	8.6	0.4	3	

Supplementary Table S4 Upper Brembana Valley elevational transect: codes, optima, tolerances and number of occurrences of all taxa included in the pollen sum. Taxa are arranged in optima order. The response models are restricted to taxa with ten or more occurrences in the elevational transect.

	optima (°C)	tolerances (°C)	type of eHOF response models
Abies	13.5	3.1	VII
Acer type	14.3	3.2	IV
Achillea type	9.9	3.3	II
Aconitum type	11.3	2.9	
Adonis type	15.5	1.1	
Aesculus	13.0	2.9	
Alchemilla	9.4	2.1	I
Allium type	7.7	2.9	
Alnus undiff	12.1	3.5	II

Ambrosia type	11.1	3.0	I
Anacardiaceae	17.0	1.9	
Androsace	13.4	5.3	
Anemone nemorosa type	9.4	1.9	I
Anthemis type	15.9	3.1	
Anthericum type	17.2	2.9	
Anthoxanthum	7.8	2.9	
Anthriscus sylvestris type	11.5	2.4	
Apiaceae	13.5	3.6	II
Arctostaphylos	9.0	0.8	
Arenaria type	6.2	2.4	
Armeria maritima type	8.9	3.2	
Arnica montana	10.1	1.5	
Artemisia	12.2	4.0	II
Astragalus alpinus type	4.4	3.6	
Astrantia type	13.0	2.3	
Athamanta cretensis	11.0	2.9	
Avena Triticum type	11.5	2.5	
Bartsia type	8.0	2.7	I
Berberis type	10.2	2.9	
Betula	13.2	3.7	II
Boraginaceae undifferentiated	12.3	3.8	I
Brassicaceae undifferentiated	11.9	3.7	II
Bupleurum type	11.2	3.9	
Buxus	13.9	3.9	
Calluna	11.8	2.9	I
Campanula	11.1	1.8	I
Campanulaceae	11.3	3.5	I
Cannabaceae type	10.5	2.7	I
Cannabis	10.1	2.1	I
Cardamine pratensis type	9.2	2.9	
Cardamine type	7.8	2.9	
Carduus type	10.1	2.3	I
Carlina type	8.1	1.9	
Carpinus	15.3	3.6	II
Carum carvi	11.5	4.4	
Caryophyllaceae	10.4	3.3	II
Castanea sativa	14.1	4.3	VII
Cedrus	16.1	3.6	I
Celastraceae	14.7	2.9	
Centaurea collina	12.8	2.9	
Centaurea cyanus type	12.6	3.0	
Centaurea montana type	13.8	4.3	
Centaurea nigra type	12.7	3.6	I
Centaurea scabiosa type	14.2	6.1	

Centaurea type	16.5	2.3	I
Cerastium type	9.1	3.9	I
Cerealia	13.8	3.7	I
Chaerophyllum type	10.8	3.4	I
Chenopodiaceae Amaranthaceae	12.7	3.7	I
Chrysanthemum alpinum	7.8	2.9	
Cirsium type	11.8	4.6	
Cistus	10.7	2.9	
Compositae subfam Asteroideae	12.4	3.5	I
Compositae subfam Cichorioideae	11.7	3.4	II
Convolvulaceae	17.6	0.7	
Cornus	9.2	2.9	
Corylus	13.8	3.7	II
Crassulaceae	11.5	3.8	I
Crepis	7.8	2.9	
Cupressus type	16.2	2.8	
Cuscuta europaea type	14.8	3.8	
Cyclamen hederifolium	18.2	1.6	
Daucus type	7.7	2.6	
Deschampsia	7.8	2.9	
Dianthus type	13.7	4.3	I
Dipsacaceae	13.5	2.7	I
Drosera	12.2	2.9	
Empetrum type	9.1	0.6	
Ephedra distachya type	14.5	5.2	
Ephedra fragilis type	10.9	3.9	
Ephedra type	10.6	2.9	
Epilobium type	13.2	3.1	I
Ericaceae	11.9	2.9	I
Erigeron	9.0	2.1	I
Eryngium type	10.0	2.9	
Eucalyptus	12.6	2.8	
Euonymus	18.6	2.9	
Euphorbia	9.8	2.9	
Euphorbiaceae	16.6	2.7	
Euphrasia type	15.3	2.9	
Fabaceae	13.2	3.9	I
Fagopyrum	17.5	0.3	
Fagus	13.7	3.5	VII
Filipendula type	13.0	3.5	I
Frangula	8.5	1.0	
Fraxinus	13.8	3.6	II
Galeopsis type	11.7	2.9	
Galium type	16.5	2.5	I
Gentiana	14.8	1.7	

Gentiana nivalis type	7.8	2.9	
Gentiana pneumonanthe type	9.7	1.9	I
Gentiana purpurea type	7.8	2.9	
Gentianaceae	11.1	2.5	I
Gentianella campestris type	9.3	1.7	
Geranium type	12.3	3.5	I
Geum type	8.3	2.3	
Globularia	6.8	2.9	
Gnaphalium type	8.5	2.1	
Gypsophila repens type	4.7	2.9	
Gypsophila type	18.0	2.9	
Hedera type	16.0	4.2	
Helianthemum type	12.8	3.5	I
Heracleum type	9.0	2.8	I
Herniaria type	4.1	2.9	
Hippophae	16.2	3.2	I
Homogyne	7.9	1.8	
Hordeum type	11.7	3.7	
Humulus type	9.0	2.9	I
Hypericum perforatum type	10.3	1.4	I
Hypericum type	17.7	2.0	
Ilex	18.6	2.9	
Inula type	11.9	2.9	
Iris type	13.6	2.9	
Jasione type	11.3	2.9	
Juglans	13.7	3.7	II
Juncaceae	10.1	2.9	
Juniperus type	11.7	3.8	II
Knautia type	12.1	1.2	
Labiatae	12.7	3.4	I
Laburnum anagyroides	14.9	1.6	
Larix	11.4	2.7	IV
Laserpitium prutenicum	13.8	6.1	
Legousia	13.2	2.9	
Leontodon helveticus	7.8	2.9	
Ligusticum mutellina	8.0	1.5	I
Ligustrum vulgare type	13.9	5.9	
Liliaceae type	12.7	2.6	I
Lilium	17.2	2.9	
Linaria type	11.7	4.5	
Linum	13.9	3.0	
Lloydia serotina	9.2	2.9	
Lonicera type	11.4	2.0	
Lotus type	11.0	3.4	I
Luzula	11.4	3.8	I
Lythrum	16.5	4.5	
Melampyrum	11.8	3.6	I

Mentha type	9.4	2.7	I
Mercurialis	17.2	2.6	I
Mercurialis annua type	9.8	2.8	
Meum	12.8	0.8	
Minuartia	12.3	1.2	
Minuartia rubra type	5.6	4.3	
Minuartia verna type	6.3	1.1	
Moehringia type	8.7	4.7	
Myosotis type	10.1	2.9	
Myrtus	12.9	2.9	
Nardus	7.8	2.9	
Odontites type	10.0	2.9	
Olea	12.3	2.9	I
Oleaceae	14.8	2.7	I
Onobrychis type	12.7	4.1	I
Ononis type	10.2	2.9	
Ostrya type	15.5	4.3	IV
Oxalis	13.6	2.9	
Oxyria type	7.8	2.9	
Papaver	18.9	2.9	
Papaver rhoeas group	10.1	2.9	
Papilionaceae	10.0	3.0	I
Parietaria	9.2	2.9	
Parnassia type	13.2	3.5	I
Paronychia type	10.9	2.6	I
Pedicularis	11.1	2.9	
Pedicularis palustris type	10.3	1.6	
Petasites type	9.2	2.9	
Peucedanum ostruthium	7.8	2.9	
Peucedanum type	11.2	3.0	I
Phillyrea type	15.6	3.3	
Phyteuma type	9.7	2.7	I
Picea	12.5	3.3	VII
Pimpinella major type	10.2	1.4	
Pinus undifferentiated	12.7	3.6	V
Pirus type	11.9	2.9	
Pistacia terebinthus	18.2	2.9	
Pistacia type	17.9	2.9	
Plantago lanceolata type	11.1	3.3	II
Plantago major type	10.7	2.8	I
Plantago maritima alpina type	10.2	2.1	III
Plantago media type	11.8	2.4	I
Plantago montana type	11.2	1.2	
Plantago type	14.5	3.0	III
Platanus	15.1	4.8	I
Poaceae	12.0	3.6	VII
Polygala vulgaris type	11.3	2.9	

Polygala type	14.1	5.4	
Polygonum alpinum	7.3	2.9	
Polygonum aviculare type	9.2	2.9	
Polygonum bistorta type	12.2	3.1	
Polygonum viviparum	12.7	2.9	
Polygonum type	13.6	3.4	I
Populus	13.9	3.2	I
Potentilla aurea	7.8	2.9	
Potentilla type	10.3	2.3	III
Poterium type	18.0	1.1	
Primula hirsuta type	8.7	1.8	
Primulaceae	12.8	4.2	
Prunus type	16.4	3.8	
Pulsatilla	10.1	1.9	
Quercus	13.7	3.6	II
Ranunculaceae	12.5	3.4	I
Ranunculus type	12.3	4.4	I
Ranunculus acris type	10.0	1.9	I
Rhamnaceae	19.5	2.9	
Rhamnus type	11.6	2.7	I
Rhinanthus type	14.9	3.3	
Rhododendron type	9.7	1.6	IV
Rhus	11.8	2.9	
Ribes	13.6	2.7	
Rosaceae	12.7	3.4	I
Rosa type	13.3	4.8	
Rubiaceae	12.6	4.1	I
Rubus type	12.7	2.7	
Rumex acetosa type	9.8	2.4	I
Rumex acetosella type	9.3	2.5	I
Rumex alpinus	9.7	1.9	I
Rumex conglomeratus type	5.7	2.9	
Rumex obtusifolius type	10.7	2.3	I
Rumex type	13.5	3.5	II
Sagina type	11.7	1.7	I
Salix	11.9	4.4	II
Salix helvetica type	7.8	2.9	
Salix herbacea type	7.8	2.9	
Sambucus	15.5	3.7	I
Sambucus nigra	10.0	3.4	I
Sambucus racemosa	9.8	1.2	
Sanguisorba minor type	15.8	4.0	I
Sanguisorba officinalis	12.8	3.8	
Sanguisorba type	14.5	1.8	
Sanicula type	16.4	1.2	
Sarothamnus scoparius	7.3	2.9	
Saussurea type	10.2	2.9	

Saxifraga	9.8	2.9	I
Saxifraga granulata type	9.3	2.5	I
Saxifraga oppositifolia type	9.0	2.4	II
Saxifraga paniculata type	10.0	1.3	
Saxifraga stellaris type	9.2	2.1	
Saxifragaceae	10.1	0.1	
Scabiosa type	12.6	5.1	
Scrophulariaceae	12.3	3.3	I
Scrophularia type	14.0	2.2	I
Secale type	11.5	3.5	I
Sedum type	11.4	3.8	I
Sempervivum	11.2	2.9	
Senecio type	10.3	3.6	I
Serratula type	10.5	1.8	
Setaria	4.7	2.9	
Silene dioica type	7.4	2.3	
Silene rupestris	7.8	2.9	
Silene vulgaris type	8.1	3.4	I
Silene type	12.5	1.4	
Solanaceae	8.6	2.9	
Solanum nigrum	9.6	2.9	
Soldanella	10.1	2.1	
Solidago type	12.7	4.7	I
Sorbus type	14.0	3.5	I
Spergula type	8.6	2.9	
Spermatophyta	15.6	2.9	
Stachys type	9.6	2.9	
Stellaria type	8.6	2.9	
Succisa pratensis type	17.2	2.9	
Taxus	15.1	1.6	
Teucrium type	18.0	1.6	
Thalictrum	9.7	3.1	I
Thesium	11.3	2.9	
Tilia	14.4	3.9	II
Trifolium alpinum type	10.9	0.9	
Trifolium badium type	12.9	0.2	
Trifolium pratense type	9.0	3.4	
Trifolium repens type	8.1	1.9	
Trifolium type	12.0	3.8	I
Trollius type	11.5	2.0	I
Ulmus	12.3	3.3	I
Urticaceae	13.3	3.6	I
Urtica type	10.2	2.5	II
Vaccinium	10.0	1.4	IV
Valeriana	13.9	1.1	
Valeriana officinalis type	11.7	2.9	
Valeriana tripteris type	10.9	2.6	

Valerianaceae	14.7	2.0	
Varia	9.2	2.9	
Veratrum type	9.7	0.6	
Veronica type	11.5	3.5	I
Viburnum	15.5	4.1	
Vicia	7.3	2.9	
Viola	9.8	0.2	
Viscum	18.4	2.9	
Vitis	13.6	4.4	I
Xanthium_type	16.4	3.4	I
Zea	12.1	3.2	

Supplementary Table S5 Calibration set 234 EMPD sites. Taxa are arranged in alphabetical order. The response models are restricted to taxa with ten or more occurrences.

	optima (°C)	tolerances (°C)	type of eHOF response models
Abies	13.1	3.2	VII
Acer type	14.4	3.1	IV
Achillea type	9.1	2.6	II
Aconitum type	11.3	2.8	
Adonis type	15.5	1.1	
Aesculus	13.0	2.8	
Alchemilla	9.4	2.1	I
Allium type	7.7	2.8	
Alnus glutinosa type	12.8	3.6	II
Alnus viridis	11.2	2.9	III
Ambrosia type	11.1	3.0	I
Androsace	13.4	5.3	
Anemone nemorosa type	9.5	2.0	I
Anthericum type	17.2	2.8	
Anthoxanthum	7.8	2.8	
Anthriscus sylvestris type	11.5	2.4	
Apiaceae	13.3	3.5	II
Arctostaphylos	9.0	0.8	
Arenaria type	6.2	2.4	
Armeria maritima type	8.9	3.2	
Arnica montana	10.1	1.5	
Artemisia	11.2	3.5	II
Astragalus alpinus type	4.4	3.6	
Astrantia type	13.0	2.3	
Athamanta cretensis	11.0	2.8	
Avena Triticum type	11.5	2.5	
Bartsia type	8.0	2.7	I

Betula	12.9	3.7	VII
Boraginaceae undifferentiated	12.6	3.8	I
Brassicaceae undifferentiated	11.5	3.5	I
Bupleurum type	11.6	4.2	
Buxus	12.4	3.7	
Calluna	11.0	2.6	I
Campanula	11.3	1.7	I
Campanulaceae	11.2	3.3	I
Cannabaceae type	10.2	1.2	
Cannabis	10.1	2.1	I
Cardamine type	7.8	2.8	
Carduus type	10.1	2.3	I
Carlina type	8.1	1.9	
Carpinus	15.3	3.6	II
Carum carvi	11.5	4.4	
Caryophyllaceae	10.3	3.1	II
Castanea sativa	14.1	4.3	VII
Cedrus	16.7	3.1	I
Celastraceae	14.7	2.8	
Centaurea collina	12.8	2.8	
Centaurea cyanus type	12.6	3.0	
Centaurea montana type	10.2	2.8	
Centaurea nigra type	12.7	3.6	I
Centaurea scabiosa type	14.2	6.1	
Centaurea type	14.4	2.8	
Cerastium type	9.7	3.7	I
Cerealia	13.4	3.6	II
Chaerophyllum type	10.8	3.4	I
Chenopodiaceae Amaranthaceae	12.1	3.6	I
Chrysanthemum alpinum	7.8	2.8	
Cirsium type	9.1	2.1	
Cistus	10.7	2.8	
Compositae subfam Asteroideae	11.8	3.3	I
Compositae subfam Cichorioideae	11.2	3.1	II
Convolvulaceae	18.4	2.8	
Cornus	9.2	2.8	
Corylus	13.4	3.7	VII
Crassulaceae	11.5	3.8	I
Crepis	7.8	2.8	
Cupressus type	16.2	2.8	
Cuscuta europaea type	14.4	4.2	
Cyclamen hederifolium	18.2	1.6	
Daucus type	7.7	2.6	
Deschampsia	7.8	2.8	
Dianthus type	13.7	4.3	I
Dipsacaceae	12.1	1.9	
Empetrum type	9.1	0.6	

Ephedra distachya type	8.6	2.8	
Ephedra fragilis type	11.9	5.8	
Ephedra type	10.6	2.8	
Epilobium type	13.5	2.6	I
Ericaceae	11.5	2.6	I
Erigeron	9.0	2.1	I
Eryngium type	10.0	2.8	
Eucalyptus	12.6	2.8	
Euonymus	18.6	2.8	
Euphorbia	9.8	2.8	
Euphorbiaceae	16.6	2.7	
Fabaceae	11.8	3.7	I
Fagus	13.6	3.4	VII
Filipendula type	13.2	3.8	I
Frangula	7.8	2.8	
Fraxinus	14.0	3.6	VII
Galeopsis type	11.7	2.8	
Gentiana nivalis type	7.8	2.8	
Gentiana pneumonanthe type	9.7	1.9	I
Gentiana purpurea type	7.8	2.8	
Gentianaceae	11.8	2.0	I
Gentianella campestris type	9.3	1.7	
Geranium type	12.6	3.3	I
Geum type	8.3	2.3	
Globularia	6.8	2.9	
Gnaphalium type	8.5	2.1	
Gypsophila type	18.0	2.8	
Hedera type	16.5	4.2	
Helianthemum type	11.9	3.3	I
Heracleum type	9.0	2.8	I
Herniaria type	4.1	2.8	
Hippophae	14.3	5.6	
Homogyne	7.9	1.8	
Hordeum type	12.1	3.9	
Humulus type	9.0	2.9	I
Hypericum perforatum type	10.3	1.4	I
Hypericum type	17.7	2.0	
Ilex	18.6	2.8	
Inula type	11.9	2.8	
Jasione type	11.3	2.8	
Juglans	13.0	3.6	I
Juncaceae	10.1	2.8	
Juniperus type	10.8	3.2	II
Knautia type	12.1	1.2	
Labiatae	12.5	3.4	I
Laburnum anagyroides	14.9	1.6	
Larix	11.2	2.6	IV

Laserpitium prutenicum	13.8	6.1	
Legousia	13.2	2.8	
Leontodon helveticus	7.8	2.8	
Ligusticum mutellina	8.0	1.5	I
Ligustrum vulgare type	13.9	5.9	
Liliaceae type	12.7	2.8	I
Lilium	17.2	2.8	
Linaria type	11.7	4.5	
Linum	10.9	0.3	
Lloydia serotina	9.2	2.8	
Lonicera type	12.2	3.0	
Lotus type	11.0	3.4	I
Luzula	11.4	3.8	I
Lythrum	15.6	6.4	
Melampyrum	10.0	2.0	I
Mentha type	9.2	2.5	I
Mercurialis	18.1	2.1	
Mercurialis annua type	9.8	2.8	
Meum	12.8	0.8	
Minuartia	12.3	1.2	
Minuartia rubra type	5.6	4.3	
Minuartia verna type	6.3	1.1	
Moehringia type	8.7	4.7	
Myosotis type	10.1	2.8	
Myrtus	12.9	2.8	
Nardus	7.8	2.8	
Odontites type	10.0	2.8	
Olea	12.3	2.9	I
Oleaceae	12.5	3.5	
Onobrychis type	12.7	4.1	I
Ostrya type	11.4	4.1	I
Oxalis	13.6	2.8	
Oxyria type	7.8	2.8	
Papaver	18.9	2.8	
Papaver rhoeas group	10.1	2.8	
Papilionaceae	9.6	2.4	
Parietaria	9.2	2.8	
Parnassia type	11.7	2.6	
Paronychia type	10.7	2.6	I
Pedicularis palustris type	10.3	1.6	
Peucedanum ostruthium	7.8	2.8	I
Peucedanum type	11.2	3.0	
Phyteuma type	9.9	2.6	I
Picea	12.2	3.2	VII
Pimpinella major type	10.2	1.4	
Pinus undifferentiated	11.8	3.3	IV
Pistacia type	17.9	2.8	

Plantago lanceolata type	10.8	3.1	II
Plantago major type	10.6	2.9	I
Plantago maritima alpina type	10.3	2.1	III
Plantago media type	11.3	1.2	I
Plantago montana type	11.2	1.2	
Plantago type	13.7	3.0	I
Platanus	15.0	5.0	I
Poaceae	11.6	3.4	VII
Polygala vulgaris type	11.3	2.8	
Polygala type	14.1	5.4	
Polygonum alpinum	7.3	2.8	
Polygonum bistorta type	12.4	3.3	
Polygonum viviparum	12.7	2.8	
Polygonum type	11.7	2.9	I
Populus	14.8	2.5	I
Potentilla type	10.2	2.2	III
Primula hirsuta type	8.7	1.8	
Primulaceae	13.8	3.9	
Prunus type	16.4	3.8	
Pulsatilla	10.1	1.9	
Quercus	13.0	3.5	II
Ranunculaceae	12.0	3.3	I
Ranunculus acris type	10.0	1.9	I
Rhamnus type	10.1	0.6	
Rhinanthus type	11.7	2.8	
Rhododendron type	9.8	1.6	IV
Rhus	11.8	2.8	
Ribes	14.4	1.0	
Rosaceae	12.4	3.3	I
Rosa type	10.6	1.6	
Rubiaceae	12.3	4.0	I
Rubus type	11.8	0.8	
Rumex acetosa type	9.8	2.4	I
Rumex acetosella type	9.3	2.6	I
Rumex alpinus	9.7	1.9	I
Rumex conglomeratus type	5.7	2.8	
Rumex obtusifolius type	10.7	2.3	I
Rumex type	13.3	3.6	II
Sagina type	11.8	1.6	I
Salix	11.4	4.3	II
Salix helvetica type	7.8	2.8	
Salix herbacea type	7.8	2.8	
Sambucus	14.8	3.9	
Sambucus nigra	10.2	4.5	
Sambucus racemosa	9.7	1.3	
Sanguisorba minor type	15.7	4.1	I
Sanguisorba officinalis	10.2	2.8	

Sanguisorba type	13.9	0.8	
Sanicula type	16.4	1.2	
Sarothamnus scoparius	7.3	2.8	
Saxifraga	9.7	2.9	I
Saxifraga granulata type	9.4	2.4	I
Saxifraga oppositifolia type	9.1	2.4	II
Saxifraga stellaris type	7.2	2.8	
Saxifragaceae	10.1	0.1	
Scabiosa type	12.6	5.1	
Scrophulariaceae	12.5	3.1	I
Secale type	10.6	3.0	I
Sedum type	11.4	3.9	I
Sempervivum	11.2	2.8	
Senecio type	9.5	2.3	
Serratula type	10.5	1.8	
Silene dioica type	7.4	2.3	
Silene rupestris	7.8	2.8	
Silene vulgaris type	8.1	3.4	I
Silene type	12.8	0.9	
Solanum nigrum	9.6	2.8	
Soldanella	10.1	2.1	
Solidago type	9.6	1.5	
Sorbus type	14.5	3.3	I
Spergula type	8.6	2.8	
Stachys type	9.6	2.8	
Stellaria type	8.6	2.8	
Succisa pratensis type	17.2	2.8	
Taxus	14.6	1.9	
Teucrium type	18.0	1.6	
Thalictrum	9.6	3.4	I
Thesium	11.3	2.8	
Tilia	14.1	4.0	II
Trifolium alpinum type	10.9	0.9	
Trifolium badium type	12.9	0.2	
Trifolium pratense type	9.0	3.4	
Trifolium repens type	8.1	1.9	
Trifolium type	12.0	3.8	I
Trollius type	11.5	2.0	I
Ulmus	12.1	3.2	I
Urticaceae	13.7	3.5	I
Urtica type	10.0	2.4	II
Vaccinium	9.9	1.1	IV
Valeriana	13.9	1.1	
Valeriana officinalis type	11.7	2.8	
Valeriana tripteris type	10.9	2.6	
Valerianaceae	14.8	2.2	
Veratrum type	10.0	2.8	

Veronica type	8.0	2.6	
Viburnum	15.1	4.5	
Vicia	6.3	2.6	
Viola	9.8	0.2	
Viscum	18.4	2.8	
Vitis	11.6	4.3	I
Xanthium type	16.4	3.4	I
Zea	12.6	3.5	

Supplementary Table S6 Calibration set 170 EMPD sites. Taxa are arranged in alphabetical order. The response models are restricted to taxa with ten or more occurrences.

Manuscript 2

(In preparation for Review of Palaeobotany and Palynology)

Modern pollen assemblages-vegetation-climate relationships along an elevational transect in the Upper Brembana Valley (Central Alps)

Giulia Furlanetto[1,2], Lorena Garozzo[2], Michele Brunetti[3], Cesare Ravazzi[2]

1 Univ. of Milano - Bicocca, Dept. of Environmental and Earth Sciences, Piazza della Scienza 1, Milano (I)

2 CNR - Institute for the Dynamics of Environmental Processes (IDPA), Laboratory of Palynology and Palaeoecology, Piazza della Scienza 1, Milano (I)

3 CNR- Institute of Atmospheric Sciences and Climate (ISAC), Bologna, Italy

1. Introduction

In mountain areas, climate parameters vary strongly with elevation, largely determining the zonation of vegetation, reflected in turn by the pollen rain record at different elevations. However, if relationships between plant composition in different vegetation belts and relative pollen percentages recorded in spectra from high-elevation sites are affected by local vegetation cover, they also depend on local slopes, exposure to dominant winds, and aspect. Very few studies of modern pollen deposition have been attempted in mountain environments of southern European countries (Court-Picon et al., 2005, 2006; Cañellas-Boltà et al., 2009; Ortu et al., 2010). Analyses of modern pollen assemblages are essential for a better understanding of fossil pollen sequences in a particular region, and thus for pollen-based palaeoenvironment and palaeoclimate reconstructions. Moss samples are commonly used as surface samples for local modern pollen deposition. They are assumed to record an average of several years of pollen deposition (Räsänen et al., 2004; Pardoe et al., 2010; Lisitsyna and Hicks, 2014) and can be profitably used as analogues for fossil pollen assemblages. Instead, pollen traps can be espressed both as percentages and Pollen Accumulation Rates (PAR). PAR measurements can be used as a modern

reference to estimate past plant population densities buffering the study site (Hicks, 2001; Tinner and Theurillat, 2003; Badino et al., 2018).

The aim of this study is to investigate modern pollen assemblages-vegetation-climate relationships along an elevational gradient. This paper presents a new elevational transect developed in the Upper Brembana Valley (Orobie Alps). Here modern pollen assemblages (pollen traps and moss samples), vegetation and climate have been collected at 16 sampling sites placed along an elevational gradient stretching from 1240 m asl to 2390 m asl. The transect has been designed (1) to understand how is the modern vegetation reflected in modern pollen assemblages from pollen traps and moss samples; (2) to estimate the relationships linking modern assemblages, vegetation, elevation and climate; (3) to provide a robust modern reference for reliable palaeoenvironmental and quantitative interpretations of past vertical shifts and changes in vegetation composition, as recognized in the pollen records from high-elevation sites.

2. Study area

The Upper Brembana Valley elevational transect extends along the uppermost section of a typical prealpine valley open to moist southern winds orographically forced uphill, between 1100 m and the headwalls at 2500-2700 m asl (**Fig. 1**). This region is marked by a *Dfc* climate (Köppen, 1923), i.e. nival, persistently wet throughout the year; locally, the annual temperature is 1.3 °C and lapse rate ranges from 0.56 °C/100 m in the mountain belt to 0.77 °C/100 m above the open forest limit. Mean annual precipitation is not significantly related with elevation (see **Table 1**). The site actually represents a snowfall extreme in the entire Alps, snow accumulation being concentrated in late winter and spring, and net snow accumulation summing up to 7 m at 1950 m asl (1964-1973 period, Belloni and Pelfini, 1990). The glacier Equilibrium Line Elevation under current climate conditions exceeds the mountain peaks; it was about 2600 m in 1994 AD (Caccianiga et al., 1994). The vegetation of the area provides a representative example of elevational ecological gradient in an oceanic climatic regime common in the Eastern and Northern Alps, and heavily affected by pastoralism. A belt of deciduous broad-leaved forest, largely fragmented by clearings, mowed meadows, and human settlements, extends between 1100 and 1400 m on sunny aspects. Here the dominant taxa are *Acer pseudoplatanus* and *Corylus avellana*. Chestnut and walnut trees (*Castanea sativa* and *Juglans regia*) have been planted up to 1100 m asl

on sunny slopes. A dark coniferous forest (*Picea abies, Abies alba, Larix decidua*) occurs only on shaded slopes, while wide areas in the subalpine belt (1400 to 2200 m asl) are covered by low pollen-producing larch forest. The canopy density of the larch forest is usually low, allowing the massive development of *Alnus viridis* understory thickets. The open forest upper limit is formed by larch at 2140 m asl. The uppermost limit of *Alnus viridis* is at 2240 m, while larch treeline reaches up 2220 m. At dry edaphic sites, isolated stands of mountain dwarf pine (*Pinus mugo*) form part of the timberline structure at 1800-2000 m asl. The crown cover of *Pinus cembra* is negligible. The wide development of graminoid-dominated alpine pastures and of xerophytic grasslands at timberline elevations and up to 2400 m is driven primarily by oceanic climates and by human impact in the last 4 ka (Furlanetto et al., 2018).

3. Materials and methods

3.1. Development of an elevational transect and sampling strategy

A transect composed by 16 sampling sites was developed (**Fig. 1**). The precise location and descriptive information of the sampling sites are listed in **Table 1**. At the center of each site, a pollen trap was located on the ground fixed to iron bars, three moss samples were collected within a circular area of 1.8 m radius (see **Fig. 2**, zone A) and mixed together (Cañellas-Boltà et al., 2009), while concentric circles of 1.8 and 10 m-radius were considered for vegetation surveys following the Braun-Blanquet method (**Fig. 2**). Furthermore, main arboreal species were listed and a cover estimation was carried out within a 100 m radius circle.

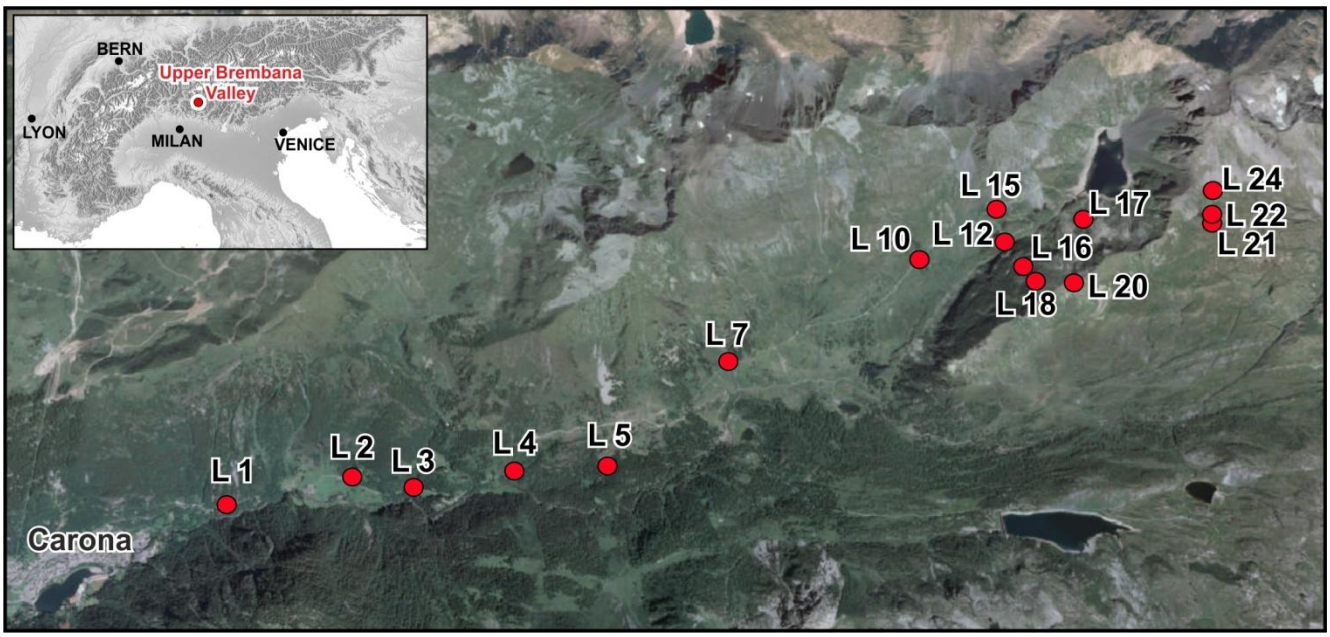

Fig. 1 Sampling sites for modern pollen assemblages and vegetation data stretching along an elevational gradient of 1200 m in the Upper Brembana Valley.

3.2. Estimation of climate normals along the elevational transect

Site-specific instrumental temperature and precipitation series, covering the 1951-2015 period, were reconstructed for each sampling site by means of the anomaly method (New et al., 2000; Mitchell and Jones, 2005) as described in Brunetti et al. (2012), to obtain a climate reconstruction as much representative of the specific locations as possible, thanks to the huge amount of meteorological observations available for Italy and surrounding areas. The interpolation procedure consists in the independent reconstruction of the climatological normals over a given reference period (i.e. climatologies) and the departures from them (i.e. the anomalies): the former, characterized by remarkable spatial gradients, were reconstructed by evaluating the local dependence of the meteorological variable on elevation (Brunetti et al., 2014; Crespi et al., 2018), and a high spatial density network of stations (even if with a limited temporal coverage) was used; anomalies are linked to climate variability and are characterized by a higher spatial coherence, therefore, a more simple interpolation technique and a low spatial density of stations are enough, but long temporal coverage and accurate homogenization (i.e. the procedure that removes the non-climatic signals introduced by stations and instruments relocation, changes in measurement practices and so on) are mandatory. Finally, climatologies and anomalies were superimposed to get temperature and precipitation monthly series in absolute values

for each sampling site. Information about the techniques and their accuracy are provided in Brunetti et al. (2014), Brunetti et al. (2012), and Crespi et al. (2018). From these monthly series, mean temperature of the warmest month (July), coldest month (January) and the total annual precipitation over the 1981–2010 period were calculated for the sampled sites.

Site acronym	Landscape and vegetation main features (from site center to 100 m radius)	Latitude (site centre)	Longitude (site centre)	Elevation m asl	Tjuly (°C)	Tjan (°C)	Pann (mm)
L 24	Open air shed ("bàrech") with droppings and discontinuous ruderal vegetation, in the distance petrophytic herb vegetation.	46° 2' 33.189" N	9° 52' 43.901" E	2393	11.5	-4.6	1865
L 22	Wet, low-tall grassland (*Nardus*) bordering a sedge peat bog and parcels of snow-bed and scree vegetation (*Salix herbacea, Chrysanthemum alpinum*).	46° 2' 26.642" N	9° 52' 44.263" E	2345	11.1	-4.9	1865
L 21	Tussock grassland (*Festuca* and *Nardus*)	46° 2' 25.534" N	9° 52' 44.319" E	2341	10.3	-5.5	1858
L 20	Juniper-Ericaceae dwarf heath (*Vaccinium* and *Rhododendron*) beyond the treeline, not grazed.	46° 2' 14.601" N	9° 52' 4.840" E	2283	9.5	-6.0	1843
L 18	Continuous *Rhododendron*-heath with larch tree individuals (4 m high, 30/40 years old).	46° 2' 15.344" N	9° 51' 51.616" E	2180	10.0	-5.7	1838
L 17	Ericaceae heaths in mosaic with low tall grassland and scattered larch trees.	46° 2' 26.690" N	9° 52' 6.433" E	2169	10.0	-5.7	1838
L 16	Mountain alder scrub with continuous understory of Ericaceae heath, and residual pasture clearings.	46° 2' 18.490" N	9° 51' 48.631" E	2106	11.2	-5.0	1852
L 15	Tussock grassland (*Festuca* gr. *varia*) with mountain alder groves and scattered larch individuals.	46° 2' 28.870" N	9° 51' 40.735" E	2105	11.5	-4.6	1864
L 12	Tussock grassland (*Festuca* gr. *varia*) in mosaic with juniper and Ericaceae dwarf scrub and a parcel of pasture	46° 2' 22.194" N	9° 51' 43.051" E	2009	12.1	-4.3	1865
L 10	Mountain alder scrub with thickets of the endemic tall herb *Sanguisorba dodecandra*.	46° 2' 18.621" N	9° 51' 18.009" E	1941	12.5	-4.1	1866
L 7	Grassland rich in basophilous herbs and petrophytic vegetation along an avalanche corridor.	46° 1' 57.943" N	9° 50' 21.535" E	1776	13.3	-3.5	1842
L 5	Pasture at the border of a mixed coniferous forest (*Larix* and *Picea*).	46° 1' 37.134" N	9° 49' 45.206" E	1672	13.9	-3.1	1834
L 4	Tussock grasslands (*Festuca* gr. *varia*), legume bushes (*Genista radiata*) in mosaic	46° 1' 36.211" N	9° 49' 17.909" E	1552			

	with mountain alder scrubs and tall herbs; thickets of the endemic tall herb *Sanguisorba dodecandra*.				14.6	-2.7	1828
L 3	River corridor and waterfalls with mountain alder scrub and tall herbs (including *Sanguisorba dodecandra*). In the surroundings, coniferous woodlands (*Picea-Larix), Larburnum* understory and mowed leans (*Pimpinella* and *Rumex)*.	46° 1' 33.239" N	9° 48' 48.401" E	1422	15.4	-2.2	1820
L 2	Mowed leans surrounded by thickets of broad-leaved trees (*Acer, Fraxinus*)	46° 1' 35.235" N	9° 48' 30.007" E	1360	15.7	-2.0	1821
L 1	Hazelnut scrubland and mixed coniferous (*Picea-Larix*), broad-leaved forests (*Sorbus aucuparia*, *Sorbus aria*), petrophytic habitats.	46° 1' 29.681" N	9° 47' 53.160" E	1244	16.4	-1.7	1783

Table 1 Site metadata for the Upper Brembana Valley elevational transect.

3.3. Vegetation data: surveying strategy (Braun-Blanquet system)

At each sampling site, vegetation surveys were carried out using the Braun–Blanquet abundance/dominance scale (Braun–Blanquet, 1979) within circular areas of 1.8 m radius (ca 10 m^2) and 10 m radius (ca 314 m^2). In this system, a semi-quantitative abundance-dominance index is used to estimate the plant cover for each species, according to the following scale: 5 (80-100%), 4 (60-80%), 3 (40-60%), 2 (20-40%), 1 (1-20%), + (scarce), r (rare). Finally, within the circular areas of 100 m radius was estimated the cover of the main species. This methodology was focused on producing good estimates of the abundance of the major taxa (the producers of the pollen types which are the major components of current and past pollen deposition in the study area) rather than recording every species present. Compared to plant species identification, pollen usually presents lower taxonomic resolution, in most cases only reaching genus or family level. To facilitate comparative data analyses plant species recorded in the vegetation surveys were grouped into higher taxonomic levels to match their corresponding pollen types and presented as percentages (see **Fig. 5**).

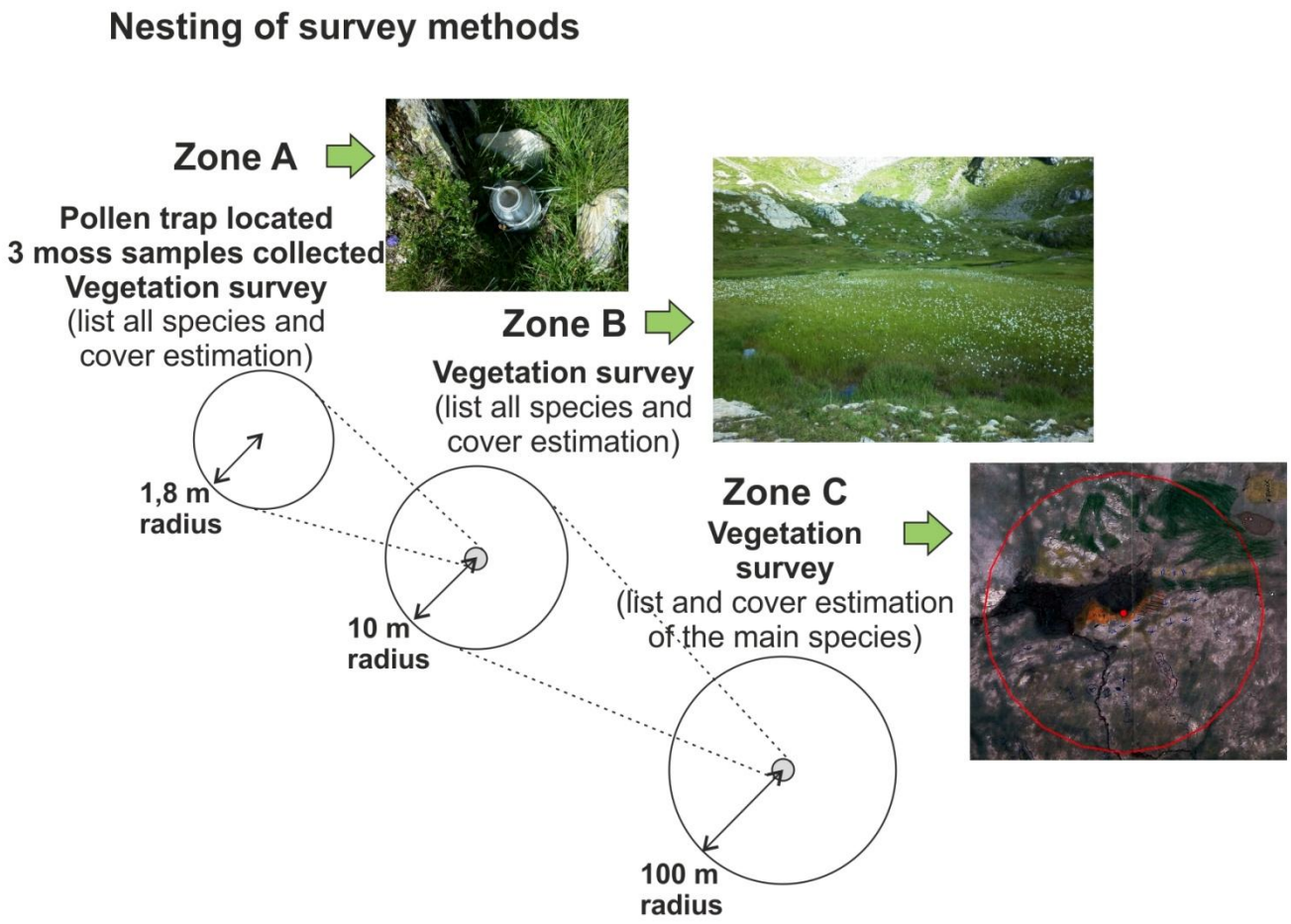

Fig. 2 Vegetation sampling method scheme used for each site of the Upper Brembana Valley elevational transect.

3.4. Pollen analysis - modern pollen assemblages

At the center of each site, a pollen trap was located (**Fig. 2**). The trap has a circular opening on top (4.5 cm in diameter), through which the airborne pollen can freely enter. Glycerine and thymol were placed in the trap to inhabit the growth of mould and the opening was covered by a 2 mm mesh fixed to the trap with duct tape. Pollen monitoring data represents the period 2016-2017. In each site, three moss polsters were also collected within a circular area of 1.8 m radius (ca 10 m^2) and mixed into one sample. Mosses were sampled down to, but not including, the mineral soil. Samples were processed following standard methods at the Laboratory of Palynology and Palaeoecology of CNR-IDPA in Milano, after adding *Lycopodium* tablets for pollen and pollen-slide microcharcoal concentration estimations (Stockmarr, 1971). A minimum count of 600 pollen grains was obtained at each sampling site, aquatics, spores and non-pollen

palynomorphs were excluded from the pollen sum. Identification was carried out at x400, x630 and x1000 magnifications under a Leica DM-LB light microscope. Pollen identification followed Moore et al. (1991), Punt and Blackmore (1976-2009), Reille (1992-1998), Beug (2004) and the CNR pollen reference collection. Pollen of *Pinus cembra* is separated from *Pinus sylvestris/mugo* type based on the following criteria: (1) presence of verrucae on the ventral surface of the grain body, (2) shape of sacci, more elongated than in *Pinus sylvestris*, (3) occurrence of a slightly undulating outer layer on the proximal surface of the grain body towards the sacci. Size classes of Alpine Poaceae pollen were distinguished by measuring grain diameter (D) and annulus diameter (d). Grains with D > 47 µm and d > 11 µm have been referred to cereals (cultivated *Avena* and *Triticum* species, i.e. Cerealia type *sensu* Joly et al., 2007). These size limits (Joly et al., 2007), more restrictive than those currently used in the Alpine region (Andersen, 1979), allow to separate an intermediate type having D 37-47 µm and D > 47 + d < 11 µm which includes both wild and cereal species (Andersen, 1979; Joly et al., 2007), e.g. a few wild *Avena* species previously listed in the *Avena*-*Triticum* group such as *Avena versicolor* which occurs at the site. We preferred to use a sum of apophytes and cultivated plants instead of anthropogenic indicators. Microbiological particles were named after van Geel et al. (1981), van Geel (1978) and van Geel and Aptroot (2006) and expressed as % out of the pollen sum. Among the Sordariaceae family, spores of several dung fungi were identified (*Sporormiella*-like, *Sordaria*, *Podospora* spores). The *taxon* Sordariaceae undiff. includes spores not assigned to a specific genus and sharing the same morphological aspect, i.e. dark brown to black in color, smooth surface, apical pore(s), one flat or slightly pointed end. The Sordariaceae undiff. curve does not include *Gelasinospora* and *Neurospora*, sporadically encountered in the analyzed samples and identified based on their characteristic morphology. Pollen-slide microcharcoal particles were counted under a light microscope at 400x. Black, completely opaque and angular fragments (Clark, 1988) were identified as charcoal and grouped in two size classes (10–50 µm and 50–250 µm length).

3.5. Data analyses

Ordination techniques are considered appropriate for assessing and displaying the relationship between pollen percentages recorded in modern pollen assemblages, vegetation data, elevation and climatic parameters. These statistical analyses have been

frequently used to detect structures or patterns within pollen and vegetation data. They provide an efficient low-dimensional representation of complex multivariate data and serve to indicate their major gradients and the relative contribution of each *taxon* to each of these gradients. All the plants present an ecological optimum and tolerance to most environmental gradients, justifying the use of a biological unimodal response model (ter Braak, 1987, 1988). In this work, Canonical Correspondence Analysis (CCA), the constrained form of CA (ter Braak 1986) was used as direct gradient analysis to highlight the relationships between pollen, vegetation, elevation and climate. Several CCA ordinations have been performed using elevation, July temperature, January temperature and annual precipitation as the sole constraining variable to assess their importance on the variance of pollen and vegetation (1.8 m and 10 m radius) assemblages (see **Table 2**). Prior to the CCA analysis, pollen percentages were square-root transformed, for variance stabilization (Prentice, 1980) and pollen taxa with percentages below 2%, were removed. In the vegetation analysis, rare elements (those designed with '+' and 'r') were not considered. The significance of all CCA were tested with ANOVA (p <0.05, after 999 unrestricted permutations).

Individual responses of uphill transported pollen types and potential indicator taxa from the subalpine belt were obtained using the Extended Huisman-Olff-Fresco fitting method (**Figs. 6-7**), which considers a set of hierarchical models in a generalized linear modelling framework (Huisman et al., 1993; Jansen and Oksanen, 2013) with eHOF package (Jansen and Oksanen, 2017). These models are designed as I (flat response, no optima), II (monotonic, optima is at the gradient extremes), III (plateau, there is an optimum range), IV (symmetric unimodal, single point optima), V (skewed unimodal, single point optima), VI (symmetric bimodal, two optima) and VII (skewed bimodal, two optima).

4. Results

4.1. Modern pollen assemblages and their relationship to vegetation

The pollen spectra of 18 pollen traps and 16 moss samples are presented in synthetic percentage diagrams, which include selected pollen types and total microcharcoal concentrations (**Figs. 3-4**). Plant species recorded in the 10 m vegetation surveys,

grouped into higher taxonomic levels to match their corresponding pollen types are presented in a synthetic percentage diagram (**Fig. 5**).

In the site L 1 located at 1244 m asl (**Fig. 5**) the main vegetation species are *Corylus avellana*, *Picea abies* and *Larix decidua* among trees and shrubs; *Festuca* sp. and *Laserpitium halleri* and *Laserpitium krapfii* among herbs. In the pollen traps the dominant taxa are *Picea*, *Corylus* and Poaceae (see **Fig. 3**, TL1-TL2) while *Corylus*, *Ostrya* type, *Fraxinus excelsior* type, *Pinus sylvestris/mugo,* and *Larix* represent the main taxa in the moss samples (see **Fig. 4**, ML1-ML2). Pollen taxa from broad-leaved tree species 10 to 20 km distant from the lowermost site in the elevational transect (e.g. *Castanea*, and *Ostrya* type) are washed out by orographic rain or transported by winds and occur in high proportions (see **Figs. 3a-4a**). *Alnus viridis* reaches high cover percentages (10-30%) in sites L 3 and L 4 located next to streams and also in the site L 10 (30%) located in an avalanche corridor/stream (**Fig. 5**), this abundance in *Alnus viridis* is also presented in modern pollen assemblages (**Figs. 3a-4a**). Sites L 3 and L 4 show also high cover percentages of *Festuca scabriculmis* (50-70%)*, Galium lucidum* (30%)*, Pimpinella major* (10%) and the endemic tall herb *Sanguisorba dodecandra* (10%)*,* while the site L 10 shows the 50% of *Agrostis* sp., 30% of *Festuca scabriculmis* and 30% cover of *Sanguisorba dodecandra*. The sites L 2 and L 5 are respectively located in mowed leans surrounded by thickets of broad-leaved trees and in a pasture at the border of a mixed coniferous forest. In the 10 m vegetation survey (L 2) *Pimpinella major* has the 30% of cover, followed by the 10% of *Alchemilla vulgaris*, *Geranium sylvaticum*, *Heracleum sphonodylium, Rumex scutatus*, *Trifolium pretense* and *Polygonum bistorta;* in the site L 5 *Laburnum alpinum* has the 50% of cover, *Picea abies* 20 %, *Larix decidua* 10%, among herbs *Festuca pratensis* has the 20 % of cover. The site L 7, a grassland along an avalanche corridor presents the 10 % of *Picea abies* and *Larix decidua* (**Fig 5a**); among herbs the 30% of *Calamagrostis* sp., *Rhinanthus* sp. and *Sanguisorba dodecandra*. *Sanguisorba dodecandra* is well represented in the pollen trap (trap TL7, **Fig. 3b**) reaching the 18%. The sites L 12–L 18 are located in the upper subalpine belt with Ericaceae moorlands (*Erica* carnea, Vaccinium *gaultherioides*, *Vaccinium myrtillus Rhododendron ferrugineum* and *Loiseleuria procumbens*) and *Alnus viridis* thickets with *Larix decidua* individuals; larch treeline is located at 2220 m. *Juniperus nana* shows high cover percentages in the sites L 12 and L 15. In the sites (L 12-L 18) the pollen trap and moss sample assemblages are dominated by *Alnus viridis*, *Pinus sylvestris/mugo,* and Poaceae, the Ericaceae moorland is well represented by *Vaccinium* while *Erica*, *Rhododendron* and

Loiseleuria show sporadic occurrences (see **Figs. 3a-4a**). Above 2100 m asl the wind-driven uphill transport of pollen from the lower belts shows increased percentages of *Pinus sylvestis/mugo*, *Betula*, *Corylus*, *Ostrya* type, *Fagus,* and *Carpinus betulus* in the moss samples and increased percentages of *Picea*, *Betula*, *Corylus* and *Castanea* in the pollen traps. In sites (L 21-L 24) the 10 m vegetation is dominated by *Festuca scabriculmis*, *Festuca quadriflora*, *Carex sempervirens* (L 21); *Salix herbacea*, *Chrysanthemum alpinum Potentilla aurea* (L22); *Cirsium spinosissimum*, *Poa alpina*, *Rumex alpestris* and *Potentilla aurea* (L 24). The site L 24 (2390 m asl) is located in an extensive pasture, reflected in modern pollen assemblages by high percentages of Poaceae and of dung spores (Sordariaceae undiff., *Sporormiella*-like spores*,* and *Podospora*).

Fig. 3 Percent diagram of pollen traps from the Upper Brembana Valley elevational transect showing selected pollen taxa and main vegetation zones.

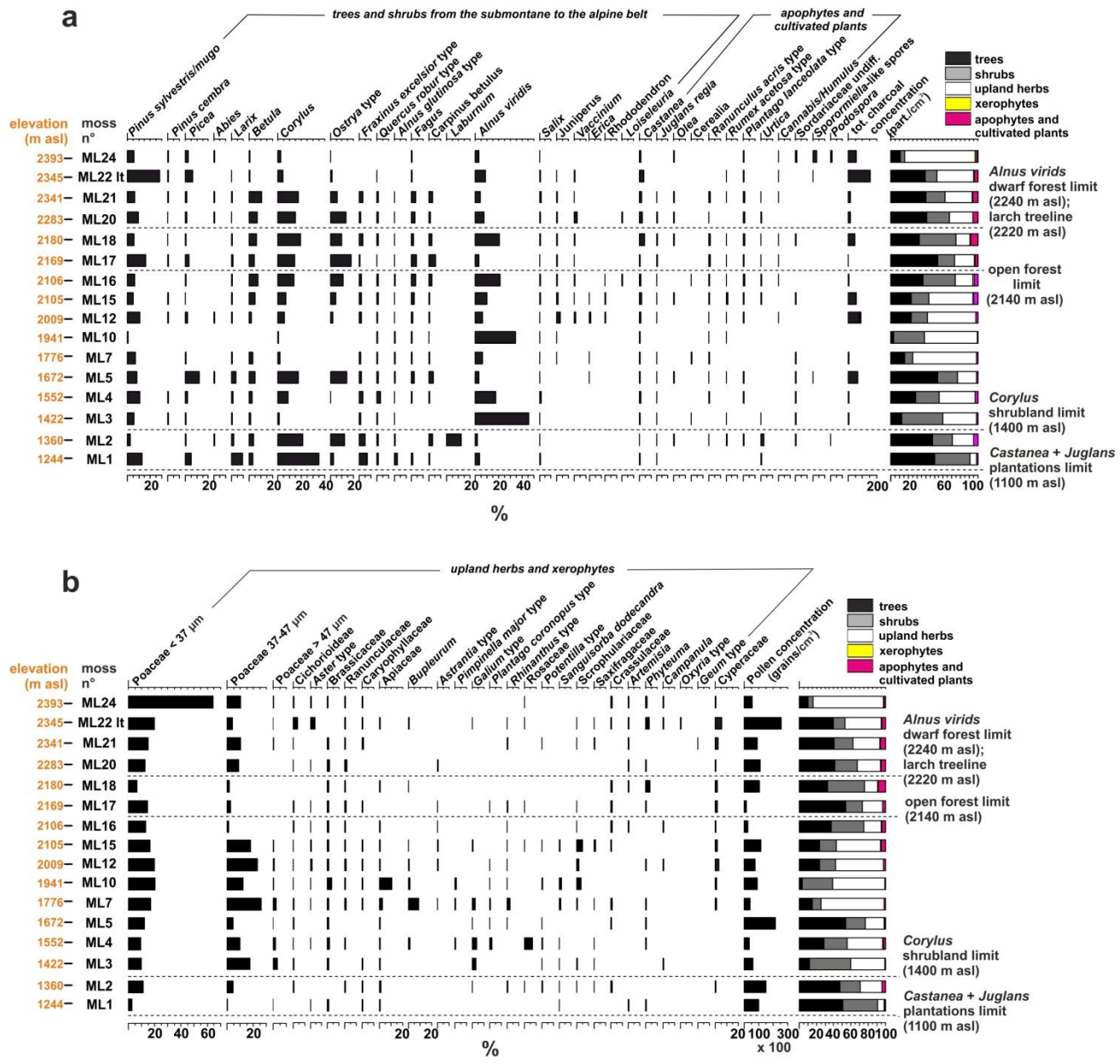

Fig. 4 Percent diagram of moss samples from the Upper Brembana Valley elevational transect showing selected pollen taxa and main vegetation zones.

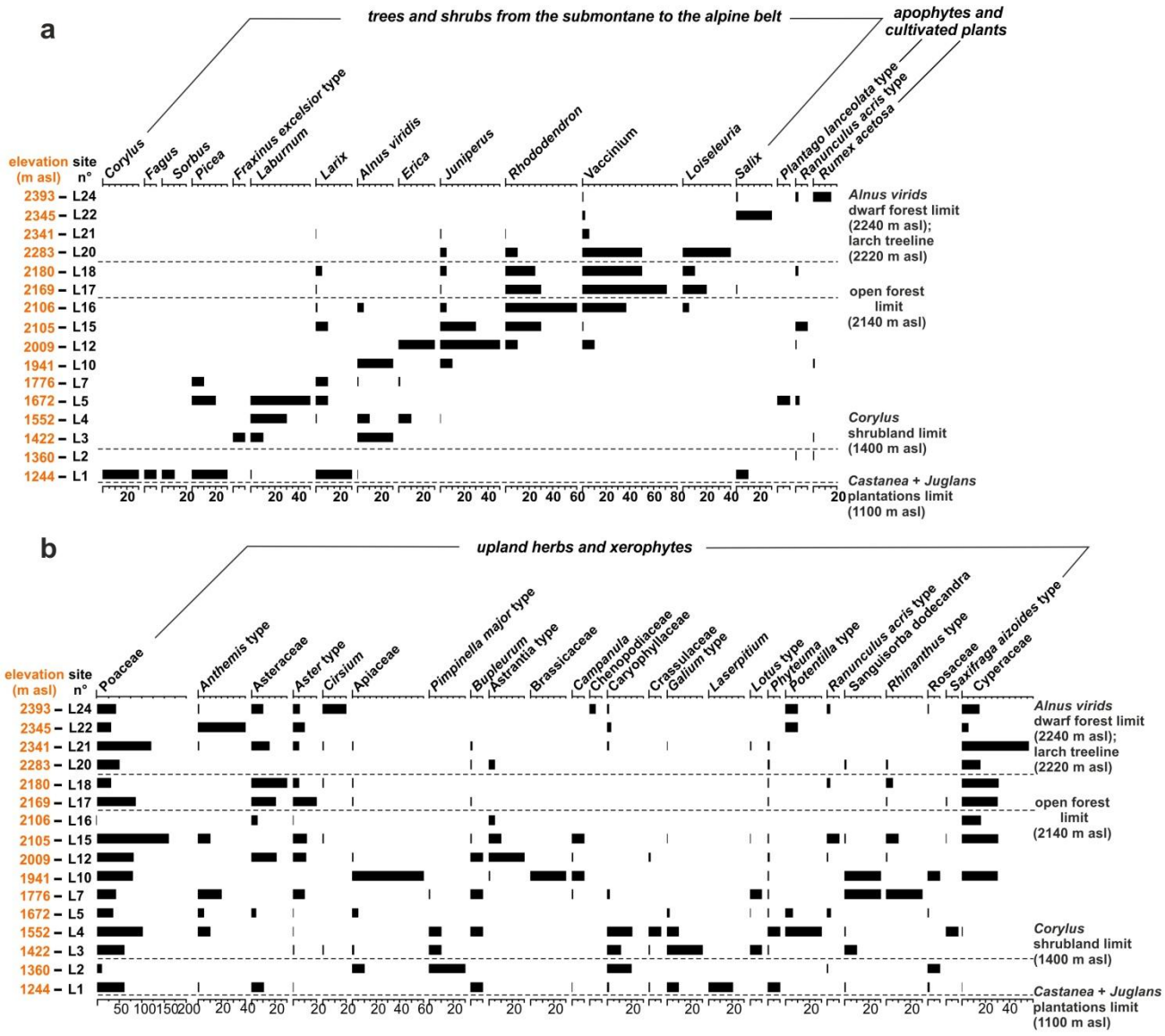

Fig. 5 Percent diagram of selected plant species from the Upper Brembana Valley elevational transect recorded in the 10 m vegetation surveys. Species were grouped into higher taxonomic levels to match their corresponding pollen types. In order to allow comparison with pollen assemblages the same taxa presented in the pollen diagrams were selected.

4.2. Canonical Correspondence Analysis (CCA)

This study aims at emphasizing pollen/vegetation/climate relationships at a local scale. Indeed, although extra-local and regional non-arboreal pollen is present in the modern pollen spectra, herbaceous pollen assemblages appear to reflect predominantly local vegetation rather than wider landscape units, as also demonstrated by Caseldine and Pardoe (1994), Hjelle (1999) and Pardoe (2001). The variances explained by elevation and each climate parameter (Tjuly, Tjan and Pann), calculated with CCA ordinations with unique constrained, are presented in **Table 2**. The Canonical Correspondence Analysis (CCA) of the vegetation data and pollen assemblages suggests that the variation in vegetation and pollen is strongly correlated to the elevational gradient (**Table 2**). In both vegetation data and pollen assemblages elevation explains more variance than the climate parameters. For the pollen traps the variance explained by elevation is 17 %, by Tjuly 16.6%, by Tjan 16.9 and by Pann 12.7 %. For the moss samples the variance explained by elevation is 14.6 %, by Tjuly 14.4 %, by Tjan 14.5 % and by Pann 10.9 %. Pann is not significant in the moss samples assemblage ($p > 0.05$, after 999 unrestricted permutations). For the vegetation 1.8 m the variance explained by elevation is 12.6 %, by Tjuly 12.3 %, by Tjan 12.4 % and by Pann 12 %. Finally for the vegetation 10 m the variance explained by elevation is 15.6%, by Tjuly 15.4 %, by Tjan 15.4 % and by Pann 14 %.

Pollen traps				
	elevation	Tjuly	Tjan	Pann
variance explained	17.06	16.61	16.91	12.66
p	0.001 ***	0.001 ***	0.001 ***	0.009 **
Moss samples				
	elevation	Tjuly	Tjan	Pann
variance explained	14.58	14.41	14.49	10.87
p	0.005 **	0.008 **	0.01 **	0.108
Vegetation 1.8 m Radius				
	elevation	Tjuly	Tjan	Pann
variance explained	12.64	12.34	12.35	12.02
p	0.001 ***	0.003 **	0.001 ***	0.001 ***

Vegetation 10 m Radius				
	elevation	Tjuly	Tjan	Pann
variance explained	15.61	15.39	15.43	13.99
p	0.001 ***	0.001 ***	0.001 ***	0.001 ***

Significance codes: *** 0.001; **0.01

Table 3. Proportions of variance explained by each explanatory variable as the sole constrained and permutational-repeated measures analysis (ANOVA) obtained for modern pollen assemblages (pollen traps and moss samples) and vegetation data (surveys at 1.8 m and 10 m radius circles).

5. Discussion

5.1. Pollen-vegetation-elevation relationships

Our data are in agreement with previous studies which identified elevation as the main gradient controlling modern pollen assemblages and vegetation distribution across mountain regions (Bonnefille et al., 1993; Vincens et al., 1997; Weng et al., 2004; Court-Picon 2005, 2006; Rull, 2006; Cañellas-Boltà et al., 2009). The Canonical Correspondence Analysis (CCA) showed that elevation explains the major percentage of variance in both vegetation data and pollen assemblages (**Table 2**).

5.1.1. Uphill pollen transport

The uphill transport of pollen by wind to subalpine and alpine zones was first recorded in the European Alps (Markgraf, 1980; David, 1997; Frei, 1997; Brugiapaglia et al., 1998; Ortu, 2002). Markgraf (1980) showed that, in a steep valley-slope system of Alpine type, the proportion of pollen dispersal from local uphill winds in daytime decreases with increasing elevation in favor of regional (medium-distance) dispersal. This high-elevation dispersal component relies significantly on pollen washout by rain, which cleans the atmosphere of suspended pollen (Markgraf, 1980). Pollen belts tend to be wider and with less defined boundaries than vegetation; this is likely due to the homogenizing effect of wind dispersal, especially from lower to upper altitudinal levels. Thus, if it is possible to identify the major vegetation types by means of their modern pollen deposition, it becomes more difficult to identify specific thresholds (e.g. treeline).

The over-representation of *Pinus* in the pollen assemblages is well documented by numerous authors (e.g. Broström et al. 1998; Brugiapaglia et al. 1998; Ortu et al. 2005, 2006; Court- Picon et al., 2005, 2006, Cañellas-Boltà et al., 2009). The strong pollen signal of *Pinus sylvestris/mugo* is recorded in the moss samples above the treeline (see **Fig. 4a**, ML17-24), while *Pinus mugo* is not recorded in the vegetation data (see **Fig. 5-6**). In the study area, isolated stands of mountain dwarf pine (*Pinus mugo*) form part of the timberline structure at 1800-2000 m asl at dry edaphic sites.

A dark coniferous forest (*Picea abies, Abies alba, Larix decidua*) occurs only on shaded slopes, therefore *Picea abies* appears in the 10 m vegetation surveys only in sites L 1, L 5 and L 7 (**Fig. 5a**) and shows a monotonic response (**Fig. 6**). In the pollen traps and moss samples *Picea* shows a flat response with no optima (**Fig. 6**) and a marked uphill transport to subalpine and alpine zones in the pollen traps (**Fig. 3a**).

Deciduous trees of the mountain belt (e.g. *Corylus, Betula, Ostrya, Castanea*) also show uphill wind transport. *Castanea* uphill transport is marked in pollen traps (**Figs. 3a-6**) while *Corylus* and *Ostrya* show high percentages in the moss samples ML16-21 between 2106 and 2341 m asl (**Fig. 4a**). The influence of upslope wind dispersal of medium- to long-distance transported pollen types (e.g. *Castanea* and *Ostrya* type) have to be taken into account and interpreted with caution in the fossil records.

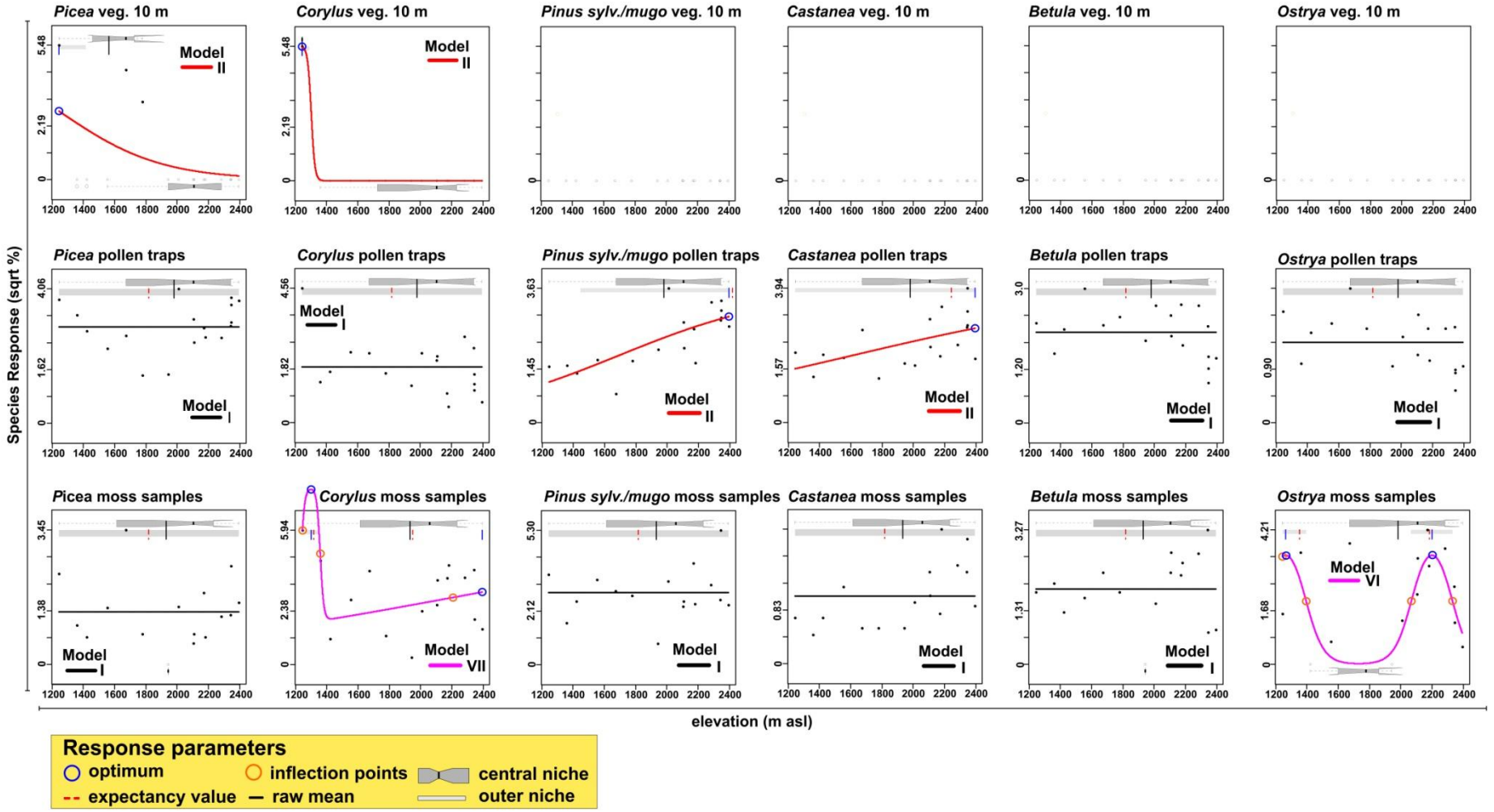

Fig. 6 Diagrams showing the simplest statistically significant response model for *Picea*, *Corylus*, *Pinus sylvestris mugo*, *Castanea*, *Betula* and *Ostrya* from the vegetation data (10 m radius) and modern pollen assemblages (pollen traps and moss samples) in relation to elevation as assessed by a hierarchical set of *taxon* response models within the framework of generalized linear modelling.

5.1.2. Potential indicator taxa of subalpine/alpine belts

Extensive mountain alder shrublands develop in the subalpine elevational belt under oceanic, cool temperate climates, that hinder cembran pine fitness. Edaphic geodiversity allows mountain alder to compete with dwarf pine (*Pinus mugo*), the latter also tolerating oceanic climates, but escaping edaphic wetness. *Alnus viridis* shows a skewed bimodal response (model VII) in both pollen traps and moss samples (**Fig. 7**). *Alnus viridis* vegetation needs a continuous water supply during the growing season, enhanced by high annual snowfall rate and good soil water balance (Richard, 1968, 1969; Mauri and Caudullo, 2016). In Alpine oceanic climates, its ecological range expands downstream especially along avalanche corridors but also on northern slopes, due to a general increase in soil moisture, and thus optima are shifted towards lower elevations (**Fig. 7**). For this reason it shows a symmetric unimodal response in the 10 m radius vegetation data but with lower elevation optima compared to continental inner valleys (Furlanetto et al., accepted) and a skewed bimodal distribution in pollen traps and moss samples.

Ericaceae is considered an excellent indicator of the montane/subalpine belts (Cañellas-Boltà et al., 2009). In our study, the identification of pollen types within this family allows to highlight different altitudinal patterns of pollen and relative parent taxa. In the 10 m vegetation surveys *Erica*, *Vaccinium* and *Rhododendron* show a symmetric unimodal response, while *Loiseleuria* a skewed unimodal response (**Fig. 7**). Interestingly, *Vaccinium*, *Rhododendron* and *Loiseleuria* show a consistent pollen–vegetation elevational pattern restricted to the belt between 2000 and 2300 m asl. Whereas *Erica* pollen type shows a wider distribution especially in pollen traps from 1422 to 2345 m asl (**Fig. 3a**) even though it is recovered in the 10 m vegetation surveys between 1550 and 2000 m asl (**Fig. 5**).

Also *Juniperus* shows a symmetric unimodal response in both vegetation and pollen traps with an optima at ca. 2000 m (**Fig. 7**).

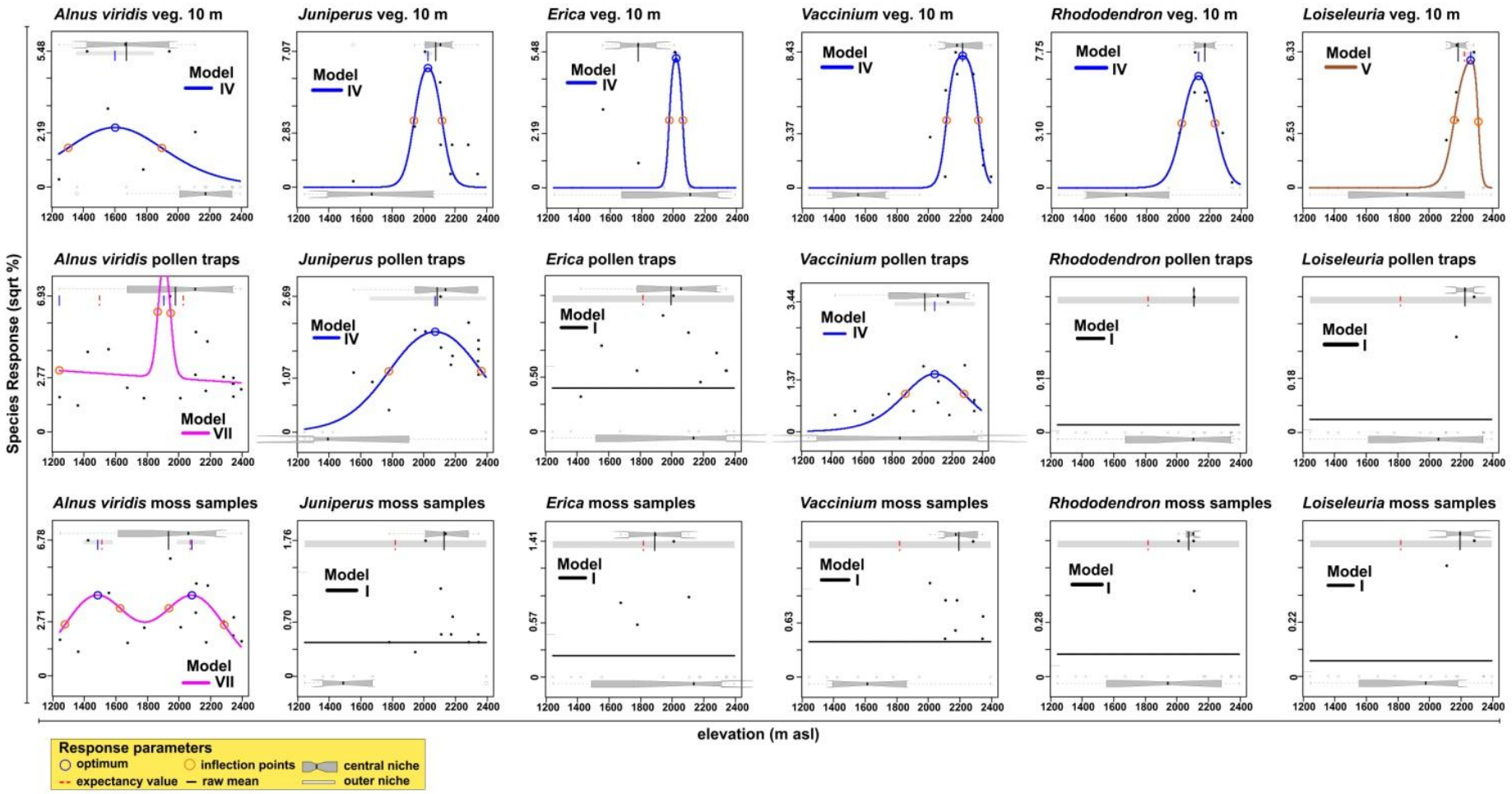

Fig. 7 Diagrams showing the simplest statistically significant response model for *Alnus viridis*, *Juniperus*, *Erica*, *Vaccinium*, *Rhododendon* and *Loiseleuria* from the vegetation data (10 m radius) and modern pollen assemblages (pollen traps and moss samples) in relation to elevation as assessed by a hierarchical set of *taxon* response models within the framework of generalized linear modelling.

6. Conclusions

The development of an elevational transect in the Upper Brembana Valley (Central Alps) represents a first step in understanding the complex relationships between modern pollen assemblages, vegetation, elevation and climate. The results of CCA analysis demonstrated a general good agreement with previous studies, which identified elevation as the main gradient in the variation of modern pollen and vegetation assemblages in mountain areas.

The uphill transport of pollen by wind to subalpine and alpine zones implies wider pollen belts with less defined boundaries than vegetation. This is mainly due to the increase in extra-local transport of strong pollen producers (e.g. *Pinus sylvestris/mugo*, *Picea*, *Castanea*, *Corylus* and *Ostrya*) and lead to some homogenization of pollen assemblages. Thus, if it is possible to identify the major vegetation types by means of their modern pollen deposition, it becomes more difficult to identify specific thresholds (e.g. treeline). To overcome these limitations, potential indicator pollen taxa of alpine/subalpine belts documented in this study could be useful for this purpose: *Vaccinium*, *Rhododendron*, *Loiseleuria*.

Local studies along elevational gradients orientated to facilitate the interpretation of past vertical shifts and changes in vegetation composition.

References

Andersen, S.T., 1979. Identification of wild grass and cereal pollen. Årbog, Danmarks Geologiske Undersoegelse 1978, 69-92.

Badino, F., Ravazzi, C., Vallè, F., Pini, R., Aceti, E., Brunetti, M., Champvillair, E., Maggi, V., Maspero, F., Perego, R., Orombelli, G., 2018. 8800 years of high-altitude vegetation and climate history at the Rutor Glacier forefield, Italian Alps. Evidence of middle Holocene timberline rise and glacier contraction. Quaternary Science Reviews 185, 41-68.

Belloni, S., Pelfini, M., 1990. La nevosità in Lombardia nel periodo 1964-1973. Natura Bresciana 25, 63-108.

Beug, H.J., 2004. Leitfaden der Pollenbestimmung für Mitteleuropa und angrenzende Gebiete. Verlag Dr. Friedrich Pfeil, München, Germany.

Bonnefille, R., Buchet, G., Friis, I.B., Kelbessa, E., Mohammed, M.U., 1993. Modern pollen rain on an altitudinal range of forests and woodlands in South West Ethiopia. Opera Botanica 121, 71-84.

Braun-Blanquet, J., 1979. Fitosociologica. Blume, Madrid.

Brugiapaglia, E., de Beaulieu, J.L., Guiot, J., Reille, M., 1998. Transect de pluie pollinique et étagement de la végétation dans le massif du Taillefer (Isère, France). Géographie physique et Quaternaire 52(2), 209-218.

Brunetti, M., Lentini, G., Maugeri, M., Nanni, T., Simolo, C., Spinoni, J., 2012. Projecting North Eastern Italy temperature and precipitation secular records onto a high-resolution grid. Physics and Chemistry of the Earth 40–41, 9–22.

Brunetti, M., Maugeri, M., Nanni, T., Simolo, C., Spinoni, J., 2014. High-resolution temperature climatology for Italy: interpolation method intercomparison. International Journal of Climatology 34(4), 1278–1296.

Caccianiga, M., Ravazzi, C., Zubiani, P., 1994. Storia del ghiacciaio del Trobio (Alpi Orobie, Bergamo) e colonizzazione della vegetazione nelle aree liberate dopo la Piccola Età Glaciale. Natura Bresciana 29, 65-96.

Cañellas-Boltà, N., Rull, V., Vigo, J., Mercadé, A., 2009. Modern pollen-vegetation relationships along an altitudinal transect in the central Pyrenees (southwestern Europe). The Holocene 19(8), 1185-1200.

Caseldine, C., Pardoe, H., 1994. Surface pollen studies from alpine/sub-alpine southern Norway: applications to Holocene data. Review of Palaeobotany and Palynology 82(1), 1-15.

Clark, J.S., 1988. Particle motion and the theory of charcoal analysis: source area, transport, deposition, and sampling. Quaternary Research 30(1), 67-80.

Court-Picon, M., Buttler, A., de Beaulieu, J.L., 2005. Modern pollen–vegetation relationships in the Champsaur valley (French Alps) and their potential in the interpretation of fossil pollen records of past cultural landscapes. Review of Palaeobotany and Palynology 135(1), 13-39.

Court-Picon, M., Buttler, A., de Beaulieu, J.L., 2006. Modern pollen/vegetation/land-use relationships in mountain environments: an example from the Champsaur valley (French Alps). Vegetation history and Archaeobotany 15(3), 151-168.

Crespi, A., Brunetti, M., Lentini, G., Maugeri, M., 2018. 1961–1990 high-resolution monthly precipitation climatologies for Italy. International Journal of Climatology 38, 878–895.

David, F., 1997. Holocene tree limit history in the northern French Alps stomata and pollen evidence. Review of Paleobotany and Palynology 97, 227–237.

Frei, T., 1997. Pollen distribution at high elevation in Switzerland: Evidence for medium range transport. Grana 36, 34–38.

Furlanetto, G., Ravazzi, C., Pini, R., Vallè, F., Brunetti, M., Comolli, R., Novellino, M.D., Garozzo, L., Maggi, V., 2018. Holocene vegetation history and quantitative climate reconstructions in a high-elevation oceanic district of the Italian Alps. Evidence for a middle to late Holocene precipitation increase. Quaternary Science Reviews 200, 212-236.

Hicks, S., 2001. The use of annual arboreal pollen deposition values for delimiting tree-lines in the landscape and exploring models of pollen dispersal. Review of Palaeobotany and Palynology 117(1-3), 1-29.

Hjelle, K.L., 1999. Modern pollen assemblages from mown and grazed vegetation types in western Norway. Review of Palaeobotany and Palynology 107(1), 55-81.

Huisman, J., Olff, H., Fresco, L.F.M., 1993. A hierarchical set of models for species response analysis. Journal of Vegetation Science 4, 37–46.

Jansen, F., Oksanen, J., 2013. How to model species responses along ecological gradients – Huisman–Olff–Fresco models revisited. Journal of Vegetation Science 24, 1108–1117.

Jansen, F., Oksanen, J., 2017. Extended HOF (Huisman-Olff-Fresco) Models. R Package Version 1.8.

Joly, C., Barillé, L., Barreau, M., Mancheron, A., Visset, L., 2007. Grain and annulus diameter as criteria for distinguishing pollen grains of cereals fromwild grasses. Review of Palaeobotany and Palynology 146, 221-233.

Lisitsyna, O.V., Hicks, S., 2014. Estimation of pollen deposition time-span in moss polsters with the aid of annual pollen accumulation values from pollen traps. Grana 53(3), 232–248.

Markgraf, V., 1980. Pollen Dispersal in a Mountain Area. Grana 19, 127–146.

Mauri, A., Caudullo, G., 2016. *Alnus viridis* in Europe: distribution, habitat, usage and threats. In: San-Miguel-Ayanz J, De Rigo D, Caudullo G, Houston Durrant T, Mauri A (eds) European Atlas of Forest Tree Species. Publication Office of the European Union, Luxembourg, p. 68.

Mitchell, T.D., Jones, P.D., 2005. An improved method of constructing a database of monthly climate observations and associated high-resolution grids. International Journal of Climatology 25(6), 693-712.

Moore, P.D., Webb, J.A., Collinson, M.E., 1991. Pollen analysis. Blackwell Scientific Publications, Oxford.

New, M., Hulme, M., Jones, P., 2000. Representing twentieth-century space-time climate variability. Part II: Development of 1901-96 monthly grids of terrestrial surface climate. Journal of Climate 13, 2217-2238.

Ortu, E., 2002. Reconstruction sur base pollinique de la dynamique de la végétation tardiglaciaire et holocène dans les Alpes Maritimes Italiennes. PhD Thesis, University d'Aix-Marseille III, F.

Ortu, E., Klotz, S., Brugiapaglia, E., Caramiello, R., Siniscalco, C., 2010. Elevation-induced variations of pollen assemblages in the North-western Alps: An analysis of their value as temperature indicators. Comptes rendus biologies 333(11), 825-835.

Pardoe, H.S., 2001. The representation of taxa in surface pollen spectra on alpine and sub-alpine glacier forelands in southern Norway. Review of Palaeobotany and Palynology 117(1), 63-78.

Pardoe, H.S., Giesecke, T., van der Knaap, W.O., Svitavská-Svobodová, H., Kvavadze, E.V., Panajiotidis, S., Gerasimidis, A., Pidek, I.A., Zimny, M., Święta-Musznicka, J., Latałowa, M., Noryśkiewicz, A.M., Bozilova, E., Tonkov, S., Filipova-Marinova, M.V., van Leeuwen, J.F.N., Kalniņa, L., 2010. Comparing pollen spectra from modified Tauber traps and moss samples: examples from a selection of woodlands across Europe. Vegetation History and Archaeobotany 19, 271–283.

Prentice, I.C., 1980. Multidimensional scaling as a research tool in Quaternary palynology: a review of theory and methods. Review of Palaeobotany and Palynology 31, 71-104.

Punt, W., Blackmore, S., (Eds) (1976–2009). The Northwest European Pollen Flora. Vol. I-IX. Elsevier Publishing Company.

Räsänen, S., Hicks, S., Odgaard, B.V., 2004. Pollen deposition in mosses and in a modified 'Tauber trap' from Hailuoto, Finland: what exactly do the mosses record? Review of Palaeobotany and Palynology 129, 103–116.

Reille, M., 1992-1998. Pollen et spores d'Europe et d'Afrique du Nord. Laboratoire de Botanique historique et palynologie, Marseille.

Richard, L., 1968. Écologie de l'aune vert (*Alnus viridis*): facteurs climatiques et édaphiques. Documents pour la Carte de Végétation des Alpes 6, 107–158.

Richard, L., 1969. Une interprétation éco-physiologique de la répartition de l'aune vert (*Alnus viridis*). Documents pour la Carte de Végétation des Alpes 7, 7–23.

Rull, V., 2006. A high mountain pollen-altitude calibration set for palaeoclimatic use in the tropical Andes. The Holocene 16, 105–107.

Stockmarr, J., 1971. Tablets with spores used in absolute pollen analysis. Pollen et Spores 13, 615–621.

ter Braak, C.J., 1986. Canonical correspondence analysis: a new eigenvector technique for multivariate direct gradient analysis. Ecology 67(5), 1167-1179.

ter Braak, C.J., 1987. The analysis of vegetation-environment relationships by canonical correspondence analysis, in: Theory and models in vegetation science. Springer Netherlands, pp. 69-77.

ter Braak, C.J., Prentice, I.C., 1988. A theory of gradient analysis. Advances in Ecological Research 18, 271-317.

Tinner, W., Theurillat, J.P., 2003. Uppermost limit, extent, and fluctuations of the timberline and treeline ecocline in the Swiss Central Alps during the past 11,500 years. Arctic, Antarctic, and Alpine Research 35(2), 158-169.

van Geel, B., 1978. A palaeoecological study of Holocene peat bog sections in Germany and The Netherlands, based on the analysis of pollen, spores and macro- and microremains of fungi, algae, cormophytes and animals. Review of Palaeobotany and Palynology 25, 1–120.

van Geel, B., Aptroot, A., 2006. Fossil ascomycetes in Quaternary deposits. Nova Hedwigia 82, 313-329.

van Geel, B., Bohncke, S.J.P., Dee, H., 1981. A palaeoecological study of an upper Late Glacial and Holocene sequence from 'De Borchert', The Netherlands. Review of Palaeobotany and Palynology 31, 367-449.

Vincens, A., Ssemmanda, I., Roux, M., Jolly, D., 1997. Study of the modern pollen rain in Western Uganda with a numerical approach. Review of Palaeobotany and Palynology 96(1), 145-168.

Weng, C., Bush, M.B., Silman, M.R., 2004. An analysis of modern pollen rain on an elevational gradient in southern Peru. Journal of Tropical Ecology 20(01), 113-124.

Manuscript 3

(Quaternary Science Reviews 200 (2018) 212-236)

Holocene vegetation history and quantitative climate reconstructions in a high-elevation oceanic district of the Italian Alps. Evidence for a middle to late Holocene precipitation increase.

Giulia Furlanetto[1,2], Cesare Ravazzi[2], Roberta Pini[2], Francesca Vallè[1], Michele Brunetti[3], Roberto Comolli[1], Massimo Domenico Novellino[2], Lorena Garozzo[2], Valter Maggi[1].

1 Univ. of Milano - Bicocca, Dept. of Environmental and Earth Sciences, Piazza della Scienza 1, Milano (I)

2 CNR - Institute for the Dynamics of Environmental Processes (IDPA), Laboratory of Palynology and Palaeoecology, Piazza della Scienza 1, Milano (I)

3 CNR- Institute of Atmospheric Sciences and Climate (ISAC), Bologna, Italy

Abstract

We reconstructed the vegetation and climate history during the last 10 ka in a high-elevation sedimentary record (Armentarga peat bog, 2345 m asl) on the southern flank of the European Alps through the study of paleoecological and sedimentary proxies. We included a specific elevational transect of modern Pollen Accumulation Rates for timberline-forming trees and shrubs (*Alnus viridis, Pinus sylvestris/mugo, Pinus cembra*). Quantitative reconstructions of July temperature and annual precipitation were obtained by applying numerical transfer functions built on an extensive pollen-climate calibration set from the European Alps. Changes in elevational vegetation arrangement were primarily driven by phases of precipitation increase, and to a lesser extent by millennial-scale temperature changes already known from glacier, timberline, chironomids and speleothem records at Alpine scale. Changes in pollen-inferred annual precipitation occurred in three main steps. An early Holocene moderately humid phase is mirrored by the early spread of

Alnus viridis dwarf forests. Precipitation started to increase at 6.2 ka cal BP. A further, prominent step forward at the Middle to Late Holocene transition led to the high values of snowfall and runoff characterizing today's oceanic elevational climates of the outer Italian Alps. This change led to timberline depression and grassland expansion. Locally, human impact was weak at the Late Neolithic / Bronze Age transition. This event correlates with lake level oscillations in the northern Mediterranean borderlands, suggesting intensification of southern air masses conveyed by Tyrrhenian cyclones towards windward districts.

Keywords Holocene, Paleoclimatology, Europe, Vegetation dynamics, Stratigraphy, Timberline, Pollen Accumulation Rates

1. Introduction

Montane vegetation is traditionally known to be particularly sensitive to climate changes (Birks and Ammann, 2000; Wick, 2000). The strong elevational climatic gradient that characterises mountain areas results in a steep ecological slope, with several ecotones occurring in a small area. Regional climate signal is amplified with elevation (Beniston et al., 1997), and this effect is illustrated by the strong impact of recent climate variations on montane ecosystems (Houghton et al., 2001; Qin et al., 2009; Pepin et al., 2015). Being able to assess the impacts of climatic fluctuations on past biodiversity in mountain regions will help in choosing suitable management strategies in the near future. Pollen sequences investigated in or shortly above the modern timberline ecotone are ideal archives to analyze the relationships between climate and ecosystems, offering a millennial perspective to the ongoing trends and allowing to decouple the role of different predictors (e.g. July temperature, annual precipitation, pastoralism), acting at different time scales (Tinner and Theurillat, 2003; Badino et al., 2018).

A large number of independent natural archives and proxies complement palaeoecology in reconstructing the climate history of the high-elevation Alps during the present interglacial. The sedimentary record of glacier activity, the most sensitive proxy of climate change, is well assessed but highly discontinuous, thereby making it difficult to decouple temperature and snowfall contributions to glacial advances or to the even more puzzling phases of glacier retreats (Holzhauser et al., 2005; Le Roy et al., 2015). Continuous isotopic and

biological records can be obtained either from speleothems, lakes or peat bogs in high-elevation areas. However, a precipitation signal is hardly discriminated in isotopic records from Alpine speleothem (Fohlmeister et al., 2012), while most high-elevation biological proxies respond primarily to summer temperature modulations (e.g. chironomids and *Pinus cembra* timberlines) (Wick et al., 2003; Nicolussi et al., 2005; Ilyashuk et al., 2011). Up to now, available validated precipitation records derive from dendroclimatic series only (Büntgen et al., 2011).

Here we focus on a high-elevation site located in the outer Italian Alps (Armentarga peat bog), an area characterized by an oceanic climate with high precipitation (**Fig. 2B**), with snowfall and cloudiness significantly influencing ecological gradients (Belloni and Pelfini, 1990). An expanded array of biological proxies, including pollen and other microbiological particles (pteridophytes, bryophytes and fungal spores, algae, animal remains, etc.), pollen-slide microcharcoal, sieved charcoal, and biogeochemical proxies (water content, total organic matter, silicoclastic + oxides contents, magnetic susceptibility, phosphorus concentrations) was obtained from the study site. Pollen Accumulation Rates (PAR) were calculated to detect absolute pollen changes, which may reflect either population fluctuations (Tinner and Theurillat, 2003; Badino et al., 2018) or snowmelt runoff. Quantitative techniques were applied on fossil spectra to obtain estimates of past climate parameters (Birks and Seppä, 2004; Brewer et al., 2007; Birks et al., 2010; Juggins and Birks, 2012). Site-specific instrumental temperature and precipitation series and climatologies were obtained for the study site. Modern vegetation was surveyed and pollen deposition was studied in natural (mosses) and artificial pollen traps. Such modern references allow the so-called “site calibration” to be defined, accounting for site-specific features affecting either climate parameters and pollen deposition, such as local topography and sedimentary processes, and the local influence of runoff and, most conspicuously, snow runoff on PAR, barely considered in traditional palaeoecological studies. The methodology for site calibration is also inherent to the original procedure for climate reconstruction developed in the present paper.

2. Physical setting, modern climate, and elevational ecological gradient

We selected a high-elevation site (Armentarga peat bog, 2345 m asl, N 46° 2' 26.642"; E 9° 52' 44.263") on the headwall of a main valley cutting N-S and draining the external belt of the Alpine edifice in front of the Po Plain (Orobie Alps, **Fig. 1**). The bedrock geology is characterized by a low-permeability sedimentary and volcano-sedimentary sequence of claystone, siltstone, sandstone and tufites of Permian age. The area was occupied by valley glaciers during the last glaciation, while highest peaks preserve a horn-shape typical for nunataks emerging from cirque glaciers (Forcella, 1988; see **Fig. 3E**). Deglaciation age will be determined in the present paper for the first time. Several lakes and peat bogs developed since then. The modern setting of the Armentarga peat bog (**Fig. 3C,E**) results from the infilling of a small lake either by an inlet on its NE side and by biogenic-biochemical deposits. The basin is surrounded by a roche moutonnées landscape (see **Fig. 3E**).

This region is marked by a *Dfc* climate (Köppen, 1923), i.e. nival, persistently wet throughout the year (**Fig. 2B**); locally, the annual temperature is 1.3 °C (**Fig. 3B**) and lapse rate ranges from 0.56 °C/100 m in the mountain belt to 0.77 °C/100 m above the open forest limit. Mean annual precipitation (Pann, 1838 mm at the study site) is not significantly related with elevation. The site actually represents a snowfall extreme in the entire Alps (**Fig. 2B**), snow accumulation being concentrated in late winter and spring, and net snow accumulation summing up to 7 m at 1950 m asl (1964-1973 period, Belloni and Pelfini, 1990). The glacier Equilibrium Line Elevation under current climate conditions exceeds the mountain peaks; it was about 2600 m in 1994 AD (Caccianiga et al., 1994). The pollen-climate elevational transect (see section 4.5.) specifically designed for this area extends along the uppermost section of a typical prealpine valley open to moist southern winds orographically forced uphill, between 1100 m and the headwalls at 2500-2700 m asl.

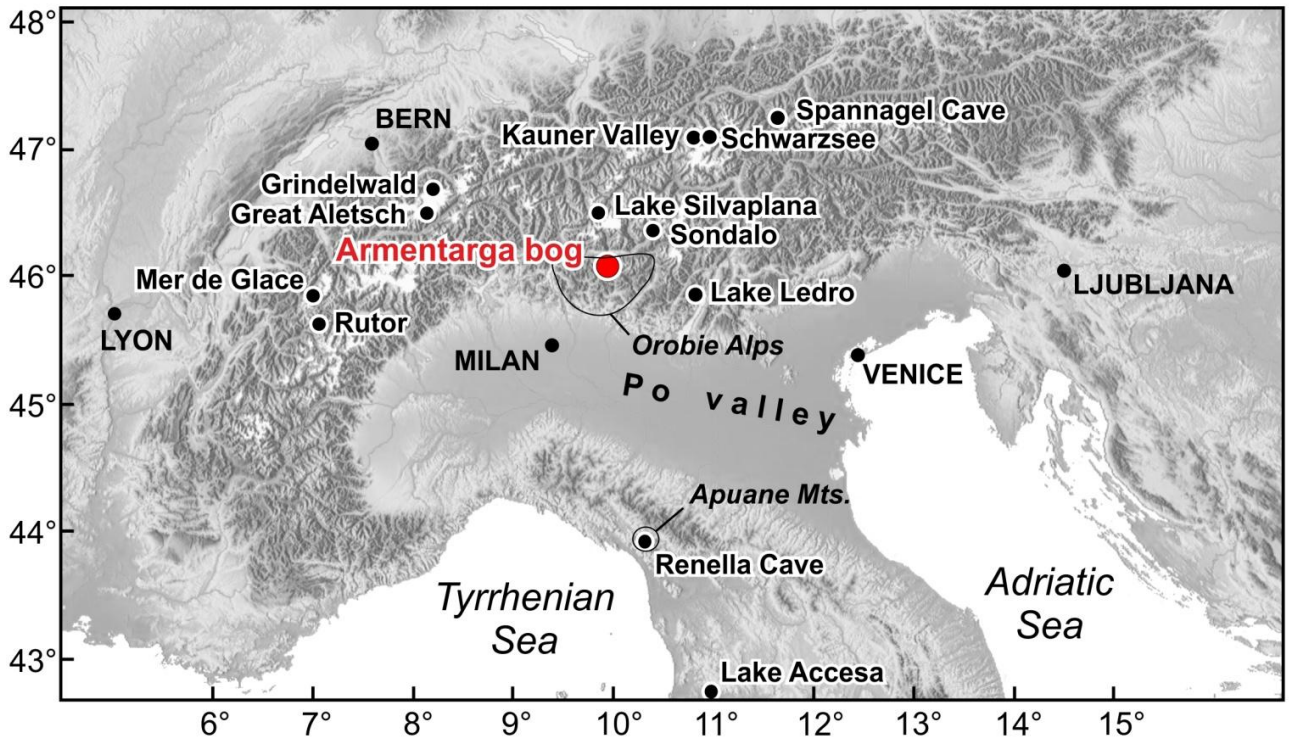

Fig. 1. The European Alps and the northern Mediterranean borderlands showing the location of the study site and of the other sites mentioned in the text.

The vegetation of the area provides a representative example of elevational ecological gradient in an oceanic climatic regime (**Figs. 3A,B**) common in the Eastern and Northern Alps, and heavily affected by pastoralism. Deciduous broad-leaved forests (mainly *Acer pseudoplatanus* and *Corylus avellana*) extend between 1100-1400 m on sunny aspects, being fragmented by clearings, mowed meadows and human settlements. Chestnut and walnut trees (*Castanea sativa* and *Juglans regia*) grow up to an elevation of 1100 m asl on sunny slopes, i.e. up to a Tjuly limit of about 17°C. Patches of dark coniferous forest (*Picea abies, Abies alba, Larix decidua*) occupy shadow slopes only, while large areas in the subalpine belt (1400-2200 m asl) are covered by a low-pollen producer larch forest. Here, low canopy density allows for a massive development of *Alnus viridis* understory thickets. The timberline is very complex due to the disruption of pristine subalpine forest by shepherds and miners, especially on sunny slopes (see **Fig. 3A**). A field survey of the 20 km^2 area partly included in **Fig. 3A** shows the following elevational timberline thresholds.
The open forest upper limit and dwarf forest limit are formed either by larch or by *Alnus viridis* groves at 2140 m asl on bedrock conductive to fine-grained regolith and by *Pinus mugo* (mountain dwarf pine) scrub at 2130 m on massive bedrock conductive to coarse

regolith (dry edaphic sites). Here, isolated stands of *Pinus mugo* form part of the timberline structure at 1800-2130 m asl. Current larch treeline extends farther up to 2220 m on rock emergencies at about 11°C Tjuly and 1860 mm Pann. Only larch individuals with >2 m erect stems less than 50 yrs old occur above 2130 m, suggesting treeline expansion uphill in recent decades, most probably in the postwar period. Swiss stone pine (*Pinus cembra*) is present but extremely rare (Andreis et al., 2005; **Fig. 3A**); its crown cover in the pollen source area is negligible. The wide development of alpine pastures and of xerophytic grasslands at timberline elevations and between 1800-2600 m asl is driven primarily by oceanic climate and human impact. For details on grassland ecology at the elevation of the study site see **Fig. 3E**.

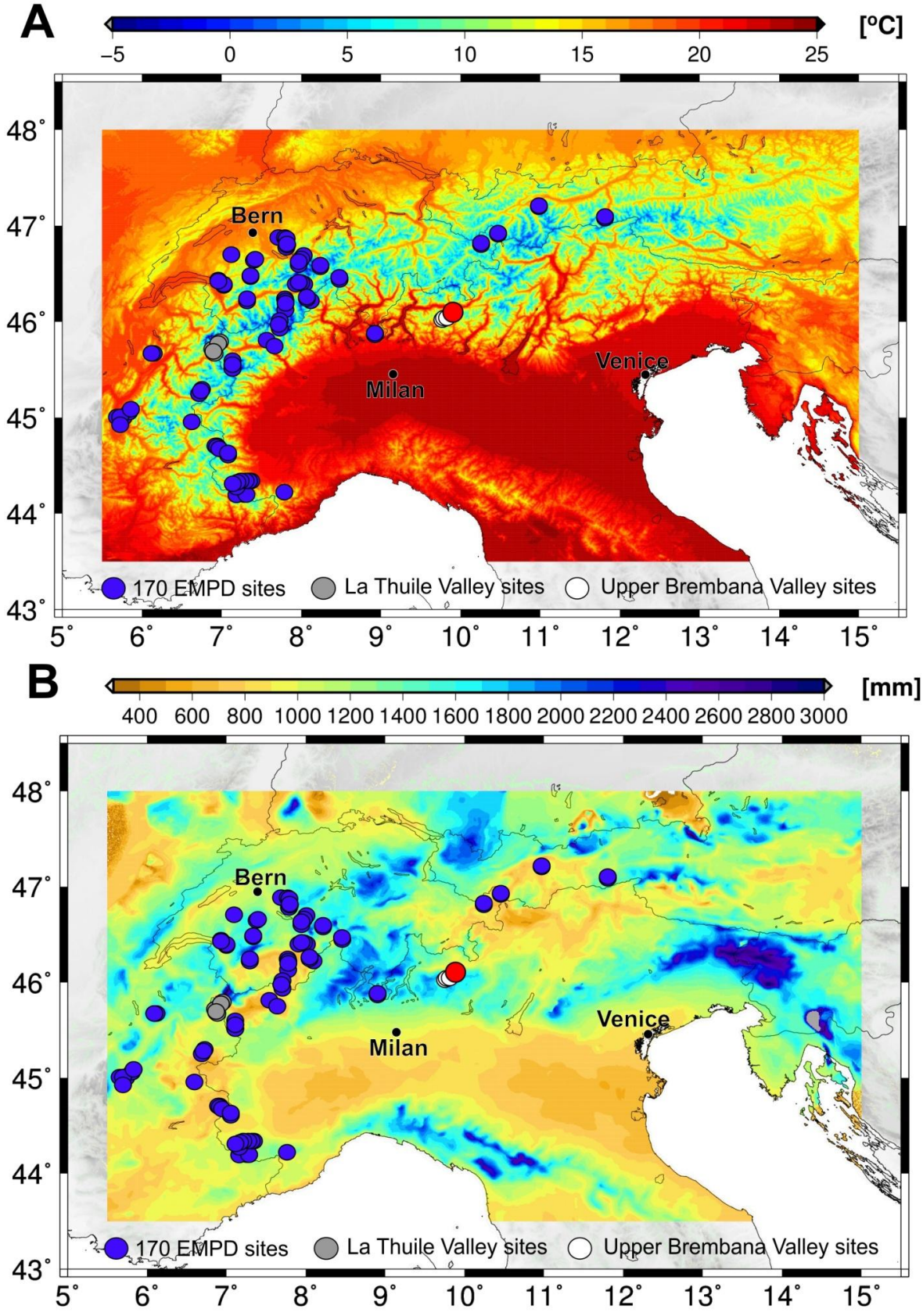
A
[°C]
−5
0
5
10
15
20
25
48°
47°
46°
45°
44°
43°
Bern
Milan
Venice
170 EMPD sites
La Thuile Valley sites
Upper Brembana Valley sites
5°
6°
7°
8°
9°
10°
11°
12°
13°
14°
15°
B
[mm]
400
600
800
1000
1200
1400
1600
1800
2000
2200
2400
2600
2800
3000
48°
47°
46°
45°
44°
43°
Bern
Milan
Venice
170 EMPD sites
La Thuile Valley sites
Upper Brembana Valley sites
5°
6°
7°
8°
9°
10°
11°
12°
13°
14°
15°

Fig. 2. A) Map of July temperature climatology (1961-1990) and B) Map of annual precipitation climatology (1961-1990) with reported the modern calibration set formed by selected European Modern Pollen Database (EMPD) sites and elevational transects sites (Furlanetto et al., accepted); for details see section 3.5.1. A red dot indicates Armentarga peat bog (2345 m asl).

2.1. Archaeological and documentary evidence

The studied mountain region is lying 25-30 km NW of the Valcamonica, the famous rock-art valley which become inhabited since the Middle Neolithic (Poggiani, 2010), after an earlier Paleolithic-Mesolithic peopling (Pini et al., 2016b). Despite extensive surveys so far carried out (Poggiani, 2007), earliest evidence for human presence in a radius of 5 km around the Armentarga peat bog is starting with rock engravings from the late Iron Age, III century BC (Casini et al., 2010, see **Fig. 3A,C**). A mining village dating back to the early Middle Ages (Longobard Age) has been recently discovered and excavated (Museo Archeologico di Bergamo, unpublished data, see **Fig. 3A**). The name “Armentarga” means “site of herds”, and indeed the existence of summer pastoralism here in the Middle Ages is testified by a written document dating back to AD 1148 (Zonca, 1998).

3. Materials and methods

The centre of the Armentarga basin (**Fig. 3E**) was manually drilled down to 258 cm depth by percussion coring to obtain 6 cm-diameter sediment cores. Due to the scarcity of plant macrofossils in the lower section, four parallel cores (ARMA 4-5-6-7) were drilled to retrieve as much material as possible for ^{14}C dating. Cores were examined, photographed and visually correlated *in situ*; more precise correlation at cm-detail was obtained through multiple LOI determination. To provide chronostratigraphic evidence for the age of basin formation, we insisted coring down into coarse sediment and obtained two copies of the transitional interval from gravels to fine lacustrine sediments (252-247 cm depth in **Fig. 4**). Lithozones, represented beside the summary stratigraphic log (**Fig. 4**), were obtained from LOI data by a constrained incremental sum of squares cluster analysis, using the Cavalli Sforza's chord distance as dissimilarity coefficient (CONISS, Grimm, 2015).

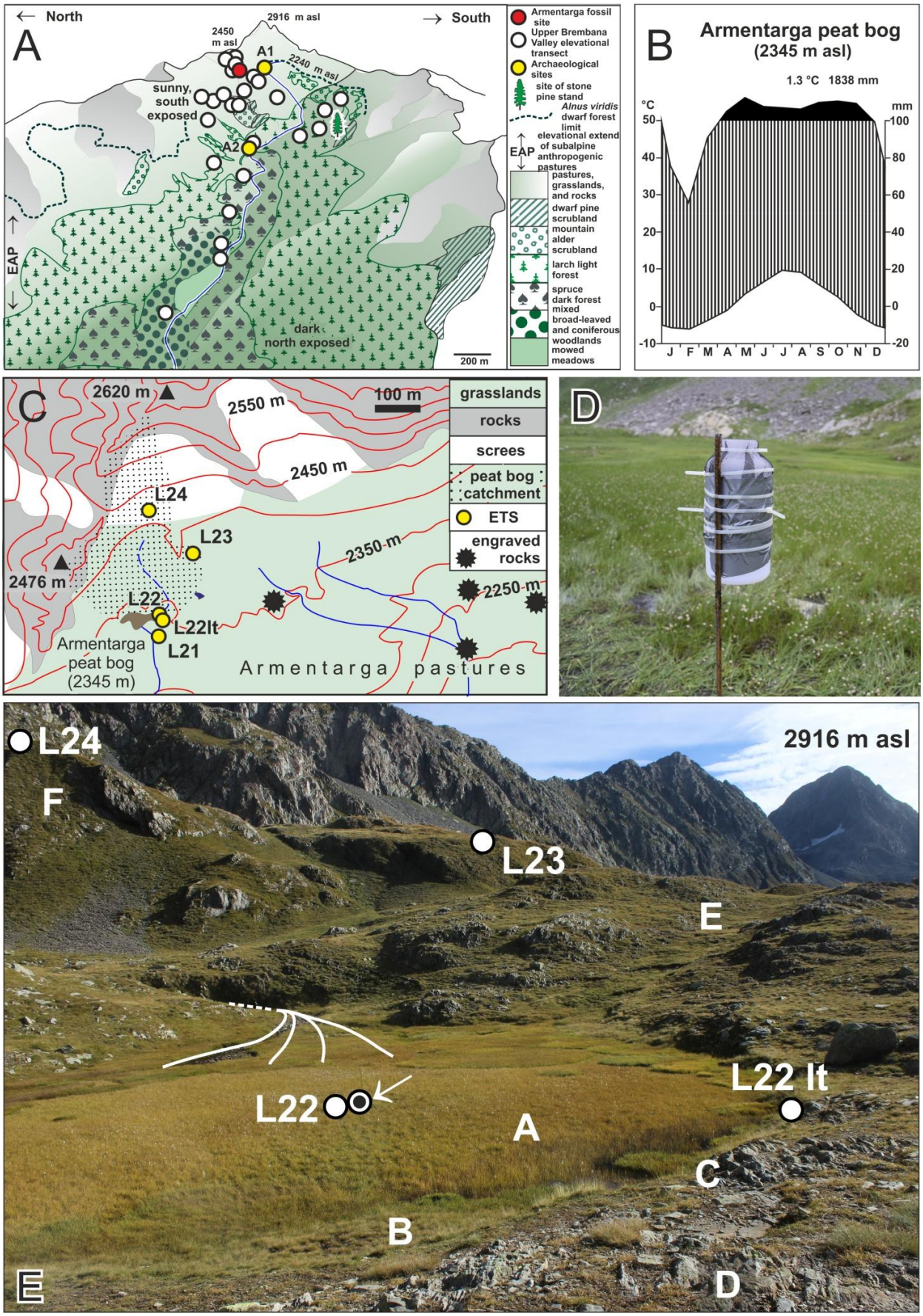
A
North
South
2916 m asl
2450 m asl
2240 m asl
A1
A2
sunny, south exposed
dark north exposed
EAP
200 m
Armentarga fossil site
Upper Brembana Valley elevational transect
Archaeological sites
site of stone pine stand
Alnus viridis dwarf forest limit
elevational extend of subalpine anthropogenic pastures
pastures, grasslands, and rocks
dwarf pine scrubland
mountain alder scrubland
larch light forest
spruce dark forest
mixed broad-leaved and coniferous woodlands
mowed meadows
B
Armentarga peat bog
(2345 m asl)
1.3 °C 1838 mm
°C
mm
J F M A M J J A S O N D
C
2620 m
2550 m
2450 m
2350 m
2250 m
2476 m
100 m
L24
L23
L22
L22lt
L21
Armentarga peat bog (2345 m)
Armentarga pastures
grasslands
rocks
screes
peat bog catchment
ETS
engraved rocks
D
E
2916 m asl
L24
F
L23
E
L22
L22 lt
A
C
B
D

Fig. 3. A) Sketches summarizing the elevational arrangement of the main ecosystems in the study area (modified from Furlanetto et al., accepted). The panorama views were drawn on Google Earth images. The scale bar (down on the right) refers to the foreground frame. The linear distance covered by the elevational transect is 7 km; Archeological sites A1 engraved rocks - Late Iron Age, A2 Piani di Sasso village - Middle Ages; B) Walter climate diagram reconstructed for the site of Armentarga peat bog (reference period 1981-2010); C) Map of the area of the Armentarga peat bog, showing the location of the elevational transect sites (ETS) and the basin catchment. Equidistance is 50 m; D) Pollen trap TL22 located in Armentarga peat bog; E) The Armentarga peat bog in autumn 2017 (A = *Carex fusca* - *Eriophorum scheuchzeri* plant formation) with the coring site (concentric point indicated by an arrow). Numbered dots are sites of the pollen-vegetation-climate elevational transect (L 22, L 22 lt, L 23, L 24). The basin is surrounded by a highland shaped in bedrock, forming roches moutonnées; in the background glacially-eroded precipitous headwalls forming peaks and cirques stand out at 2650-2914 m asl, preserving small glaciers. Peat bog borders host discontinuous snow-beds and Alpine rocky vegetation (B = "hygronardetum" wet *Nardus*; C = *Salix herbacea* and D = *Chrysanthemum alpinum* formations). Gentle slopes support a low-tall Poaceae-dominated pasture (E = *Nardus stricta* - *Festuca curvula* - *Avenula versicolor*). A xerophytic tussock grassland (F = *Festuca luedii* formations) extends on steeper slopes in the left background. The dotted line shows the inlet and its clastic fan prograding on NE peatbog border.

3.1. Dating and age-depth model

We radiocarbon-dated plant material from three parallel cores (**Table 1**). All AMS ^{14}C dates derive from upland plants remains (e.g. terrestrial mosses, leaves and wood) after wet sieving. To date the basal sediments (devoid of any macrofossil) we concentrated and decontaminated sieved charcoal through an aggressive attach by sodium hypochlorite and 10% sodium hexametaphosphate and subsequent picking of individual charcoal fragments at the stereomicroscope. We checked for thermally-altered, detrital organic matter (e.g. reworked from bedrock) which was not detected while picking charcoal fragments. We applied this method of decontamination to most of the samples prepared for AMS ^{14}C (UBA-37489, UBA-37490, UBA-33046, UBA-35688, UBA-35687, RCMIB001) in order to avoid reservoir effect (see **Table 1**). Radiocarbon ages were calibrated using Calib 7.0.2 (Stuiver et al., 2013) based on the IntCal 13 calibration curve (Reimer et al., 2013). Deposition rates were modelled through the software Bacon v 2.2 (R interface) (Blaauw and Christen, 2011) from 54 to 220 cm depth. Two different models were built. The first model implies a continuous sedimentation, so deposition rates were modelled using radiocarbon ages as parameters; the second model drops the assumption of a continuous sedimentation since several stratigraphic proxies (pollen and phosphorus) display an

abrupt, though subtle offset, suggesting that a hiatus of centennial duration may have perturbed the long-term patterns. A hiatus is properly defined by a basal and top age, the basal age at 112 cm was obtained by modelling while the top age could be only estimated inferring a steady accumulation rate. Bacon's modelled ages are graphically presented in **Fig. 4** and numerically expressed by their wmean throughout the text, whereas calibrated ages (unmodelled) are expressed by their median probability.

3.2. Biogeochemistry

93 volumetric samples were taken from core ARMA5, weighted and progressively heated at 105 °C, 550 °C and 980 °C to estimate water, total organic matter + sulphides (TOM + sulphides) and the silicoclastic + oxides contents (RES) (Gustafsson et al., 2001). Total organic carbon (TOC) and the carbonate fraction, which includes also both sulphides and sulphates ($CaCO_3$ + $S^{2-}X$ +$SO_4^{-2}X$; Földvári, 2011), were determined stoichiometrically (Dean, 1974).

Magnetic susceptibility was measured with a Bartington MS2 device equipped with a MS2E core logging sensor. Measures were taken on wet sediment every 2 cm, and repeated to check environmental conditions changes.

Minerogenic particles of the size classes 500 μm - 1 mm and > 1 mm were counted in gridded Petri dish under a stereoscope at 40x.

Phosphorus occurring in lake sediments could originate both from apatite dissolution and intake of livestock manure. Variations in phosphorus concentrations and chemical forms can provide hints on the occurrence of wild or domesticated animals, as well as human settlements (Boyle et al., 2015; Pini et al., 2017).

Phosphorus concentrations (organic, inorganic and available) were obtained following soil chemistry procedures (Colombo and Miano, 2015). Total P was determined spectrophotometrically via blue phosphomolybdate complex. Organic P was calculated as difference between P obtained after sulphuric acid treatment with and without heating at 550 °C; inorganic P was calculated as the difference between total and organic P. Available P was extracted with sodium bicarbonate (Olsen method; Schoenau and O'Halloran, 2008).

3.3. Pollen, microbiological proxies and stomata

Samples for pollen analysis were processed following standard methods at the Lab. of Palynology and Palaeoecology of CNR-IDPA in Milano, after adding *Lycopodium* tablets for pollen and pollen-slide microcharcoal concentration estimations (Stockmarr, 1971). A minimum count of 600 pollen grains was reached for each sample; aquatics, spores and microbiological particles other than pollen were excluded from the pollen sum. Identification was carried out at x400, x630 and x1000 magnifications under a Leica DM-LB light microscope. Pollen identification followed Beug (2004), Moore et al. (1991), Punt and Blackmore (1976-2009), Reille (1992-1998) and the CNR pollen reference collection. Pollen zonation was obtained by a constrained incremental sum of squares cluster analysis, using the Cavalli Sforza's chord distance as dissimilarity coefficient (CONISS, Grimm, 2015). Clustering was restricted to taxa whose pollen reached over 2%. At the optical microscope, we distinguished individual pollen of *Pinus cembra* from *Pinus sylvestris/mugo* type; additionally, we identified *Pinus mugo* and *Pinus sylvestris* pollen at SEM on selected samples. Readers are referred to **Supplementary Table S1** and **Fig. S1** for further taxonomic details.

Size classes of Alpine Poaceae pollen were distinguished by measuring grain diameter (D) and annulus diameter (d). Grains with D > 47 µm and d > 11 µm have been referred to cereals (cultivated *Avena* and *Triticum* species, i.e. Cerealia type *sensu* Joly et al., 2007). These size limits (Joly et al., 2007), more restrictive than those currently used in the Alpine region (Andersen, 1979), allow to separate an intermediate type having D 37-47 µm and D > 47 + d < 11 µm which includes both wild and cereal species (Andersen, 1979; Joly et al., 2007), e.g. a few wild *Avena* species previously listed in the *Avena-Triticum* group such as *Avena versicolor* which occurs at the site.

Plantago maritima type is named after Beug (2004) and includes *Plantago alpina*, *Plantago maritima* and *Plantago maritima* subsp *serpentina*. Ranunculaceae undiff. includes pollen grains not identified at the genus or type level and it does not include *Ranunculus* and *Ranunculus acris* type. We preferred to use a sum of apophytes and cultivated plants instead of anthropogenic indicators. Microbiological particles were named after van Geel et al. (1981), van Geel (1978) and van Geel and Aptroot (2006) and expressed as % out of the pollen sum. Among the Sordariaceae family, spores of several dung fungi were identified (*Sporormiella*-like, *Sordaria*, *Podospora* spores). The *taxon* Sordariaceae undiff. includes spores not assigned to a specific genus and sharing the

same morphological aspect, i.e. dark brown to black in color, smooth surface, apical pore(s), one flat or slightly pointed end. The Sordariaceae undiff. curve does not include *Gelasinospora* and *Neurospora*, sporadically encountered in the analyzed samples and identified based on their characteristic morphology. Pollen-slide microcharcoal particles were counted under a light microscope at 400x. Black, completely opaque and angular fragments (Clark, 1988) were identified as charcoal and grouped in two size classes (10–50 μm and 50–250 μm length). We also recognized charcoal particles from 92 samples processed following Whitlock and Larsen (2001); each sample was wet-sieved through metal-screened filters with mesh sizes of 62, 125, 500 μm and 1 mm. Samples were then placed into a gridded Petri dish, and the charcoal in each size class was counted under a stereoscope at 40× (Whitlock and Larsen, 2001; Enache and Cumming, 2007; Jensen et al., 2007). Charcoal counts were expressed as particles/cm^3. Diagrams were drawn using Tilia ver. 2.0.41 (Grimm, 2015) and Corel Draw X7 for further graphic elaborations.

3.4. Pollen Accumulation Rates (PAR)

Pollen monitoring using annual pollen traps helps to quantify and calibrate pollen deposition with present-day vegetation and meteorological conditions, as well as providing insights into local pollen dispersal and sedimentation mechanisms (Hicks, 2001). Pollen Accumulation Rates (PAR) measurements can also be used as a modern reference to estimate past plant population densities buffering the study site (Hicks, 2001; Tinner and Theurillat, 2003; Badino et al., 2018). We compared fossil PAR of *Alnus viridis*, *Pinus cembra* and *Pinus sylvestris/mugo* with modern PAR values from the Armentarga peat bog (see **Table 2** and **Fig. 3E**, traps TL22 and TL22 lt) and with modern PAR threshold values estimated at the timberline ecotone (van der Knaap et al., 2001; Sjögren et al., 2008; Bjune, 2014) to detect absolute pollen changes, which may reflect either population fluctuations or snowmelt runoff. Subsequently, we compared fossil PAR values with independent sediment proxies for alluvial events at the study site.

3.5. Pollen-based July temperature and annual precipitation reconstructions

Quantitative methods (Modern Analogue Technique and Weighted Averaging Partial Least Squares) were applied to the Armentarga fossil record to estimate the temperature of the warmest month (Tjuly) and annual precipitation (Pann) during the last 10 ka. We adopted the same procedure to obtain a modern site calibration by comparing pollen-inferred Tjuly and Pann from modern pollen traps (see **Fig. 3D,E**, trap TL22) with instrumental data.

3.5.1. Modern pollen-climate calibration set

A modern calibration set (cs223) was created merging two subsets, retaining taxonomical distinction between *Alnus viridis* and *Alnus glutinosa/incana*, in order to maintain the potential indicator value of these taxa. A first subset of 170 alpine sites was selected from the EMPD-European Modern Pollen Database (Davis et al., 2013). A second subset of 53 sites originates from two new elevational transects, one from an oceanic outer district of the Central Alpine chain (Upper Brembana Valley; Furlanetto et al., accepted), and the other from a continental inner valley of the Western Alps (La Thuile Valley; Badino et al., 2018; Furlanetto et al., accepted) (**Fig. 2**). Prior to the calculations, pollen taxonomy of modern and fossil data was harmonized. Poaceae were included in the pollen sum of both calibration and fossil datasets, while Cyperaceae were excluded.

Site-specific instrumental temperature and precipitation series, covering the 1951-2015 period, were computed for each sampling site of both elevational transects (data accessible in Furlanetto et al., accepted) and for the 170 alpine sites selected from the EMPD-European Modern Pollen Database (Davis et al., 2013), by means of the anomaly method (New et al., 2000; Mitchell and Jones, 2005) as described in Brunetti et al. (2012), to obtain a climate reconstruction as much representative of the specific locations as possible, thanks to the huge amount of meteorological observations available for Italy and surrounding areas. The interpolation procedure consists in the independent reconstruction of the climatological normals over a given reference period (i.e. climatologies) and the departures from them (i.e. the anomalies): the former, characterized by remarkable spatial gradients, were reconstructed by evaluating the local dependence of the meteorological variable on elevation (Brunetti et al., 2014; Crespi et al., 2018), and a high spatial density

network of stations (even if with a limited temporal coverage) was used; anomalies are linked to climate variability and are characterized by a higher spatial coherence, therefore, a more simple interpolation technique and a low spatial density of stations are enough, but long temporal coverage and accurate homogenization (i.e. the procedure that removes the non-climatic signals introduced by stations and instruments relocation, changes in measurement practices and so on) are mandatory. Finally, climatologies and anomalies were superimposed to get temperature and precipitation monthly series in absolute values for each sampling site. Information about the techniques and their accuracy are provided in Brunetti et al. (2014), Brunetti et al. (2012), and Crespi et al. (2018). From these monthly series, mean temperature of the warmest month (July) and the total annual precipitation over the 1981–2010 period were calculated for the sampled sites in the two elevational transects. For the 170 alpine sites selected from the EMPD mean July temperature and total annual precipitation over the 1951–2000 reference period were calculated.

3.5.2 Numerical methods

Reconstruction of July temperature (Tjuly) and annual precipitation (Pann) were carried out by means of (a) the Modern Analogue Technique (MAT: Guiot, 1990) and (b) Weighted Averaging Partial Least Squares (WA-PLS) regressions (ter Braak and Juggings, 1993; ter Braak, 1995). The reconstructed temperature value obtained with MAT is the weighted-mean of the climate values associated to the k best analogues (k=3) (Jackson and Williams, 2004; Simpson, 2007). The goodness of the selected analogues for each fossil assemblage was evaluated by looking at their squared-chord distances and at their associated temperature standard deviations. All distances smaller than the 10th percentile indicate that the fossil sample has good analogues, while distances higher than the 10th percentile suggest no analogues in the calibration set (Simpson, 2012). WA-PLS optimal number of components was selected on the basis of the lower root mean square error of prediction (RMSEP), low maximum bias, high coefficient determination (r^2) between observed and predicted values of Tjuly and Pann, and the smallest number of “useful” components (Birks, 1998). MAT and WA-PLS model performances were assessed in leave-one-out cross-validation; models development, their evaluation and the temperature reconstructions were performed with the program R 3.2.3 version (R Core Team, 2013) and the R Rioja package (Juggins, 2017). The statistical significance of key taxa individual

responses to Tjuly and Pann was tested using the Extended Huisman-Olff-Fresco fitting method, which considers a set of hierarchical models in a generalized linear modelling framework (Huisman et al., 1993; Jansen and Oksanen, 2013) using the R eHOF package (Jansen and Oksanen, 2017). In addition, the statistical significance of the Pann inferred with MAT method was tested with the method of Telford and Birks (2011a) using the R package palaeoSig (Telford, 2015). The pollen-based temperature and precipitation series were smoothed with a LOESS smoother (span = 0.1) in order to better evaluate the reconstructed trends with respect to the noise. Finally, numerical reconstructions from the studied site (Tjuly and Pann) were compared with climate reconstructions based on independent records from the Alpine area.

4. Results and interpretation

4.1. Age-depth model

The age-depth model was developed from 54 to 220 cm depth and includes 8 calibrated ^{14}C dates (**Fig. 4**). The model extends for about 10 millennia between 10.3-0.35 ka cal BP (wmean). The age obtained at 163-165 cm depth was excluded from model computing after considering its poor agreement with the model. Actually, this sample did not undertake decontamination through an aggressive attach before wet sieving (see section 3.1. and **Table 1**), a treatment which could have been able to remove organic particles affected by reservoir effect, such as aquatic CO_2 from dissolved carbonates occurring in the catchment. The model solution does not extend below 220 cm depth, as lithofacies changes might perturbate the sedimentation rate (see log in **Fig. 4**). Further features of the modelled Holocene chronostratigraphy will be presented in comparison with the chronosequence of sedimentary environments (section 4.2.). An alternative model for the interval 4.7 to 2.9 ka cal BP has been developed (see **Fig. 4**) due to a possible hiatus occurred at 112 cm. A calendar age (3.9 ka cal BP) was included in the model at the depth of sedimentation resumption. For details see section 4.2. and caption in **Fig. 4**.

Information on the age of the unmodelled basal portion of the sequence may be derived from pollen-stratigraphical events which proved to be synchronous at centennial scale on the southern flank of the Italian Alps, i.e. the rapid *Corylus* expansion at the very beginning of the early Holocene warming, starting between 11.7 and 11.2 ka cal BP (Wick, 1996;

Pini, 2002; Finsinger et al., 2006). In the Armentarga record this occurs at 242 cm depth (see *Corylus* % curve and biochronological event in **Fig. 4**). This biostratigraphic event is accompanied by a temporary fall of pine pollen and by its subsequent recovery, another feature visible in other Lateglacial to early Holocene pollen records of the Italian Alps (e.g. Scaife, 1997). These biostratigraphic ties suggest discarding an age obtained from a moss sample at 238-239 cm depth, missing an aggressive pre-treatment (**Table 1**). The age of the very basal interval (245-250 cm) of fine sediment (median probability 14.079 ka cal BP) is intriguing as it should refer to the Bølling-Allerød interstadial, rarely radiocarbon dated in high-elevation Alps (Gehrig, 1997; Scaife, 1997; Brisset et al., 2015). Being obtained on a microcharcoal fraction submitted to ABOX pre-treatment, a reservoir effect may be excluded here. Further support to a Lateglacial setting for the onset of basin sedimentation at the study site is provided by a nearby high-elevation pollen site, which also includes evidence for the Younger Dryas.

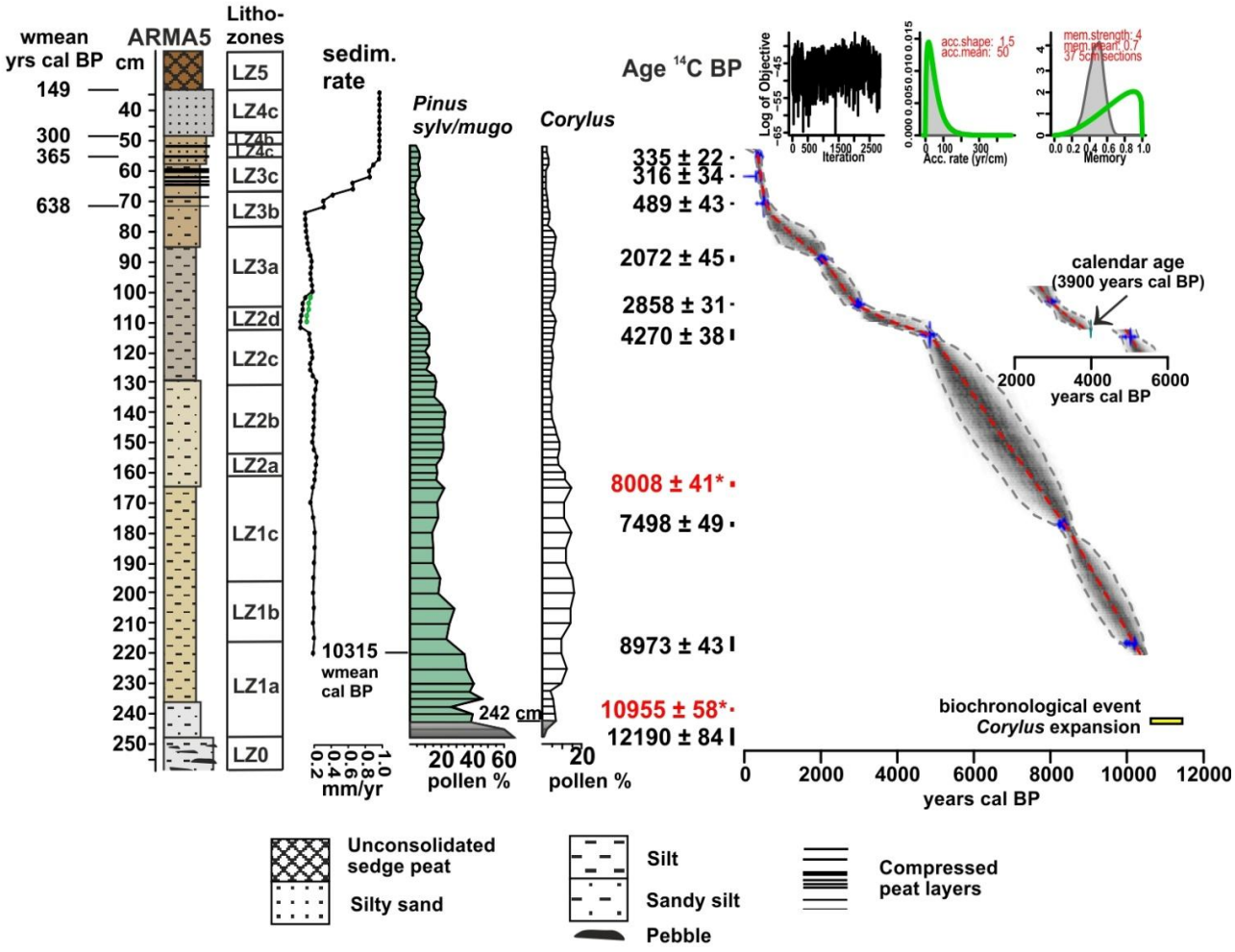

Fig. 4. Armentarga composite stratigraphic log (ARMA5) and chronostratigraphy including age-depth model. Bacon output graphs on the right. Blue: calibrated ^{14}C dates; red stippled curve shows single 'best' model based on the weighted mean age for each depth. An alternative model for the interval 4.7 to 2.9 ka cal BP is also shown adding a calendar age (3.9 ka cal BP) at the sedimentation resumption depth. This age is the most parsimonious solution considering a steady accumulation rate (see the green curve in the sedimentation rate). The lithozones, and the sedimentation rate, *Pinus sylvestris/mugo* and *Corylus* pollen % are also presented.

4.2. The chronosequence of sedimentary environments

The drilling in the centre of the Armentarga basin did not reach the bedrock but stopped at clast-supported gravels (LZ0, 258-252 cm depth, **Fig. 4**) interpreted as an alluvial pavement. No glacigenic deposits were found. At 252-247 cm a transition to matrix-supported fine gravels followed by micaceous sandy silts rich in algae (**Figs. 4-5**) testifies to the development of a limnic environment. We infer very low average sedimentation rates in the basal segment between the age of 14.079 ka cal BP (245-250 cm depth Table 1) and the subsequent biochronological marker at 11.7-11.3 ka cal BP. Re-elaboration processes related to sediment erosion and focusing may have affected this basal transitional interval. Condensed sedimentary sequences typically occur in the shallower zones of lake basins (Blais and Kalff, 1995) and in temporary nival ponds drying out at the end of the snow-free season (Wissinger et al., 2016). Due to the envisaged discontinuous sedimentary pattern, the basal segment (below 244 cm depth) has been excluded from the historical reconstruction of vegetation and climate.

Most of the record starting shortly after the Holocene onset (LZ1, 230-165 cm depth) represents stable, shallow limnic, fine detrital sedimentation, as shown by its discontinuous, faintly laminated, minerogenic silty lithofacies, and confirmed by the assemblage of planctonic algae. In a first phase (LZ1) organic input by limnic organisms is significant (**Fig. 5**); then lake productivity decreases (LZ2). Although the lake was probably very small and supplied by an inlet on its NE side, the sedimentation rate remained stable until wmean 4.7 ka cal BP (112 cm depth), suggesting low supply changes in the inlet on its NE side. At 112 cm depth, pollen and phosphorus stratigraphic proxies display an abrupt, though subtle offset, mirrored by sedimentation rate changes, suggesting that a hiatus of centennial duration may have perturbed the long-term patterns of LOI, pine pollen proportion and phosphorus concentration decreases (yellow belt in **Figs. 5-6**). An unconformity however is not apparent from sedimentary structures, as frequently happens

in drilled cores from lake stratigraphies. We thus produced two age-depth model solutions (**Fig. 4**, see discussion in section 5.2.2.). Inferring a steady accumulation rate, hiatus duration may extend no more than 800 yrs, in latter case spanning between 4.7 and 3.9 ka cal BP (see alternative age-depth model in **Fig. 4**). The intercalation of peat layers since 72 cm depth, with a modelled age of 0.638 ka cal BP (wmean) marks an advanced phase of lake infill. The macrobotanical analysis suggests a first phase (LZ3c) of littoral belt expansion by terrestrial peat vegetation (Cyperaceae), subsequently followed by progradation of an alluvial fan, as shown by embedded sand lens at 55 cm depth and upward. The final lake infill is accompanied by increasing sedimentation rate (0.97 mm / yr). The peat bog was buried by a tabular body of coarse sand with a wmean modelled age of 0.318 ka cal BP (1630 AD, close to the onset of the Little Ice Age). Peat vegetation developed again in recent decades (see caption **Fig. 3**) covering the sandy layers (**Fig. 4**).

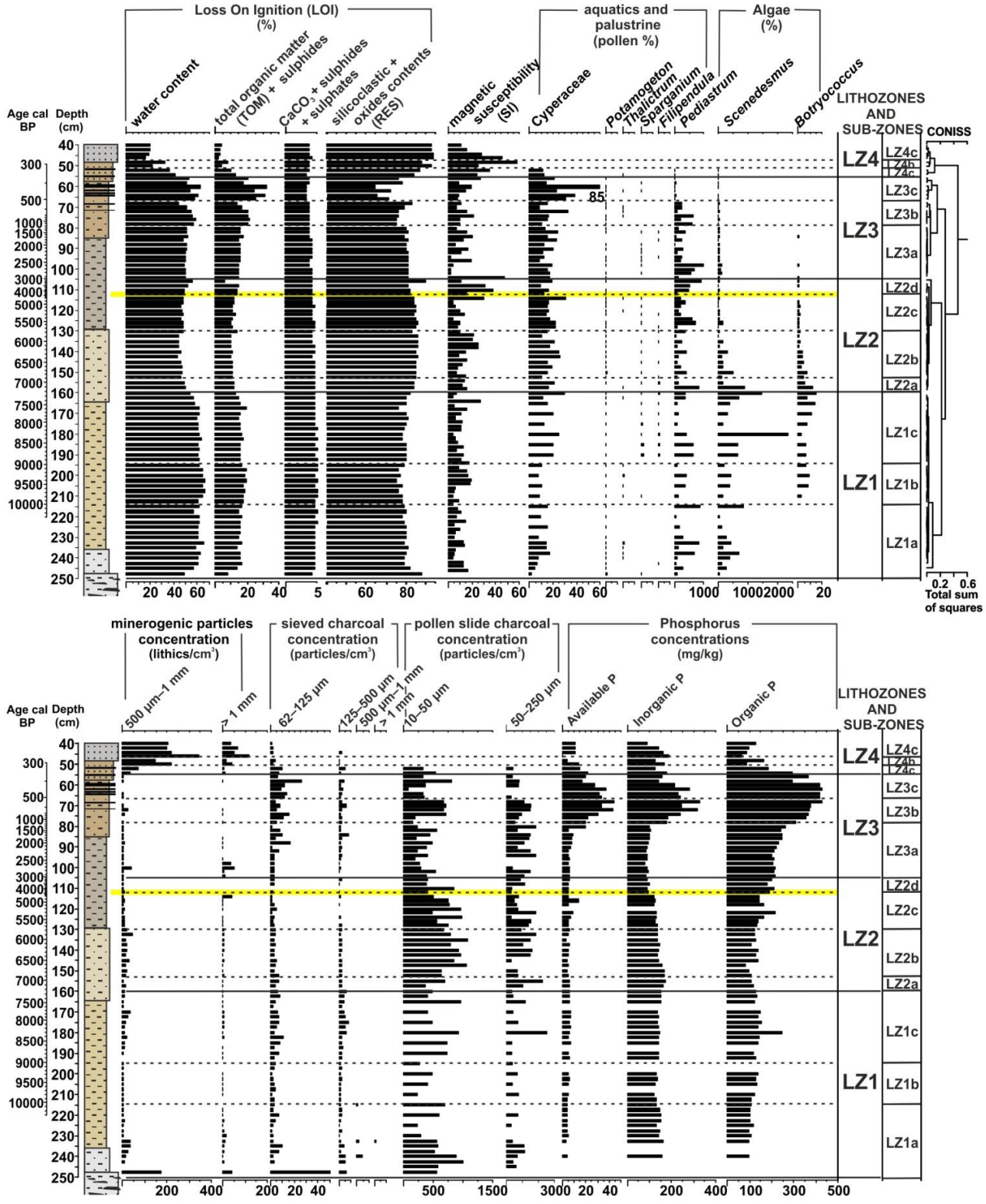

Fig. 5. Armentarga biogeochemical and sedimentary proxies. Upper panel: LOI data (water content % based on the initial sample weight, other LOI parameters % based on dry sample weight); magnetic susceptibility; aquatic and palustrine taxa and algae are shown (expressed as % based on the main pollen sum). Lower

panel: sieved charcoal, minerogenic particles, pollen slide charcoal and phosphorus concentrations are presented. At 112 cm depth, a yellow belt marks a possible hiatus of centennial duration.

4.3. Biogeochemical and sedimentary proxies for environmental and climate change

Lithofacies units were obtained by clustering LOI data in 4 main lithozones and 13 subzones (**Fig. 5**). The lowermost lithozone (LZ1, 247.5-160 cm) is characterized by mean values of water content, TOM + sulphides and RES respectively 60%, 20% and 80% (see section 3.2. and **Fig. 5**). Peaks of organic P concentrations, *Scenedesmus* % and pollen-slide charcoal concentrations occur at 180 cm depth. Lithozone LZ2 (160-105 cm) displays a decrease of water content and TOM + sulphides and increase of RES (85%). At 124 cm (5.4 ka cal BP) a first increase of organic P concentration and *Sporormiella*-like spores % (see Figs. 5-6) occurs. This increase is more pronounced in lithozone LZ3 (subzone a) in a phase of precipitation rise (see later, MAT Pann) as nutrients transfer to water bodies (see section 5.1.3). Intriguingly, these changes are in phase with an overall precipitation rise (see later, MAT Pann). Disentangling the role of climate and of human interference in LZ3a will be discussed in section 5.1.3. Subzones LZ3b, LZ3c show an increase of sediment water and of TOM + sulphides in phase with higher sieved charcoal concentrations, phosphorus concentrations (**Fig. 5**) and plant indicators of human activities (e.g. *Plantago lanceolata* type, *Cannabis/Humulus* type, Cerealia, **Figs. 6-7** and section 5.1.2.) indicating enhanced human interference. LZ4 (55-40 cm) is marked by a sharp increase of RES, magnetic susceptibility and minerogenic particles concentration and decrease of water content, TOM + sulphides and P concentrations.

4.4. Pollen Accumulation Rate (PAR)

Alnus viridis, the main woody species forming the dwarf forests in the Upper Brembana Valley timberline ecotone, shows a specific elevational PAR arrangement under modern climate conditions (**Table 2**). The highest PAR values in the local elevational transect are observed in sites L 3 and L 10 (1420 and 1940 m asl, respectively) in river corridors and waterfalls with mountain alder scrub. Here PAR values range between 2400 and 3100 pollen grains cm^{-2} yr^{-1} (**Table 2**, traps TL3 and TL10). On the other hand, pollen traps at

subalpine elevation (**Table 2**, traps TL16, TL18; respectively 2100 and 2180 m asl), located at the border of mountain alder scrub with continuous understory of Ericaceae, display PAR values of about 700 pollen grains cm^{-2} yr^{-1}. Modern PAR data of *Alnus viridis*, *Pinus cembra* and *Pinus sylvestris/mugo* from the Armentarga peat bog (**Fig. 3E**) range from ca. 70 to 430 pollen grains cm^{-2} yr^{-1} (**Table 2**, traps TL22 and TL22 lt). These PAR measurements can be used as a modern reference to estimate past plant population densities (**Fig. 7**). Caution is due because the pattern of decreasing pollen production with elevation (Furlanetto et al., 2018) also affects PAR values.

4.5. Reconstruction of the vegetation history

The complex vegetation history depicted by the % pollen diagram (**Fig. 6**) is clustered in 6 pollen zones and 14 subzones. Information from pollen proportions is integrated by PAR and sieved charcoal concentrations (**Table 2** and **Figs. 5-7**); we have also taken into account the scanty macrofossil data from stomata and carpoflora, and the results of SEM morphoscopy on pine pollen (see **Supplementary Table S1** and **Fig. S1**).

The AR1a subzone is dominated by *Pinus mugo* pollen, followed by *P. sylvestris* and *P. cembra* and by broad-leaved trees. The basal portion of this subzone (248-244 cm depth) represents a condensed sedimentary record of lateglacial age (see sections 4.1.-4.2.) not suitable for detailed vegetation reconstructions. *Corylus* pollen appears and expands in the second part of subzone AR1a, suggesting development of hazel woodlands in the lower elevation. This palynological event marks the Early Holocene onset in the Italian Alps (section 4.1.).

In subzone AR1b (10.7-10.4 ka cal BP) *Pinus mugo* pollen dominates over *P. sylvestris* and *P. cembra*, followed by pollen of deciduous broad-leaved trees and grassland herbs. Around 10.6 ka cal BP, the occurrence of pine stomata suggests that pine (most probably dwarf pine) grew close to the site. However, pine PAR values do not reach the timberline threshold (**Fig. 7**), thus we infer that the peat bog remained in the Alpine zone, more precisely over the top of the open forest (i.e. extensive scrubs of dwarf pine). Subalpine forest included *Pinus sylvestris* and *P. cembra* downward in contact with warm-temperate broad-leaved forests.

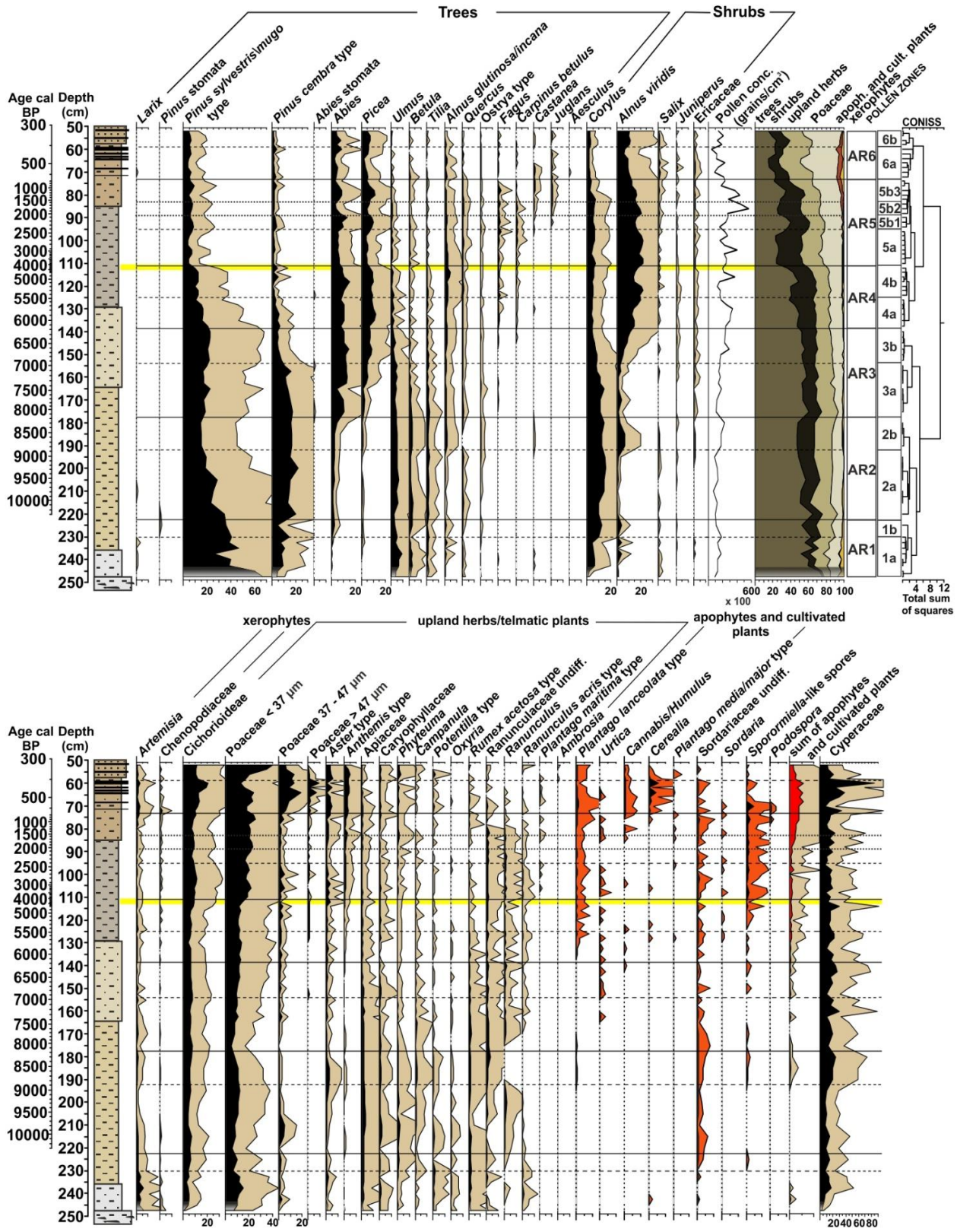

Fig. 6. Armentarga pollen and spore fossil record: Percentage palynological record of selected taxa plotted versus depth. Pollen sum used for % calculations does not include aquatics/wetland species. A grey white filling pattern marks high proportion of floated pollen (AR 1a- pollen zone). Magnification of percentage

curves: x5. A red filling pattern marks coprophilous fungi and anthropogenic indicators (both expressed as % based on the main pollen sum), for which a larger representation scale has been adopted: x10. Details on identification criteria and on the nomenclature used in the pollen diagram can be found in section 3.3. At 112 cm depth, a yellow belt marks a possible hiatus of centennial duration.

In subzone AR2a (10.4-8.8 ka cal BP) changing pine pollen proportions suggest the expansion of Swiss stone pine progressive regression of dwarf and scots pines. Broad-leaved tree pollen also reaches a maximum. We suggest this change to reflect a millennial forest dynamic: the early successional, pioneer dwarf pine being replaced by the late successional Swiss stone pine. However, according to pollen percentages and PAR (**Fig. 7**), this tree didn't establish a full forest in the upper subalpine belt, differently from other Alpine districts where populations spread successfully (Tinner and Theurillat, 2003; Pini et al., 2017; Badino et al., 2018), neither reached the elevation of the Armentarga peat bog. The belt of warm-temperate deciduous broad-leaved trees reached its maximum expansion in this subzone.

Subzone AR2b (8.8–8.1 ka cal BP) marks the first expansion of *Alnus viridis* which however remained well below its current PAR values, and well below pine PAR. Small stands of green alder may have competed with pines at wettest sites in the timberline ecotone. The spread of Alpine grasslands around the site is shown by persistently high values of herb taxa. Spores of coprophilous fungi (Sordariaceae undiff. and *Sporormiella*-like spores) suggest that herb vegetation supported pastures by native herbivores. Palaeoecological researches on lake sequences both in mediterranean and alpine areas (Anderson et al., 2011; Etienne et al., 2013) during pre-anthropic times stress the predictive power of dung spores as indicators of grazing by wild animals. Interestingly, the same areas will often be chosen later on by humans to develop seasonal pastoral activities for domesticated herbivores, in turn marked by increasing concentrations and accumulation rates of dung-related spores.

Expansion of *Abies* (ca. 10%) and *Picea* took place in zone AR3a (8.1-7 ka cal BP). The occurrence of isolated *Abies* stomata even at the high-elevation of the site is not surprising, being recorded over 2000 m asl in Swiss Alps (Wick, 2000). However, judging from the absence of correlation between *Abies* and *Pinus cembra* pollen patterns, the elevational niche of *Abies* may not have occupied the timberline ecotone.

In pollen subzone AR3b (7-6.1 ka) a massive expansion of *Alnus viridis* drives the most significant change in pollen proportions implying high within-cluster dispersion and

accumulation of dissimilarity with the subsequent AR4a zone (see dissimilarity values in clustering subzones AR3b and AR4a, **Fig. 6**). Competition with Swiss stone pine is shown by negative correlation; indeed, both species show their ecological optima in the subalpine belt. Swiss stone pine is finally reduced (in zone AR4) to the present abundance values, thus between 7-5.6 ka cal BP it disappeared from dominant forests towards its modern relict stands (see **Fig. 3A**). There are no effects on *Abies* and *Picea*. In this zone a continuous record of *Urtica*, which was completely absent before 7.3 ka cal BP, suggests the development of new ruderal nitrophilous habitats. The appearance of *Urtica* may be related to the Neolithization process in Central Alps, indeed its age is consistent with the early Neolithic migration across N-Italy at 7.3 ka cal BP (Starnini et al., 2017). *Urtica* is a large pollen producer: its pollen can easily reach the open areas above timberline sourcing from km-distances and it does not constitute a strict pastoral indicator (Mazier et al., 2006), at least when low values are recorded. There is no specific pollen indication for human activities close to the site.

Pollen zone AR4 (6.1-ca 4.7 ka cal BP) shows a further expansion of *Alnus viridis* pollen with PAR values consistent with the establishment of stands at the elevation of the Armentarga site (i.e. 2345 m asl). Replacement over the dwarf and Swiss stone pines in the subalpine belt is clearly shown by a fall of pine PAR values in subzone AR4b. The pollen production of herbs is only slightly affected by such timberline changes, suggesting that herbs and forbs persisted to dominate in the surrounding of the site. The increase of *Plantago lanceolata* (ribwort plantain) pollen between 6-5.6 ka cal BP points to a second step of human inhabitation of the Central Alps. Like *Urtica*, also plantain pollen is effectively dispersed and reaches high-elevation open lands (Bröstrom et al., 2004; Mazier et al., 2006); this long-distance transport is also shown by modern pollen deposition and vegetation surveys in the elevational transect specifically developed for the study area (Furlanetto et al., accepted). An increase of *Sporormiella*-like spores in the second part of the zone suggests increased grazing. These changes may be related to the early spread of the Camuni culture in Valle Camonica, which occurred between 6.0 and 5.5 ka cal BP (Poggiani, 2010; Pini et al., 2016b).

Pollen zone AR5a (ca 4.7 / 3.9-2.3 ka cal BP) records a sharp decrease in tree pollen, either in percentages and PAR (pines, *Abies* and *Picea*) or only in PAR (*Alnus*).

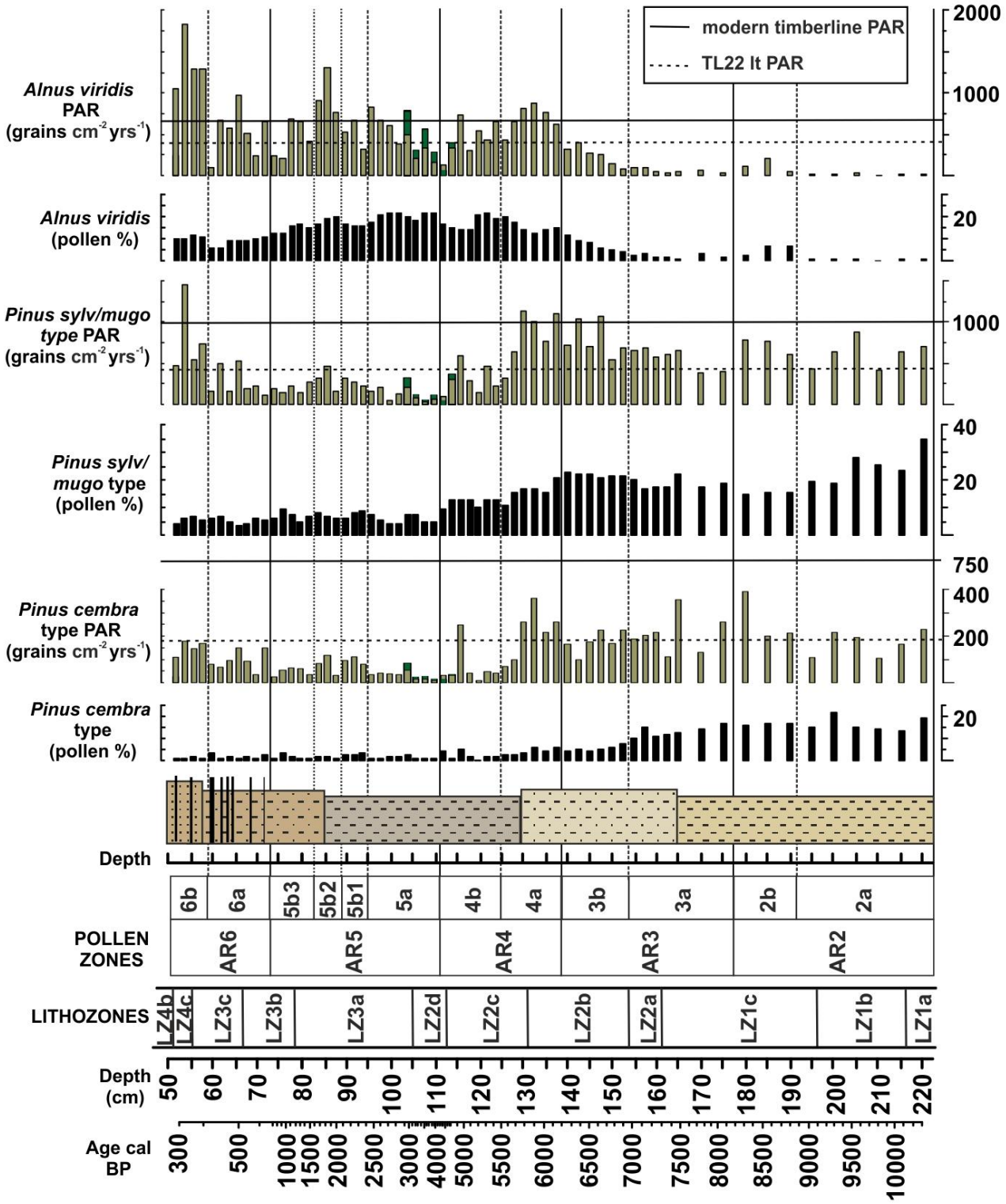

Fig. 7. Fossil pollen % and Pollen Accumulation Rates of *Pinus cembra*, *Pinus sylvestris/mugo* and *Alnus viridis*; black dashed line indicates the modern PAR value at the Armentarga peat bog (see Fig. 3E); black line indicates modern timberline PAR measurements (see section 3.4.); dark green histograms indicate PAR data from the alternative age-depth model (interval 2.9-4.8 ka cal BP); multiproxy stratigraphy is also plotted.

Conversely there is a substantial increase of pollen types from grassland vegetations and of coprophilous fungi, especially *Sporormiella*-like spores. The increasing amount and diversification of Poaceae and Asteraceae reach values similar to today's pasture vegetation ecology of the area. This pattern speaks for a lowering of the timberline ecotone and coeval expansion of grass vegetation around the site. The main step of this change is sharply recorded at 112 cm depth, with a wmean modelled age of 4.34 ± 0.3 ka cal BP, which will be discussed in section 5.1.3.

Zones AR5b and AR6 document the complex vegetation history during the late protohistory and historical ages, from the Late Iron Age to the onset of the Little Ice Age. Zone AR5b1 (2.3-2.1 ka cal BP, 94-90 cm depth) shows a first increase in sieved charcoal particles (wmean 2.23 ± 0.4 ka cal BP) while Arboreal Pollen is rising. The first occurrences of *Castanea* and *Juglans* pollen in AR5b2 likely represent long-distance transport from Celtic and Roman settlements south of the Alps. Here, cultivation started around the onset of the Current Era (Gobet et al., 2000; Pini et al., 2016a) although *Juglans* already occurred during the Late Iron Age at the Etruscan sites further south (Ravazzi et al., 2013). During the Roman Age (2.0-1.6 ka cal BP, 88-84 cm depth, AR5b2), we observe a peak in PAR values of *Alnus viridis*, a rise of sieved charcoal particles and of total and organic phosphorus (2.0-1.6 ka cal BP, 88-84 cm depth, AR5b2) suggesting that the *Alnus* dwarf forest exceeded the elevation of the study site, though being exploited and burnt. A first deforestation event (1.6-1.2 ka cal BP, early subzone AR5b3) is indicated by a new peak of sieved charcoal particles.

A further withdrawal of *Alnus viridis* dwarf forests from the Armentarga mountain took place at a modelled age of 1.2 ka cal BP (79 cm depth, late subzone AR5b3), mirrored by an increase of pasture plants pollen (*Plantago lanceolata* and *Rumex acetosa* type) and a fall of forbs (Ranunculaceae). This event is in phase with the installation of a human settlement nearby (see section 5.1.4 for further information).

Subzone AR6a (0.65-0.40 ka cal BP, that is, from 1300 to 1550 AD, 72-60 cm) shows a sharp rise of several synanthropic plants, including large cereal pollen (Cerealia type *sensu* Joly et al., 2007, i.e. D > 47 µm + d > 11 µm) but mainly intermediate types Poaceae (D > 47 µm + d < 11 µm; and D 37 - 47 µm) which may be related to *Avena* cultivation or mowing *Avena versicolor*-dominated seminatural grasslands even at high-elevation. This grassland formation still occurs on sunny slopes surrounding the

Armentarga peat bog (see caption and **Fig. 3**). Long-distance transported *Cannabis* pollen most probably originates from farming activities close to mountain villages. All these anthropogenic signals mark the late Medieval expansion of human-managed mountain landscape since the XI-XII century AD (Zonca, 1998) and installation of stable villages in the mountains of Lombardy Alps.

The subzone AR6b, dated to the XVI-XVII centuries, records a rise of *Alnus* PAR (see section 5.1.), and the decline of cultural plants. A contemporary increase in runoff and snow accumulation in the Armentarga basin catchment is indicated by the sedimentary proxies, pointing to the effects of the Little Ice Age (see section 4.2.).

4.6. Pollen-inferred temperature and precipitation reconstructions

MAT and WA-PLS model performances were evaluated in leave-one-out cross-validation. Both MAT and WA-PLS models are able to estimate the central part of the temperature and precipitation gradients covered in the calibration set, as shown by the R^2 and their root mean square error of prediction (RMSEP) values (**Fig. 9**). The residuals (predicted values minus observed values) of the calibration set show respectively a slight underestimation of the low values of July temperature and annual precipitation and an overestimation at the high values (**Fig. 9**). Overall, the MAT model (k=3 analogues) performs better (e.g. higher R^2 and lower RMSEP in **Fig. 9**) than WA-PLS model.

eHOF fitting for key taxa (*Pinus, Alnus viridis, Abies* and *Picea*) shows that these taxa have a significant relationship with Tjuly and Pann being monotonic (e.g. **Fig. 8f**), symmetric unimodal (**Fig. 8a,g**) and skewed bimodal (**Fig. 8b,c,d,e,h**). Pann frequency distribution in contrast to Tjuly frequency shows an uneven sampling of the precipitation gradient in the calibration set (**Fig. 8e,f,g,h**, see discussion in Telford and Birks, 2011b). For this reason only the MAT Pann reconstruction is here presented and discussed.

In **Fig. 10** Tjuly and Pann inferred from pollen trap TL22 and Armentarga fossil pollen record are presented. The comparison between modern Tjuly inferred with MAT method (i.e. TL22 9.85 °C) and instrumental Tjuly value (i.e. 10 °C) at 2345 m asl (Armentarga peat bog) reveals only a slight difference resulting in an underestimation of 0.15 °C in the MAT reconstruction and an overestimation of 0.35 °C in the WA-PLS reconstruction; while the comparison between modern Pann inferred with MAT method and instrumental annual precipitation shows an underestimation of 280 mm in the reconstruction of the pollen trap

located in the peat bog (TL22) (**Fig. 10**). The direct comparison between the pollen-inferred values and the instrumental data at the study site, serve as a general estimation of the model performance specifically at the study site.

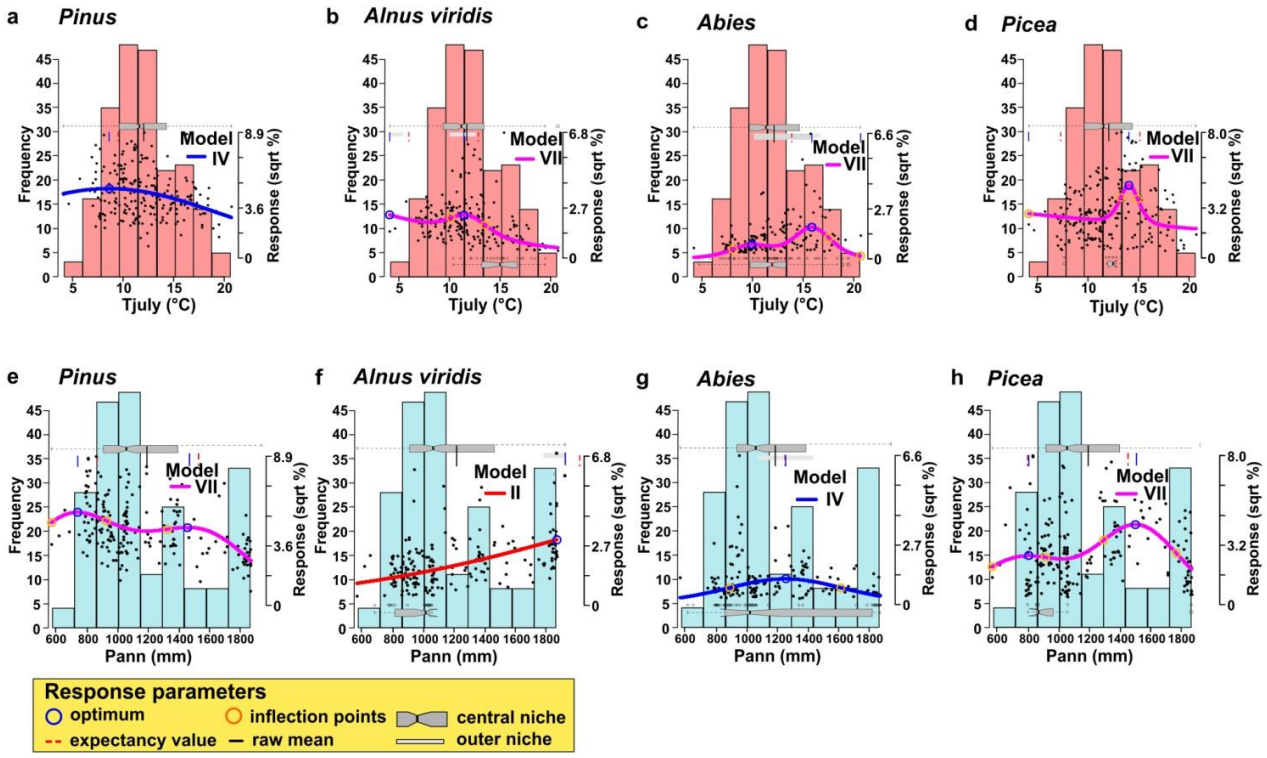

Fig. 8. Diagrams showing the simplest statistically significant response model for *Pinus, Alnus viridis, Abies* and *Picea* from the calibration set in relation to Tjuly (a to d) and Pann (e to h) as assessed by a hierarchical set of *taxon* response models within the framework of generalized linear modelling plotted on the Tjuly and Pann frequency distribution (respectively pink and light blue histograms).

The reconstructed Tjuly series obtained by the two methods throughout the fossil record (ca. 10.3-0.3 ka cal BP) show similar trends. A distinct cool event is shown around 8.5-8.7 ka cal BP when WA-PLS-inferred Tjuly dropped by about 0.8 °C, compared to the previous period. MAT reconstruction also shows decreasing temperature between 8.7-8.5 ka cal BP in comparison with the fossil samples of the previous interval having good analogues (see **Fig. 10**). The interval between 8.3-7.0 ka cal BP lacks good analogues (see **Fig. 10**, square chord distance). For this reason MAT Tjuly estimates might be too low. Considering that WA-PLS does not depend on analogue selection we rely on WA-PLS reconstruction that in this interval displays a phase of higher temperatures. After 5.0 ka cal BP a general decrease in Tjuly suggests a cooling trend up to the end of the sequence

(ca. 0.3 ka cal BP, **Fig. 10**) interrupted by a warmer period. During this phase, a drop in temperature is documented in both reconstructions at around 2.9 ka cal BP in the Early Iron Age. After a warmer period around 2.8-1.5 ka cal BP, a new cooling trend appears from the Late Middle Age to Modern times in a phase of higher human impact (see section 5.1 and **Fig. 11**). Pann (MAT) reconstruction shows a first interval of low annual precipitation from 10.3 to 6.4 ka cal BP interrupted by a phase of higher precipitation values (ca. + 300 mm) between 9.0-8.3 ka cal BP (**Fig. 10**) considering the samples which have good analogues in this interval (analogues with square chord distances lower than 10th percentile). Two increasing steps are visible from 6.4-1.5 ka cal BP, the first between 6.4 and 5.5 ka cal BP, the second between ca. 4.5 and 1.0 ka cal BP, reaching the maximum reconstructed values during the Late Roman Age-Early Middle Ages (estimated 1770 mm). The pollen-based Pann reconstruction obtained with MAT acknowledges a statistically significance (p=0.001) to the method proposed by Telford and Birks (2011a), which is based on the assumption that a significant reconstruction must explain most of the variance in the fossil data. Specifically, our Pann MAT-inferred reconstruction explains more variance in the Armentarga fossil record than reconstructions based on random environmental variables (Telford and Birks, 2011a; Telford, 2015; see **Supplementary Fig. S3**).

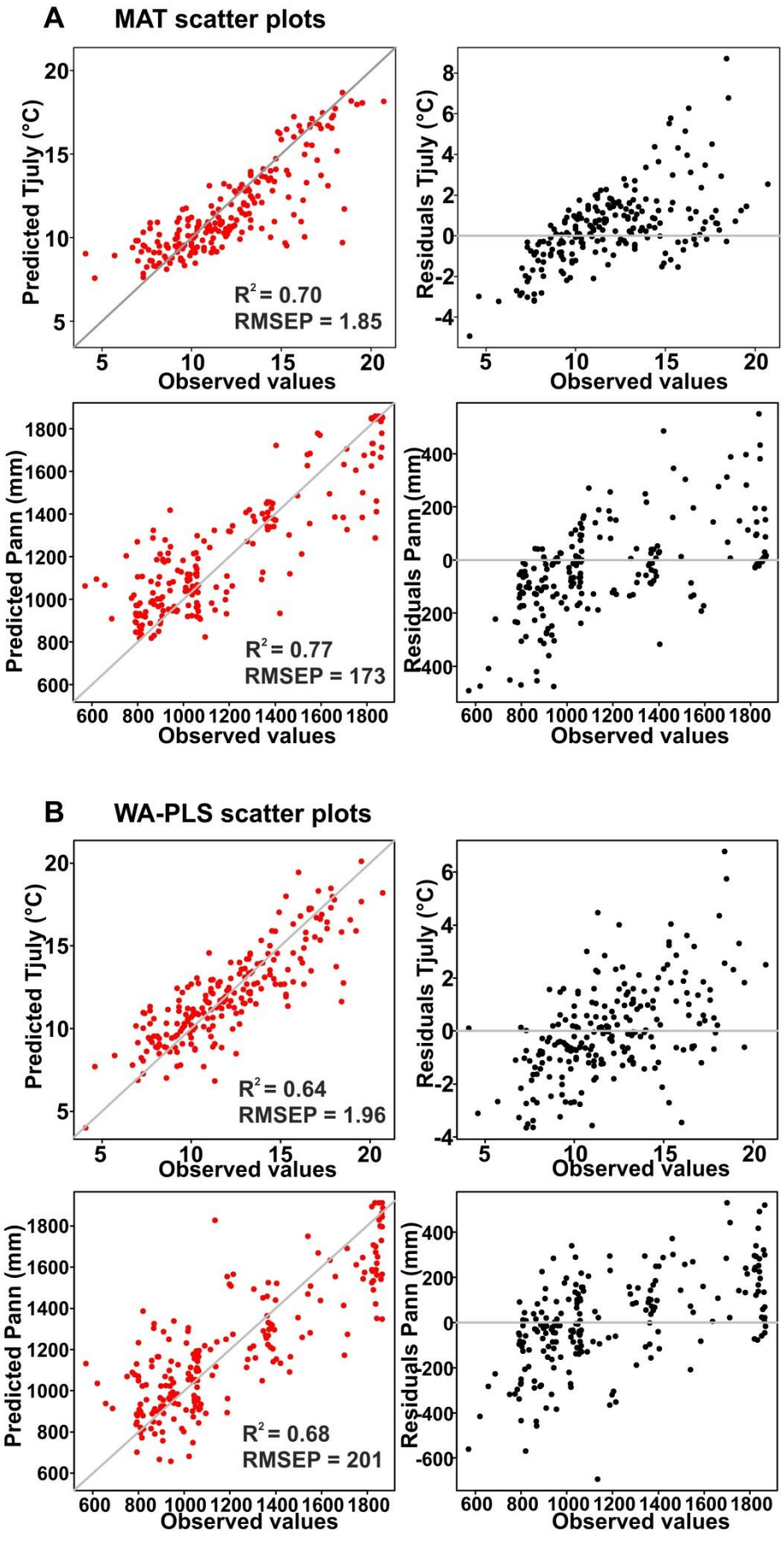
A
MAT scatter plots
Predicted Tjuly (°C)
Observed values
R² = 0.70
RMSEP = 1.85
Residuals Tjuly (°C)
Observed values
Predicted Pann (mm)
Observed values
R² = 0.77
RMSEP = 173
Residuals Pann (mm)
Observed values
B
WA-PLS scatter plots
Predicted Tjuly (°C)
Observed values
R² = 0.64
RMSEP = 1.96
Residuals Tjuly (°C)
Observed values
Predicted Pann (mm)
Observed values
R² = 0.68
RMSEP = 201
Residuals Pann (mm)
Observed values

Fig. 9. A) Mean Tjuly and Pann predicted by MAT (Modern Analogue Technique) against observed July temperature and annual precipitation. Plots on the right show relationship between residuals (e.g. predicted - observed temperature and precipitation) and observed temperature and precipitation. Root mean square of predictions (RMSEP) and R^2 are also shown. B) Tjuly and Pann predicted by WA-PLS (Weighted Averaging Partial Least Squares) against observations. Plots on the right show relationship between residuals (e.g. predicted - observed temperature and precipitation) and observed temperature and precipitation. Root mean square of predictions (RMSEP) and R^2 are also shown.

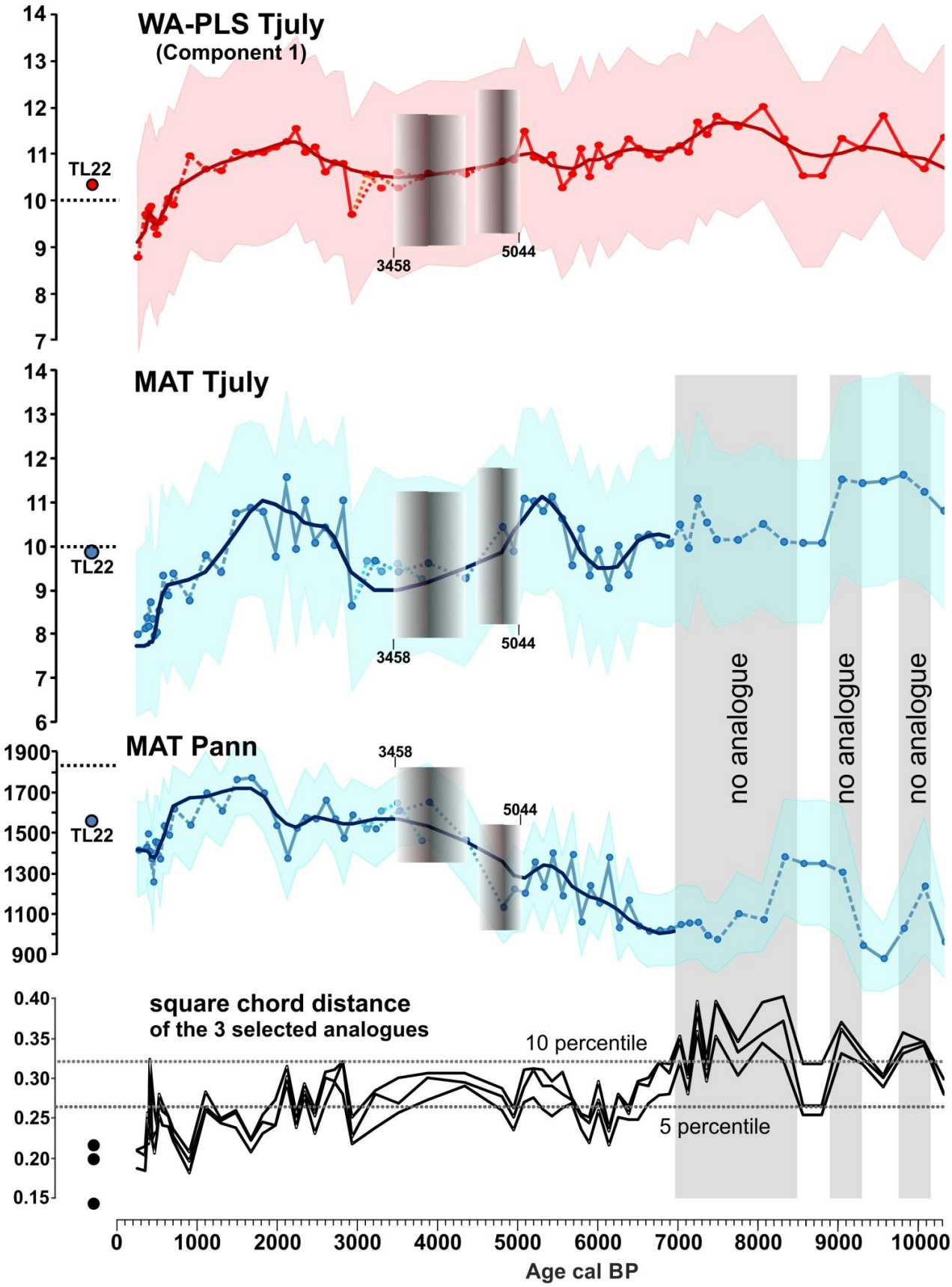
WA-PLS Tjuly
(Component 1)
TL22
3458
5044
MAT Tjuly
TL22
3458
5044
no analogue
no analogue
no analogue
MAT Pann
3458
5044
TL22
square chord distance
of the 3 selected analogues
10 percentile
5 percentile
Age cal BP

Fig. 10. Pollen-inferred Tjuly (MAT and WA-PLS) and Pann (MAT) reconstructions from the 'Armentarga record'. Pann frequency distribution in contrast to Tjuly frequency shows an uneven sampling of the precipitation gradient in the calibration set for this reason the pollen-inferred Pann WA-PLS reconstruction was not considered. A LOESS smoother (span 0.1) is fitted to the reconstructed values (solid line) plotted together with sample-specific standard errors of prediction (SSEP, light red and light blue envelope). The min and max age cal BP for the samples 110 and 114 cm depth given by Bacon is presented with grey shaded rectangles. The modern reconstructed Tjuly and Pann values (red and blue dots) and instrumental data (black dashed lines) are plotted. MAT reconstructions are evaluated checking the square chord distance of the three selected analogues. All distances smaller than 10th percentile indicate that the fossil sample has good analogues, while distances higher than 10th percentile suggest no analogues in the calibration set. Grey uniform bands and dashed lines connecting the reconstructed points indicate samples having no analogues. Dashed lines also indicate the Middle Age interval affected by strong human impact.

5. Discussion

5.1. The history of human interference and its effects on pollen-based climate reconstruction

5.1.1. Calibration of the pollen-climate elevational transect for anthropic interference and the analogue goodness

Human impact on vegetation is a potential source of bias in climate reconstruction models based on pollen. In a companion study, Furlanetto et al. (accepted) have tested the specific pollen-climate elevational transect for the site under study (Upper Brembana Valley) checking for anthropic bias using a WA-PLS model and found a temperature underestimation due to the signal of synanthropic herb vegetation, more important at lower (mountain) elevation compared to high elevation. The calibration between pollen-reconstructed Tjuly and instrumental values at the Armentarga site revealed only a slight difference, resulting in an overestimation of 0.35 °C in the WA-PLS reconstruction and an underestimation of 0.15 °C in the MAT reconstruction (**Fig. 10**), suggesting that the analogues included in the calibration set used for climate reconstruction are able to account for the present-day state of anthropic alterations to climate-vegetation relationships at the study site. This ensures models robustness even if timberline is locally depressed, and even if modern pollen proportions are altered by pastoralism and forest clearing (see section 5.1.2.). However, this conclusion is not to be extended back in time, as far as modern available analogues may not match past pollen images. An evaluation of

the goodness of the selected analogues is given in **Fig. 10** (lower panel, square chord distance). Two intervals are critical (i) the time span before 7 ka cal BP, due to missing analogues in our calibration set, i.e. cohexistence of oceanic and continental dwarf forest in the timberline ecotone. Here, our reconstructions suffer from an uneven distribution of available analogues along the precipitation gradient, only partly constrained by our sampling strategy along elevational vegetation transects. (ii) the Middle Ages, due to strong human impact exceeding the modern values. Reconstructed Tjuly and Pann for intervals (i) and (ii) will be marked by a dashed line (**Figs. 10-13**). The main changes in precipitation observed in the second half of the Holocene are supported by good analogues both before and after the expansion of the *Alnus viridis* dwarf forest. A drought season, which has a strong impact on Mediterranean vegetation and may be cause of bias in semiarid regions with poor analogue coverage and strong fire disturbance (Samartin et al., 2017), is to be excluded for the oceanic Alps, either in contemporary and in the Middle Holocene times.

5.1.2. The historical record of plant indicators of human activities

In order to disentangle human impacts from the complex of climate-human interactions, we compared several proxies of anthropic activities, i.e. coprophilous fungi, pointing to herbivores dung in the runoff catchment supplying the depositional basin; phosphorus forms, helping to investigate the fertilization of the terrestrial and aquatic environments; and the pollen of synanthropic plants. Our modern elevational transect (Furlanetto et al., accepted) revealed that pollen of synanthropic plants such as *Urtica, Plantago, Cannabis, Castanea* and *Juglans* undertake moderate (2-5 km) to long (> 5 km) distance transport from lower vegetation belts, and that pollen deposition with low percentages (< 2%) in the elevational treeless area is a marker of lowland and mountain human settlements, rather than local activities (**Supplementary Fig. S4**). A method to effectively disentangle human impact relies on tracing baseline patterns of apophytes (i.e. native plants whose abundance was enhanced by human activities) prior to the first sign of farming, i.e. prior to the Neolithization of the Italian Alps between 7.3-6 ka cal BP (Pessina, 2000; Poggiani, 2010). The quantification of such a “pristine baseline” (Willis et al., 2005) is necessary, if primary habitats are to be kept distinct from human-made secondary ones. When doing so, most of the so-called “anthropogenic indicators” (Behre, 1981) such as *Rumex acetosa*

type and the large group of Ranuculaceae (the genera *Aconitum, Trollius, Anemone, Pulsatilla* widely occur in natural habitats) do not show changes exceeding natural disturbance before the Middle Ages (see curve of apophytes and cultivated plants in **Fig. 6**). This feature may be related to the elevational location of our site which remained above the upper forest limit before and after the Neolithization. We conclude that human interference remained weak along the pre-historical ages in our study area. In a wider perspective, we warn against using apophyte pollen occurrence alone to predict human impact at or above upper timberline elevations in the Alps.

5.1.3. The environmental changes at the Middle to late Holocene transition evidence of grazing by native herbivores

The pollen record from the Armentarga site revealed a sharp vegetation change, i.e. expansion of nutrient-rich plant communities and timberline depression, in the final steps of zone AR4 around 4.34 ± 0.3 ka cal BP (or between 4.7 and 3.9 ka cal BP according to the alternative age-depth model, see **Fig. 4**). An increase of dung spores, notably *Sporormiella*-like spores (van Geel and Aptroot, 2006), co-occurs at the time of the timberline depression (**Fig. 6** and **Supplementary Fig. S4**, section 4.5.). Sordariaceae and especially *Sporormiella*-like spores are found to mark local grazing, both in our elevational transect and in the literature (Doyen and Etienne, 2017). We already noticed that at our site dung spores occurred even in pristine grasslands before the Neolithization, thus we infer grazing of native herbivores (mostly ungulates, notably ibex). Direct analysis of fossil dung from the discovery site of the Late Neolithic Iceman has proved this circumstance in another high-elevation mat in the Eastern Alps (Oeggl, 2009). The dung spores increase observed at 4.7 / 3.9 ka cal BP may be related either to the expansion of grassland vegetation and intensification of grazing by native herbivores (Anderson et al., 2011) and/or domesticated ones (Etienne et al., 2013), and/or to an increased runoff and notably snow runoff combined with long-term population changes in ungulates (Jacobson et al., 2004; Holtmeier, 2009; Oeggl, 2009; Etienne et al., 2013; **Supplementary Fig. S2** and **Table S2** for further arguments on snow runoff). We have shown that natural grasslands persisted throughout the pre-anthropic Holocene at our high-elevation site, thus we expect both effects to be summed up. Such situations urge the need for independent proxies disentangling human from climate triggers. In the previous section we

highlighted that indicators of local human impact (excluding long-distance transport) did not show a significant response. On the other hand, we inferred a coeval strong increase in reconstructed annual precipitation (**Fig. 10**), which may have triggered grassland expansion and increase of snow runoff. The same applies to organic and total phosphorus, showing a weak increase meanwhile. Dissolved phosphorus forms are mainly transferred from grazed grassland to stream and lake sediments by surface runoff (Jordan et al., 2005; Kurz et al., 2006). In turn, runoff and phosphorus transfer depend primarily on rainfall and then on grazing intensity. All together, these arguments suggest that sharp vegetation change, i.e. expansion of nutrient-rich plant communities and timberline depression observed at 4.7 / 3.9 ka cal BP, was mostly triggered by a phase of precipitation and runoff increase and was accompanied by an intensification of grazing. In turn, climate change may account for enhanced animal husbandry observed elsewhere in the Alps (Magny and Haas, 2004). This scenario will be supported by comparing independent proxies for climate change in the nearby mountain areas (section 5.2.).

5.1.4. The Middle Ages phase of human interference

A phase of intense human impact started at wmean age 1.1 ka cal BP (late subzone AR5b3 starting from phosphorus increase at level AR5b-78 cm; early Middle Ages, locally Longobard Age) and ended at wmean age 0.385 ka cal BP (Little Ice Age onset). Here, a withdrawal of *Alnus viridis* dwarf forests from the Armentarga mountain is mirrored by the expansion of low pollen-producers apophytes and cultivated plants, such as Poaceae (*Hordeum* type*, Avena*, partly cultivated, partly apophytes), cereals and pasture plants (*Plantago* and *Rumex acetosa* type). Doubling total and organic phosphorus concentrations recall the records from Alpine water basins with animal watering (Pini et al., 2017). Furthermore, a coeval increase in sieved charcoal particles and a fall in *Alnus viridis* PAR point to the exploitation of dwarf forests in the timberline ecotone belt fringing the study site just below 2345 m asl, most probably for charcoal production. Indeed, several charcoal kiln platforms were found in the subalpine belt underlying the Armentarga site and radiocarbon dated to the early Middle Ages (Casini et al., 2010 and personal communication). In turn, these kiln ages were found to be in phase with a nearby mining village active between the VII-XV centuries AD (the “Piani di Sasso village” **Fig. 3A**) (Riceputi, 2004). During the Middle Ages, due to the need of metal processing, subalpine

dwarf and coppiced forests (especially *Alnus viridis, Pinus mugo*, and *Fagus sylvatica*) were widely exploited in the Alps for charcoal production (Cucini Tizzoni, 1994; Castelletti et al., 2011).

In the early Middle Age (Longobard Age), forest clearing, farming and pastoralism were more intense than today, thus we cannot exclude biases on numerical reconstruction of climate parameters, as shown in **Figs. 10** and **11**. The main steps of human interference recorded at the Armentarga peat bog have been fixed in **Supplementary Fig. S4**.

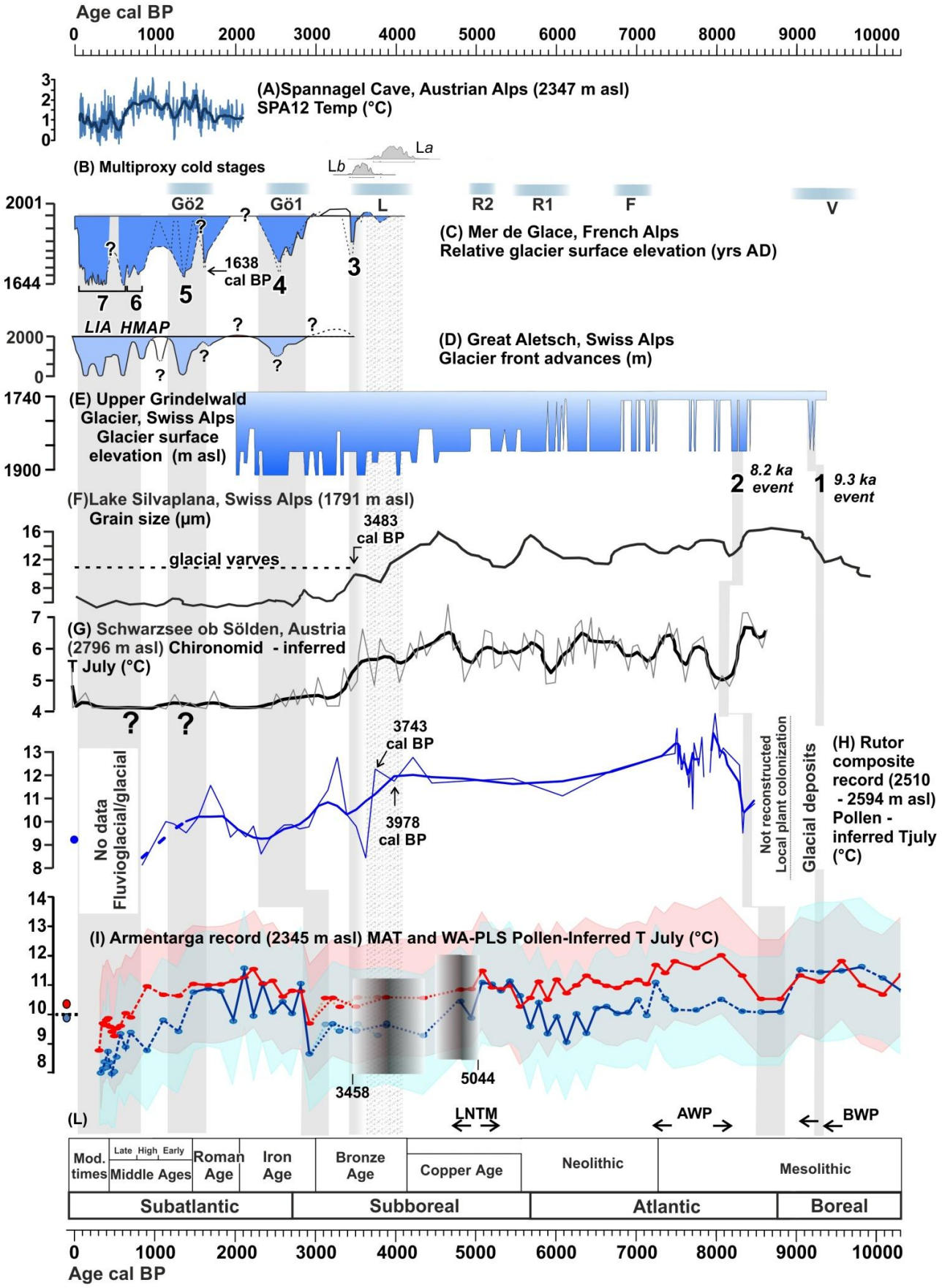
Age cal BP
0 1000 2000 3000 4000 5000 6000 7000 8000 9000 10000
(A)Spannagel Cave, Austrian Alps (2347 m asl)
SPA12 Temp (°C)
(B) Multiproxy cold stages
La
Lb
Gö2
Gö1
L
R2
R1
F
V
(C) Mer de Glace, French Alps
Relative glacier surface elevation (yrs AD)
1638 cal BP
LIA HMAP
(D) Great Aletsch, Swiss Alps
Glacier front advances (m)
(E) Upper Grindelwald Glacier, Swiss Alps
Glacier surface elevation (m asl)
8.2 ka event
9.3 ka event
(F)Lake Silvaplana, Swiss Alps (1791 m asl)
Grain size (µm)
3483 cal BP
glacial varves
(G) Schwarzsee ob Sölden, Austria
(2796 m asl) Chironomid - inferred
T July (°C)
3743 cal BP
3978 cal BP
No data
Fluvioglacial/glacial
Not reconstructed
Local plant colonization
Glacial deposits
(H) Rutor composite record (2510 - 2594 m asl) Pollen - inferred Tjuly (°C)
(I) Armentarga record (2345 m asl) MAT and WA-PLS Pollen-Inferred T July (°C)
3458
5044
(L)
LNTM
AWP
BWP
Mod. times
Late High Early
Middle Ages
Roman Age
Iron Age
Bronze Age
Copper Age
Neolithic
Mesolithic
Subatlantic
Subboreal
Atlantic
Boreal
0 1000 2000 3000 4000 5000 6000 7000 8000 9000 10000
Age cal BP

Fig. 11. Selected series of climate proxies from the high altitude Alps (speleothems, glaciers, chironomids, lake sediments) have been plotted according to their calendar chronology (taken from Badino et al., 2018) and compared with Armentarga pollen-inferred Tjuly. Proposed alignments of climate events are indicated by grey belts and by acronyms of warm phases (L). A dotted belt in the Early Bronze Age interval underlines a regime shift in temperature, which apparently is evident only in proxies measured in continuous stratigraphies (chironomids, pollen and lake sediment derived proxies).

Key to numbers of climate events: (1) 9.3 ka cal BP event identified in the NGRIP $\delta^{18}O$ record; (2) 8.2 ka cal BP event identified in the NGRIP $\delta^{18}O$ record; (3-4-5-6-7) Mer de Glace advances.

Key to panels: (A) Temperature (°C) Spannagel Cave SPA 12 (Mangini et al., 2005). (B) Multiproxy cold stages in the Alps - V: Venediger oscillation (Patzelt and Bortenschlager, 1973); F: Frosnitz advance periods; R 1-2: Rotmoos advance periods; L: Löbben oscillation (La and Lb: Calibration intervals for ages 3576 (median) ± 140 yrs cal BP and 3811 (median) þ 180/-203 yrs cal BP (Patzelt and Bortenschlager, 1973); Gö 1-2: Göschenen periods (Zoller et al., 1966); (C) Relative surface elevation of the Mer de Glace (Le Roy et al., 2015); (D) Great Aletsch glacier front advances (Holzhauser et al., 2005); (E) Synthesis of Upper Grindelwald Glacier surface elevation changes interpreted from the Milchbach Cave speleothems (Luetscher et al., 2011); (F) Grain size variation in Lake Silvaplana (Leemann and Niessen, 1994) plotted against recalculated calibrated ages; (G) Chironomid-inferred temperature from Schwarzsee ob Sölden, Austria (Ilyashuk et al., 2011); (H) Rutor composite record reconstructed past and modern Tjuly using the Modern Analogue Technique (MAT). Error bar for the modern value represents the RMSEP of the model (Badino et al., 2018). (I) Armentarga record reconstructed past and modern Tjuly using the MAT (blue) and the WA-PLS methods (red) plotted together with sample-specific standard errors of prediction (light red and light blue envelope). The modern reconstructed Tjuly values (red and blue dots) and instrumental data (black dashed line) are plotted. The intervals with missing analogues for MAT reconstruction or Middle Ages strong human impact are presented with dashed lines. (L) Holocene warm phases presented in section 5.2.1.: Boreal Warm Period (BWP), Atlantic Warm Period (AWP) and Late Neolithic Thermal Maximum (LNTM).

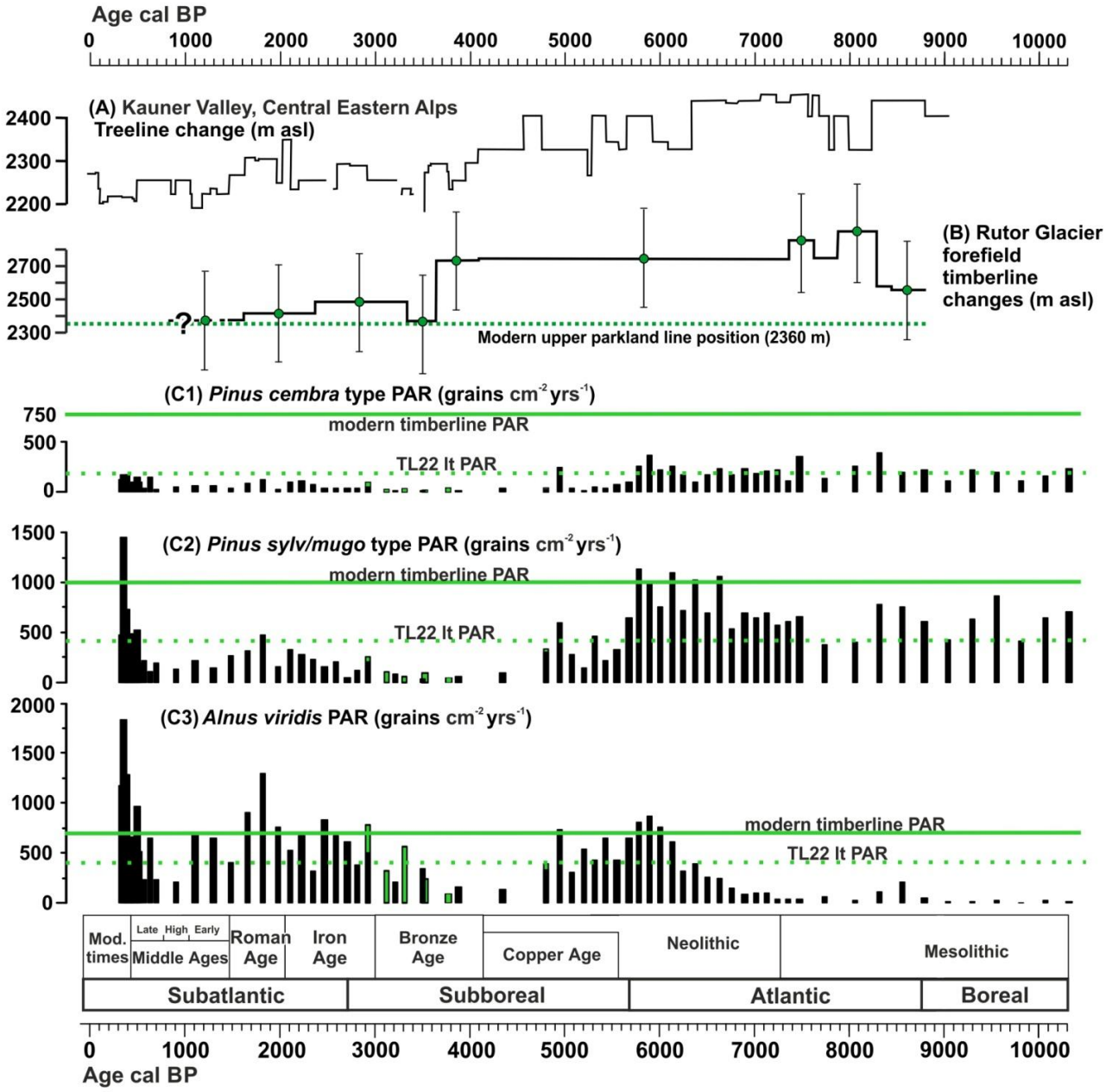

Fig. 12. (A) Reconstructed treeline position from Kauner Valley, Central Eastern Alps (Nicolussi et al., 2005). (B) Rutor Glacier forefield reconstructed timberline position with standard error bars averaged for pollen zones (Badino et al., 2018); (C) Fossil *Alnus viridis*, *Pinus sylvestris/mugo* and *Pinus cembra* Pollen Accumulation Rate data from Armentarga record; green histograms indicate PAR data from the alternative age-depth model (interval 2.9-4.8 ka cal BP).

5.2. The proxy record of Mid to late Holocene thermal oscillations and precipitation increase in the Alps and their borders

The Holocene-scale reconstructions of both Tjuly and Pann obtained at a high-elevation site in the oceanic Italian Alps show a series of temperature changes and a pronounced pattern of precipitation changes. We anticipate the analysis of temperature changes in the high mountains as they are dependent mostly on lapse rate, and related process of amplification, so that trends can be easier compared to other, independent high-elevation records in the Alps (section 5.2.1, **Figs. 11-12**). On the other hand, the analysis of the main change in precipitation observed at the Middle to Late Holocene transition must take into account the marked regionalization which opposes the inner to the outer belts of the Alps and their foothills (section 5.2.2., **Figs. 13-14**).

5.2.1. Disentangling the sequence of Holocene thermal anomalies from precipitation changes

During the last 10 ka the Tjuly anomaly remained in a range of 2.4° ± 1.8° C (WA-PLS model). There is an overall declining trend from the early peak at 8 ka cal BP (Atlantic Warm Period, AWP) to the onset of the Little Ice Age at 0.38 ka cal BP. This trend has been found to match the pattern of middle latitude insolation both at continental (Mauri et al., 2015) and alpine scale (**Fig. 11**). AWP is preceded by a cold event dated 8.5-8.7, which interrupted a previous warm phase (Boreal Warm Period, BWP, 9-10.4 ka cal BP) (see **Fig. 11**). The resolution of our record does not allow centennial events to be resolved, still we suggest this cold event could match the Venediger glacial advance at 9-9.4 ka cal BP, more pronounced than the Greenland event at 8.2 ka cal BP (Rasmussen et al., 2007), the former being found at several glacial records in eastern Alps (**Fig. 11**; Muscheler et al., 2000; Luetscher et al., 2011; Badino et al., 2018). At the Armentarga site, the AWP apparently spanned a millennium between ca. 8.2-7.2 ka cal BP (WA-PLS pollen-inferred Tjuly), matching the phase of maximum timberline positions recorded in the Alps (see **Fig. 12**; Nicolussi et al., 2005; Badino et al., 2018). In the outer Italian Alps, however, the timberline remained below the site and did rise only later on (**Fig. 7** and section 4.5.). Here we recall to the negative effect of oceanicity on spread of the main tree species forming thermal timberlines in continental climates, i.e. *Pinus cembra*, and despite

a coeval precipitation minimum occurs in phase with AWP (**Fig. 13**). This question will be discussed in section 5.2.3.

A further warm phase is centered at ca. 5 ka cal BP, although MAT and WA-PLS provide different results as for amplitude and pattern of this event, which is commonly, though informally, referred to “Late Neolithic Thermal Maximum” (Grosjean et al., 2007). Notice a late precipitation minimum at ca. 4.8 ka cal BP (Late Neolithic; otherwise “late Copper Age” according to the archaeological periodization in the Italian Alps, see **Fig. 11**), not in phase with the thermal acme (**Fig. 13**).

Unfortunately, the Middle / Late Holocene transition (Mayewski et al., 2004; Walker et al., 2012) between 4.7-3.9 ka cal BP and the so called “4.2 ka cal BP event” (4.25-3.9 ka cal BP according to Zanchetta et al., 2016) could not be detailed in our record, as the modelled age at 4.34±0.3 ka cal BP represents just the intermediate point of a main temperature decline and a remarkable precipitation increase marking the most important Holocene change in the climatic regime. The “4.2 ka cal BP event” may possibly be represented by a hiatus (see next section). The overall temperature drop between the Late Neolithic Thermal Maximum and the Iron Age minimum (locally dated 2.9 ka cal BP – we propose correlation with Göschenen I, 2.9-2.6 ka cal BP, **Fig. 11**), however, remained within 2.0 °C (MAT) or 1.8°C (WA-PLS).

The Late Iron Age and Roman Age records a timberline rise and warm conditions, modulated by intervening precipitation oscillations, notably a dry-warm phase characterized the Roman Imperial Age and an extreme wet, still warm phase occurred during the Late Roman – early Middle Age (**Figs. 11-13**). These in phase moisture and temperature changes are widely documented in the western Mediterranean and related to NAO intensity changes (Olsen et al., 2012; Di Rita et al., 2018). Differences among our models and discrepancies with the reference Alpine temperature record (Mangini et al., 2005, **Fig. 11A**) are visible since the onset of the Middle Ages, possibly due to intervening strong human impact. We therefore refrain from any paleoclimate interpretation during historical times.

5.2.2. Towards wetter orographic climates – changes in the weather system at the Middle / Late Holocene transition in the outer belts of the Italian Alps

Nowadays, the precipitation pattern in the Alps shows several oceanic-like climate zones in the outer belts and their foothills (Crespi et al., 2018). The southern flank of the Alps hosts two main districts characterized by oceanic-like precipitation regime marked by annual rainfall between 1600 and > 3000 mm (an except shown in **Fig. 2B**), i.e. the Insubria-Lepontine-Lombardy Alps and the Julian Alps. These mountains are affected by substantial advection of southern air masses driven by Atlantic trough extending over the Mediterranean basin enhancing orographic precipitation (Rotunno and Houze, 2007; Davolio et al., 2016). The maximum precipitation in the Insubria-Lepontine-Lombardy Alps is associated to the frequency of Mediterranean cyclones in winter, conveying air masses from the Mediterranean towards the Alps. Due to the low elevation of the Apennine chain at its NW limit, southern air masses are able to flow over the Apennines and reach the Alps where they are uplifted providing substantial orographic rainfall (Buzzi et al., 2003; Rotunno and Houze, 2007; **Figs. 2B-14**). The Armentarga site is located at the northern border of the oceanic district on the highest chain divide, exposed to these air masses (**Fig. 14**). This regional feature is associated with a pressure ridge over the eastern Euro-Mediterranean region. On the whole, changes on cyclones pathways northward or southward of the Alps are expected to deeply affect this precipitation mechanism.

In **Fig. 13** we compared precipitation and lake level reconstructions at three sites along the orographic rainfall gradient so far described. The first site of Lake Accesa (Magny et al., 2007) is from mountain foothills windward to the Apennine barrier (i.e. the Apuane Alps, see **Fig. 14** and **Supplementary Fig. S5**); the second one of Lake Ledro (Magny et al., 2012) is in the Italian Alps, at low elevation (**Fig. 14**); the third one is the Armentarga site presented in this paper. We argue for a similar pattern of Holocene precipitation change at all these sites throughout the Holocene, indicating a similar weather system determinant. When the antithetic Eastern Mediterranean is included, an opposite Holocene pattern has been shown, partly related to changes of NAO intensities (Bar-Matthews et al., 1998; Magny et al., 2011, 2012; Di Rita et al., 2018).

Timing and climate dynamics across the Middle to Late Holocene transition in the Alps require high-resolution multiproxy data and robust chronologies which are currently poorly or not available. The average age obtained for the high-elevation Armentarga site (4.34 ± 0.3 ka cal BP) and intervening small gaps in stratigraphy are not enough precise for fine

correlation. Prominent lake level rise at Lake Ledro is assigned an age of 4.5 ka cal BP and an outstanding shift of + 4.5 m (Magny et al., 2012), which may be updated to 4.2 ka cal BP and + 2.5 m once sediment subsidence and correlation with early Bronze age pile dwelling is reconsidered (red line in **Fig. 13**). An age of 3.9 ka cal BP would match the sharp lake level rise at Accesa (Magny et al., 2007, with chronological updates, see caption **Fig. 13**) and other alpine studies on soil erosion (Arnaud et al., 2012; Brisset et al., 2013). A double sequence of sharp changes in isotopic composition between 4.5-3.8 ka cal BP, suggesting sharp changes in seasonal precipitation, is shown in Alpine (Fohlmeister et al., 2012) and N-Apennine (Zanchetta et al., 2016) speleothems. However, discontinuities in lacustrine records (**Fig. 13**), and difficulties in comparing radiocarbon, U/Th and tephra chronologies at centennial scale hampers disentangling the centennial climate history across the Middle to Late Holocene transition on the northern Mediterranean borderland, an argument requiring further effort beyond the scope of the present paper.

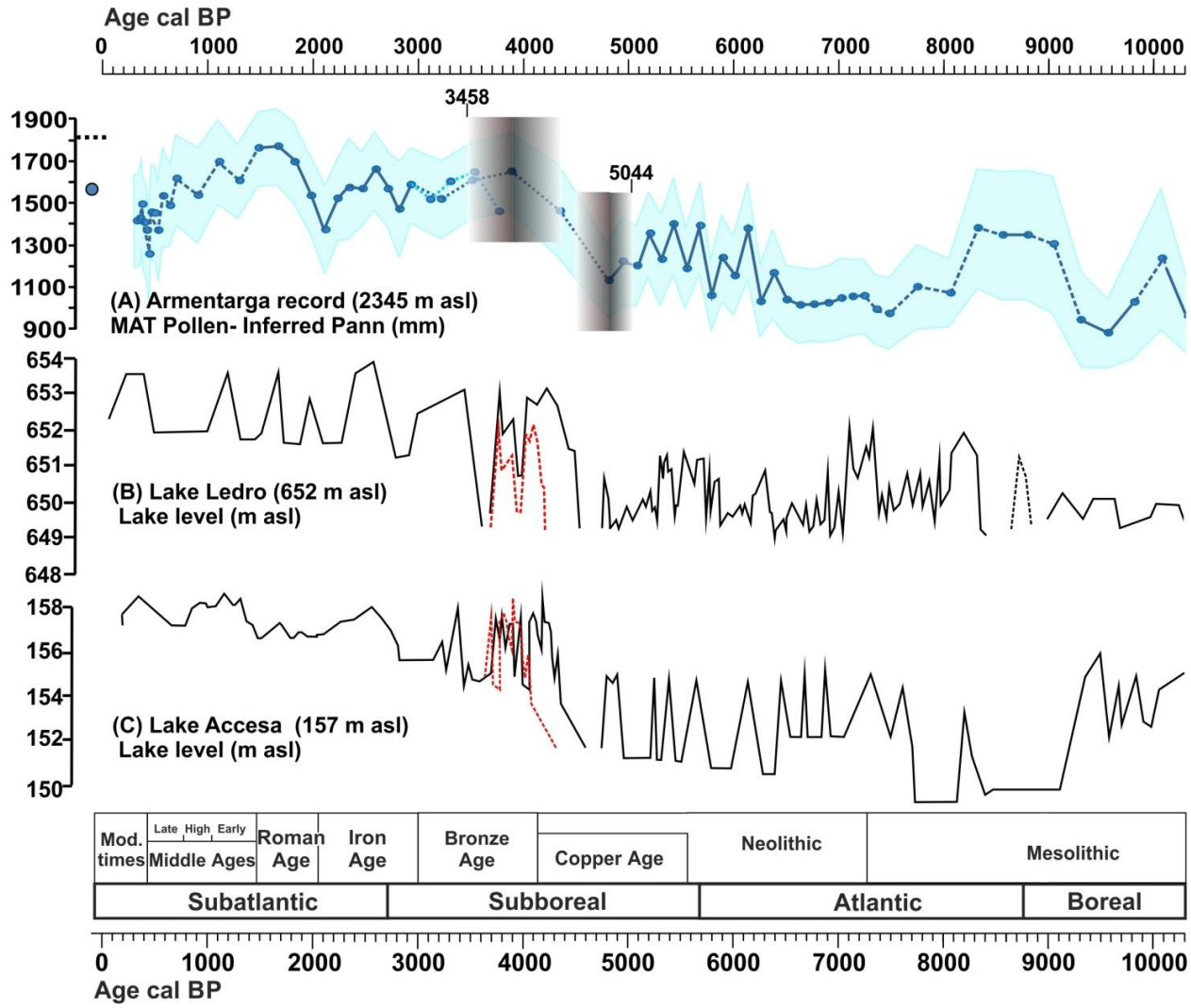

Fig. 13. (A) Armentarga record reconstructed past and modern annual precipitation using Modern Analogue Technique plotted in comparison to lake level reconstructions on the northern Mediterranean borderland at sites windward to the Tyrrhenian cyclones. The sites are respectively at the southern border of the oceanic Italian Alps (panel B - Lake Ledro, black line, from Magny et al. 2012; red line alternative age model for Ledro, see section 5.2.2.) and at the foothills of the northern Apennine (panel C – Lake Accesa, from Magny et al. 2007, age of Avellino tephra updated according to Sevink et al., 2011 (red dashed line)).

5.2.3. The timberline replacement of pines by broad-leaved dwarf forest under the pressure of precipitation increase

The most common type of timberline ecotone today in the Alps is formed by *Pinus cembra* developing in inner continental ranges under 600-1100 mm Pann (Ellenberg, 1988). Several types of dwarf forest, either conifer (*Pinus mugo*) or broad-leaved dominated (*Alnus viridis, Sorbus aucuparia, S. chamaemespilus*) take place in more oceanic ranges

(Jobbagy and Jackson, 2000), especially in the eastern Alps and the Carpathians (Holtmeier, 2009; Mauri and Caudullo, 2016; see **Fig. 14B**). Despite larch takes part in the modern timberline ecotone, its local pollen representation is too low (see **Fig. 3** in Furlanetto et al., accepted) to allow any precise consideration about its past occurrence. In today's snow-rich and summer-rainy ranges of the Eastern Alps, *Pinus cembra* is endangered and underfit by parasitic snow fungi, especially due to slow growth of seedlings, strongly affecting survival (Senn, 1999; Holtmeier, 2009). On the other hand, *Pinus mugo* is competing with broad-leaved forest at timberline on an edaphic base, i.e. it occupies dry sites, such as massive bedrock conductive to coarse regolith (Ballian et al., 2016), whilst broad-leaved are on other bedrock types or parent materials, conductive to fine-grained regolith. Competition is expected to have also happened in the first half of the Holocene below the elevation of our site, as both timberline shrubs together with Swiss stone pine occurred there since the early Holocene. Our data show that time displacements in favor of the broad-leaved scrub was climate-driven and started as early as 9 ka cal BP as a consequence of a temporary precipitation increase (**Figs. 10-13**). A second step of dwarf broad-leaved forest increase at 6.2 ka cal BP (**Fig. 7**) took place at reconstructed annual precipitation of 1300 mm. *Alnus viridis* became dominant at the time of further prominent precipitation increase, i.e. at the Middle-Late Holocene transition, leading to the current relict state of *Pinus mugo* and *P. cembra* populations as early as 3.9 ka cal BP (**Fig. 7** and **Supplementary Fig. S1**) at reconstructed annual precipitation of 1600 mm (**Fig. 10**). The process of timberline replacement by the dwarf broad-leaved forest was already completed at the onset of human deforestation, in the Iron Age. Despite a strong interference by pastoralism and mining since the early Middle Ages, the structure of the current timberline residual forest spots in the outer Italian Alps still reflect the dominance of oceanic dwarf forests, which become established in the second half of the Holocene.

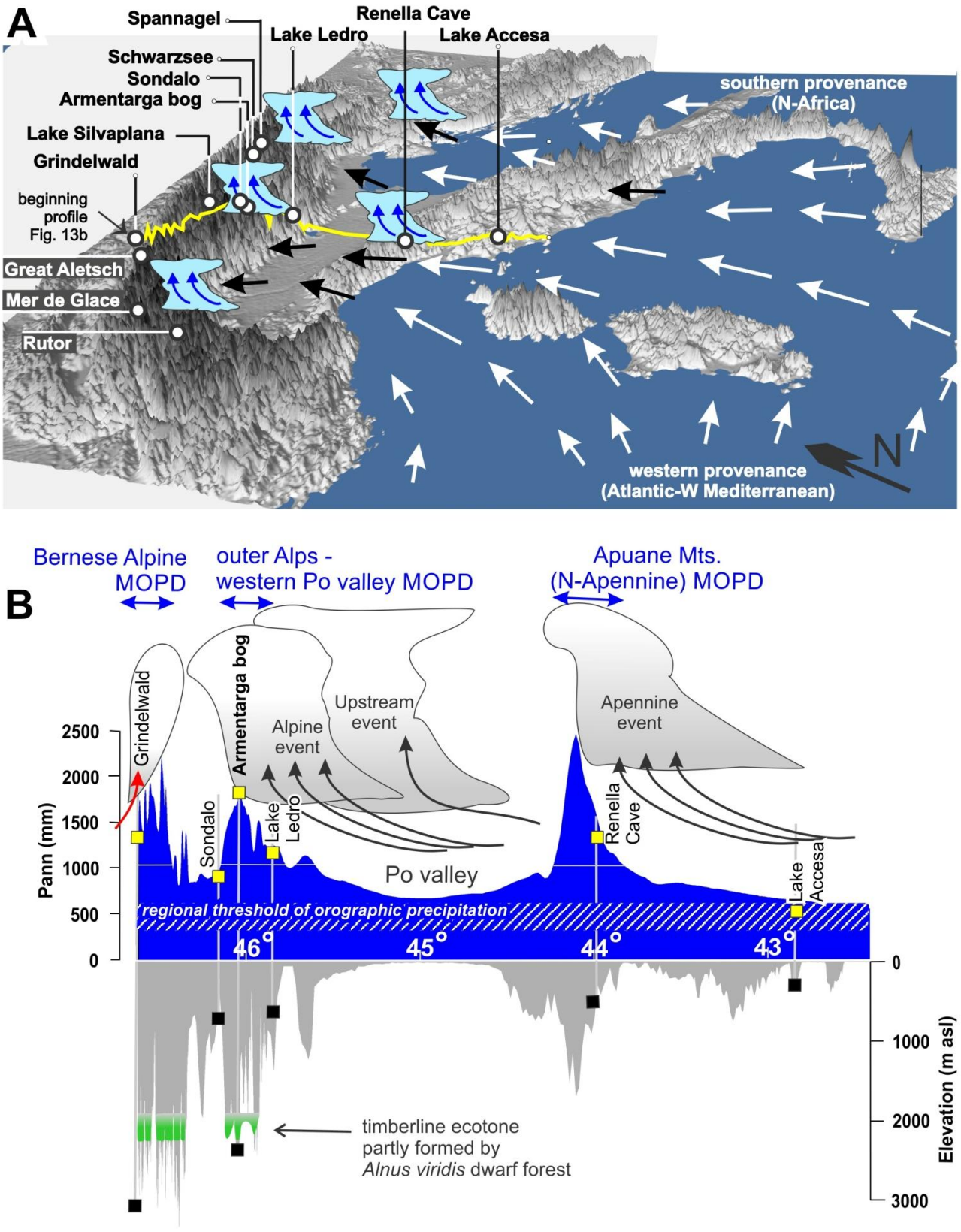

Fig. 14. Orographic precipitation on the northern Mediterranean borderlands. A) Wind field at 500 hPa at a case of heavy rainfall due to orographic precipitation on the southern flank of the Alps (from Rotunno and Houze, 2007, their Fig. 4) associated with a typical W-Mediterranean cyclone. Notice western Atlantic

moisture sourcing, not extending to the Eastern Mediterranean. B) Annual precipitation (Pann) and relief latitudinal profiles (from N 42° to N 47°) across the Apuane Mts., the Po valley and the southern flank of the Alps showing the location of the records of hydrological changes on the northern Mediterranean borderland and the elevational position of the broad-leaved dominated dwarf forest in the oceanic mountain districts. The figure also conceptualizes the main regional topographic factors involved in orographic precipitation related to Tyrrhenian cyclones. MOPD = Maximum orographic precipitation district. Circulation and precipitation patterns are from Rotunno and Houze (2007) and Davolio et al. (2016).

6. Conclusions

The stratigraphic study of paleoecological and sedimentary proxies in the Armentarga peat bog allowed to reconstruct the vegetation and climate history during the last 10 ka in a high-elevation, oceanic district of the Italian Alps. Quantitative reconstructions of Tjuly and Pann were obtained and validated by applying numerical transfer functions built on an extensive calibration pollen-climate dataset. These models proved to be effective even on the modern landscape marked by weak to moderate human impact, with the exclusion of Middle Age phases that suffered stronger alterations due to deforestation and pastoralism. The reconstruction of timberline structure and elevations was supported by an additional elevational transect on modern and past Pollen Accumulation Rates of the main tree and shrub species building the timberline ecotone.

In this area, the modern timberline ecotone shows a peculiar arrangement with a widespread belt of broad-leaved dwarf forest, in agreement with high annual precipitation, while the continental timberline formed by *Pinus cembra* is absent.

The palaeobotanical record of the Armentarga peat bog has shown this elevational vegetation arrangement to be primarily driven by a Middle to late Holocene precipitation increase, substantially independent from the millennial sequence of thermal anomalies already known from other high-elevation Alpine proxies (i.e. glaciers, timberline, chironomids, speleothems).

Changes in annual precipitation occurred in three main steps during the Holocene, starting with a moderately humid early Holocene marked by early occurrence of the *Alnus viridis* dwarf forests, and followed by a first step of precipitation increase starting at 6.2 ka cal BP. A prominent step forward occurred at the Middle to Late Holocene transition, dated between 4.7 and 3.9 ka at the Armentarga site, which led to present values typical for oceanic mountain climates (Pann 1700-1850 mm) and was probably accompanied by

increased snowfall and runoff, and had a major impact on timberline depression and grassland expansion. Evidence for a concurrent trigger by human activities at the Late Neolithic / Bronze Age transition are weak, although climate change favored a subsequent development of pastoralism in the Alpine highlands.

We also highlighted that a phase of precipitation increase at Middle to Late Holocene transition actually found straightforward correlation with other proxies of hydrological changes, such as lake level increase in the circumalpine area and in the northern Mediterranean borderlands. The paleoclimatic structure of the event recalls an intensification of the southern air masses conveyed by Tyrrhenian cyclones towards the windward districts of outer Italian Alps and antithetic processes of aridification in southern Italy and the eastern Mediterranean.

Author contributions

GF, MDN and LG performed palynological analysis, GF and RC biogeochemical analysis and RP supervised sieved charcoal analysis. GF and FV elaborated pollen-based quantitative climate reconstructions. MB provided the modern climate framework. GF designed the age-depth model. CR and GF wrote the paper. VM provided the glaciological background. All authors shared the ideas of the paper and reviewed earlier drafts of the manuscript**.**

Acknowledgements

This paper is the result of a PhD project at Milano-Bicocca University, cotutored by CNR-IDPA. Research on the vegetation history in the Upper Brembana Valley was co-funded by Parco delle Orobie Bergamasche (Delib. 12/2017). Thanks are due to S. Casini (Museo Archeologico di Bergamo) for help with the archaeological history and to M. Zanon (University of Kiel), author of a preliminary study. Support to quantitative reconstructions of climate parameters was provided by the CNR-DTA Project of Interest ‘NextData’. We wish to acknowledge the strong coring team and the self-control in facing the several hurricanes monsoonal episodes marking the field work (years 2012-2017). Thanks are due to two anonymous reviewers for constructive comments and suggestions.

References

Andersen, S.T., 1979. Identification of wild grass and cereal pollen. Årbog, Danmarks Geologiske Undersoegelse 1978, 69-92.

Anderson, R.S., Jiménez-Moreno, G., Carrión, J.S., Pérez-Martínez, C., 2011. Postglacial history of alpine vegetation, fire, and climate from Laguna de Río Seco, Sierra Nevada, southern Spain. Quat. Sci. Rev. 30, 1615-1629.

Andreis, C., Armiraglio, S., Caccianiga, M., Bortolas, D., Broglia, A., 2005. *Pinus cembra* L. nel settore sud-alpino lombardo (Italia Settentrionale). Natura Bresciana 34, 19-39.

Arnaud, F., Révillon, S., Debret, M., Revel M., Chapron, E., Jacob, J., Giguet-Covex, C., Poulenard, J., Magny, M., 2012. Lake Bourget regional erosion patterns reconstruction reveals Holocene NW European Alps soil evolution and paleohydrology. Quaternary Science Reviews 51, 81-92.

Badino, F., Ravazzi, C., Vallè, F., Pini, R., Aceti, E., Brunetti, M., Champvillair, E., Maggi, V., Maspero, F., Perego, R., Orombelli, G., 2018. 8800 years of high-altitude vegetation and climate history at the Rutor Glacier forefield, Italian Alps. Evidence of middle Holocene timberline rise and glacier contraction. Quaternary Science Reviews 185, 41–68.

Ballian, D., Ravazzi, C., De Rigo, D., Caudullo, G., 2016. *Pinus mugo* in Europe: distribution, habitat, usage and threats, in: San-Miguel-Ayanz, J., de Rigo, D., Caudullo, G., Houston Durrant, T., Mauri, A. (Eds.), European Atlas of Forest Tree Species. Publ. Off. EU, pp. 124-125.

Bar-Matthews, M., Ayalon, A., Kaufman, A., 1998. Middle to Late Holocene (6,500 Yr. Period) Paleoclimate in the Eastern Mediterranean Region from Stable Isotopic Composition of Speleothems from Soreq Cave, Israel, in: Issar, A.S., Brown, N. (Eds) Water, Environment and Society in Times of Climatic Change, Water Science and Technology Library, vol 31, Springer, Dordrecht.

Behre, K.-E., 1981. The interpretation of anthropogenic indicators in pollen diagrams. Pollen et Spores 23, 225-245.

Belloni, S., Pelfini, M., 1990. La nevosità in Lombardia nel periodo 1964-1973. Natura Bresciana 25, 63-108.

Beniston, M., Diaz, H.F., Bradley, R.S., 1997. Climatic change at high elevation sites: an overview. Climate Change 36, 233–251.

Beug, H.J., 2004. Leitfaden der Pollenbestimmung für Mitteleuropa und angrenzende Gebiete. Verlag Dr. Friedrich Pfeil, München, Germany.

Birks, H.H., Ammann, B., 2000. Two terrestrial records of rapid climatic change during the glacial–Holocene transition (14,000–9,000 calendar years B.P.) from Europe. PNAS 97, 1390–1394.

Birks, H.J.B., 1998. Numerical tools in palaeolimnology - Progress, potentialities, and problems. Journal of Paleolimnology 20, 307-32.

Birks, H.J.B., Heiri, O., Seppä, H., Bjune, A.E., 2010. Strengths and weaknesses of quantitative climate reconstructions based on Late-Quaternary biological proxies. Open Ecology Journal 3, 68-110.

Birks, H.J.B., Seppä, H., 2004. Pollen-based reconstructions of late-Quaternary climate in Europe e progress, problems, and pitfalls. Acta Palaeobotany 44, 317-334.

Bjune, A.E., 2014. After 8 years of annual pollen trapping across the tree line in western Norway: are the data still anomalous? Vegetation History and Archaeobotany 23, 299–308.

Blaauw, M., Christen, J.A., 2011. Flexible paleoclimate age-depth models using an autoregressive gamma process. Bayesian Analysis 6(3), 457-474.

Blais, J.M., Kalff, J., 1995. The influence of lake morphometry on sediment focusing. Limnology Oceanography 40(3), 582-588.

Boyle, J.F., Chiverrell, R.C., Davies, H., Alderson, D.M., 2015. An approach to modelling the impact of prehistoric farming on Holocene landscape phosphorus dynamics. The Holocene 25(1), 203-214.

Brewer, S., Guiot, J., Barboni, D., 2007. Pollen data as climate proxies, in: Elias, S.A. (Ed.), Encyclopedia of Quaternary Science, first ed. Elsevier Science, pp. 2497-2508.

Brisset, E., Guiter, F., Miramont, C., Revel, M., Anthony, E.J., Delhon, C., Arnaud, F., Malet E., de Beaulieu, J.-L., 2015. Lateglacial/Holocene environmental changes in the Mediterranean Alps inferred from lacustrine sediments. Quaternary Science Reviews 110, 49-71.

Brisset, E., Miramont, C., Guiter, F., Anthony, E.J., Tachikawa, K., Poulenard, J., Arnaud, F., Delhon, C., Meunier, J.-D., Bard, E., Suméra, F., 2013. Non-reversible geosystem destabilisation at 4200 cal. BP: Sedimentological, geochemical and botanical markers of soil erosion recorded in a Mediterranean alpine lake. The Holocene 23(12), 1863–1874.

Broström, A., Sugita, S., Gaillard, M.J., 2004. Pollen productivity estimates for the reconstruction of past vegetation cover in the cultural landscape of southern Sweden. The Holocene 14(3), 368-381.

Brunetti, M., Lentini, G., Maugeri, M., Nanni, T., Simolo, C., Spinoni, J., 2012. Projecting North Eastern Italy temperature and precipitation secular records onto a high-resolution grid. Physics and Chemistry of the Earth 40–41, 9–22.

Brunetti, M., Maugeri, M., Nanni, T., Simolo, C., Spinoni, J., 2014. High- resolution temperature climatology for Italy: interpolation method intercomparison. International Journal of Climatology 34(4), 1278–1296.

Büntgen, U., Tegel, W., Nicolussi, K., McCormick, M., Frank, D., Trouet, V., Kaplan, J.O., Herzig, F., Heussner, K.-U., Wanner, H., Luterbacher, J., Esper, J., 2011. 2500 Years of European Climate Variability and Human Susceptibility. Science 331(6017), 578-582.

Buzzi, A., D'Isidoro, M., Davolio, S., 2003. A case study of an orographic cyclone formation south of the Alps during the MAP-SOP. Q. J. R. Meteorological Society 129, 1795-1818.

Caccianiga, M., Ravazzi, C., Zubiani, P., 1994. Storia del ghiacciaio del Trobio (Alpi Orobie, Bergamo) e colonizzazione della vegetazione nelle aree liberate dopo la Piccola Età Glaciale. Natura Bresciana 29, 65-96.

Casini, S., Longhi, C., Castellano, L., Croce, E., Lando, A., 2010. Un santuario celtico a Carona (Bergamo). Ricerche e ritrovamenti nell'area del masso inciso CMS1. Notizie Archeologiche bergomensi 18, 133-154.

Castelletti, L., Martinelli, E., Michetti, A.M., Motella De Carlo, S., 2011. Anthropic land use and vegetation dynamics in mountain areas of Cavargna Valley (Lepontine Alps, Lombardy, N-Italy) during the Holocene. INQUA Congress - Bern (Switzerland), 20-27 July 2.

Clark, J.S., 1988. Particle motion and the theory of charcoal analysis: source area, transport, deposition, and sampling. Quaternary Research 30(1), 67-80.

Colombo, C., Miano, T.M. (Eds.), 2015. Metodi di analisi chimica del suolo. 3ª versione, SISS, Pubblicità e Stampa, Bari, Italy.

Crespi, A., Brunetti, M., Lentini, G., Maugeri, M., 2018. 1961–1990 high-resolution monthly precipitation climatologies for Italy. International Journal of Climatology 38, 878–895.

Cucini Tizzoni, C., 1994. Miniere e metallurgia in alta Val Brembana-Bergamo (secoli XII-XVI). Bergomum 2, 47-98.

Davis, B.A.S., Zanon, M., Collins, M., Mauri, A., Bakker, J., Barboni, D., Barthelmes, A., Beaudouin, C., Birks, H.J.B., Bjune, A.E., et al., 2013. The European modern pollen database (EMPD) project. Vegetation History and Archaeobotany 22(6), 521–530.

Davolio, S., Volonte', A., Manzato, A., Pucillo, A., Cicogna, A., Ferrario, M.E., 2016. Mechanisms producing different precipitation patterns over North-Eastern Italy: insights from HyMeX-SOP1 and previous events. Q. J. R. Meteorological Society 142, 188-205.

Dean, W.E., Jr., 1974. Determination of carbonate and organic matter in calcareous sediments and sedimentary rocks by loss on ignition: comparison with other methods. Journal of Sedimentary Research 44(1), 242-248.

Di Rita, F., Fletcher, W.J., Aranbarri, J., Margaritelli, G., Lirer, F., Magri, D., 2018. Holocene forest dynamics in central and western Mediterranean: periodicity, spatio-temporal patterns and climate influence. Scientific Reports 8, 8929.

Doyen, E., Etienne, D., 2017. Ecological and human land-use indicator value of fungal spore morphotypes and assemblages. Vegetation History and Archaeobotany 26, 357-367.

Ellenberg, H., 1988. Vegetation Ecology of Central Europe. Cambridge University Press.

Enache, M.D., Cumming, B.F., 2007. Charcoal morphotypes in lake sediments from British Columbia (Canada): an assessment of their utility for the reconstruction of past fire and precipitation. Journal of Paleolimnology 38, 347–363.

Etienne, D., Wilhelm, B., Sabastier, P., Reyss, J.-L., Arnaud, F., 2013. Influence of sample location and livestock numbers on *Sporormiella* concentrations and accumulation rates in surface sediments of Lake Allos, French Alps. Journal of Paleolimnology 49, 117-127.

Finsinger, W., Tinner, W., van der Knaap, W.O., Ammann, B., 2006. The expansion of hazel (*Corylus avellana* L.) in the southern Alps: a key for understanding its early Holocene history in Europe? Quaternary Science Reviews 25, 612–631.

Fohlmeister, J., Vollweiler, N., Spötl, C., Mangini, A., 2012. COMNISPA II: Update of a mid-European isotope climate record, 11 ka to present. The Holocene 23(5), 749-754.

Földvári, M., 2011. Handbook of thermogravimetric system of minerals and its use in geological practice. Vol. 213. Geological Institute of Hungary Budapest.

Forcella, F., 1988. Assetto strutturale delle Orobie Orientali tra la Val Seriana e la Val Camonica. Rendiconti della Società Geologica Italiana 11, 269-278.

Furlanetto, G., Ravazzi, C., Brunetti, M., Garozzo, L., 2018. *Alnus viridis* a sensitive snowfall indicator for past oceanic timberlines in the Alps. Alpine and Mediterranean Quaternary 31, 131-134.

Furlanetto, G., Ravazzi, C., Badino, F., Brunetti, M., Champvillair, E., Maggi, V. Elevational transects of modern pollen samples - site specific temperatures as a tool for paleoclimate reconstructions in the Alps. The Holocene accepted.

Gehrig, R., 1997. Pollenanalytische Untersuchungen zur Vegetations- und Klimageschichte des Val Camonica (Norditalien). Dissertatione Botanicae, 276. J. Cramer, Berlin - Stuttgart, pp. 152.

Gobet, E., Tinner, W., Hubschmid, P., Jansen, I., Wehrli M., Ammann, B., Wick., L., 2000. Influence of human impact and bedrock differences on the vegetational history of the Insubrian Southern Alps. Vegetation History and Archaeobotany 9, 175-178.

Grimm, E.C., 2015. Tilia/TGView 2.0.41. Illinois State Museum, Research and Collections Center, Springfield, IL.

Grosjean, M., Suter, P.J., Trachsel, M., Wanner, H., 2007. Ice-borne prehistoric finds in the Swiss Alps reflect Holocene glacier fluctuations. Journal of Quaternary Science 22 (3), 203-207.

Guiot, J., 1990. Methodology of the last climatic cycle reconstruction in France from pollen data.

Palaeogeography, Palaeoclimatology, Palaeoecology 80(1), 49-69.

Gustafsson, Ö., Bucheli, T.D., Kukulska, Z., Andersson, M., Largeau, C., Rouzaud, J.N., Reddy, C.M., Eglinton, T.I., 2001. Evaluation of a protocol for the quantification of black carbon in sediments. Global Biogeochemical Cycles 15(4), 881-890.

Hicks, S., 2001. The use of annual arboreal pollen deposition values for delimiting tree-lines in the landscape and exploring models of pollen dispersal. Review of Palaeobotany and Palynology 117(1-3), 1-29.

Holtmeier, F.-K., 2009. Mountain timberlines. Ecology, Patchiness, and Dynamics. Springer, Berlin, pp. 437.

Holzhauser, H., Magny, M., Zumbühl, H.J., 2005. Glacier and lake-level variations in west-central Europe over the last 3500 years. The Holocene 15(6), 789-801.

Houghton, J.T., Ding, Y., Griggs, D.J., Noguer, M., van der Linden, P.J., Dai, X., Maskell, K., Johnson, C.A., 2001. IPCC, 2001: Climate Change 2001: The Scientific Basis. Contribution of Working Group I to the Third Assessment Report of the Intergovernmental Panel on Climate Change. Cambridge University Press, Cambridge, United Kingdom and New York, NY, USA, pp. 881.

Huisman, J., Olff, H., Fresco, L.F.M., 1993. A hierarchical set of models for species response analysis. Journal of Vegetation Science 4, 37–46.

Ilyashuk, E.A., Koinig, K.A., Heiri, O., Ilyashuk, B.P., Psenner, R., 2011. Holocene temperature variations at a high-altitude site in the Eastern Alps: a chironomid record from Schwarzsee ob Sölden, Austria. Quaternary Science Reviews 30(1), 176-191.

Jackson, S.T. and Williams, J.W., 2004. Modern analogs in Quaternary paleoecology: Here today, gone yesterday, gone tomorrow? Annual Reviews Earth and Planetary Sciences 32, 495-537.

Jacobson, A.R., Provenzale, A., Von Hardenberg, A., Bassano, B., Festa-Bianchet, M., 2004. Climate forcing and density dependence in a mountain ungulate population. Ecology 85(6), 1598-1610.

Jansen, F., Oksanen, J., 2017. Extended HOF (Huisman-Olff-Fresco) Models. R Package Version 1.8.

Jansen, F., Oksanen, J., 2013. How to model species responses along ecological gradients – Huisman–Olff–Fresco models revisited. Journal of Vegetation Science 24, 1108–1117.

Jensen, K., Lynch, E.A., Calcote, R., Hotchkiss, S.C., 2007. Interpretation of charcoal morphotypes in sediments from Ferry Lake, Wisconsin, USA: do different plant fuel sources produce distinctive charcoal morphotypes? The Holocene 17, 907-915.

Jobbagy, E.G., Jackson, R.B., 2000. Global controls of forest line elevation in the northern and southern hemispheres. Global Ecology and Biogeography 9(3), 253-268.

Joly, C., Barillé, L., Barreau, M., Mancheron, A., Visset, L., 2007. Grain and annulus diameter as criteria for distinguishing pollen grains of cereals fromwild grasses. Review of Palaeobotany and Palynology 146, 221-233.

Jordan, P., Arnscheidt, J., McGrogan, H., McCormick, S., 2005. High-resolution phosphorus transfers at the catchment scale: the hidden importance of non-storm transfers. Hydrology and Earth System Sciences Discussions, European Geosciences Union 9(6), 685-691.

Juggins, S., 2017. Rioja: Analysis of Quaternary Science Data, R package version 0.9-15. Available at: http://cran.r-project.org/package=rioja.

Juggins, S., Birks, H.J.B., 2012. Quantitative Environmental Reconstructions from Biological Data, Chapter 14, in: Birks, H.J.B., et al. (Eds.), Tracking Environmental Change Using Lake Sediments, Developments in Palaeoenvironmental Research 5. Springer Science+Business Media, pp. 431-483. B.V. 2012.

Köppen, W., 1923. Die klimate der Erde, in: Grundriss der klimakunde. de Greuter, W., (Ed.), Berlin.

Kurz, I., O'Reilly, C.D., Tunney, H., 2006. Impact of cattle on soil physical properties and nutrient concentrations in overland flow from pasture in Ireland. Agriculture, Ecosystems and Environment 113, 378–390.

Leemann, A., Niessen, F., 1994. Holocene glacial activity and climatic variations in the Swiss Alps: reconstructing a continuous record from proglacial lake sediments. The Holocene 4(3), 259-268.

Le Roy, M., Nicolussi, K., Deline, P., Astrade, L., Edouard, J.L., Miramont, C., Arnaud, F., 2015. Calendar-dated glacier variations in the western European Alps during the Neoglacial: the Mer de Glace record, Mont Blanc Massif. Quaternary Science Reviews 108, 1-22.

Luetscher, M., Hoffmann, D.L., Frisia, S., Spötl, C., 2011. Holocene glacier history from alpine speleothems, Milchbach cave. Switzerland. Earth and Planetary Science Letters 302(1), 95-106.

Magny, M., De Beaulieu, J.-L., Drescher-Schneider, R., Vannièr, B., Walter-Simonnet, A.-V., Miras, Y., Millet, L., Bossuet, G., Peyron, O., Brugiapaglia, E., Leroux, A., 2007. Holocene climate changes in the central Mediterranean as recorded by lake-level fluctuations at Lake Accesa (Tuscany, Italy). Quaternary Science Reviews 26, 1736–1758.

Magny, M., Haas, J.N., 2004. A major widespread climatic change around 5300 cal. yr BP at the time of the Alpine Iceman. Journal of Quaternary Science 19(5), 423–430.

Magny, M., Vannière, B., Calo, C., Millet, L., Leroux, A., Peyron, O., Zanchetta, G., La Mantia, T., Tinner, W., 2011. Holocene hydrological changes in south-western Mediterranean as recorded by lake-level fluctuations at Lago Preola, a coastal lake in southern Sicily, Italy. Quaternary Science Reviews 30, 2459-2475.

Magny, M., Joannin, S., Galop, D., Vannière, B., Haas, J.N., Bassetti, M., Bellintani, P., Scandolari, R., Desmet, M., 2012. Holocene palaeohydrological changes in the northern Mediterranean borderlands as reflected by the lake-level record of Lake Ledro, northeastern Italy. Quaternary Research 77, 382–396.

Mangini, A., Spötl, C., Verdes, P., 2005. Reconstruction of temperature in the Central Alps during the past 2000 yr from a $\delta^{18}O$ stalagmite record. Earth and Planetary Science Letters 235, 741–751.

Mauri, A., Davis, B.A.S., Collins, P.M., Kaplan, J.O., 2015. The climate of Europe during the Holocene: a gridded pollen-based reconstruction and its multi-proxy evaluation. Quaternary Science Reviews 112, 109-127.

Mauri, A., Caudullo, G., 2016. *Alnus viridis* in Europe: distribution, habitat, usage and threats, in: San-Miguel-Ayanz, J., De Rigo, D., Caudullo, G., Houston Durrant, T., Mauri, A. (Eds), European Atlas of Forest Tree Species. Publication Office of the European Union, Luxembourg, p. 68.

Mayewski, P.A., Rohling, E.E., Stager, J.C., Karlénd, W., Maascha, K.A., Meekere, L.D., Meyersona, E.A., Gassef, F., Van Kreveldg, S., Holmgrend, K., Lee-Thorph, J., Rosqvistd, G., Racki, F., Staubwasserj, M., Schneiderk, R.R., Steigl, E.J., 2004. Holocene climate variability. Quaternary Research 62, 243-255.

Mazier, F., Galop, D., Brun, C., Buttler, A., 2006. Modern pollen assemblages from grazed vegetation in the western Pyrenees, France: a numerical tool for more precise reconstruction of past cultural landscapes. The Holocene 16(1), 91-103.

Mitchell, T.D., Jones, P.D., 2005. An improved method of constructing a database of monthly climate observations and associated high-resolution grids. International Journal of Climatology 25(6), 693-712.

Moore, P.D., Webb, J.A., Collinson, M.E., 1991. Pollen analysis. Blackwell Scientific Publications, Oxford.

Muscheler, R., Beer, J., Wagner, G., Finkel, R.C., 2000. Changes in deep-water formation during the Younger Dryas event inferred from ^{10}Be and ^{14}C records. Nature 408(6812), 567-570.

New, M., Hulme, M., Jones, P., 2000. Representing twentieth-century space-time climate variability. Part II: Development of 1901-96 monthly grids of terrestrial surface climate. Journal of Climate 13, 2217-2238.

Nicolussi, K., Kaufmann, M., Patzelt, G., van der Plicht, J., Thurner, A., 2005. Holocene tree-line variability in the Kauner Valley, Central Eastern Alps, indicated by dendrochronological analysis of living trees and subfossil logs. Vegetation History and Archaeobotany 14(3), 221-234.

Oeggl, K., 2009. The significance of the Tyrolean Iceman for the archaeobotany of Central Europe. Vegetation History and Archaeobotany 18, 1–11.

Olsen, J., Anderson, N.J., Knudsen, M.F., 2012. Variability of the North Atlantic Oscillation over the past 5,200 years. Nature Geoscience 5, 808-812.

Patzelt, G., Bortenschlager, S., 1973. Die postglazialen Gletscher- und Klimaschwankungen in der Venedigergruppe (Hohe Tauern, Ostalpen). Zeitschrift für Geomorphologie N.F. 16, 25-72. Suppl. Bd.

Pepin, N., Bradley, R.S., Diaz, H.F., Baraer, M., Caceres, E.B., Forsythe, N., Fowler, H., Greenwood, G., Hashmi, M.Z., Liu, X.D., Miller, J.R., Ning, L., Ohmura, A., Palazzi, E., Rangwala, I., Schöner, W., Severskiy, I., Shahgedanova, M., Wang, M.B., Williamson, S.N., Yang, D.Q., 2015. Elevation-dependent warming in mountain regions of the world. Nature Climate Change 5(5), 424-430.

Pessina, A., 2000. Il primo Neolitico dell'Italia Settentrionale. Problemi generali. In (Pessina, A., Muscio, G., a cura di) La Neolitizzazione tra Oriente e Occidente. Museo Friulano di Storia Naturale, pp. 81-90.

Pini, R., 2002. A high-resolution Late Glacial – Holocene pollen diagram from Pian di Gembro (Central Alps, northern Italy). Vegetation History and Archaeobotany 11(4), 251-262.

Pini, R., Ravazzi, C., Raiteri, L., Guerreschi, A., Castellano, L., Comolli, R., 2017. From pristine forests to high-altitude pastures: an ecological approach to prehistoric human impact on vegetation and landscapes in the western Italian Alps. Journal of Ecology 105, 1580–1597.

Pini, R., Castellano, L., Perego, R., Ravazzi, C., Chiesa, S., De Amicis, M., Poggiani Keller, R., 2016a. Nuovi dati sulla storia ambientale del centro abitato di Bergamo Alta tra la fase arcaica dell'età del Bronzo e il Medioevo. Stratigrafia, paleoecologia e archeobotanica dei depositi del Palazzo del Podestà (Piazza Vecchia). Atti dell'Ateneo di Scienze, Lettere ed Arti, Bergamo, LXXIX, 349-371.

Pini, R., Ravazzi, C., Aceti, A., Castellano, L., Perego, R., Quirino, T., Vallè, F., 2016b. Ecological changes and human interaction in Valcamonica, the Rock Art Valley, since the last deglaciation. Alpine and Mediterranean Quaternary 29(1), 19-34.

Poggiani, K., 2010. La Valcamonica fra Preistoria e Protostoria, in: Maretta, A., Cittadini, T. (Eds), I parchi con arte rupestre della Valcamonica - Guida ai percorsi di visita. Centro Camuno Studi Preistorici, pp. 30-33.

Poggiani, K., 2007. L'età del Ferro. Dall'*oppidum* degli Orobi alla formazione della città sul colle, in: Fortunati, M., Poggiani, R. (Eds). Storia Economica e Sociale di Bergamo. I primi millenni, 1, 147-189.

Punt, W., Blackmore, S., (Eds) (1976–2009). The Northwest European Pollen Flora. Vol. I-IX. Elsevier Publishing Company.

Qin, J., Yang, K., Liang, S., Guo, X., 2009. The altitudinal dependence of recent rapid warming over the Tibetan Plateau. Climatic Change 97, 321–327.

R Core Team, 2013. R: A language and environment for statistical computing. R Foundation for Statistical Computing, Vienna, Austria. Available at: http://www.R-project.org/.

Rasmussen, S.O., Vinther, B.M., Clausen, H.B., Andersen, K.K. 2007. Early Holocene climate oscillations recorded in three Greenland ice cores. Quaternary Science Reviews 26(15), 1907-1914.

Ravazzi, C., Marchetti, M., Zanon, M., Perego, R., Deaddis, M., De Amicis, M., Margaritora, D., Quirino, T., 2013. Lake evolution and landscape history in the lower Mincio River valley, unravelling drainage changes in the central Po Plain (N-Italy) since the Bronze Age. Quaternary International 288, 195-205.

Reille, M., 1992-1998**.** Pollen et spores d'Europe et d'Afrique du Nord. Laboratoire de Botanique historique et palynologie, Marseille.

Reimer, P.J., Bard, E., Bayliss, A., 2013. IntCal13 and Marine13 radiocarbon age calibration curves 0-50,000 years cal BP. Radiocarbon 55, 1869-1887.

Riceputi, F., 2004. Li homini de Fondra, Branciis, Carona, Valle Levi et Populo. Ferrari Edizioni.

Rotunno, R., Houze, R.A.J., 2007. Lessons on orographic precipitation from the Mesoscale Alpine Programme. Q. J. R. Meteorological Society 133, 811–830.

Samartin, S., Heiri, O., Joos, F., Renssen, F., Franke, J., Brönnimann, S., Tinner, W., 2017. Warm Mediterranean mid-Holocene summers inferred from fossil midge assemblages. Nature Geoscience 10, 207-214.

Scaife, R., 1997. Pollen analysis of the Laghetti del Crestoso corrie basin, in: Baroni, C., Biagi, P. (Eds.), Excavations at the high-altitude Mesolithic site of Laghetti del Crestoso (Bovegno - Brescia, Northern Italy). Ateneo di Brescia, Accademia di Scienze, Lettere e Arti, pp. 64-77.

Schoenau, J.J., O'Halloran, I.P., 2008. Sodium bicarbonate-extractable phosphorus. Soil Sampling and Methods of Analysis, 2nd edn (eds Carter, M.R. and Gregorich, E.G.), CRC Press, Boca Raton, FL, USA, pp. 89–94.

Senn, K., 1999. Tree mortality caused by *Gremmeniella abietina* in a subalpine afforestation in the central Alps and its relationships with duration of snow cover. European Journal of Pathology 29, 65-74.

Sevink, J., van Bergen, M.J., van der Plicht, J., Feiken, H., Anastasia, C., Huizinga A., 2011. Robust date for the Bronze Age Avellino eruption (Somma-Vesuvius): 3945 ± 10 calBP (1995 ± 10 calBC). Quaternary Science Reviews 30, 1035-1046.

Simpson, G.L., 2012. Analogue Methods in Palaeolimnology, in: Smol, J.P., Birks, H.J.B., Last, W.M. (Eds.), Tracking environmental change using lake sediments. Developments in Palaeoenvironmental Research 5. Springer Science+Business Media, pp. 431-483. B.V.

Simpson, G.L., 2007. Analogue Methods in paleoecology: using the analogue package. Journal of Statistical Software 22(2), 1-29.

Sjögren, P., van der Knaap, W.O., Huusko, A., van Leeuwen, J.F.N., 2008. Pollen productivity, dispersal, and correction factors for major tree taxa in the Swiss Alps based on pollen-trap results. Review of Palaeobotany and Palynology 152, 200–210.

Starnini, E., Biagi, P., Mazzucco, N., 2017. The beginning of the Neolithic in the Po Plain (northern Italy): Problems and perspectives. Quaternary International 1-17.

Stockmarr, J., 1971. Tablets with spores used in absolute pollen analysis. Pollen et Spores 13, 615–621.

Stuiver, M., Reimer, P.J., Reimer, R., 2013. Radiocarbon Calibration Program Revision 7.0.2.

Telford, R.J., 2015. palaeoSig: Significance Tests for Quantitative Palaeoenvironmental Reconstructions, R Package Version 1.1-3. http://cran.r-project. org/package=palaeoSig.

Telford, R.J., Birks, H.J.B., 2011a. A novel method for assessing the statistical significance of quantitative reconstructions inferred from biotic assemblages. Quaternary Science Reviews 30, 1272-1278.

Telford, R.J., Birks, H.J.B., 2011b. Effect of uneven sampling along an environmental gradient on transfer-function performance. Journal of Paleolimnology 46, 99–106.

ter Braak, C.J.F., 1995. Non-linear methods for multivariate statistical calibration and their use in palaeoecology: a comparison of inverse (k-nearest neighbours, partial least squares and weighted averaging partial least squares) and classical approaches. Chemometrics and Intelligent Laboratory Systems 28, 165-180.

ter Braak, C.J.F., Juggings, S., 1993. Weighted averaging partial least squares regression (WA-PLS): an improved method for reconstructing environmental variables from species assemblages. Hydrobiologia 269/270, 485–502.

Tinner, W., Theurillat, J.P., 2003. Uppermost limit, extent, and fluctuations of the timberline and treeline ecocline in the Swiss Central Alps during the past 11,500 years. Arctic, Antarctic, and Alpine Research 35(2), 158-169.

van der Knaap, W.O., van Leeuwen, J.F., Ammann, B., 2001. Seven years of annual pollen influx at the forest limit in the Swiss Alps studied by pollen traps: relations to vegetation and climate. Review of Palaeobotany and Palynology 117(1), 31-52.

van Geel, B., 1978. A palaeoecological study of Holocene peat bog sections in Germany and The Netherlands, based on the analysis of pollen, spores and macro- and microremains of fungi, algae, cormophytes and animals. Review of Palaeobotany and Palynology 25, 1–120.

van Geel, B., Aptroot, A., 2006. Fossil ascomycetes in Quaternary deposits. Nova Hedwigia 82, 313-329.

van Geel, B., Bohncke, S.J.P., Dee, H., 1981. A palaeoecological study of an upper Late Glacial and Holocene sequence from 'De Borchert', The Netherlands. Review of Palaeobotany and Palynology 31, 367-449.

Walker, M.J., Berkelhammer, M., Björck, S., Cwynar, L.C., Fisher, D.A., Long, A.J., Lowe, J.J., Newnham, R.M., Rasmussen, S.O., Weiss, H., 2012. Formal subdivision of the Holocene Series/Epoch: a Discussion Paper by a Working Group of INTIMATE (Integration of ice-core, marine and terrestrial records) and the Subcommission on Quaternary Stratigraphy (International Commission on Stratigraphy). Journal of Quaternary Science 27(7), 649-659.

Whitlock, C., Larsen, C., 2001. Charcoal as a fire proxy, in: Smol, J.P., Birks, H.J.B., Last, W.M. (Eds.), Tracking environmental change using lake sediments. Volume 3: terrestrial, algal, and siliceous indicators. Kluwer Academic Publishers, pp. 75–97.

Wick, L., 2000. Vegetational response to climatic changes recorded in Swiss Late Glacial lake sediments. Palaeogeography, Palaeoclimatology, Palaeoecology 159, 231–250.

Wick, L., 1996. Late-glacial and early-Holocene palaeoenvironments in Brianza, N Italy. Il Quaternario Italian Journal of Quaternary Sciences 9(2), 653-660.

Wick, L., van Leeuwen, J.F., van der Knaap, W.O., Lotter, A.F., 2003. Holocene vegetation development in the catchment of Sägistalsee (1935 m asl), a small lake in the Swiss Alps. Journal of Paleolimnology 30(3), 261-272.

Willis, K.J., Gillson, L., Brncic, T.M., Figueroa-Rangel, L., 2005. Providing baselines for biodiversity measurement. TRENDS in Ecology and Evolution 20 (3), 107-108.

Wissinger, S.A., Oertli, B., Rosset, V., 2016. Invertebrate Communities of Alpine Ponds, in: Baltzer, D., Boix, D. (Eds), Invertebrates in Freshwater Wetlands. An International Perspective on their Ecology. Chapter 3. Springer, 55-103.

Zanchetta, G., Regattieri, E., Isola, I., Drysdale, R.N., Bini, M., Baneschi, I., Hellstrom, J.C., 2016. The so-called “4.2 event” in the Central Mediterranean and its climatic teleconnections. Alpine and Mediterranean Quaternary 29(1), 5-17.

Zoller, H., Schindler, C., Röthlisberger, H., 1966. Postglaziale Gletscherstände und Klimaschwankungen im Gotthardmassiv und Vorderrheingebiet. Verh. Naturforsch. Ges. Basel 77(2), 97-164.

Zonca, A., 1998. Gli uomini e le terre dell’Abbazia San Benedetto di Vallalta (secoli XII-XIV). Civica Biblioteca Angelo Mai, Bergamo, pp. 78-86.

Appendix A. Supplementary data

Identification of *Pinus* pollen grains in Holocene deposits from the Central Alps: features at LO and SEM

At the optical microscope, pollen of *Pinus cembra* was systematically distinguished from *Pinus sylvestris/mugo* type based on the following criteria: (1) presence of verrucae on the ventral surface of the grain body, (2) shape of sacci, more elongated than in *Pinus sylvestris*, (3) occurrence of a slightly undulating outer layer on the proximal surface of the grain body towards the sacci. The distinction of pollen of *Pinus mugo* from *Pinus sylvestris* was performed at SEM based on the criteria indicated by Klaus (1978) and our original observations (**Supplementary Fig. S1** and **Table S1**). The main features used for the species distinction are the arrangements of tectum sculptures on the grain corpus (chamber caps of unequal size - height and distribution in *P. mugo*, while equal in *Pinus sylvestris*) and the number of perforations on the sacci (much higher in *Pinus sylvestris* than in *P. mugo*).

CAPPA	*Pinus sylvestris*	*Pinus mugo*
Size of chamber caps (in an area of 25 μm^2)	Equal (0,57-1,33 μm)	Unequal (0,4-2 μm)
Heigth of caps	Equal	Wide, changing from cap to cap
Density of caps	Medium (33/25 μm^2)	Medium (32/35 μm^2)
Trenches between caps	Broad	Narrow and deep
Microgranula	Numerous	Absent
Shape of caps	Irregular, polygonal, equally distributed over the square space	Extremely irregular (partly elongated, rounded and undulated), unequally distributed over the surface
Cappa exine sculpture	Irregularly verrucate- rugulate	Verrugate- rugulate
Fusions of caps	Almost absent	Occasionally fused
Micrograna	Almost absent	Present but irregularly distributed over the surface
Perforations	Occur (6-8/25 μm^2)	Almost absent (1-2/25 μm^2)

SACCUS	*Pinus sylvestris*	*Pinus mugo*
Perforations (in an area of 25 μm^2)	63/25 μm^2	31/25 μm^2 Few (almost absent)
Chamber caps	Lepros-vermiculate, occasionally flattered	Reticulate
Microgranula	Numerous, densely spaced	Numerous
Micrograna	Absent	Occur

Supplementary Table S1. Criteria for *Pinus sylvestris* and *Pinus mugo* SEM distinction. Diagnostic characters verified from Klaus, 1978.

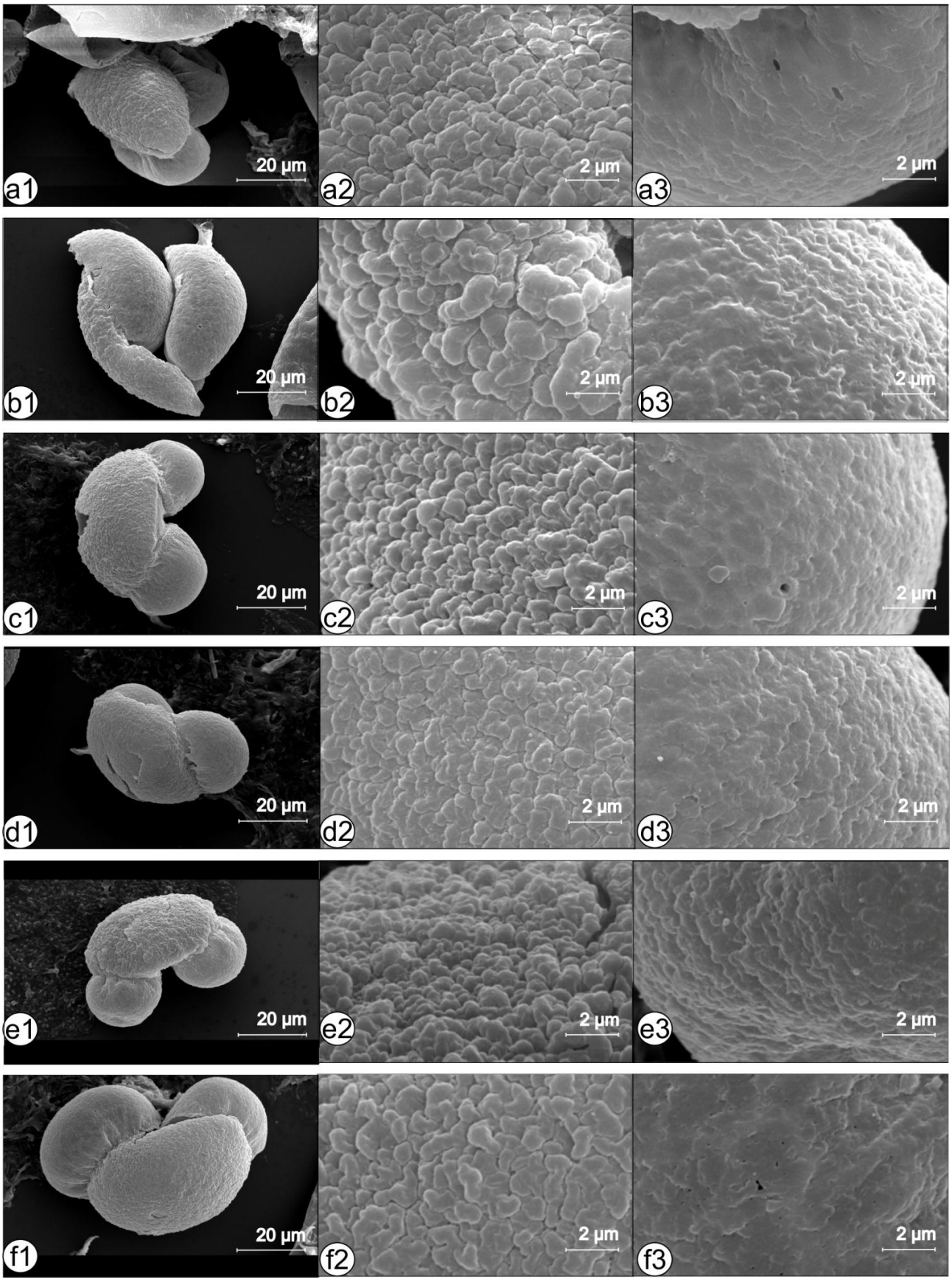

Supplementary Fig. S1. Scanning Electron Microscope (SEM) micrographs of fossil pine grains from the Armentarga succession.

a-c-e) *Pinus mugo* from 85, 194 and 241,5 cm depth. a1-c1-e1: grains in lateral view, x1300; a2-c2-e2: chamber caps on the grain corpus, x10000; a3-c3-e3: details of the grain saccus, x10000.

b-d-f) *Pinus sylvestris* from 85, 194 and 241,5 cm depth. b1-d1-f1: grains in lateral view, x1300; b2-d2-f2: chamber caps on the grain corpus, x10000; b3-d3-f3: details of the grain saccus, x10000.

Supplementary Fig. S2. Examples of snow runoff carrying nutrients from dust deposition and from droppings of native ungulates during the melting season in the Italian Alps.

Panel A and B – Native ungulates populations (reintroduced ibex and native chamois) exploit the fringe of snowmelt patches in late spring to obtain salts from dripping water and water-satured soils, and also graze on young shoots of *Juniperus nana*, *Carex sempervirens, Homogyne* in a *Nardus*-dominated grassland (pictures taken at Passo Laghi Gemelli, Orobie Alps, 2140 m asl, June 17, 2018). Local shepherds, after interviews by one of us (C.R.), support either native *Capra ibex* or domesticated *Capra hircus* to exploit snowmelt and browse on juniper shoots in early spring to obtain salt and thus nutrients. Dust deposition to snow cover is likely responsible for accumulation of nutrients on water snowmelt (e.g. Steltzer et al., 2009). Ungulates typically defecate in front of melting snow patches while snow runoff is active. We checked these droppings to have been always deposited on soil surface after snow melting occurred. Palynological analysis of both droppings and water-satured soil highlights abundance of coprohilous fungi likely originating from infiltering meltwater and also include juniper stomata (see **Supplementary Table S2**). This mountain region in the Italian Alps also supports transhumance of domesticated livestock, which, however, is taken on high pastures only after the end of snow melt season (i.e. June 15 at stables around 2000 m asl, but later on, after onset July, at higher elevations). Hence, droppings from livestock virtually do not contribute to snow runoff but are concentrated on watering sites. Accumulation of both coprophilous fungi and phosporus has been documented from several prehistoric watering sites in the Alps (Etienne et al., 2013; Pini et al., 2017).

Panel C – Melting snow patches with fresh ungulate droppings (arrow) at the border of Lake Malgina, 2339 m, Orobie Alps, June 24, 2018.

	ungulates droppings	water satured soil
Alnus glutinosa/A. incana	0.9	1.1
Betula	0.6	2
Castanea	0.6	1.6
Fagus	0.2	2.9
Fraxinus excelsior type	0.7	0.9
Ostrya type	0.6	1.4
Picea	2.8	5.2
Pinus cembra	0.2	1.4
Pinus sylvestris/mugo type	1.8	12.9
Salix	0.2	5.4
Alnus viridis	54.9	6.5
Corylus	4.8	22.1
Vaccinium	1.8	0.7
Juniperus stomata	3.1	0
Brassicaceae	1.1	2
Cichorioideae	0.2	4.7
Cirsium	1.1	0
Gentiana pneumonanthe type	3.5	1.4
Plantago lanceolata type	0.2	1.4
Poaceae < 37 µm	9.4	13.3
Poaceae 37-47 µm	1.8	1.8
Potentilla type	2.8	0
Cyperaceae	0.7	1.4
Podospora	0.6	0

Glomus	0	1.4
Sordariaceae undiff.	7.3	0.2
Sordaria	9.7	0.2
Sporormiella-like type	38.5	0.9
Delitschia	1.3	1.4
charcoal conc. 10-50 µm	0	215
pollen conc.	39463	48760
trees	8.1	34.5
shrubs	62.4	30.7
upland herbs	27.7	29.3
apophytes and cultivated plants	1.8	3.8
xerophytes	0	1.6
pollen sum	545	443

Supplementary Table S2. Results from palynological analysis of droppings and water-satured soil. The table reports the main pollen types (> 1 %). The Sordariaceae does not include *Gelasinospora* and *Neurospora* which can be distinguished on a morphological basis.

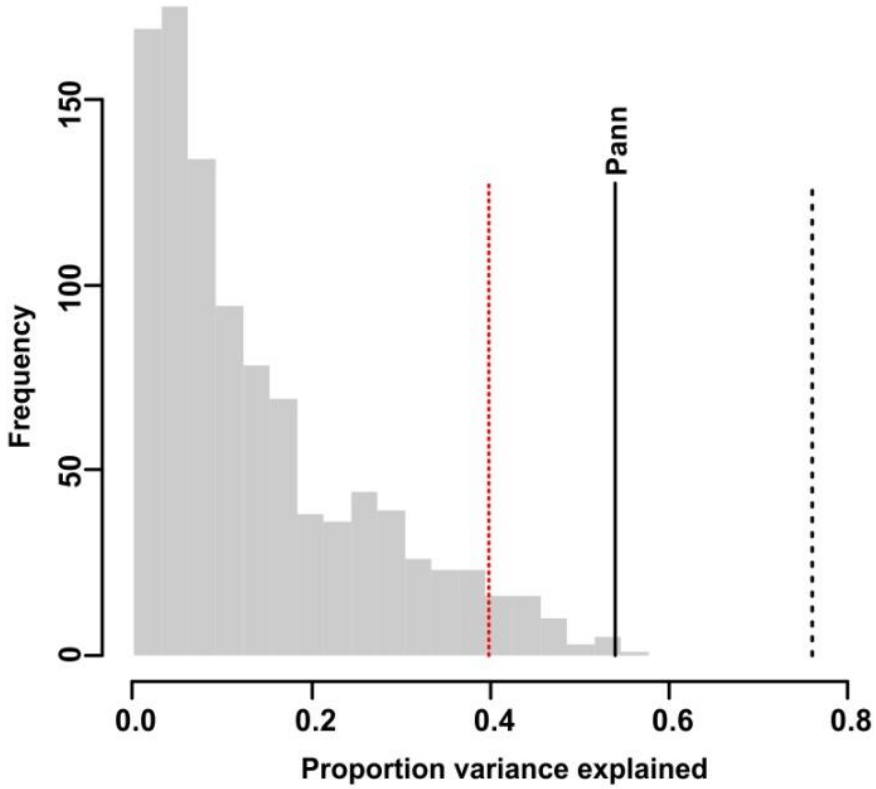

Supplementary Fig. S3. Pann reconstruction statistically significant (p =0.001) to the novel method proposed by Telford and Birks (2011).

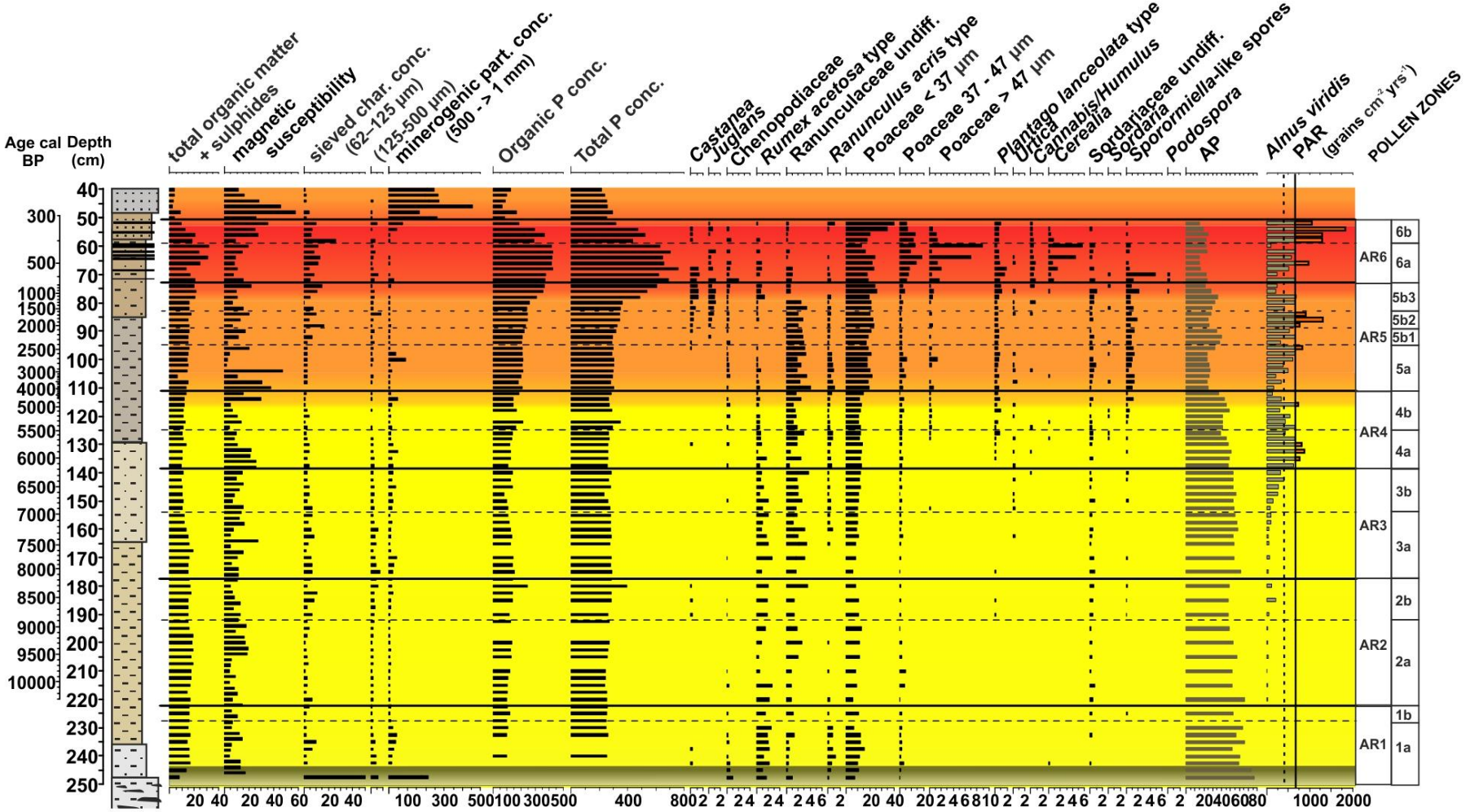

Supplementary Fig. S4. Synthetic figure for the history of human interference. Yellow – Grazing and fertilization by native ungulate: Orange – Intensified fertilization by native ungulates and by transhumant livestock; Red – Forest clearing and burning, charcoal production, livestock watering with intense fertilization. The Sordariaceae does not include Gelasinospora and Neurospora which can be distinguished on a morphological basis.

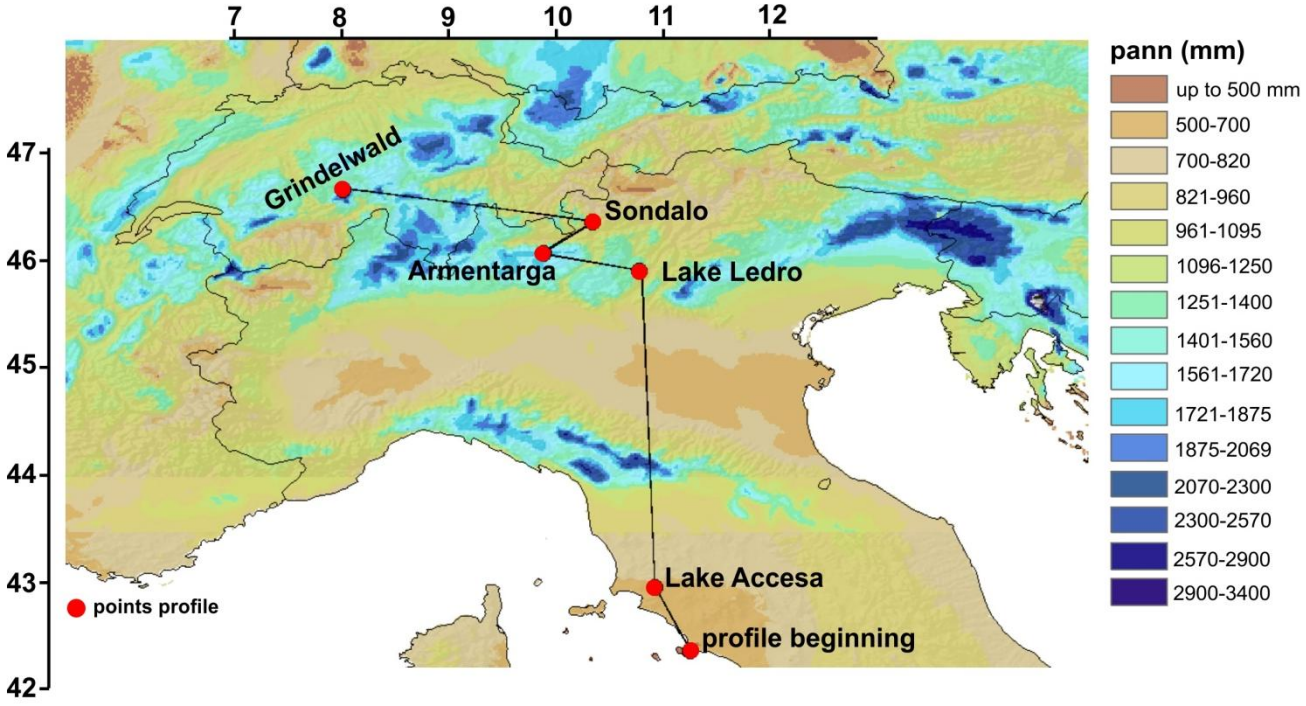

Supplementary Fig. S5. Latitudinal transect across the precipitation gradient from the Tyrrhenian Sea to the Alps. The profile is used in Fig. 14 Classified annual precipitation climatology (1961-1990) between Lat 42.404 to Lat 46.621 N and transect line. Red dots indicate sites discussed in the text (see section 5.2.2).

References

Etienne, D., Wilhelm, B., Sabastier, P., Reyss, J.-L., Arnaud, F., 2013. Influence of sample location and livestock numbers on *Sporormiella* concentrations and accumulation rates in surface sediments of Lake Allos, French Alps. Journal of Paleolimnology 49, 117-127.

Klaus, W., 1978. On the taxonomic significance of tectum sculpture characters in alpine Pinus species. Grana 17, 161-166.

Pini, R., Ravazzi, C., Raiteri, L., Guerreschi, A., Castellano, L., Comolli, R., 2017. From pristine forests to high- altitude pastures: an ecological approach to prehistoric human impact on vegetation and landscapes in the western Italian Alps. Journal of Ecology 105, 1580–1597.

Steltzer, H., Landry, C., Painter, T.H., Anderson, J., Ayres, E., 2009. Biological consequences of earlier snowmelt from desert dust deposition in alpine landscapes. PNAS 106(28), 11629-11634.

Telford, R.J., Birks, H.J.B., 2011. A novel method for assessing the statistical significance of quantitative reconstructions inferred from biotic assemblages. Quaternary Science Reviews 30, 1272-1278.

Final remarks

The aim of this PhD research was to test and prove the suitability of pollen data for quantitative paleoclimate estimations.

First (**Manuscript 1**) was demonstrated the importance of local elevational transects of modern pollen samples with site-specific temperature as a tool for paleoclimate reconstructions in the Alps. The two elevational transects (La Thuile Valley and Upper Brembana Valley) were developed to derive consistent local pollen-climate correlations, to find sensitive pollen taxa useful for paleoclimate reconstructions; to estimate the effects of local parameters (elevational lapse rate, climate, uphill pollen transport and human impact) and were used as test sets to evaluate pollen-climate models based on calibration sets extracted from the European Modern Pollen Database. This procedure can be applied to other high mountain ranges with Alpine-types of elevational biodiversity gradients in the mid-latitudes of the Eurasian and American continents.

The modern pollen assemblages-vegetation-climate relationships along an elevational gradient in the Upper Brembana Valley were investigated (**Manuscript 2**). The results of CCA analysis demonstrated a general good agreement with previous studies, which identified elevation as the main gradient in the variation of modern pollen and vegetation assemblages in mountain areas. Potential indicator pollen taxa of alpine/subalpine belts (e.g. *Vaccinium*, *Rhododendron*, *Loiseleuria*) were documented in this study.

Pollen-based quantitative estimations of July temperature and annual precipitation were obtained from a high-elevation site (Armentarga peat bog, 2345 m asl) during the last 10 ka (**Manuscript 3**). The models proved to be effective even on the modern landscape marked by weak to moderate human impact, with the exclusion of Middle Age phases that suffered stronger alterations due to deforestation and pastoralism. Changes in annual precipitation occurred in three main steps during the Holocene, starting with a moderately humid early Holocene marked by early occurrence of the *Alnus viridis* dwarf forests, and followed by a first step of precipitation increase starting at 6.2 ka cal BP. A prominent step forward occurred at the Middle to Late Holocene transition, dated between 4.7 and 3.9 ka, which led to present values typical for oceanic mountain climates (Pann 1700-1850 mm).